MESOSCALE MODELLING OF THE ANTARCTIC KATABATIC WIND OVER THE LAMBERT BASIN

by

Richard Andrew Dare, B.Sc.(Hons.).

Submitted in fulfilment of the
requirements for the degree of
Doctor of Philosophy

University of Tasmania

March, 1995

DECLARATION AND AUTHORITY OF ACCESS

The material contained in this thesis is original except where due acknowledgement is given, and the material has not been accepted for the award of any other degree or diploma.

This thesis may be made available for loan and limited copying in accordance with the Copyright Act 1968.

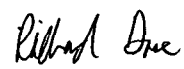

ABSTRACT

The Lambert Glacier drainage basin is a large area of the Antarctic which has been devoid of conventional meteorological observations, apart from the coastal meteorological stations. A mesoscale atmospheric model is adapted for use over the Antarctic continent, and is used with the coastal meteorological records to simulate boundary layer climatologies over the region. The results are well validated by new data from oversnow traverses and automatic stations around the basin. The CSU-Pielke (Pielke and Martin (1981)) numerical mesoscale model was tested for its suitability over Antarctica. Problems with the surface energy balance iteration scheme, sea ice surface temperatures, boundary layer height parameterisation and the representation of cloud in the radiation scheme over the Antarctic plateau needed to be overcome. Following sensitivity tests to surface parameters, mean summer and winter modelling results were verified using interpolated fields from observations available around the Lambert Basin. Analyses of the meteorological records at Mawson station showed that warm, moist blizzard winds were associated with cyclonic forcing, and average katabatic winds consisted of cold, dry air originating further south and flowing as a shallow surface density current to the coast. "Katabatic-blizzard" winds were the strongest mean winds found, forced by a combination of cyclonic and drainage flows. The mesoscale modelling clarified the observations and showed that downslope winds are likely to be influenced by SW - W synoptic wind directions during July. Near-surface jets complicated relationships between surface and synoptic winds because they are fairly independent of synoptic control, existing as relatively dense parcels of air draining downslope from the plateau. Observations showed that during summer, wind speed increases were accompanied by increases in thermal stability, but during winter, by reductions in stability. During January, upper winds directly influence surface winds through direct transfer of momentum in the vertical, but during July, vectorial components contribute to the surface flow forcing. The modelling explained the differences in boundary layer structure between summer and winter, associated with the seasonal differences in synoptic flow and also explained why Mawson station is a site of strong, persistent winds. Once appropriately adapted for Antarctic use, the numerical model was found to produce reasonable thermal fields with corresponding wind regimes. It then served as a powerful tool for improving the general understanding of air flow over Antarctica, on the regional scale, and also for explaining relationships between surface winds and synoptic forcing over Mawson station.

ACKNOWLEDGMENTS

The content of this thesis represents the results of several years work under the guidance and advice of my supervisor, Prof. W. F. Budd. I am grateful for his enthusiasm and expertise in the field of Antarctic Meteorology. I would also like to thank my co-supervior, Dr. T. T. Gibson for reviewing drafts of this thesis.

I am grateful to Dr. B. van Meurs of the University of Melbourne for her guidance during the initial stages of this research. I would also like to thank Dr. D. Jenssen of the University of Melbourne for his encouragement and enthusiasm in the fields of Computers and Meteorology during my years as an undergraduate and postgraduate.

I would like to thank Dr. I. Allison of the Australian Antarctic Division for providing me with data collected from the Lambert Glacier Basin region of Antarctica. Thanks also to Dr. D. Russell-Head and the Bureau of Meteorology for supplying me with data from Mawson and Davis stations.

Finally, I would like to thank the staff and students of I.A.S.O.S. at the University of Tasmania.

Contents

List of Figures

List of Tables

ABBREVIATIONS

ABL - Atmospheric Boundary Layer

AGCM - Atmospheric General Circulation Model

AUW - Antarctic Upper Wind (data set)

AWS - Automatic Weather Station

PBL - Planetary Boundary Layer

SHANAL - Southern Hemisphere Analyses

Abbreviated names of wind types are noted in Chapter 3.

Chapter 1

INTRODUCTION

The Antarctic Ice Sheet still has large areas of over 1000 kilometres in extent devoid of conventional meteorological observations. The surface heat balance and development of pronounced boundary layer inversions, with shallow katabatic drainage, which is strongly influenced by the irregular passage of coastal depressions, form an important part of the Earth's atmospheric energy balance.

The development of numerical models to simulate the Antarctic boundary layer well has been impaired by the lack of data available over large parts of the interior for validation. The opportunity arose with the recent traverses around the Lambert Glacier Basin, making surface observations, and establishing a series of new Automatic Weather Stations, to examine how well a mesoscale model can simulate the boundary layer conditions in the interior in advance of the new data which could then be used for validation.

The primary aims of this project are to establish mean seasonal (particularly summer and winter) atmospheric boundary layer meteorological conditions over the Lambert Glacier Basin Region of East Antarctica and to clarify the relationship between synoptic weather conditions and surface winds at Mawson station. Mean January and mean July conditions are used to represent mean summer and mean winter conditions respectively.

Past work on Antarctic atmospheric planetary boundary layer meteorology is reviewed in Chapter 2. This includes discussions on the "inversion winds" over the plateau, the coastal and katabatic winds, the transition between plateau and

coastal winds, pressure jumps in the coastal zone, depressions that pass through coastal areas and their effects and also non-Antarctic work on katabatic winds that is relevant.

This review provides a basis upon which the entire project may be undertaken. Work in later chapters is often compared and referred back to the review, which is helpful in assessing the validity of the project's results and in determining the path which the research was to take at different stages.

In Chapter 3, measurements from the Lambert Glacier Basin of East Antarctica are examined to establish the validity of compiling a climatology of this region. It is concluded that presently, due to the sparseness of the data coverage and short periods of time that Automatic Weather Stations (AWSs) have been deployed, a reliable climatology cannot be calculated, over the interior directly from the observations, but useful estimates of meteorological variables are found. Several different types of winds are also analysed from observations at Mawson and Davis stations, showing the meteorological conditions accompanying katabatic and blizzard winds.

The CSU-Pielke numerical mesoscale model is introduced in Chapter 4, for the purpose of attempting to model the boundary layer over the region of interest. Mean January and mean July conditions are modelled, so that climatological conditions can be determined over regions where real data are absent. However, before these can be derived, several modifications need to be made to the 1981 version of this model so that it can function suitably in Antarctic meteorological conditions. A change to the surface balance iteration scheme is described.

Chapter 5 discusses comparisons between observed and modelled surface temperature fields. It is found that over the sea ice region of the model domain, surface temperatures in the model drop dramatically and unrealistically due to the flat terrain, relatively calm winds and little mixing of air. These conditions lead to the formation of a strong inversion, that is unrealistic for the sea ice region; surface temperatures of sea ice are relatively warm compared with those

over the Antarctic plateau due to heat conduction through the ice from the water below and also because of the relatively warm air that is advected from the north.

Several methods are tested to adjust the sea ice temperatures to realistic values, but because the modelling carried out is not interseasonal, and does not include a sea ice model, the method adopted here is to prescribe the monthly mean sea ice surface temperatures as observed. The surface temperatures of the firn (snow and ice) over the continent are calculated at every timestep during a model run.

The 1981 version of the CSU-Pielke model used the Deardorff (1974) scheme for predicting the height of the atmospheric planetary boundary layer (PBL). This is suitable for conditions where there is surface heating, such as in the Wangara Experiement, from which the Deardorff formulation is derived. However, over the Antarctic plateau strong inversions can form due to significant loss of long-wave radiation. Where the ice slopes are small, wind speeds are low and vertical mixing is inhibited. Inversions over the Antarctic plateau can be most intense up to about 25 metres above the surface. The PBL depth predicted using the Deardorff scheme becomes very shallow under these Antarctic plateau conditions. The values are unrealistic when compared with the real atmosphere, so the PBL heights are calculated using a different formulation. This modification and subsequent model test runs are discussed in Chapter 5.

Chapter 6 contains discussions on the tuning of the model's radiation with respect to cloud influences, based on detailed cloud and radiation observations at Mawson, but less reliable cloud climatology over the interior. Cloud had not previously been included in the model, apart from emissivities at different levels due to water vapour. This process had not taken into account cloud albedo, absorption of long-wave radiation or variations in these factors due to cloud amount. These are represented in the model by making simple adjustments to the long-wave output and short-wave input terms in the surface energy balance equation.

Other related experiments, such as sensitivity to changes in surface albedo,

are also discussed. These are followed by verifications; results are discussed in relation to observations, including data from oversnow traverses and automatic stations. Presentations are made of the mean January and mean July boundary layer climatologies over the Lambert Glacier Basin region.

Winds at Mawson station and relationships between synoptic conditions and surface winds are investigated using the observational data (from several different sources), in Chapter 7. These discussions expand upon the work of Chapter 3.

As a result of the modifications described in earlier chapters, the numerical model is now capable of explaining many of the interrelationships between synoptic conditions and surface winds in the vicinity of Mawson. Results from this modelling are presented in Chapter 8.

Chapter 2

REVIEW OF PAST WORK ON ANTARCTIC BOUNDARY LAYER METEOROLOGY

2.1 INTRODUCTION

This review of boundary layer meteorology over Antarctica is divided into four sections (2.2 - 2.5). Section 2.2 describes boundary layer processes over inland Antarctica, those which occur over the plateau regions. The plateau region of West Antarctica is defined by Dalrymple (1966) to be that with terrain elevations greater than about 1500 metres and terrain slope less than $2x10^{-2}$. The East Antarctic plateau region, relevant to this study, is defined as terrain with elevation above 2000 metres and slope less than $2x10^{-2}$. Terrain slopes of the high plateau are very small, 10^{-4} or less, as noted by Parish (1984).

The review of meteorological conditions over the plateau is important because this study focusses on a region of East Antarctica, of which over fifty-five percent of terrain heights are above 2000 metres. The mean height of East Antarctica is 2450 metres, Linacre and Hobbs (1977). The relatively small slopes of these inland areas influence boundary layer air flow in a dramatically different way to the air over the steeper coastal terrain.

Section 2.3 discusses air flow on the steep slopes of Antarctica. Such slopes may be greater than $2x10^{-2}$, although the katabatic flow characteristic of these slopes, in contrast to the plateau wind regime, can occur over slopes that are only

greater than $2x10^{-3}$, Ball (1960). The Antarctic continent, and East Antarctica in particular, may be idealised as a circular dome, with greatest terrain slopes near the coastal boundaries. Such idealisations were made by Miller (1974) and Parish (1984) in their studies of boundary layer meteorology.

In reference to East Antarctica, slopes of large magnitude are usually found in coastal areas, where strong winds have been observed at numerous locations. However, as mentioned in the Introduction, the Lambert Glacier - Amery Ice Shelf region is a major indentation into East Antarctica, in terms of disturbing the "dome-like" continent, and it is a location where there are steep slopes, not just at the coast but hundreds of kilometres inland.

Section 2.4 discusses meteorological conditions in coastal regions associated with passing cyclonic systems.

Section 2.5 covers past work on katabatic winds and flow related to drainage winds and nocturnal boundary layers in areas other than Antarctica. This is useful for revealing general characteristics of katabatic winds.

Conclusions, regarding the purpose of this review, are discussed in Section 2.6.

A discussion of the numerical model used in this study is presented in Chapter 4. Other references, particularly in relation to modifications, are made throughout Chapters 5 and 6.

2.2 BOUNDARY LAYER METEOROLOGY OVER INLAND PLATEAU REGIONS OF ANTARCTICA

This section contains three subsections. The first discusses the existence of the surface temperature inversion over the Antarctic plateau. The second discusses the effect that the inversion has on the surface wind regime, and the third reviews observations that were analysed by Lettau (1966) in regard to a case of katabatic flow over the plateau region.

2.2.1 THE SURFACE TEMPERATURE INVERSION OVER THE ANTARCTIC PLATEAU

Over the Antarctic plateau, the firn (ice and snow) surface has high surface albedos, typically in the range 0.80 to 0.90, Weller (1980), Dalrymple (1966). This means that most short-wave solar radiation that reaches the surface is reflected. The high latitudes of the plateau region also mean that the sun is low in the sky even during the summer months (December and January). Because of this small solar elevation the atmosphere is a relatively thick barrier to incoming solar radiation, compared with lower latitudes, and therefore a larger proportion of solar radiation is likely to be absorbed or scattered before reaching the surface. In terms of long-wave radiation escaping to space though, the atmosphere is relatively thin due to the high terrain elevations and it can easily escape upwards to space.

The seasons in Antarctica are often not as clearly defined as they are for lower latitude regions, where there are four seasons, each of approximately three months. Schwerdtfeger (1970) described the seasons, depending on the annual temperature wave, as consisting of a short summer, short autumn and spring and a long winter.

During the winter months of June and July, solar radiation input over the plateau is absent. Even in coastal regions, such as at Mawson station, a considerable distance north of plateau regions, the sun only rises above the horizon by a few degrees during these months, and has a negligible effect on temperature and wind fields, Shaw (1957).

These radiation conditions lead to significant loss of long-wave radiation at the firn surface. This leads to the formation of a strong ground based inversion. The mean annual surface air temperature isotherms, Figure 2.1, as reproduced from Rusin (1961), are shown to be strongly dependent on terrain elevations and continentality. This figure is in good agreement with the 10-metre depth firn temperatures of Dalrymple (1966). Generally, these values are within about one

degree of the annual mean firn surface temperature at a given location, Budd, Jenssen and Radok (1971). Dalrymple (1966) states that the 10-metre depth firn temperatures are close approximations to the mean annual surface air temperatures; there is a significant correlation between surface firn and surface air temperatures, with the firn temperatures generally lower than the air temperatures.

The continentality of Antarctica is increased during winter when sea ice forms and surrounds the continent for hundreds of kilometres. The peak sea ice extent, and maximum thickness of ice, usually occur during September.

Wendler and Kodama (1993) discussed the "kernlose" (coreless) winter in the region of Adelie Coast, East Antarctica. For the six winter months, there was no systematic temperature change. This pattern was evident for stations from near-coastal regions to far inland at Dome C. With lack of solar radiation input during this season, temperature changes can be largely influenced by advection of air.

Gravity-driven downslope air flow is not encouraged over the plateau because terrain slopes are small, and it is somewhat inhibited due to the inversion, discussed in the following section. This lowers the probability of the occurrence of turbulence and mixing, thereby contributing to the maintenance of the inversion. Disturbances due to significant synoptic activity are rare over the plateau regions, as discussed below.

The large scale atmospheric general circulation involves the presence of an anticyclone over Antarctica. Due to the high Antarctic terrain the overlying atmosphere is relatively thin and thus the surface pressures of these systems are relatively low, but it does involve the sinking of air, as is characteristic of all anticyclones. Such conditions favour the formation of nocturnal inversions, and in the same way, the inversion over the Antarctic continent.

The plateau regions are quite resistant to penetration by synoptic depressions, particularly during the winter months, which also contributes to the formation

and maintenance of the inversion. Rusin (1961) notes that cyclones that reach the Antarctic coast are prevented from moving inland due to the high ice slopes, but that they may be deformed causing relatively warm and humid air in their upper sections to move inland, but in the form of air currents, not closed pressure systems.

In reference to the Lambert Glacier region, Streten (1962) notes that there is not much evidence of the movement of low pressure systems across the continent. A high pressure ridge is often present over this region, as also shown by analyses of 700 hPa height fields in Chapter 7.

Dalrymple (1966) also notes that penetration of the Antarctic plateau by cyclones is not common. Miller (1974) is in agreement, and states that the thermal processes at the firn surface determine the meteorological conditions of the high, inland plateau. This means, in general, that the firn surface cools, as does the air near the surface, and an inversion develops.

The penetration of cyclones to the interior of the continent occurs more frequently and with greater effect during summer, when the surface inversion is weaker, Wilson (1968).

Parish (1982) showed that passing cyclones influence the interior wind field picture to a smaller degree than they do in the coastal regions.

Cyclonic systems are important in regard to coastal weather, as will be discussed in Section 2.4, and analysed in later chapters.

The mean strength of the surface temperature inversion over Antarctica during the June, July, August period was computed by Phillpot and Zillman (1970), using data from twenty-two Antarctic bases. Their results are reproduced in Figure 2.2. There is a close similarity between the inversion pattern and the surface air temperature pattern shown in Figure 2.1, suggesting that the inversion strength is related to the surface air temperature, and therefore the firn temperature and also the terrain elevation and continentality.

Phillpot and Zillman (1970) noted the relationship between variations in sur-

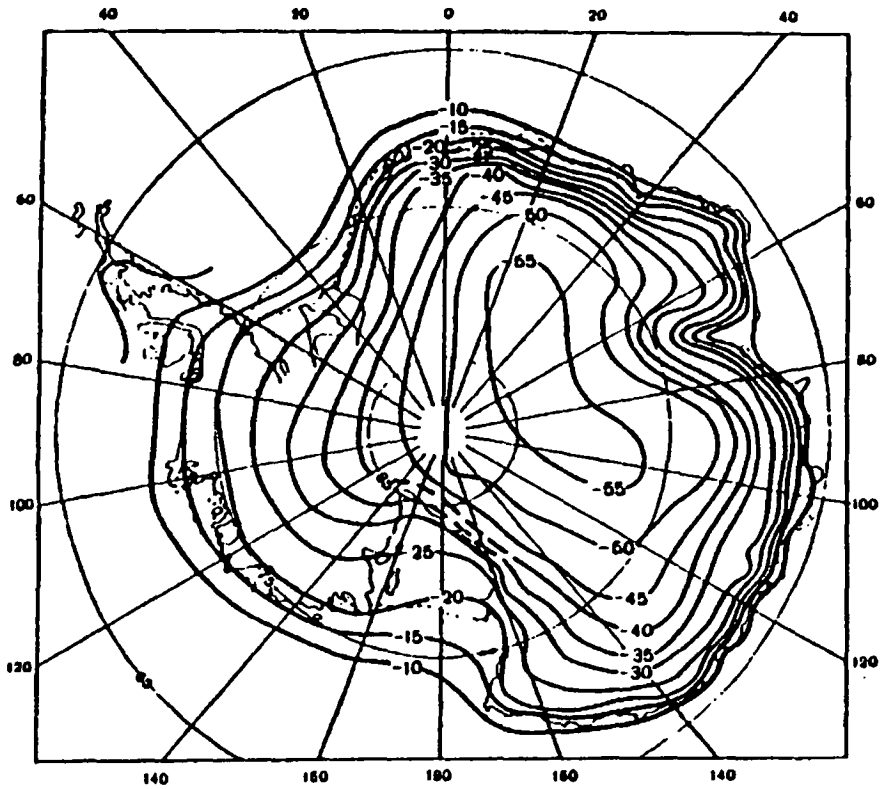

Figure 2.1: Annual mean isotherms in Antarctica, as reproduced from Rusin (1961).

face air temperature and inversion strength for the June, July, August period, and stated that the air temperature above the inversion remains fairly constant for the winter season, with surface temperatures fluctuations controlling fluctuations in the inversion strength.

This picture of the vertical structure of the temperature inversion over the plateau is supported by Schwerdtfeger (1984), who noted that during the sunlit periods of the year there is a diurnal variation of the near-surface air temperature, but the corresponding variation at elevations of several hundred metres is much smaller. This indicates that the inversion strength variation is closely related to the surface air temperature variation.

The inversion strength can grow beyond the mean values shown by Figure 2.2. Schwerdtfeger (1984) noted a value of 36°C within the lowest 400 metres of the atmosphere at Vostok in 1969. The inversion can also be destroyed, although this is rare during winter. Such a destruction occurred at Plateau station within the lowest 32 metres of the atmosphere, 18-19 August 1967. This was explained as

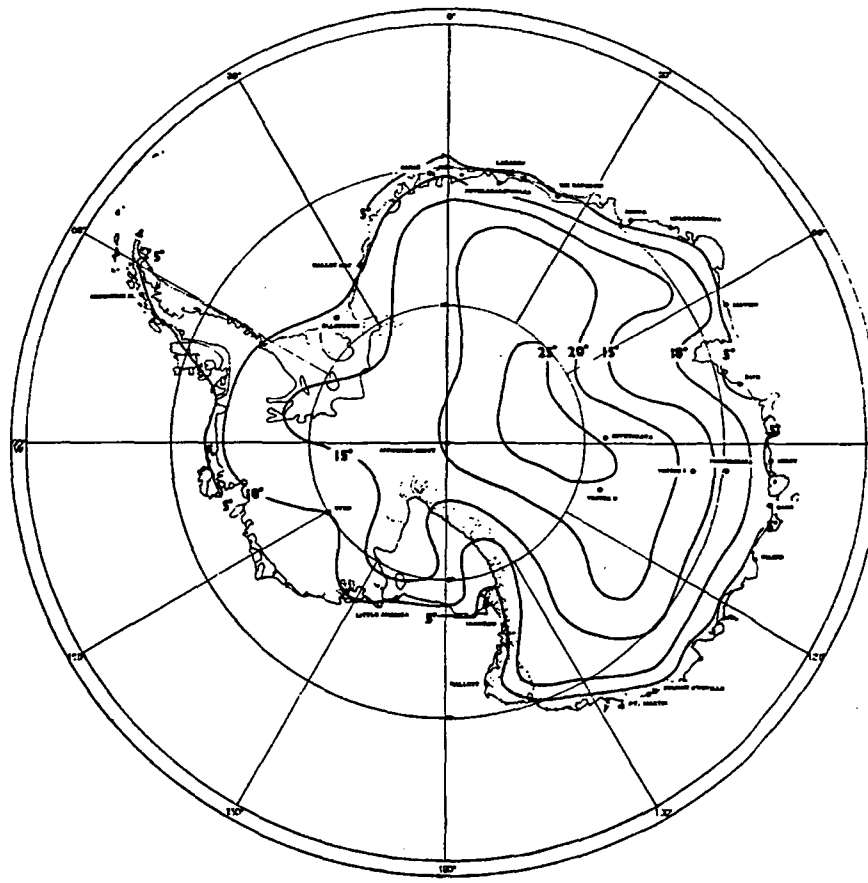

Figure 2.2: Isopleths of the average strength (C) of the surface temperature inversion over the Antarctic continent in winter (June, July, August), as reproduced from Phillpot and Zillman (1970).

being due to three physical processes; advection of warm air above the inversion, vertical mixing, and long-wave radiation prevented from escaping to space and then being supplied to the air below due to the presence of cloud. Phillpot and Zillman (1970) noted the winter inversion was destroyed by passing intense synoptic systems, but this occurred only rarely. When inversions were destroyed they reformed fairly quickly; examples given by Dalrymple (1966) for South Pole suggest that inversions destroyed by cyclonic activity can reform within 24 hours of the system passing, and within about 12 hours for cases when overcast conditions dissipate after having weakened the inversion. Parameters, such as varying cloud cover and warm air advection, do of course alter the rate of regeneration of the inversion; the time periods shown here are only approximate values used to illustrate the rate of growth of the inversion.

Inversions develop under conditions that allow long-wave radiation loss from

the surface, such as with little or no cloud to prevent this loss. Low wind speeds are also necessary so that significant amounts of turbulence are not present. Turbulence contributes to vertical mixing of air, and thus inhibits inversion formation and maintenance, because the near-surface air temperature gradient is decreased or removed.

Liljequist (1958) explains that there is a turbulent heat flux directed toward the surface from higher levels and a corresponding conduction of heat through the firn that compensates for the radiational heat loss from the surface, thereby preventing the inversion from continuing to grow in strength and in depth. This flux is present because the inversion is by definition a layer of relatively cold air below a layer of relatively warm air, and therefore there is a flux of heat from the warmer to the cooler air, which is directed downwards.

Rusin (1961) provides an analogous explanation but also takes into account the presence of humidity inversions, said to be present for 9 to 10 months of the year, as the temperature inversions are. The turbulent flux of water vapour to the surface is an important supply of snow accumulation over the plateau regions of Antarctica; water vapour sublimes in the cold surface air layer, forming ice and snow. Mists and clouds can also form, which are sources of precipitation.

Relatively warm and moist air is advected from the north at high levels, as part of the large scale general circulation and input to the top of the anticyclone. Schwerdtfeger (1984) notes that radiometer soundings at the South Pole have shown that this air loses heat via long-wave radiation to the relatively cold air both above and below it.

The structure of the temperature inversion is not linear with height. Dalrymple (1966) and Wilson (1968) both note that the lowest region of the inversion, below a height of about 10 to 20 metres, has the greatest intensity (temperature increase with height). At South Pole for example, the monthly mean inversion strength in the lowest 8 metres of the atmosphere is between 10 and 15°C.

Miller (1974) states that the observed temperature profile of the plateau in-

versions is approximately exponential, as given by Equation 2.1.

$$T = T_t - \Delta T e^{(-Z/H)} \tag{2.1}$$

where Z : height above the surface,

T_t : temperature of the free atmosphere above the inversion layer,

$\Delta T = T_t - T_{SURFACE}$: inversion strength,

H : scale height of the inversion layer.

The intense inversion strength in the lowest few metres of the atmosphere probably means that near-surface wind jets can exist because the strong stable stratification provides relatively good isolation from surface friction.

The mean depth of inversion during winter over the high plateau region was found by Phillpot and Zillman (1970) to be between 500 and 700 metres. Dalrymple (1966) and Wilson (1968) provide data that support these depths, but the depth varies between station locations. For example, the monthly mean depth of the inversion at Vostok during July 1960 was 931 metres, but for the same period at South Pole it was 629 metres. The depth also varies between summer and winter by approximately 200 to 300 metres, with depths greater during winter when the inversions are stronger.

2.2.2 PLATEAU INVERSION WIND REGIME

The wind directions over the interior plateau regions of Antarctica have been observed to lie in a direction about 30° to 60° to the "left" of the fall line; ("left" is defined here such that someone with their back to the wind would have higher terrain to their left).

Over the steeper coastal terrain the winds blow closer to the direction of maximum slope, with deviation (also to the left) due to the Coriolis force at relatively smaller angles, less than about 30°. The winds over the steeper slopes will be discussed in later sections of this chapter. The winds that blow over the plateau regions, and what drives them, are discussed in this section.

	Obs	H	Slope	Winter				Annual			
				WS	WD	q	α	WS	WD	q	α
Station	years	m	$x10^{-3}$	m/s	°		°	m/s	°		°
Plateau	3	3625	0.8	4.2	001	0.75	49	3.4	335	0.67	55
Vostok	15	3488	1.3	4.4	251	0.82	34	4.1	243	0.81	42
Mizuho	4	2230	3	11.5	099	0.97	21	9.9	098	0.96	21
South Pole	16	2835	4	5.3	038	0.80	62	4.6	039	0.79	61

Table 2.1: Winter and annual data from four East Antarctic plateau stations. Wind speeds (WS), wind directions (WD), directional constancy (q) and deviation from the fall line (α), from Schwerdtfeger (1984).

Because the winds over the plateau are directed at significant angles away from the fall line, drainage of air from the plateau is not efficient. This means however that the supply of air upwind is not easily exhausted, and it is observed that the plateau winds blow uninterrupted for long periods of time, possibly for periods of weeks.

As summarised by Schwerdtfeger (1984), the winds over the plateau are also characterised by great directional constancy; data from four East Antarctic stations each with more than one year of observations are shown in Table 2.1. The directional constancy decreases with height above the surface, towards the top of the inversion. In the region of the inversion that is most intense, near the surface, there are "remarkable" changes of wind direction with height when the inversion is strong.

A consequence of the intense inversion, particularly in the lower region of the inversion, is the strong stable vertical stratification, that allows surface friction effects to be somewhat isolated because the vertical exchange of air parcels is strongly supressed. The result is greater wind speeds nearer the surface. This represents an effective decrease in surface friction in addition to that due to the relatively flat and frictionless Antarctic plateau firn surface.

Schwerdtfeger (1984) noted that within the strong inversion there is a well defined shear layer that reaches from the surface to heights between 40 and 300 metres and is turbulent, due to strong vertical shear. The depth of this layer is generally below 100 metres, but alters depending on winds and temperatures. In regard to katabatic flow, friction and turbulence cannot be ignored either below or above the wind maximum, as noted by Manins and Sawford (1979a).

When strong surface inversions are present over plateau regions, the surface wind speed is strong, and winds aloft, at about 700 hPa are relatively weaker. This is the opposite to the "normal" wind speed profile, (such as that observed in Australia for example), where winds are stronger aloft and generally decrease in strength towards the ground due to surface friction. When the inversion is weak or absent the wind speed profile returns to the "normal" situation.

An explanation of the modification of the upper geostrophic wind through the inversion to the surface, due to thermal wind effects, is discussed below.

The surface-based temperature inversion over the interior of Antarctica is considerably stronger than that in the coastal regions. This is well illustrated by Phillpot and Zillman (1970) for the winter months of June, July and August, (Figure 2.2).

Various researchers have analysed and discussed the relationship between surface air flow and the strong inversion - see Dalrymple, Lettau and Wollaston (1966), Lettau and Schwerdtfeger (1967), Schwerdtfeger and Mahrt (1968), Miller (1974), Schwerdtfeger (1974), Schwerdtfeger (1984), and Parish (1982).

As noted previously, compared with the coastal regions, the interior plateau regions have relatively small slopes. The surface-based temperature inversion has approximately constant depth over large distances, implying that there is a strong horizontal temperature gradient. This is demonstrated schematically in Figure 2.3, reproduced from Lettau and Schwerdtfeger (1967). A stronger inversion means that the horizontal temperature gradient is also stronger because the depth of the inversion is fairly constant over large distances.

The presence of this horizontal temperature gradient means that the geostrophic wind must change with height; there will be a non-zero thermal wind. The magnitude of the inversion-thermal wind vector is proportional to the implied horizontal temperature gradient, that is proportional to the strength of the inversion. For the southern hemisphere, the direction of the thermal wind vector may be described as follows; with one's back to this "wind", there is cooler air to the right, warmer air to the left.

For this Antarctic case, the direction of the thermal wind depends on the orientation of the slope of the inversion, which in turn depends on the orientation of the terrain slope, assuming that the inversion is of approximately constant depth over large distances. Considering Antarctic terrain as an idealised "dome-shape", the thermal wind that exists due to a sloped inversion would be a "westerly", (the thermal wind is not a real wind but a change in wind with height). For several locations in Antarctica, Schwerdtfeger and Mahrt (1968) calculated the thermal winds for the inversion layer and Antarctic terrain contours, as reproduced in Figure 2.4. The thermal wind vectors tend to be closely aligned with the terrain contours.

The thermal wind vector is added to the surface wind vector to give the upper wind vector, or it is subtracted from with the upper wind vector to give the surface wind vector; these vector operations involve the geostrophic components of the wind only, not other effects such as surface friction.

Figure 2.3 shows a comparison of this vector summation for strong inversion and for lapse conditions. The resultant surface wind vector is directed about 45° to right of the resultant geostrophic wind vector at the surface. This is due to surface friction; in the Southern Hemisphere the Ekman spiral has an effect such that winds turn to the right of the geostrophic values as friction has a greater effect closer to the surface.

The greater the ratio of thermal wind to the upper geostrophic wind, the smaller is the variation of surface wind direction. This means that for a given

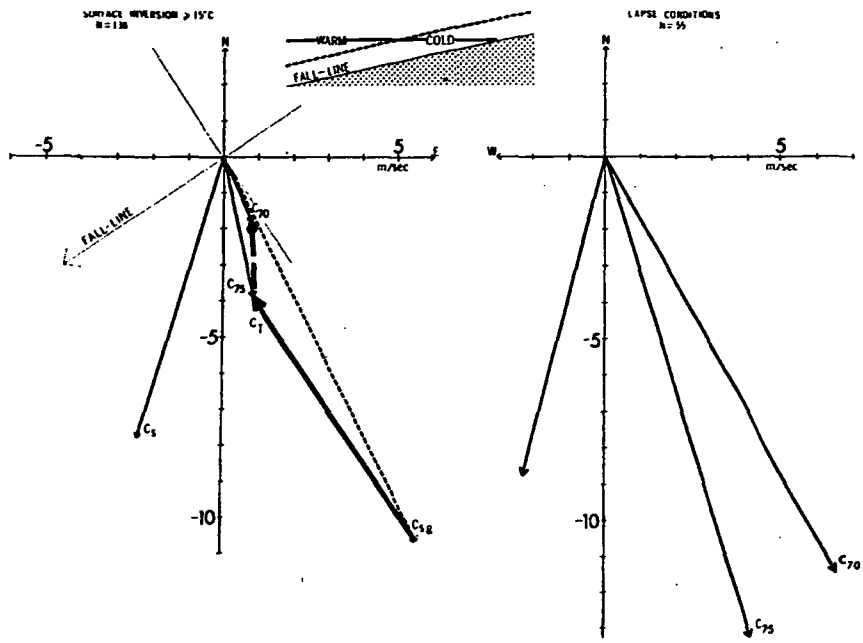

Figure 2.3: Schematic diagram demonstrating the horizontal temperature gradient caused by sloping terrain and an inversion of approximately constant depth. The surface, upper and thermal wind vectors for an inversion of 15°C at Byrd are shown on the left, and on the right is the corresponding surface and upper wind vectors for lapse conditions, as reproduced from Lettau and Schwerdtfeger (1967).

upper geostrophic wind, a stronger inversion will result in a larger thermal wind value, this ratio will be greater and the surface wind will be determined to a larger degree by the inversion, not by the upper-level gradient.

Dalrymple, Lettau and Wollaston (1966) related the "local" thermal wind to the terrain slope, as shown by Equation 2.2.

$$\vec{V_t} = \frac{g}{f}\frac{\Delta T}{\bar{T}}\vec{G} \times \vec{k} \tag{2.2}$$

Where $\vec{V_t}$ is the thermal wind vector,

g is the acceleration due to gravity, f is the Coriolis parameter,

ΔT is the temperature difference between the surface and upper air, the inversion strength,

$\bar{T}$ is the mean temperature of the inversion layer,

$\vec{G}$ is the vector representing the terrain slope; magnitude and direction, and $\vec{k}$ is the vertical unit vector.

Lettau and Schwerdtfeger (1967) analysed observations at South Pole and

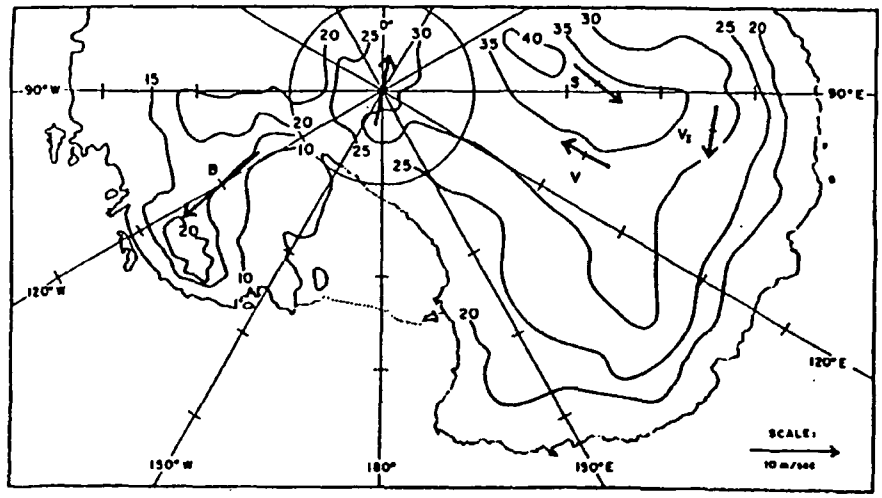

Figure 2.4: Thermal winds for the inversion layer and Antarctic surface contours, as reproduced from Schwerdtfeger and Mahrt (1968).

Byrd stations for five winter periods, April to September 1961 to 1965. Local thermal wind values between the surface and the 750 hPa level and the surface and 700 hPa level were determined. At Byrd station the 750 hPa level averaged a height of over 500 metres and the 700 hPa level averaged about 1000 metres height. These two heights were used to represent levels of "free flow" above the inversion. Data from Byrd station shown in Wilson (1968) support the use of the 750 hPa and 700 hPa levels because the mean inversion depth for April to September from years 1958 to 1961 is 578 metres, below the 750 hPa level, which means that the these two levels should be fairly representative of the "free flow".

It was shown that the direction of the geostrophic wind at the surface differed from that of the observed surface wind, measured at a height of 10 metres, by an average of 45 degrees, and the ratio of upper to surface wind speeds was 0.68. These results showed that when there is a strong inversion present ($\Delta T \geq 15°C$ over Byrd station), there are significant ageostrophic components of the wind, and the wind speeds are greater near the surface than aloft.

The winds discussed so far, over interior Antarctica, are not katabatic winds driven exclusively by gravity and are not directed downslope closer to the fall line as coastal katabatic winds generally are. Instead, they are called "thermal inversion winds" or "inversion winds" because the existence of a strong inversion

modifies the air flow near the surface.

Schwerdtfeger and Mahrt (1968) analysed observations collected from three inland Antarctic stations (Vostok, South Pole and Byrd) from winter half years. The aim of this paper was to confirm that the thermal wind effect, which is due to the sloped surface inversion layer, affects the surface wind to a significant degree, as discussed in the earlier paper by Lettau and Schwerdtfeger (1967).

Cases when the inversion was strong ($\Delta T \geq 20°C$) were considered. The synoptic-scale thermal wind present higher in the atmosphere was estimated from the isotherm patterns at various pressure levels, but it was found to be of the order of 1 m/s or less for the three stations, and therefore not significant when considering levels in the lower atmosphere, particularly when the "local" thermal wind is much larger. Observations of inversion strength, surface winds and the geostrophic wind above the inversion showed that the magnitude of the "inversion" thermal wind increased with increased inversion strength. To a lesser degree, it depends on the mean temperature of the layer and the Coriolis parameter.

The difference between the actual surface wind and the geostrophic wind at the surface is due to friction, which depends on the surface roughness and on the strength of the inversion. Differences in the frictional deviation angles exist between the three stations, but because the surface characteristics are similar, the reason for the differences may be due to different structures of the inversions in the lowest 50 metres of the atmosphere. Schwerdtfeger and Mahrt (1968) did not investigate this further.

Their observations showed that there is high directional constancy of the surface winds, due to the "inversion wind" effect.

The results of Schwerdtfeger and Mahrt (1968) supported the "inversion wind" theory as discussed above. It was shown that the wind regime was not katabatic, the winds were characterised by pronounced directional constancy, and the wind strengths were less than those observed for katabatic flow in Antarctica. An

important point made was that the winds could persist for weeks, given favourable radiation conditions, unlike the katabatic flow observed over the coastal slopes, which is relatively sporadic. The inefficiency of drainage by the inversion wind regime is important in regard to the persistence of these winds for long periods; the supply of air upwind is not easily exhausted, and air flow continues.

Katabatic flow was defined as winds that were observed on and at the base of steeper slopes, but characterised by relatively short duration. This occurs because katabatic winds cause more efficient drainage of air than do the inversion winds, and so the limited supply of cold air upstream is exhausted. This is one possible explanation for the occurrence of sudden lulls that have been observed between katabatic storms at various coastal stations, such as Cape Denison, Port Martin and Mirny. Although not discussed by Schwerdtfeger and Mahrt (1968), strong katabatic winds can persist for periods longer than a few hours. (See discussion below). Causes of these prolonged katabatic winds are discussed in Sections 2.3 and 2.4.

Schwerdtfeger and Mahrt also noted that there was ample observational evidence that was not compatible with the assumption of Ball (1960) of equilibrium flow for pure katabatic winds. However, Ball's theories and results have been supported by the results of Weller (1969) and Parish (1984) for coastal regions of Antarctica. Although an equilibrium flow that is continuous for long periods may not be established for pure katabatic winds, such winds may exist, but for periods that are relatively short compared with the length of time that "inversion winds" exist. Pettré and André (1991) noted that katabatic flow periods of one to three days occurred during field observations in Adelie Land, Antarctica. For these periods, ideas presented by Ball can be applied to katabatic flow. This is discussed in more detail in Section 2.3.

Schwerdtfeger and Mahrt (1968) also noted that the prevailing surface wind direction and strength are so closely related to the direction and steepness of the slope of the terrain, that they can be well estimated if the topography is known,

and vice versa, as shown previously, Equation 2.2 from Dalrymple, Lettau and Wollaston (1966).

During the sunlit periods there are diurnal variations in the temperature and wind fields. Over steeper slopes, and typical of coastal regions, the strength of the wind near the surface is greatest during the "night" between 00 and 06 local time, when the air has cooled and is most dense. During the "midday-afternoon" period, the temperature is a maximum and the wind speed a minimum. These patterns are discussed further in Section 2.3.

Over plateau regions the same diurnal pattern is not observed in the wind field. The temperatures reach their maximum and minimum during the same periods, but the wind speeds tend to be strongest during the "midday-afternoon" period, not during the "night". Explanations are given by Loewe (1974) and by Wendler et al. (1993). The strong inversions over the Antarctic interior vary diurnally, being strongest during the night, and this causes the transfer of momentum from upper levels to the surface to be hindered, but during the midday-afternoon the inversion is weaker, and the transfer of momentum can occur more efficiently, and a wind speed maximum is reached.

Also, the smaller slopes of the interior do not encourage downslope flow to the extent observed nearer to the coast, meaning that the air will not increase in speed to such an extent when it is most dense.

The transition from the interior plateau wind regime to that over the steeper coastal slopes is not well documented, but Schwerdtfeger (1984) provides a possible example. Mizuho station is located on the Antarctic plateau at an elevation of 2230 metres with a terrain slope of 3×10^{-3}, less than the limit set by Dalrymple (1966). It may be expected therefore that the wind regime of Mizuho would be that of the plateau, as described above, but the wind speed is actually greatest between 00 and 06 local time, a pattern characteristic of the steeper slopes in coastal regions.

2.2.3 KATABATIC FLOW OVER THE PLATEAU

Lettau (1966) discussed the rarity of katabatic flow over the Antarctic plateau, where air flow is usually characterised by "inversion winds". Micrometeorological measurements were taken at Amundsen-Scott station from February to November of 1958. The station is located on a region of the plateau that is very flat and approximates an inclined plane.

Observations had showed that about 50% of the time, the wind directions were NNE to NE, and SSE winds were observed only 0.1% of the time, and wind directions from SE to S only occurred 1.3% of the time. The slope of the topography was measured to be in a SSE direction so observations showed that truly downslope motion, which is a prerequisite for katabatic flow, is very rare in the vicinity of 90°S. (At the South Pole northerly winds are defined as those directed from 0°longitude).

As discussed in the previous section, local thermal wind effects, and not just frictional effects, are responsible for the cross slope motion of the wind in the surface layer. This leads to a tendency for the air motion in the surface layer to be an ENE wind, regardless of the wind speed and direction in the free atmosphere.

The date chosen for the case study exemplifying katabatic flow was September 17, 1958, because on this day the synoptic pressure gradient was very weak, and this was expected to allow the development of a true katabatic wind. Also, a SSE wind was observed at this time, which, as noted above, is uncommon and is the expected direction of katabatic flow. Evidence that there was katabatic flow during the period analysed is outlined below.

Defant (1951) believed there to be a critical value of slope inclination, beyond which katabatic flow motion becomes unstable. This value is 1/100, but the slope around 90°S is of the order of 1/1000, so katabatic flow there, if it exists, should be stable. However, the Reynolds number was large, indicating that the motion was not genuinely laminar.

Whereas Prandtl (1942) investigated katabatic flow by investigating wind and temperature profiles in detail, Ball (1960) looked at the problem using bulk coefficients of surface friction and bulk dimensions of the inversion layer. By looking at strong to severe types of katabatic winds, observed frequently in coastal Antarctica, and at the effects of synoptic pressure distribution, Coriolis and topographic influences, Ball produced relations among wind speed of the bulk layer, inversion height and inclination of the slope, discussed further in Section 2.3.

When these relations are applied to the region around Amundsen-Scott station, an expected bulk wind speed for katabatic flow is about 2 m/s. The data from September 17, 1958 show that this prediction is of the correct order of magnitude, and it was also observed that there was a tendency for a wind maximum at the 4-metre level, showing that the flow may well have been katabatic. Normally the work of Ball is not applied to air flow of interior Antarctica because "inversion winds" prevail, and katabatic type flow is rare.

When average profiles of temperature and wind speed were compared with what is expected from Prandtl's theory of katabatic flow, there was sufficient agreement to show that the flow was katabatic, if only for a few hours. After this time there was a radical change, and the wind profile then resembled one expected in a more usual type of surface layer structure over the plateau. When this change occurred, there was a general lowering of temperature. Measurements revealed that at the 8 metre level there was a 5°C drop in the air temperature. Also, the vertical gradients of temperature decreased, indicating that when katabatic flow breaks down there is less stability and vertical mixing occurs. This was thought to be due to local convergence of the low-level air flow, which produced a piling up of cold surface air. Sudden warming which is observed at other times is thought to be caused by the local divergence of low level air, leading to vertical advection of heat, from the relatively warmer air higher up.

The magnitude of the heat flux from the subsurface snow layer to the snow surface over this period was -1.9 ly/hour (-22.1 Wm^{-2}), but the average values,

over the months when the sun was below the horizon, were stated to be always below -0.4 ly/hour (-4.6 Wm^{-2}). Therefore this period was characterised by an extreme value, and katabatic flow would not be expected to be maintained for a long period, and probably lasted no more than a few hours.

Before the change in flow type, the profiles of wind speed and temperature appeared to correspond to those expected with true katabatic flow. After the change there was an increase in wind speed and a decrease in temperature. The cause of the temperature change cannot have been due to vertical mixing, because this would have caused some warming in the lowest layers, and this was not observed. Vertical advection due to convergence of horizontal flow can account for the observed cooling. Because the vertical temperature gradient within the inversion over the Antarctic plateau is so large, a small vertical displacement of air can produce a significant temperature change.

2.3 AIR FLOW OVER NON-PLATEAU ICE SLOPES

This section discusses the meteorological conditions over the steeper terrain slopes of Antarctica. These are the areas not defined to be "plateau". Most inhabited East Antarctic stations are located in coastal regions at or near the base of these relatively steep slopes.

This section is divided into three subsections. The first discusses the air supply from the interior to the coastal regions and the atmospheric conditions experienced a relatively short horizontal distance (below terrain elevations of about 2000 metres) from the coast. The second subsection reviews the characteristics of winds, particularly katabatic, over the steep slopes of coastal regions. The third discusses pressure jumps, or Loewe's phenomenon, as discussed by Ball (1956), Ball (1957), Lied (1964) and Pettré and André (1991).

The discussion in this section generally excludes meteorological phenomena directly associated with cyclonic systems; this is discussed in Section 2.4.

2.3.1 ATMOSPHERIC CONDITIONS INLAND FROM COAST

Parish (1982) explained that winds in coastal areas are dependent on the convergence of drainage currents over the interior. If the Antarctic continent is again idealised as a dome-shape, there is divergence of the drainage pattern downwind of "plateau" areas because the "local circumference" of the continent increases towards the coast. This means that without terrain features influencing convergence of drainage flows, there would be a general divergence in the wind field as it approaches the coast.

Apart from synoptic influences, local thermal winds associated with inversions and terrain influences (causing patterns of convergence or divergence), the drainage air flow over an idealised dome-shaped continent would be largely controlled by Coriolis, with winds turning to the left and possessing an easterly component as they approach the coast.

As shown in Figure 2.5, there are several regions of convergence over the

eastern sector of East Antarctica, as demonstrated in model studies by Parish (1982). As the modelling depended on the thermal inversion winds, discussed in Section 2.2, it was limited to the plateau regions, above 2000 metres terrain elevation. Because there must be a general divergence of air flow towards the coast and there are regions of significant convergence, there must also be regions of significant divergence; strong and persistent drainage flow must be the exception, not the norm.

Parish and Bromwich (1987) described the broadscale airflow over the Antarctic continent during winter using both diagnostic and primitive equation models. Horizontal grid spacings of 50 kilometres were used. The modelling conducted in later chapters is for both summer and winter conditions and horizontal grid spacings of higher resolution are used, at 20 kilometres. However, only a limited area is investigated, the Lambert Glacier basin.

Mather (1969) provided a time-averaged pattern of surface air flow inferred from station data and sastrugi orientations, (Figure 2.6). The pattern is relatively featureless (zones of convergence are not apparent) in comparison with that shown in Figure 2.5. This is a good demonstration of the advantages of using numerical modelling over Antarctica where observations are spatially sparse.

It has often been shown by the presence of snow drift that there were strong winds east or west of Mawson, while the station had only light winds, Shaw (1957). Dzerdzeevskii (1960) commented that strong downslope winds only occur along short stretches of the coast. They are not a regular feature of coastal Antarctica. Streten (1962) stated that the fairly constant drainage in the Mawson region was caused by the inland and coastal topography.

Bromwich and Kurtz (1984) noted that a large pool of cold air can form upstream of coastal areas when inland terrain causes convergence. This can lead to unusually strong and persistent winds at the coast. Terrain closer to the bottom of a steep ice slope may further enhance the wind. Enhancement due to cyclonic activity can also occur, and is discussed further in Section 2.4.

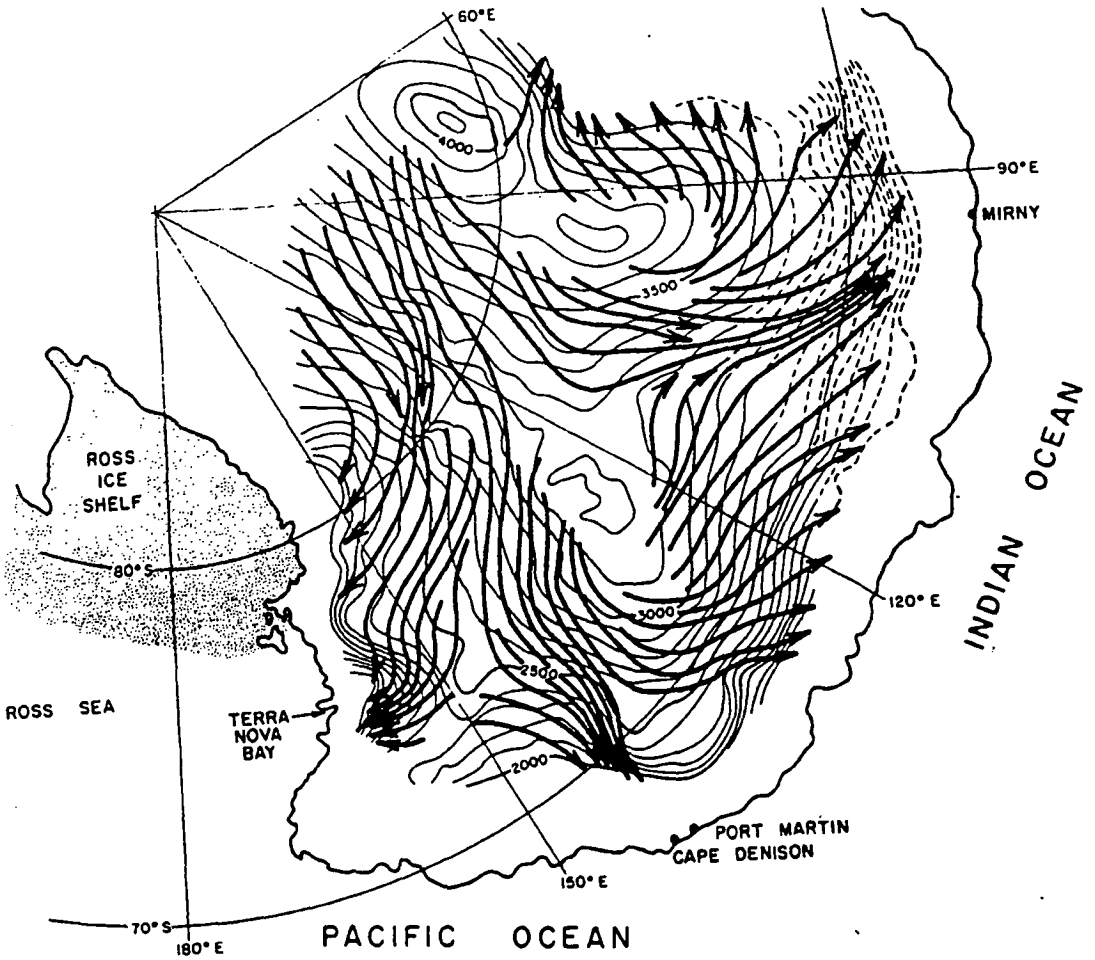

Figure 2.5: Time-average winter flow pattern over the surface of the Antarctic interior, as reproduced from Parish (1982).

The importance of an upstream supply of cold air for supporting strong katabatic winds was also noted by Parish (1984).

Bromwich, Parish and Zorman (1990) used observations of sastrugi and numerical modelling to study the effect that terrain has on the drainage pattern upwind of Terra Nova Bay, Antarctica. It was found that a confluence zone existed and played an important part in the air supply upwind of Terra Nova Bay, where katabatics have been observed to be strong and persistent. The small differences between the modelled and observed fields were likely to be caused by the relatively coarse grid spacings (32 kilometres) used in modelling, that prevented highly accurate representation of the terrain.

Ball (1960) derived relationships between katabatic wind speed, V, height of

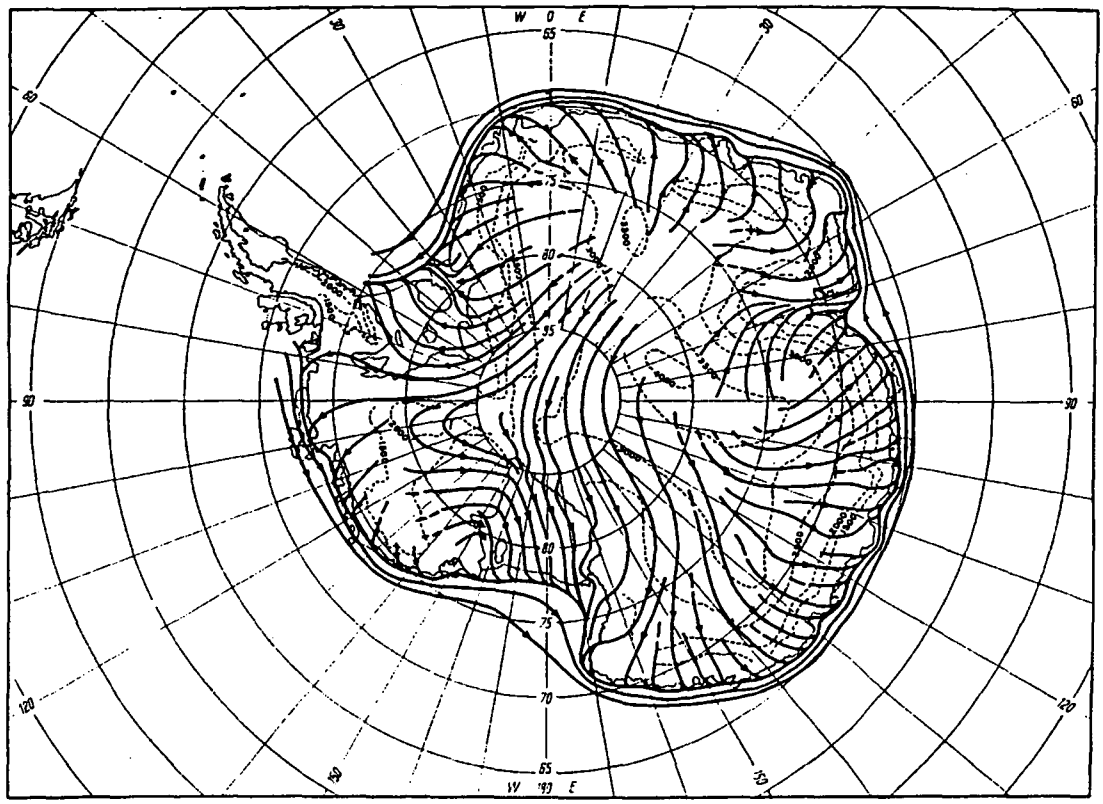

Figure 2.6: Time-averaged pattern of surface wind flow over Antarctica, inferred from predominant wind frequencies at the stations and from traverse records, as reproduced from Mather (1969).

the inversion, h, pressure gradient force, F, and the angle between direction of flow and the direction of the pressure gradient force, β, when a friction parameter, k, and the Coriolis parameter, f, are known. The cold air of the katabatic flow is assumed to be surmounted by an inversion at height h.

Relationships between these variables, shown in Equations 2.3, 2.4 and 2.5, are also illustrated in Figure 2.7, where any two of V, h, F and β can be estimated if the other two are given.

$$cos\beta = (1 + J^2)^{1/2} - J \tag{2.3}$$

$$V = (hF/k)^{1/2} = (F/f)sin\beta \tag{2.4}$$

where

$$J = hf^2/2kF \tag{2.5}$$

The pressure gradient force was calculated from the superimposed (synoptic) pressure gradient, and a parameter called the katabatic force, which depends on the terrain slope and a modified gravitational acceleration, g^*. The katabatic force, $g^*\alpha$, is stronger as the slope, α, or the inversion strength increase.

$V^2 = u^2+v^2$, where u and v are the x and y components of velocity respectively,

F is the pressure gradient force per unit mass below the inversion,

$g^* = \theta' g/\theta$, where g is the "standard" acceleration due to gravity (9.8 ms^{-2}), θ' is the inversion strength and θ is the temperature of cold air.

Ball (1960) also presented air drainage flow line patterns corresponding to idealised topographic features. Those in the neighbourhood of a bay and of a cape are shown reproduced in Figures 2.8 and 2.9 respectively. It was noted that significant variations in the speed and direction of the katabatic wind can occur with relatively minor changes to the shape of the terrain contour pattern. Patterns of convergence, and jets, may develop .

Ball also explained that usual methods of meteorological analysis must be used with caution in Antarctica, due to the strong surface inversions and katabatic winds that can develop, with those winds being influenced by the synoptic pressure distribution. When the surface slope is greater than $2x10^{-3}$ it is expected that the katabatic force will exceed the synoptic pressure gradient force.

Weller (1969) constructed and discussed a surface wind vector profile along the 62° East meridian over Antarctica. This covers an area south of Mawson through MacRobertson Land. Observations from 600 kilometres inland to 16 kilometres offshore were used. There were various recording sites near Mawson station. Almost a thousand observations of wind were made during 1961 and 1965. Wind measurements were made at between two and four metres above the surface.

Ninety-three percent of observations at Mawson showed a wind direction from between east and south. Histograms of wind direction frequencies are given for Mawson in Chapter 3.

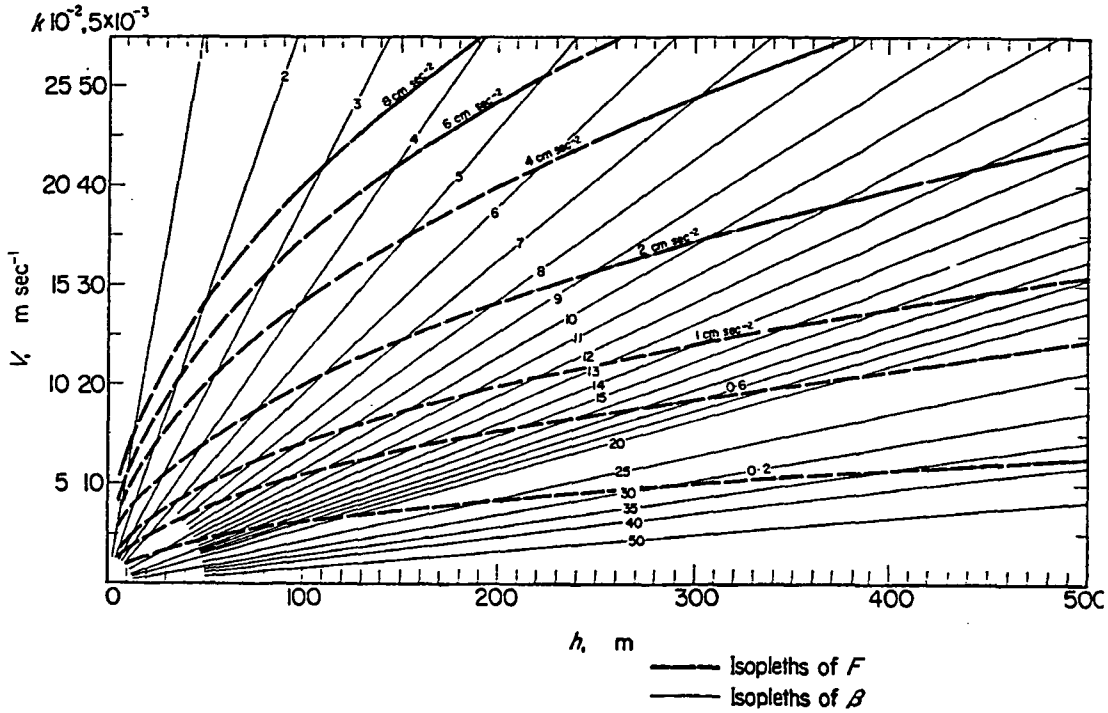

Figure 2.7: The relation between wind speed (V), height of the inversion (h), force per unit mass (F) and the angle between directions of movement and force (β), as reproduced from Ball (1960).

Winds in the coastal area were found to be of such strength that they occasionally strongly opposed the gradient flow. The katabatic wind was stronger over steeper slopes. However, observations made over extended periods showed that the wind speed was greatest inland from the coast at a distance of 20 to 30 kilometres. Weller (1969) explained this through the occurrence of hydraulic jumps (discussed in Section 2.3.3) that were generally situated up to 20 kilometres inland, that meant the strong wind was overriding the coastal area. Streten (1963) noted that only about 1% of winds at Mawson were overriding. However, in the coastal region of Mirny, Tauber (1960) discussed observations made during August of 1956, and found a different result. Wind speeds at the base of that ice slope were greater than wind speeds 10 or 25 kilometres inland. However, it is important to realise that the terrain of these two places is not identical; terrain is an important factor influencing katabatic winds near the coast, as already noted above from Ball's work. Also, Tauber's results were from only one month of measurements and observations, not a long enough period to establish a valid

climatology of winds.

Allison, Wendler and Radok (1993) used AWS data to produce a climatology of the conditions over the East Antarctic ice sheet between 100°E and 140°E. It was found that the surface wind speed was a maximum some distance inland, not at the coast. This is well illustrated in Figure 2.10, reproduced from their paper.

Weller (1969) used measurements of winds made in the hinterland of Mawson to examine the transition from the inversion wind to the katabatic. As the slope angle of the terrain increased, towards the coast, the angle between the fall line and the surface wind direction decreased, as the wind was aligned more with the direction of maximum slope. Weller concluded that Ball's model described the slope winds very successfully.

From the work of Lettau and Schwerdtfeger (1967) and Schwerdtfeger and Mahrt (1968), discussed in Section 2.2, an inversion wind regime exists over terrain of gentle slopes and where there is a strong surface inversion present. They used data from stations of interior Antarctica, including Byrd and South Pole stations. Weller (1969) concluded that inversion winds were found from 100 to 600 kilometres inland. A distance of 100 kilometres inland is relatively close to the coast, and a long way from the Antarctic plateau, as it is defined in the introduction to this chapter. Characteristics of the two different wind regimes, inversion and katabatic respectively, exist to different degrees in the transition from one to the other. Schwerdtfeger (1984) noted that there was a continuous transition from one to the other. As expected, from the coast to 100 kilometres inland, where the terrain is relatively steep, air flow was found to be purely katabatic.

Parish (1984) used a three-dimensional hydrostatic model to model the low-level air flow over the Adelie Land region. The results were in good agreement with those produced by the analytical method of Ball (1960).

vanMeurs and Allison (1986) analysed AWS data from 1982-83 at a location south of Mawson station at 1850 metres elevation. The terrain slope was 6×10^{-3}

and therefore katabatic flow was expected. The diurnal variations of winds were plotted for each season, as reproduced in Figure 2.11. There are marked diurnal rotations of wind vectors except during the winter season. At about 00 local time, the vectors are directed more downslope than they are at 12 local time. This is due to the katabatic force, as defined by Ball (1960), being stronger at night when the air is cooler and the inversion strength is larger, and therefore the synoptic pressure gradient force has a relatively smaller influence on the resultant wind.

Ball's model, described above, was tested using the collected AWS data. Predicted values of the winter and spring inversion height and strength agreed with the magnitudes shown by Phillpot and Zillman (1970) and also with observations. vanMeurs and Allison (1986) concluded that the assumption of the zero along-slope potential temperature gradient used in the model may not always be valid.

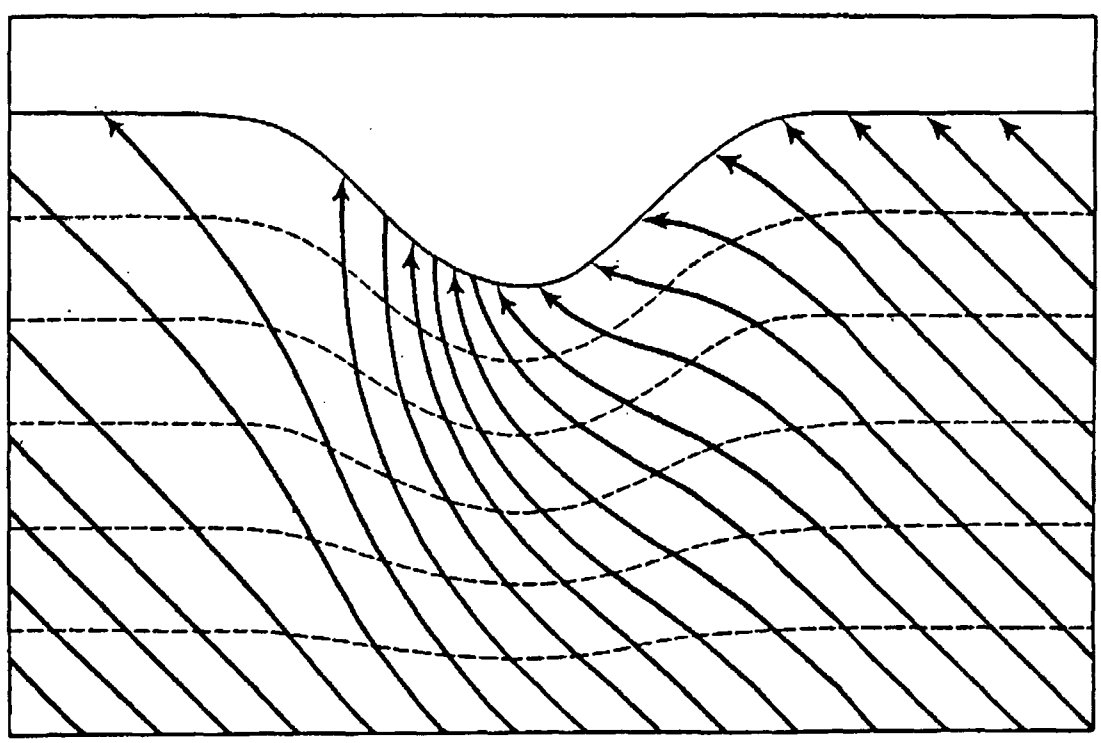

Figure 2.8: Flow in the neighbourhood of a bay, as reproduced from Ball (1960).

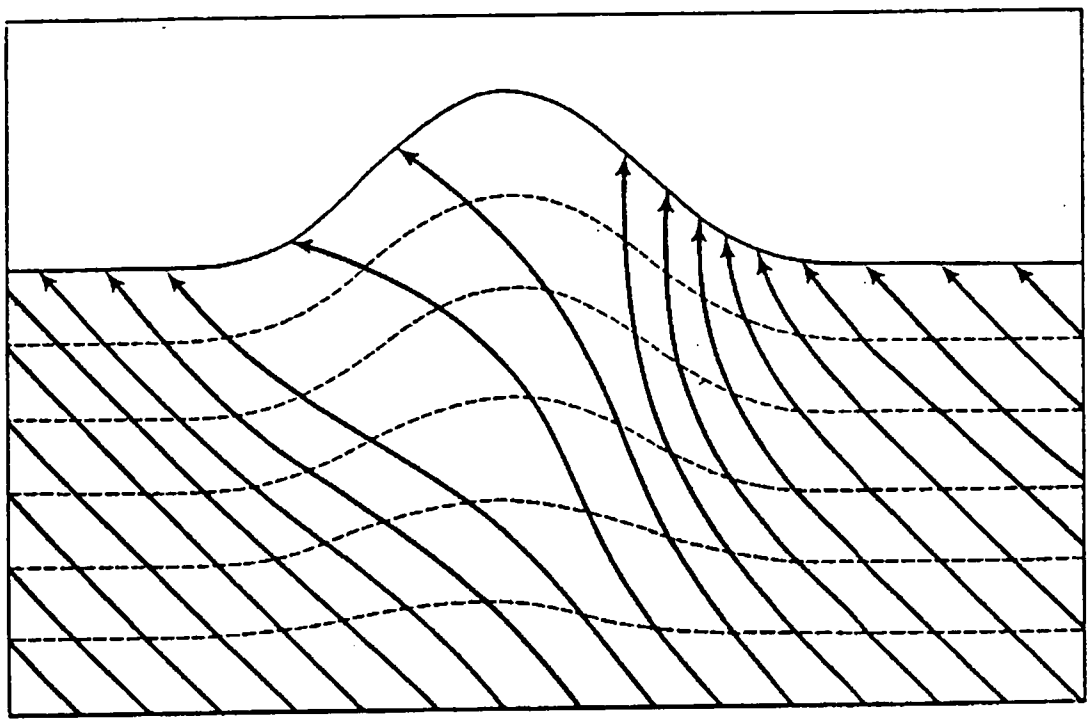

Figure 2.9: Flow in the neighbourhood of a cape, as reproduced from Ball (1960).

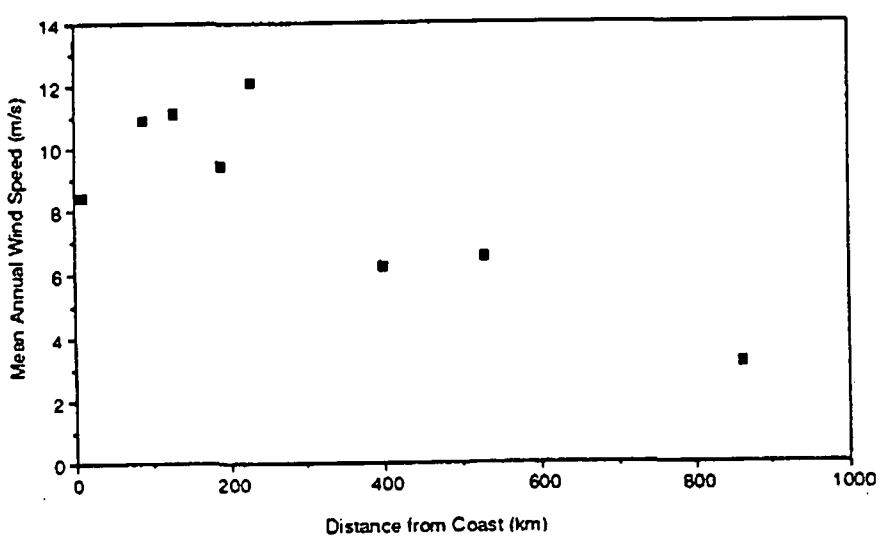

Figure 2.10: Mean annual wind speed as a function of distance from the coast, as reproduced from Allison, Wendler and Radok (1993).

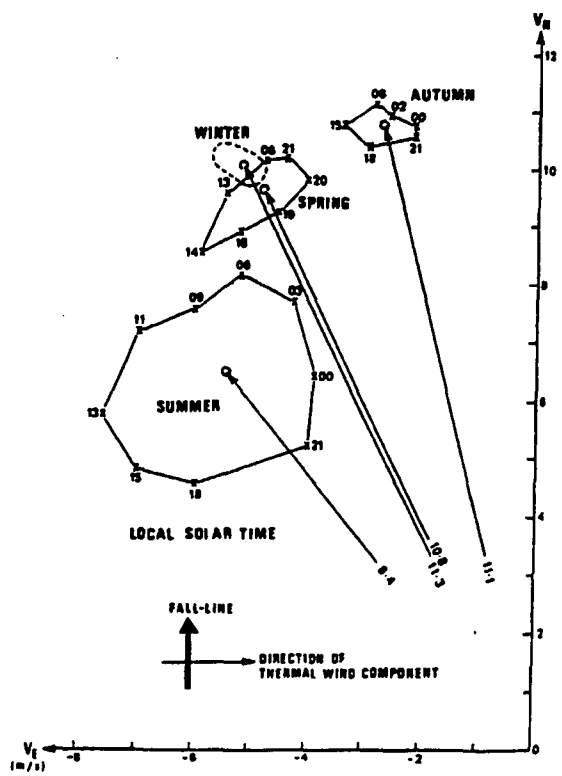

Figure 2.11: Hodographs of 3-hourly (local solar time) positions of the seasonal mean 4 metre wind vectors for 1982-1983, as reproduced from vanMeurs and Allison (1986).

2.3.2 CHARACTERISTICS OF COASTAL WINDS

The general differences between inland and coastal winds are that coastal winds are directed downslope more closely aligned with the fall line of the terrain. Also, coastal winds are stronger, but less persistent in time.

Katabatic winds flow downslope due to gravity and are generally expected to be stronger when the air being acted upon is cooler and denser. They are characterised by low level wind maxima. They constitute 40-50% of observations during summer, and 60-70% of observations during winter, at Mirny station, Rusin (1961).

Cloudless skies, steady wind speed and direction, snow drift, low temperatures and reduced atmospheric humidities characterise katabatic winds, Tauber (1960). However, blowing or drifting snow can increase the sublimation rate of the snow crystals and the moisture content of the air increases. Katabatic winds develop under weak synoptic pressure gradients, Dzerdzeevskii (1960).

Streten (1962) stated that katabatic winds are the outstanding weather feature over the slopes of Antarctica, and that there is almost continuous strong outflow in some areas, such as in the Mawson vicinity, where wind speeds average about 20 knots (about 10 m/s) throughout the year.

Mawson may be considered a "typical" Antarctic katabatic wind site. As observed by Streten (1963), the wind speed at 1000 ft (300 metres) above Mawson is similar in strength to that at the surface but the wind direction has backed (turned from southeasterly towards easterly) by 10 degrees (on average). This is in agreement with the results of Rusin (1961), who also noted that at higher levels the wind direction may then turn clockwise (from easterly towards southerly).

At 3000 ft (900 metres) the mean annual wind speed has dropped to about 65% of the strength of the surface wind, and the direction has backed by a further 20 degrees.

The level of the katabatic wind maximum is somewhat below 500 ft (150

metres) over Mawson, and over the plateau at 73°S the wind maximum was at a level of 250 ft (75 metres), Streten (1963).

Rusin (1961) found that at Mirny the height of the katabatic wind maximum was several tens of metres, but speeds between 150 and 200 metres were usually less than at ground level. This is in general agreement with the results of Tauber (1960): the level of minimum intensity of the wind was from 300 to 500 metres and the usual depth of the katabatic layer was 200 to 500 metres.

Rusin (1961) noted that katabatics are accompanied by temperature inversions in the boundary layer. Tauber (1960) stated that the upper limit of the inversion coincided with the upper limit of the katabatic cold air layer. This is not in agreement with Shaw (1960), who noted that although there were shallow katabatic layers and inversions present, their altitudes did not usually correspond.

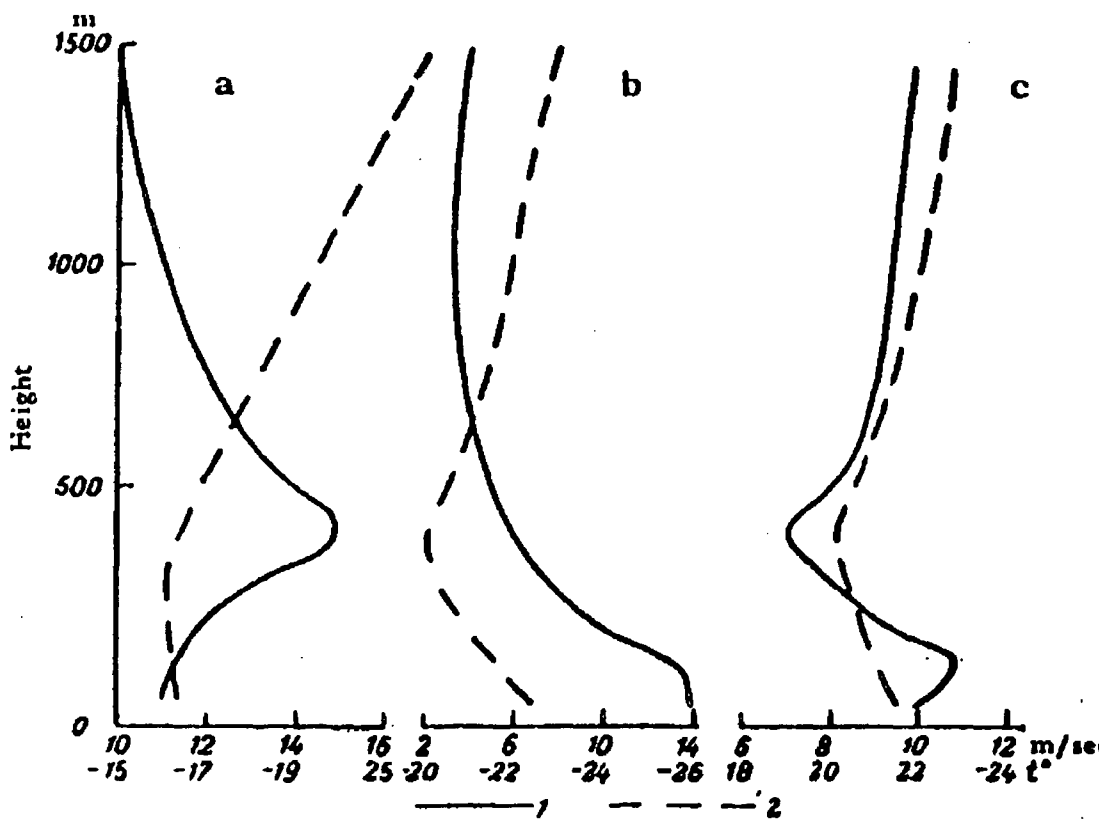

Figure 2.12: Mean aerological characteristics of katabatic, transitional and cyclonic winds at Mirny (1956), as reproduced from Rusin (1961). Wind velocities are shown by the solid lines(1) and air temperatures are shown by the dashed lines(2); a - transition from cyclone to katabatic, b - katabatic, c - transition from katabatic to cyclone.

During summer the wind speed at Mawson reaches a maximum during the

night or early hours of the morning, and a minimum at around midday, when not affected by offshore depressions. This is basically the same pattern found by vanMeurs and Allison (1986) for the AWS south of Mawson.

During winter there is no such regular diurnal pattern. Periods of calm exist between violent onsets and cessations of the katabatic, Streten (1962). Although the sun does appear above the horizon during winter at Mawson, there is no significant diurnal effect, Shaw (1957).

From 5000 ft (about 1500 metres) to 7000 ft (about 2100 metres) over Mawson station, there is frequently an inversion present that marks the boundary between the cold air draining over the continent and the warmer oceanic air above. During winter, inversions are present close to the surface and exist at the top of the katabatic layer, as defined in the model of Ball (1960).

The resultant surface wind may be expressed in terms of the gradient wind component and the katabatic component. Streten found that the katabatic component of the surface wind is influenced by the synoptic wind in a complicated manner.

At Mawson, the direction of the katabatic wind component is from 130° to 140°. When there is a katabatic wind onset at Mawson, the wind direction reverts to this direction, and the wind speed increases by about 7 m/s. There is marked gustiness involved with the onset, but cessation usually occurs gradually without sudden changes, with a mean decrease of about 8 m/s.

Turbulence is present inland and associated with wave phenomena but is most pronounced in the katabatic layer, downwind of the coastal plateau, Streten (1962). It was noted by Ball (1957) that: "...the wind is presumably retarded at its upper boundary as well as its lower boundary...". This was also noted by Manins and Sawford (1979a) for katabatic flow.

Shaw (1957) and Streten (1963) both observed periodic fluctuations in the wind speed at Mawson, with periods ranging from 5 to 20 minutes. The physical barrier of Mt. Henderson, south of Mawson, may have contributed to the

formation of waves. These are discussed further in Chapter 7.

The katabatic flow can be quite independent of the synoptic forcing, Shaw (1960). Low level katabatic winds can "...effectively mask all but the strongest..." synoptic features, Streten (1962).

Streten (1963) concluded that there does not appear to be a relationship between the strength of upper winds and the strength of the katabatic, with very strong katabatics being present when the upper winds were light and at other times strong. It was also noted that for many cases the katabatic seems to be completely uncoupled from the synoptic pattern.

Weller (1969) stated that "These [coastal katabatic] winds have been observed to exist independent of the synoptic pressure distribution..."

Parish (1984) noted that observations have shown that the katabatic wind is driven primarily by radiational cooling of the ice surface. In regard to the forcing of katabatic winds, it seems that the synoptic influence plays a secondary role. This is clarified in later chapters.

As previously noted, terrain plays a crucial role in the channelling of drainage winds. Wilson (1968) stated that: "Surface topography is of utmost importance with respect to the regional and local wind regimes." Also: "Downslope katabatic winds...are highly localised according to terrain."

Rusin (1961) stated that although katabatic winds may not be as strong as winds driven by off-shore depressions, their effects are more severe because of the cold air they transport from the interior.

In the area of Mawson station, blue ice is present because strong winds blow snow away. This was noted by Shaw (1957), Streten (1961), Streten (1962) and Weller (1980). The terrain within about 20 to 30 kilometres south of the coast consists of blue ice and rock. Beyond about 30 kilometres inland, there is an accumulation area where snow is always present on the surface.

Snow can be deposited in the vicinity of Mawson but the overall picture is the removal of snow due to strong winds. Snow can be transported to Mawson

when it is picked up from over the plateau by strong winds. Adiabatic warming can occur and some of the snow may be evaporated before reaching Mawson. When this occurs, the density of the drifting snow is lower (molecular weight of water vapour=18, molecular weight of dry air$\simeq$29), so it may be expected that the katabatic downslope force is reduced. However, as Ball (1957) explained, when fine suspended ice particles evaporate, there is a decrease in temperature, causing a lower temperature than for a similar stream of dry air. This cooling leads to an increase in density and therefore an increase in wind strength, as the katabatic flow is acted upon by gravity. The density is also increased directly by the presence of the snow particles. The suspended particles also increase surface friction but this effect is small compared with that caused by the increase in density.

Snow can also be deposited when it is precipitated from altostratus clouds. High drifting snow may be present in pressure jumps, that are discussed in Section 2.3.3. Snowfalls are also associated with cyclones that frequent coastal regions, Section 2.4.

Despite adiabatic warming that may occur, katabatic winds are cooler than cyclonic winds that transport air from the north and east from over the sea or sea ice region. This is so because katabatic winds transport air from very cold regions over the interior of Antarctica.

There are various methods by which air can warm as it flows downslope to coastal regions. Mixing may occur when the fast air flow becomes turbulent. Vertical advection of air from higher levels may occur, related to gustiness or wave motion. Adiabatic warming is another method, with air compressed as it flows downslope to lower levels but higher pressure.

As summarised by Schwerdtfeger (1984), drifting snow, below heights of about 2 metres, is maintained by wind speeds of about 5 to 10 m/s. The sizes of particles involved in drifting snow are smaller than those that occur in usual precipitation in Antarctica; this means that snow deposits can be packed very tightly. Blowing

snow occurs at heights greater than about 2 metres and may extend to heights of hundreds of metres, being driven by stronger winds.

Observations presented by Weller (1969) state that the katabatic wind dissipates by about 15 kilometres offshore. This is in fairly good agreement with Tauber (1960) who stated that the katabatic winds lose their intensity at about 10-12 kilometres offshore. These are relatively very short distances compared with the flow lines of Figure 2.6 that show air flow over distances of hundreds of kilometres before reaching the coast.

Shaw (1957) noted that in fine weather conditions the katabatic did not extend far out to sea.

The results of Bromwich (1991), that link strong katabatic outflow with mesoscale cyclogenesis in the Ross Sea, show that in some areas of Antarctica, katabatic winds do extend considerable distances offshore.

Winds to the north of these dissipation areas are controlled by the pressure gradient. Streten (1963) noted that there is: "...rapid dying away of the katabatic within a few miles of the coastal slope and with increasing predominance of the gradient wind direction giving a more easterly direction...".

Drainage winds can have a considerable effect on the sea ice near the coast. Shaw (1957) described the winds causing sea ice to be moved away from the coast northwards, leaving an open water area (polynya) along the coast. Parish (1992) noted that such regions of open water may increase the strength of the katabatic by as much as 2-3 m/s. This occurs because the polynya is a heat source and a land-breeze situation develops.

Davis is a coastal station that is not subject to katabatic winds, as it is located away from the ice slope and surrounded by bare rock and lakes of the Vestfold Hills. The predominant wind direction is northeast, and the average wind speed is about 10 knots (about 5m/s), half of that recorded at Mawson, Streten (1962). Strong winds may occur at Davis due to depressions that move into the area. Climatological conditions at Mawson and Davis stations are discussed in Chapter 3.

2.3.3 PRESSURE JUMPS ASSOCIATED WITH KATABATIC WINDS

Shaw (1957) observed that frequently a few miles inland from Mawson there were strong winds, while at Mawson and out to sea it was almost calm.

Reports by Ball (1956) and Ball (1957) are primarily of importance for the study of low level air flow around the steep slopes of coastal Eastern Antarctica, particularly in relation to "pressure jumps".

It has been observed, and was noted by Ball (1956), that there often exists a sharp boundary between the strong katabatic winds flowing down an ice slope and the synchronous comparatively calm air conditions over the sea and sea ice. Apart from the slight deviation due to the Coriolis parameter, the direction of flow of the strong katabatic winds over the slopes of the Antarctic ice cap, particularly where it is steepest near the coast, is controlled almost entirely by the topography.

Ball (1956) explained why lulls in the strong wind occur, whereas most of the time the winds are strong and persistent in both speed and direction. At the onset of a lull (observed at coastal stations, and those in the Commonwealth Bay area were used as observation points in this paper), there was a pressure rise of 2-3 hPa, accompanying the sudden drop in wind speed. At the end of a lull, as the wind speed increased suddenly, the pressure fell back. Also, during these lulls strong winds were observed higher up the slope, (with the station located at the base of the slope, by the sea).

An analogy between the hydraulics involved in the flow of water in channels and the flow of cold air down the ice cap was used by Ball to apply hydraulic theory to the katabatic flow. The depth of water flowing is assumed to be constant, so it was necessary to also have a definite and constant depth in relation to the cold air that was flowing down the slope. Ball used the height of the inversion to determine this depth.

The hydraulic theory revealed that when there is a change in the elevation of the surface from one level to another, over a small horizontal distance, what is

known as a hydraulic jump, may occur.

Upstream of a jump, the flow is shooting (fast flowing air, probably within a fairly well stratified environment) but downstream flow is tranquil. (Ball defines flow as shooting or tranquil depending on whether the Froude Number is greater than or less than unity respectively; see Equation 2.6). This is an explanation for the "mysterious lulls" that have been observed. When a jump occurs, it is situated near the base of the slope. This is where observations of the corresponding meteorological phenomena have been collected, as illustrated by Madigan's diagram in Mawson (1915). Numerous similar observations have been documented since; Shaw (1957), Lied (1964), Weller (1969) and Wilson (1992).

Generally referred to as "jumps", they are also named "hydraulic jumps" from the standard hydraulic theory discussed by Ball (1956), "pressure jumps" because of the sudden change in air pressure observed at meteorological stations, Ball (1957), and "katabatic jumps" by Lied (1964). They are also known as "Loewe's Phenomenon". Coastal stations of East Antarctica are located at the base of steep ice slopes, making them good observation points for jumps, given ideal atmospheric conditions.

If the jump moves seaward, then the station is in a region of strong winds and/or shooting flow, and if the jump moves inland, the station is in a region of tranquil flow, probably with greater mixing and turbulence.

For instances when a hydraulic jump has developed and it is stationary, (air is flowing through, but the system is not progressing either seaward/downstream or landward/upstream), it was shown theoretically that flow must change from shooting to tranquil. The mean flow energy decreases through a jump which means that this energy is transferred to other processes; for small jumps, the flow energy is transformed mainly into stationary waves, but for more intense hydraulic jumps, it is transformed into turbulence.

When considering a jump that is not stationary, it was shown that a jump moving upstream is more intense than a stationary jump, and a jump moving

seaward is weaker than a stationary one.

Whether or not a jump occurs can be indicated from the Froude number for uniform flow. This dimensionless number is a ratio of the inertial to gravity forces. The form of the Froude number as used by Ball (1956) is given in Equation 2.6.

$$F_r = \frac{\theta Q^2}{\alpha \theta' g} \tag{2.6}$$

where $Q = h.u$, a constant depending on the rate of supply of cold air from the ice plateau, h is the height of the inversion, u is the wind speed,

α is the angle of inclination of the ice slope.

θ is the potential temperature,

θ' is the potential temperature deficit of the cold air,

and g is the acceleration due to gravity.

For values of the Froude number less than 1 no jump is expected to occur, but for values greater than 1, a jump may form. These predictions are made assuming the topography is smooth, or close to smooth, and other atmospheric processes, such as convection and mixing due to a heat source, such as the sea, are ignored.

It was noted that Coriolis effects have an influence on the position of the jump. Coriolis effects contribute to turning the wind direction away from the fall line of the topography. The jump depends on the component of the wind directed downslope, and this component is reduced slightly due to the Coriolis turning. Also, it is expected that if a jump occurs when there is more veering of the wind away from the fall line, that jump is more likely to be located seawards of the coast. This is probably because a jump that occurs when there is more veering of the wind, relative to the fall line, is expected to be weaker than a jump that occurs when there is a greater downslope component of the wind, and therefore the jump occurs further seaward. Local topography can have a significant effect, and the results presented were for "ideal" conditions, as assumed in the hydraulic

theory used. Veering of the wind due to Coriolis reduces the chance of a jump forming.

Comparison with observations demonstrated that Madigan's diagram, from Mawson's (1915) publication, was a good analogy with flow in a hydraulic jump. This is shown well by Figure 2.13, as reproduced from Ball (1956).

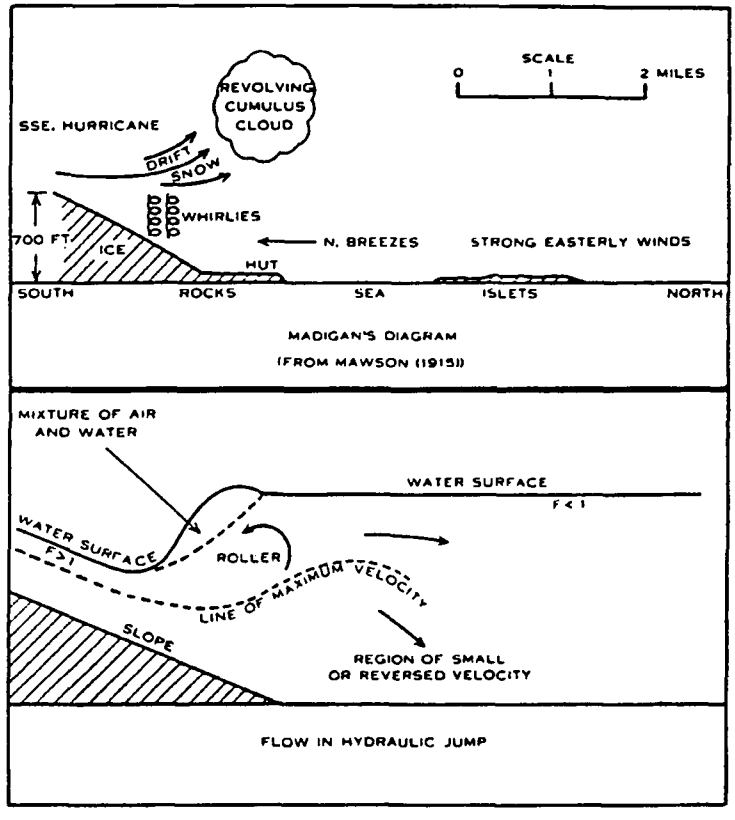

Figure 2.13: Comparison between Madigan's diagram and flow in a hydraulic jump, as reproduced from Ball (1956).

If a jump is expected to form, its position can be determined from the relative values of the upstream and downstream depths. If the depth of the inversion downstream of the jump exceeds the upstream depth by more than 50 metres, the jump is expected to form about 1/2 kilometre inland, but if the depth of the inversion upstream is more than 50 metres larger than the downstream depth, the jump is expected to form 2-4 kilometres seaward of the coast. Ball surmised that the jump would be most likely "stationary" (as defined previously), and therefore the best place for observation would be just inland from the coast.

The deviation of the direction of the flow from the fall line due to Coriolis

effects was thought to be about 16 degrees, but about 8 degrees when a stronger inversion was present. At Cape Denison the values observed were 10-15 degrees, and about 5 degrees at Port Martin. Downstream of a jump, the deviation is thought to increase from 16 to 60 degrees and 8 to 30 degrees respectively. These are predictions from equations, and these are not easily verified because of the large amount of turbulent kinetic energy generated as air passes through a jump, and this leads to variable wind directions. However, it is observed that further out to sea, the flow tends to be easterly. These predictions are made assuming that there is uniform flow, and it is noted that uniform flow is unlikely to be present, due to irregularities in the flow upstream and in the topography, and so the predicted angles are likely to be over-estimates.

Ball (1957) applied the findings from Ball (1956) to observed conditions in the neighbourhood of Commonwealth Bay, east of Dumont D'urville station. It was shown that the pressure (or hydraulic) jump that occurs at the base of the ice slope represents the boundary between the strong katabatic winds of the steep ice slopes and relative calm over the sea. When this boundary moves, the region over which strong winds occur also changes. Abrupt onsets and cessations measured at coastal stations may be caused by the movement of the pressure jump; this was well supported by qualitative predictions using this hypothesis, that were shown to be of the correct magnitude.

Mawson (1915) had noted that at Cape Denision during calm conditions, the strong winds continued overhead and at other locations along the coast. This suggested a sharp boundary between the strong winds and calm conditions. It was a localised effect.

Lied (1964) presented measurements and observations of hydraulic jumps, including those made from passing through a hydraulic jump from one side to the other. The jump was frequently located close to an ANARE weather station in the Vestfold Hills about 18 miles (about 29 kilometres) inland from Davis station. The observation period was from May 1961 to January 1962.

A wall of drift snow about 30 to 100 metres high was associated with most of the standing jumps. At the top of this wall, small fracto-type roll clouds were frequently observed, with formation to dissipation times ranging from 30 seconds to 3 minutes, as similarly observed by Madigan (1929).

A jump could be seen to extend for 10-12 miles (about 18 kilometres) along the plateau when there was a wall of drift snow, and Lied noted that gaps sometimes appeared in the wall. It seems that disturbances to the air flow caused by prominent terrain features, such as ice domes, moraines and nunataks, were an important influence on development of the gaps in the wall of drift snow.

When there was less precipitation, there was less loose surface snow available for transport by winds, and consequently less appeared as walls of drift snow, associated with hydraulic jumps. However, the presence of the katabatic flow was also evident from the roar that could be heard, Lied (1964). Madigan (1929) also mentions the roar of the wind to the south, during periods when there were calm conditions at the observer's location.

Lied (1964) stated that when the observer entered a jump from the downslope and calm side, strong updrafts and downdrafts were experienced. Also, there was a sudden pressure drop, and a rise in temperature. The edge of the jump was turbulent but further upslope the wind was stronger and the drift was denser. Changes in pressure were normally 2-3 hPa.

The descriptions of strong winds upstream of a jump, but calm conditions downstream, by Ball (1956) and Ball (1957), were well supported by Lied's observations.

Lied examined upper wind data for days when a jump, was observed. It was found that on these occasions there were strong, overriding winds at both the weather station in the Vestfold hills and at Davis station. Also, there was an inversion found on the sounding at Davis. During these events, the base of the inversion was usually at a height between 2000 and 7000 feet (about 600 to 2100 metres).

Weller (1969) noted that abrupt onsets of katabatic winds were usually accompanied by a drop in pressure by 0.5 hPa, a drop in temperature by 1 degree and a rise in relative humidity by 4 percent. Also observed were snow drift and roll clouds, as described by Lied (1964).

Despite the generally good agreement between analyses of hydraulic jumps made by Ball (1956) and the observations of Lied (1964), Ball's work does not explain all of a jump's characteristics. Shaw (1957) noted that there was good qualitative agreement between observations at Mawson station and Ball's explanations, but there were cases where another model seemed to be necessary.

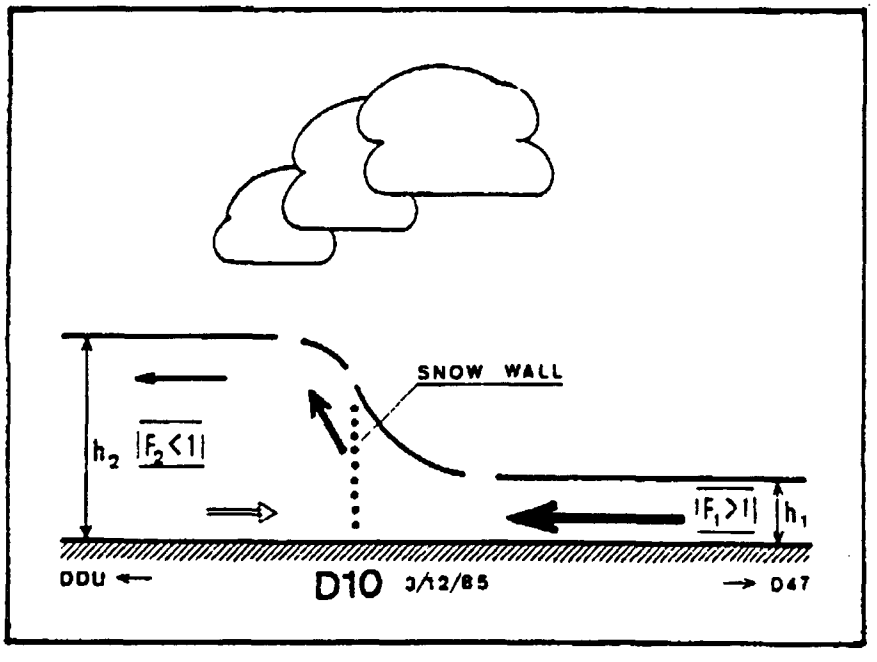

Figure 2.14: Schematic diagram of the hydraulic jump observed on 3 December 1985 at location D10 in Adelie Land, Antarctica, as reproduced from Pettré and André (1991).

Pettré and André (1991) noted that jumps usually formed after the katabatic had persisted for some period of time (hours or days), and marked the end of the katabatic flow. Downstream of a jump, reversal of flow was observed; this is likely to be associated with convergence and updraft, as was previously noted in discussions recorded in Antarctic Meteorology, Proceedings of the Symposium, Melbourne, 1959. A schematic representation of a jump observed in Adelie Land in December 1985 is shown in Figure 2.14.

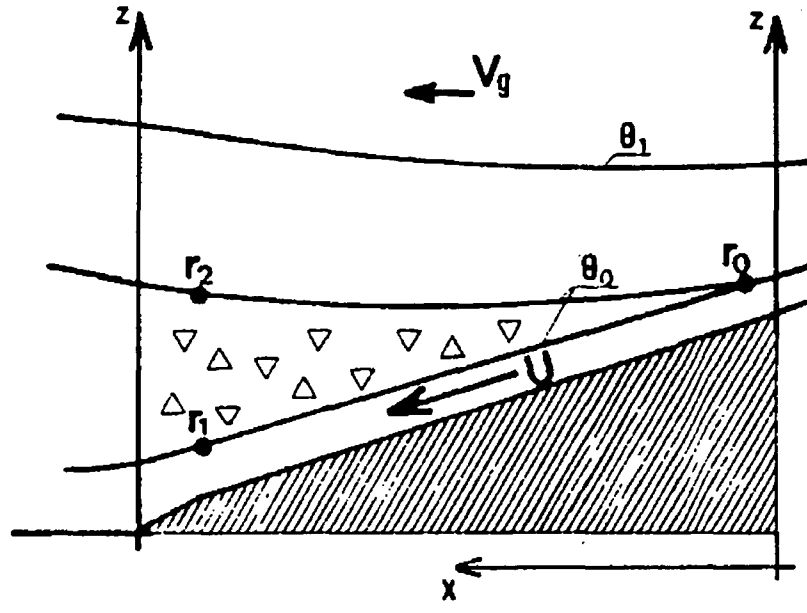

Figure 2.15: Idealised configuration of the flow before (upstream of) the occurrence of the jump (triangles indicate the unstable layer), as reproduced from Pettré and André (1991).

Pettré and André (1991) found that large pressure changes that occur through a jump, such as the near 20 hPa case observed by Lied (1964), are not explained by Ball (1956) or Ball (1957). Ball's explanation could only explain changes in pressure of 1-3 hPa.

By considering accelerations of the downslope wind, instead of simply the change in depth of the cold air layer as it passed through a jump, Pettré and André (1991) showed that the processes occurring within a jump could be better explained.

Ball (1956) used a model with a katabatic layer capped with an inversion, above which was a neutral or unstable layer, and above this was the transition to the free atmosphere. This has been shown to be successful in explaining katabatic flow, but not as effective in explaining Loewe's phenomenon, or "katabatic jumps".

Pettré and André (1991) used observations to construct a different picture of air flow over the Antarctic slopes. As shown in Figure 2.15, there is a layer of air flowing downslope adjacent to the surface, and above this is an unstable layer that thickens downslope. This unstable layer was also noted as being turbulent. Above this is the transition from the surface winds to the free atmosphere. It was

found that jumps have frontal characteristics and are too complex to be explained by the hydraulic approach of Ball (1956).

The unstable layer overlying the surface drainage layer is turbulent, and it is therefore not possible to determine air trajectories through such a layer. This illustrates the complex nature of the flow over coastal regions where jumps occur. It was found that the near 20 hPa pressure change observed by Lied (1964) may be associated with strong wind shear between the upper (above the unstable layer) and lower (below the unstable layer, at the upper boundary of the surface drainage layer) streamlines, downstream; at r_2 and r_1 respectively as shown in Figure 2.15.

2.4 SYNOPTIC INFLUENCES ON AIR FLOW AROUND COASTAL ANTARCTICA

Antarctica is encircled by a semi-permanent trough of low pressure. This separates the westerly winds of the Southern Ocean from the winds above the Antarctic continent, Streten (1962). Monthly mean pressures are displayed in Chapter 3, Figures 3.12 and 3.24.

Depressions are present in this belt of low pressure and generally move to the east or east-southeast under the control of upper winds, although they may also decay or even move westward. A schematic representation of cyclone tracks around Antarctica is shown in Figure 2.16.

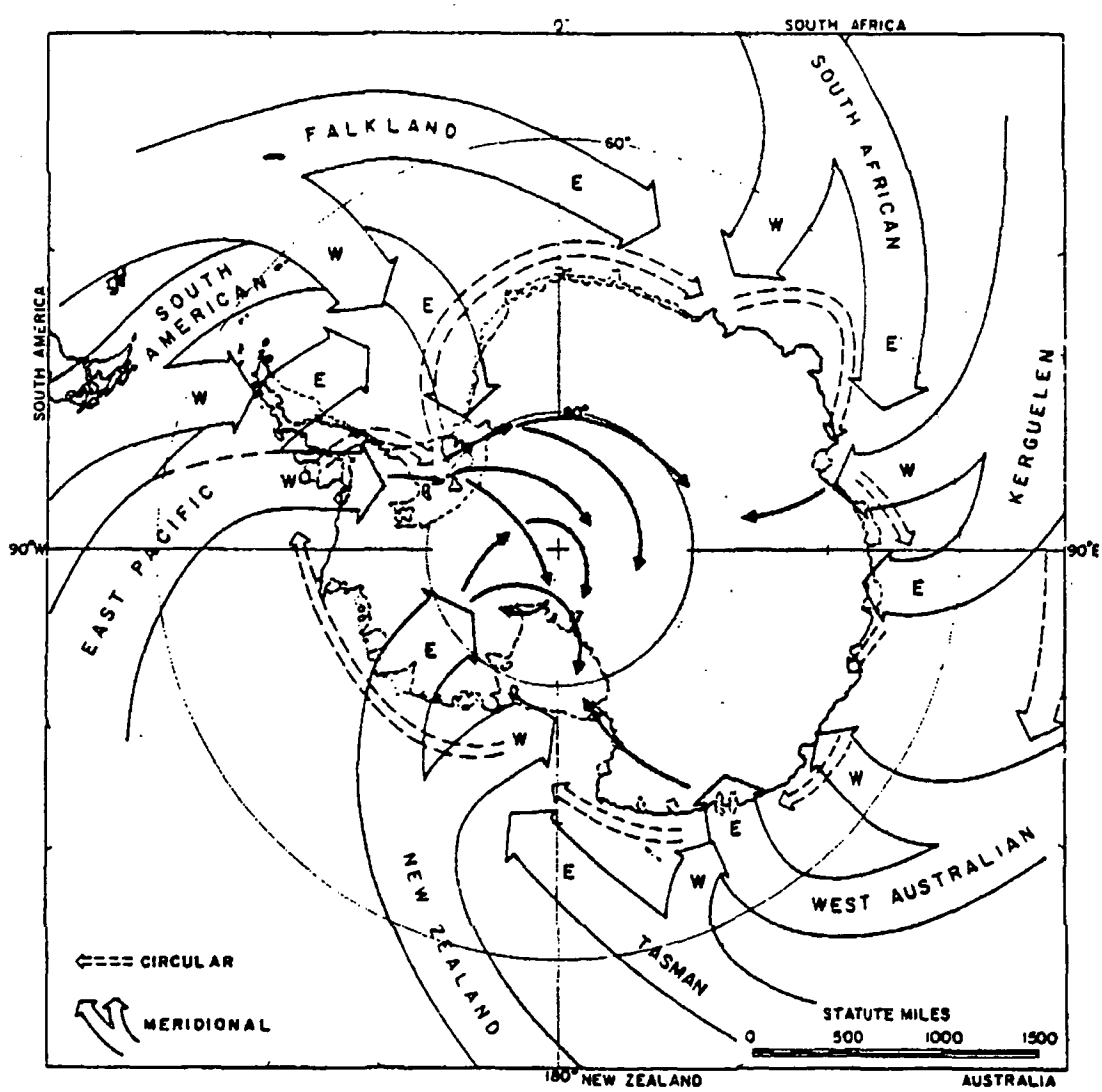

Figure 2.16: Tracks of sea-level depressions as reproduced from Alt, Astapenko and (Jr). (1959).

Depressions that caused blizzard conditions at Mawson usually approached from the sea to the north-west, Streten (1961).

Rusin (1961) noted that most meteorological elements indicated the approach of a cyclone, but pressure did not necessarily do so; there may even be a rise in pressure. It was noted that this feature occurs in coastal regions where katabatic winds are present, causing a distortion of the picture. This may be associated with changes in pressure caused by jumps, as discussed in Section 2.3.3. Also, along the East Antarctic coastline, depressions move generally eastward, and as they possess clockwise rotation in the Southern Hemisphere, the "leading edge" of a cyclone opposes the drainage air flow. This involves a drop in pressure but also a reduction in wind speed instead of an increase in wind speed. As the cyclone passes to the east, the pressure increases and the wind speed increases as the cyclonic air flow no longer opposes the drainage flow off the continent.

Rubin and Giovinetto (1962) explained snow accumulations over Antarctica in terms of cyclone tracks and topographic features. Terrain of lesser slope did not cause rapid lifting of air to the lifting condensation level and therefore there was precipitation higher on the slope, where the air later reached condensation.

Cyclones play an important part in precipitation over Antarctica. The low air temperatures over the continent limit the amount of moisture that may be carried by the air. The principal source of moisture is the ocean to the north of Antarctica, although during summer the sea surface temperatures are close to 0°C, and during winter the sea ice extends for many tens of kilometres. Polynyas and leads therefore play an important part also, providing regions of open water to interact with the atmosphere. This interaction usually takes the form of a heat and moisture supply to the atmosphere. Cyclone tracks in Figure 2.16 show the general movement of cyclones towards Antarctica to be from the north and the west. The steep coastal orography, particularly of East Antarctica, and the low air temperatures encourage precipitation relatively near to the coast.

Shaw (1957) noted that most precipitation in the Mawson region was related

to depressions.

Cyclonic wind velocities increase with height, in contrast to the wind speed profile of the katabatic, Figure 2.12b. Frequent prolonged rises in temperature may also occur due to cyclonic winds, Rusin (1961).

Ball (1960) discussed the influence that cyclones, situated off the Antarctic coast, have on the flow lines of drainage winds flowing from the interior towards from the coast. This is shown in Figure 2.17.

The flowlines due to a low pressure system situated off the Antarctic coast were shown to be similar to those around a bay. The surface wind strength in the western region of influence, however, was much stronger, but wind directions were not altered very much. As a low pressure system moves along the coast, it can therefore cause large increases in wind strength, but wind direction remains the same. This increase in wind strength causes movement in the coastal pressure jump, and, as described in Section 2.3.3, this in turn leads to the sudden onsets and cessations of the katabatic wind at coastal stations, (discussed also in Ball (1956), Ball (1957) and Schwerdtfeger (1984)).

Observations of Streten (1962) are in agreement with those of Ball (1960), with offshore depressions increasing the wind speed but not greatly affecting the direction of the wind, possibly a change of only about 10°. Streten noted that violent winds associated with synoptic systems exist typically for periods of only 24 to 48 hours.

Streten (1968b) pointed out that prolonged gales were found to be associated with synoptic disturbances. This is in contrast to pure drainage flow, which does not persist for extended periods, because the upstream air supply becomes exhausted in most regions of Antarctica.

Synoptic-scale cyclonic influence on drainage flow has been discussed. In contrast, katabatic outflow may be associated with mesoscale polar low formation. A strong katabatic jet that flows off the ice slopes may help to support cyclonic motion, if it is situated with the outflow directed into the western side of a vortex

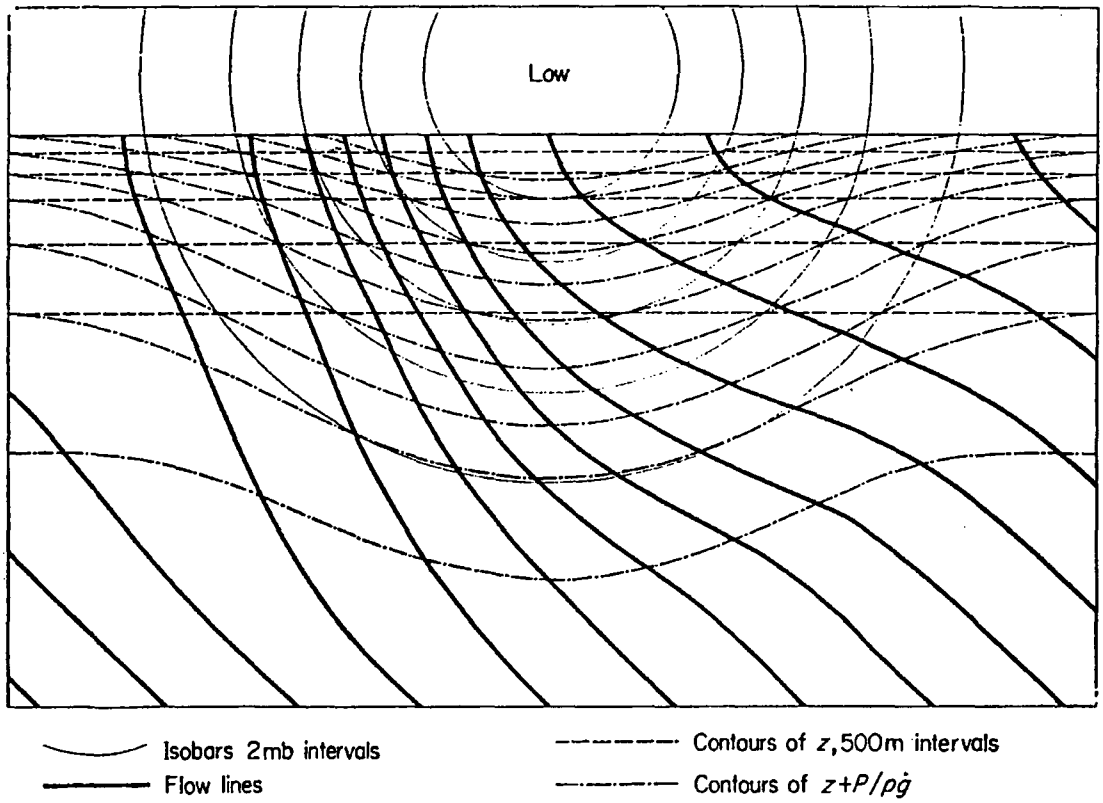

Figure 2.17: Flow lines in the neighbourhood of a depression, as reproduced from Ball (1960).

that is located to the north. A problem with this is that the relatively cold air may contribute to the "filling" of the low pressure system, causing it to dissipate rather than grow in strength, Parish (1988).

2.5 NON-ANTARCTIC KATABATIC AND DRAINAGE FLOW AND NOCTURNAL BOUNDARY LAYERS

Manins and Sawford (1979b) discussed some characteristics of katabatic flow, based on numerical modelling results. The model presented took into account entrainment of air into downslope flow, and this was shown to be a more significant retardation than surface friction. Surface stresses may be further reduced when there is strong stable stratification close to the ground, because this isolates the katabatic flow from the surface irregularities.

When shooting flow develops, breaking of interfacial waves causes strong mixing by entrainment. For steady katabatic flow, in a neutral atmosphere, the flow grows in thickness linearly with distance downslope and the rate of speed increase decreases. When a critical slope is reached and waves develop, the waves may break and this leads to entrainment, and growth of the layer.

Ambient stratification has an effect on the so-called "flux of buoyancy deficit" of katabatic flow: when there is ambient stratification downslope, cool air that arrives from upslope contributes some (relative) buoyancy because the ambient air is cooler, and so, to maintain a stable situation, a larger proportion of the cooling that occurs is used for maintaining the buoyancy deficit, and hence stable stratification.

The "flux of buoyancy deficit" increases with layer cooling, and it reaches a maximum, after which there is a decrease as the flow rate increases. On steeper slopes, the decrease of the "flux of buoyancy deficit" occurs more rapidly. This probably means that there is more mixing on steeper slopes, and the inversion may be weaker, and possibly deeper.

A cross-slope ambient wind enhances interfacial shear and may be important in determining whether a katabatic wind is observed. Kitabayashi (1977) showed that when the internal Froude number of the flow was greater than approximately 2.3, cooled air may move in the direction of the ambient wind instead of more

directly downslope.

Manins and Sawford (1979a) discussed data measured during a field case study of katabatic winds in the Latrobe Valley, Australia. The observations were made during September 1975.

Downslope flow that was measured at about 4 a.m. local time coincided with an increase in thermal stability of air below a height of 40-50 metres. At time 0610, it was found that there was an exceptionally strong temperature inversion below the level of the downslope wind velocity maximum, that was located close to a height of 40 metres. At around 100 metres height, the velocity profile changed sign and approached the ambient velocity component, which was in opposition to the downslope flow.

During both nights, a shallow flow of only several metres depth was observed at the surface. It was concluded that this flow was practically independent of the ambient wind. This is analogous to Antarctic katabatic winds, discussed in Section 2.3.2, that were found to be independent of the synoptic wind.

The interaction between the katabatic flow and the ambient air flow above leads to mixing, and consequent turbulence that is produced works in opposition to buoyancy forces. Following Turner (1973), the mixing was said to be an internal process. This means that the interaction and subsequent mixing is isolated from the surface. This was supported by computing profiles of the gradient Richardson Number (Ri) obtained from observations made during the case study of Manins and Sawford (1979a). A critical value of Ri = 0.27 ± 0.1 occurs in the region of this interaction and mixing, from about 50 metres to at least 110 metres height. The Ri profiles also show that any mixing that occurs near the surface is isolated from the mixing due to the interaction above by the relatively well stratified air flow in between.

It was concluded that the shear stress between the ambient wind and the downslope flow was more important than the surface stress, for cases when the ambient wind opposes the downslope flow. Also, the dynamics of the flow can

be influenced by the ambient wind. It was noted that this stress due to the interaction of flows cannot be parameterised simply because it was a dynamical part of the interaction process.

Rusin (1961) notes that observations of gravitational winds in Antarctica show that the eddy exchange is increased, and this causes advection of warmer air towards the surface from higher levels. However, Tauber (1960) explains that it is the presence of ground based inversions and the small roughness length of the ice and snow surface that cause a low value of the turbulent exchange coefficient despite high wind speeds. This is more likely to occur with stronger inversions that possess strong vertical stratification, as discussed in Section 2.2.

Zeman (1979) presented a model that was used to parameterise the nocturnal boundary layer (NBL) and also allow development of a nocturnal jet. This is of interest to the study of the atmospheric boundary layer over Antarctica, which has fairly continuous downslope flow that is characteristic of nocturnal flow in other parts of the world.

The nocturnal boundary layer differs from the daytime mixed layer because it cannot respond fast enough to varying boundary inputs and is continually evolving until sunrise.

The model depended on boundary layer depth, bulk wind and temperature and surface turbulent fluxes. The source of turbulence in a NBL is the mean shear. It is important that mean shear be realistically represented because if the boundary layer is turbulent, it will not be predicted well if the mean shear is incorrect. The depth of a NBL depends on turbulence and on mean flow.

Past formulae for predicting the NBL depth were only valid for a steady- state limit. The approach used here was to relate the NBL height to the dynamical parameters of the boundary layer, such as the length scale of turbulence and the mean flow.

Buoyancy and Coriolis forces control the depth of a turbulent boundary layer, and without these forces, the depth of the layer could continue to grow. Turbu-

lence is suppressed by buoyancy forces, and this leads to a decrease in the layer's depth, which leads to an increase in mean shear, and this can then cause more turbulence to be generated. Turbulence is extracted from mean flow dependent on the rate of destruction of turbulence, which depends on the buoyancy forces and viscous dissipation. These energy exchange processes take place in such a way that the Richardson number is maintained in the subcritical range.

This model predicted that after an initial collapse, the NBL depth grew at relatively small rates, but sufficient for it to double in the period from 3 to 12 hours after sunset. Due to often unreliable observations of NBLs, for verification purposes, Zeman's model was compared with a previous model (second order closure model for a horizontally homogeneous barotropic NBL) instead. Both models agreed on the overall features of the NBL dynamics, but it is important to realise that these comparisons were made using featureless terrain.

A nocturnal low-level jet was treated as an NBL feature, and the conditions that were most likely to lead to the development of a jet were noted. Large cooling rates and thus clear nights were favourable for jet development. As the NBL decays, there is an increased departure from the geostrophic wind, and this is also favourable for jet development. When there is no decay, there is less departure from the geostrophic wind in the NBL, and with a greater NBL depth, the jet is displaced higher and approaches the local value of the geostrophic wind. It is important to note that the processes described here were produced by a model, not from observations. Bulk mean shear and mean values of parameters at the top of the boundary layer were used.

Mahrt and Larsen (1982) studied drainage flow in Northeast Denmark. They showed that significant turbulence occurred above the region of cold air drainage, as discussed by Manins and Sawford (1979a). It was also shown that the head of the gravity current was a region of intense three-dimensional turbulence.

Hootman and Blumen (1983) analysed nighttime drainage winds in Boulder, Colorado, another mid-latitude region. The principal characteristics of drainage

winds were shown to be preserved as the air moved away from the foothills.

This is an interesting point in relation to flow off the coast of Antarctica, where the drainage flow has been observed to dissipate at about 15 kilometres offshore over the sea or seaice.

Blumen (1984) noted that drainage flow over complex terrain can lead to the development of billows, causing mixing between the drainage current and surrounding air.

Applying this point to East Antarctica, most terrain consists of firn surfaces that are relatively smooth compared with complex terrain, and therefore billow formations are not expected. There are relatively small regions of complex terrain in East Antarctica, such as the Prince Charles Mountains, Mawson Escarpment and Framnes Mountains. In the case of the Framnes Mountains, in the area south of Mawson, air has been observed to flow around the mountains with little disturbance other than channelling of the air, while phenomena such as hydraulic jumps depend on the air flow and terrain slope, not on complex terrain. However, Streten (1963) suggested that Mt. Henderson near Mawson may be the cause of observed atmospheric wave motions.

Clark and Farley (1984) modelled severe downslope windstorms that had occurred in Boulder, Colorado in January 1972. A possible cause of gustiness in the downslope region was presented. The terrain used during the simulations took the form of a ridge; the results may not be applicable to coastal Antarctica where the ice slopes are generalised as continuous slopes, as used in the modelling study by Parish (1984) for example, because in the case of a ridge or a hill, the air flows over the hill and not just in a general down-motion.

The hypothesis was that the lee of the ridge, where waves developed, was a region of turbulence if the waves broke. Convective instability in the wave breaking region may then cause movement of turbulent eddies to the surface via downdrafts. Such a movement produces gustiness. Periodicity of gusts may be due to competition between the production of gravity waves and their breakdown

due to convective instability.

Porch, Clements and Coulter (1991) analysed measurements of nighttime drainage winds in a valley in Western Colorado. Regular oscillations in the flow were found to be regulated by inflow from tributaries. Observations supported the hypothesis that there was a build-up of cold air in tributaries over a twenty minute period, followed by a surge into the main valley. This caused the main valley air flow to decrease in order to conserve momentum.

Coulter, Martin and Porch (1991) expanded on the work of Porch, Clements and Coulter (1991). It was concluded that the orientation of a tributary to the main valley was important in determining how much influence the inflow from a tributary has on the air flow within the main valley. As may be expected, it was found that oscillations were less pronounced and drainage mass per unit area was greater in tributaries that were more closely aligned with the main valley. Weak flow within tributaries was found to be sensitive to small terrain features. As mentioned by Schwerdtfeger (1984) for winds over the Antarctic plateau regions, and by Ball (1960) for winds on steeper slopes, terrain features are important in determining the air flow near the surface.

2.6 CONCLUSION

This chapter has reviewed past literature relevant to the Antarctic atmospheric boundary layer, and katabatic winds in general. The work in the following chapters uses this review as a base to build upon, while investigating the boundary layer over the Lambert Glacier basin region. It is helpful to compare the present project's results with this review, as a guide to its validity, and in determining the path which the research takes at various stages.

Chapter 3

CLIMATOLOGIES

3.1 INTRODUCTION

This chapter discusses the availability of meteorological data throughout the Lambert Glacier Basin Region. The sparseness of observations, in both space and time, which prevents reliable climatologies of the region being compiled, is demonstrated.

Another aim of this chapter is to analyse Antarctic Upper Wind (AUW), surface and radiosonde data in order to produce a climatology of winds and associated weather conditions at Mawson and Davis stations. Conclusions are drawn about the several wind types defined in Section 3.4. Analyses at Mawson are expanded upon in Chapters 7 and 8.

The area of interest is known as the Lambert Glacier Basin, or Lambert Glacier Drainage Basin, because winds, and streams of ice, drain into it. Mawson and Davis stations are present in coastal areas and Sovietskaya and several automatic weather stations (AWS) are present in the plateau region.

This region roughly covers from latitudes 65°S to 85°S and longitudes 50°E to 90°E. The region over which the atmosphere will be modelled (in later chapters) is shown in Figure 3.1. This figure also shows station locations.

Section 3.2 discusses the various sources of meteorological data that are available throughout the Lambert Glacier Basin region.

Section 3.3 is a brief discussion on the climatology of the plateau region of the Lambert Glacier Basin using data that are available. The discussion on the me-

teorological processes and the thermal regime that exist over the plateau region, in Chapter 2, is of use in understanding the climatological results presented here.

Section 3.4 defines terms, particularly types of winds, that are used in computing climatologies at Mawson and Davis stations. These terms are also referred to in later chapters.

Sections 3.5 and 3.6 are detailed climatologies for Mawson and Davis stations respectively. Climatologies, particularly of Mawson, have been compiled and presented by several authors, such as the numerous papers by Streten. The aim here is not to repeat or simply update this past work. Instead, these climatologies concentrate on the various wind types defined in Section 3.4, expanding upon the non-plateau type winds discussed in Chapter 2, and forming a basis for analyses and modelling throughout Chapters 7 and 8.

The conclusions in Section 3.7 are important for deciding the path that this research follows; lack of observations make numerical modelling a desirable option, provided that there have been sufficient observations for model validation to ensure reliability. Apart from helping to establish a climatology, modelling may also be a useful method for studying mechanisms behind observed winds.

Generally throughout this thesis, summer and winter seasons are represented by mean January and mean July conditions respectively.

3.2 DATA AVAILABLE THROUGHOUT THE LAMBERT GLACIER BASIN REGION

As noted in Chapter 2, the coverage of meteorological observations over Antarctica is sparse. The Lambert Glacier Basin is no exception.

Stations and their respective latitudes and longitudes are shown in Table 3.1. These are also shown in Figure 3.1.

MAWSON AND DAVIS STATIONS

Detailed analyses of surface, radiosonde and upper air wind data are presented for Mawson and Davis stations; Sections 3.5 and 3.6. These are the only two locations

Station	Latitude	Longitude	Elevation
Davis	68°34′48″S	77°58′48″E	12 m
Mawson	67°36′0″S	62°52′48″E	8
Sovietskaya	78°24′0″S	87°32′0″E	3662
LGB00	68°39′0″S	60°33′0″E	1850
LGB10	71°18′50″S	59°12′25″E	2570
LGB20	73°49′59″S	55°40′22″E	2775
LGB59	73°27′6″S	76°47′24″E	2550

Table 3.1: Station locations throughout the Lambert Glacier Basin region. Stations named LGBxx are automatic weather stations.

within the region that have long term records; refer to Table 3.2. The surface data set contains temperature, pressure, wind speed, wind direction, visibility, total cloud amount, low cloud amount and low cloud base height fields. The radiosonde data set contains temperature and mixing ratio fields at pressure levels shown in Table 3.3. The upper wind data set consists of wind speeds and wind directions at pressure levels shown in the same table.

SOVIETSKAYA STATION

Sovietskaya station was only operated during 1958, and its remote location means that the data available are valuable. However, one year of recording is not adequate to establish a reliable climatology, but the data should be representative of the magnitudes of meteorological parameters that exist over the high, and most southern, regions of the Lambert Glacier Basin. These data (temperatures, pressures, wind speeds and directions, cloud amounts and inversion strengths and depths) are shown in Figures 3.5 and 3.6.

AUTOMATIC WEATHER STATIONS

There is also a limited supply of automatic weather station (AWS) data available. As these data have only been collected in the short-term (less than 5 years for

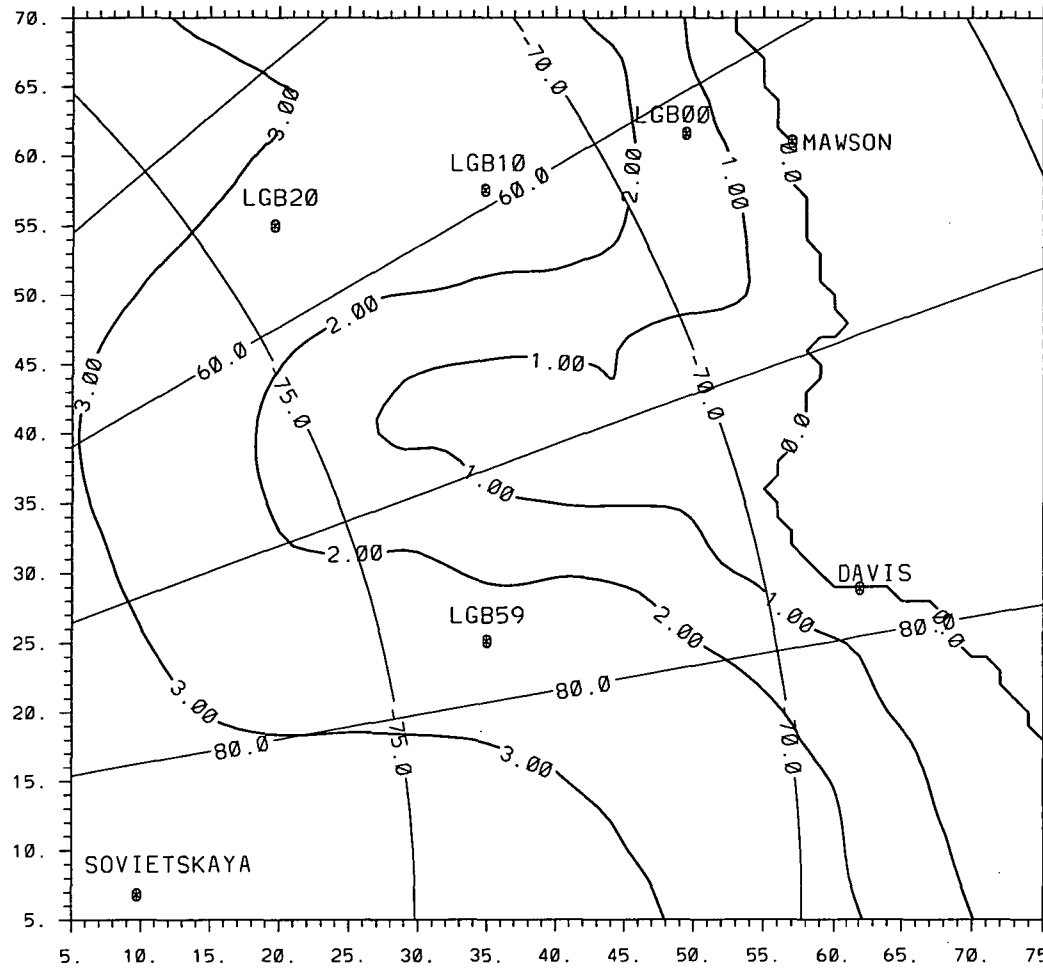

Figure 3.1: Locations of stations throughout the Lambert Glacier Basin region of East Antarctica. The unit of the terrain elevation contours (bold) is kilometre. The tick marks on the borders of this figure represent 20 kilometre spacings. The x- and y-coordinates are grid points corresponding to the grid used for numerical modelling of the atmosphere. This is explained in more detail in Chapter 4.

most stations), they can not be used to portray a reliable climatology of their locations. However, as with the data from Sovietskaya station, they are valuable because so few observations have been made in this area.

In addition to the lack of long term deployment of AWSs, there are problems with their continuous operation. During winter, ice can form on the anemometers, preventing operation. Due to their remote locations, they cannot be serviced more than once a year, during the summer. Nearer to the coast, where accumulation can be approximately one metre per year, the accuracy of measurements needs to be questioned because heights of sensors (1, 2 and 4 metres above the surface) vary throughout the year. Eventually the sensors and the entire station are covered

	Mawson	Davis
Surface	1954 - 1987	1957 - 1964, 1969 - 1987
AUW	1954 - 1987	1957 - 1964, 1969 - 1987
Radiosonde	1955 - 1987	1959 - 1964, 1969 - 1987

Table 3.2: Periods of Surface, Antarctic Upper Winds (AUW) and Radiosonde data at Mawson and Davis stations used for analyses in this chapter.

completely, with snow, unless serviced.

Monthly mean January and July air temperatures, wind speeds and wind directions, computed from AWS data, are shown and compared with modelled results in Chapter 6. January diurnal variations of these parameters are also shown.

SASTRUGI ORIENTATIONS

Sastrugi are snow dunes that are formed by accumulation of blown snow. They line up close to parallel with the surface wind direction.

Sastrugi orientation data are available from several traverses that have been made in the region south of Mawson and west of the Prince Charles Mountains. Observations from helicopter flights are also used.

These data may be used to represent the direction of wind flow near the surface at and previous to the time of measurement. Mather (1962) noted that sastrugi orientations can vary considerably at the same location. The data represent the directions of winds that have recently passed over the location in question, and are therefore only a guide to the climatological wind directions. As these measurements were made on traverses conducted during summer, the wind directions that may be inferred from the sastrugi orientations are at best representative of surface winds during this season only. These orientations are shown in Figure 3.9. They are compared with model-generated surface wind directions in Chapter 6.

Height	Radiosonde levels	Upper wind levels
0 m	Surface	Surface
370 m	—	950 hPa
740 m	900 hPa	900 hPa
1180 m	850 hPa	850 hPa
1640 m	800 hPa	—
2150 m	—	750 hPa
2360 m	700 hPa	—
3750 m	600 hPa	600 hPa
5030 m	500 hPa	500 hPa

Table 3.3: Pressure levels at which radiosonde (centre column) and upper wind (right hand column) data have been collected; levels above 500 hPa are not shown as they are not considered in this study. Heights of these pressure levels vary from season to season; the left hand column contains mean annual height values for Mawson, estimated from Streten (1962).

SPARSENESS OF OBSERVATIONS OVER THE INLAND

The AWS, sastrugi and Sovietskaya data are very useful for verifying numerical modelling results. These data can be used for this purpose because the meteorological fields are largely unknown over the area of interest, and therefore even limited data are valuable for assessing the results of numerical modelling. Except by extrapolating data over large distances (hundreds of kilometres) from stations such as Plateau and Vostok (that lie outside the area of interest), and using data from coastal stations Mawson and Davis as a guide to the climate inland, (which is not recommended due to the very different meteorological conditions of the plateau and coast), only the AWS, sastrugi and Sovietskaya data are available for verification of model results, even to the correct magnitude, over inland areas of the Lambert Glacier Basin.

3.3 OVERVIEW OF THE CLIMATE OF THE INTERIOR PLATEAU REGION

This section does not discuss the climate of the Antarctic plateaus in general, but refers specifically to the plateau that lies within the area of interest. A general discussion of the Antarctic plateau weather is included in Chapter 2.

Unlike the detailed analyses presented in Sections 3.5 and 3.6 which were calculated using AUW, surface and radiosonde data, many of the meteorological fields over this plateau region have not been compiled using raw data, but are from previous publications, noted where relevant.

Figures 3.5 and 3.6 show monthly mean values of several meteorological parameters at Sovietskaya station for most months of 1958, the only period when the station was operational. These data are from Rusin (1961) and Dalrymple (1966).

TEMPERATURE

Annual mean isotherms over Antarctica are shown by Figure 2.1, Chapter 2.

The firn surface temperature data, for the Lambert Glacier Basin region, are derived from Budd, Jenssen and Radok (1971) and Radok et al. (1986). Seasonal variations of firn surface temperatures are estimated from differences between annual and seasonal surface air temperatures at Mawson, Davis and Plateau (south of the Lambert Glacier Basin region, but representative of plateau region) stations, which are then used to estimate the summer ("day" and "night") and winter firn surface temperature fields. These are shown in Figures 3.2, 3.3 and 3.4 respectively.

An analogous method is used to estimate diurnal firn surface temperature variations during summer. These are used to adjust the summer firn surface temperature data to more precise values, when comparing these "observations" with modelling results, in Chapter 6.

Corrections and tuning to the numerical model's thermal fields, (in following

chapters), can only be as accurate as the observed data that are available. There are several sources of error in the firn temperature data. The first is to do with the dependence on the 10 metre depth firn temperature for the annual surface temperature value, which leads to a potential error of $\pm 1°C$. The second involves the interpolation of annual surface temperatures, from the few available points, to cover the large area shown in Figure 3.1; this error is estimated to be $\pm 5°C$.

The third source of error comes from the estimation of the annual surface temperature wave from the annual air temperature wave. This is probably fairly small, and is affected by a period of thermal lag, as the surface is expected to respond more slowly to temperature changes than the air. This error is estimated to be less than 1°C.

Another problem is that Mawson and Davis are coastal stations, but have a relatively greater influence on firn temperatures, at terrain elevations up to about 2000 metres, than do the data from Plateau station. However, due to lack of data, the methods used are acceptable.

The total potential error involved with the surface temperatures used to represent January and July mean values is estimated to be over 5°C. The aims of the following chapters are to improve parameterisation schemes and tune the numerical model. Considering that the derived seasonal firn temperatures are not highly accurate, modelled firn temperatures that agree within 5°C of the respective seasonal fields are acceptable.

Recent traverse and AWS results can be used in the future to improve the temperature and surface elevation data, but these were not available when this project was begun.

Monthly mean air temperatures at Sovietskaya are shown in Figure 3.5.

PRESSURE

Monthly mean pressures at Sovietskaya station are shown in Figure 3.5. The semi-annual pressure pattern that is observed around coastal Antarctica (see

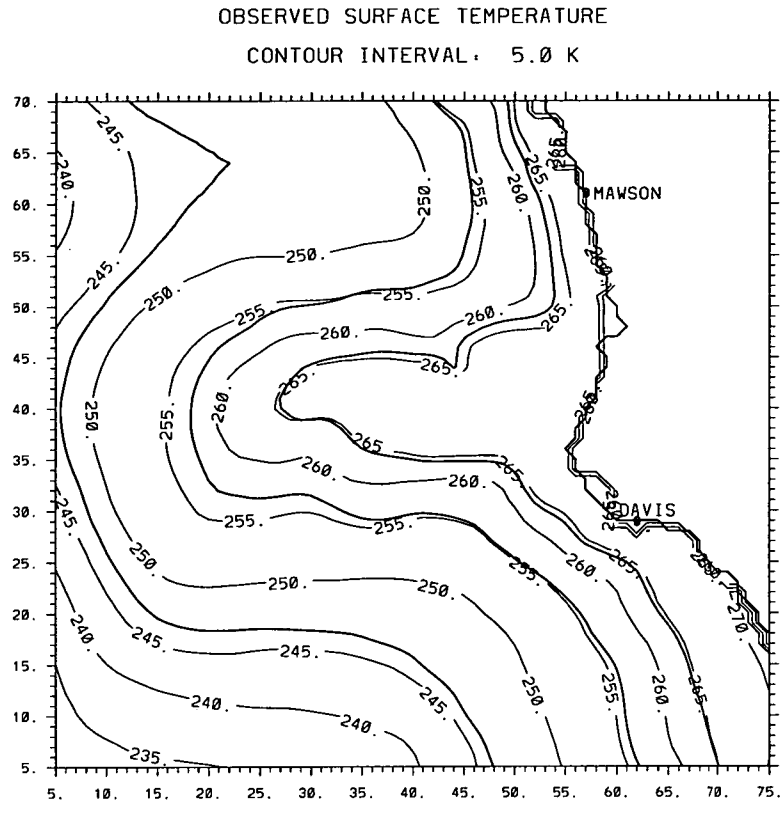

Figure 3.2: January "midday" surface firn temperatures, derived from observations of 10 metre depth firn temperatures.

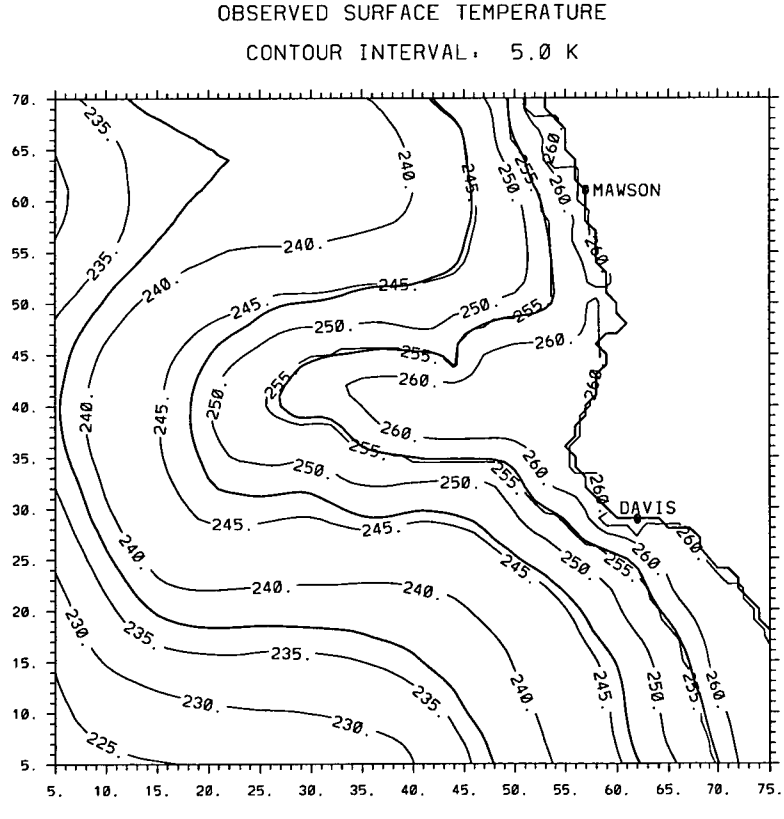

Figure 3.3: January "midnight" surface firn temperatures, derived from observations of 10 metre depth firn temperatures.

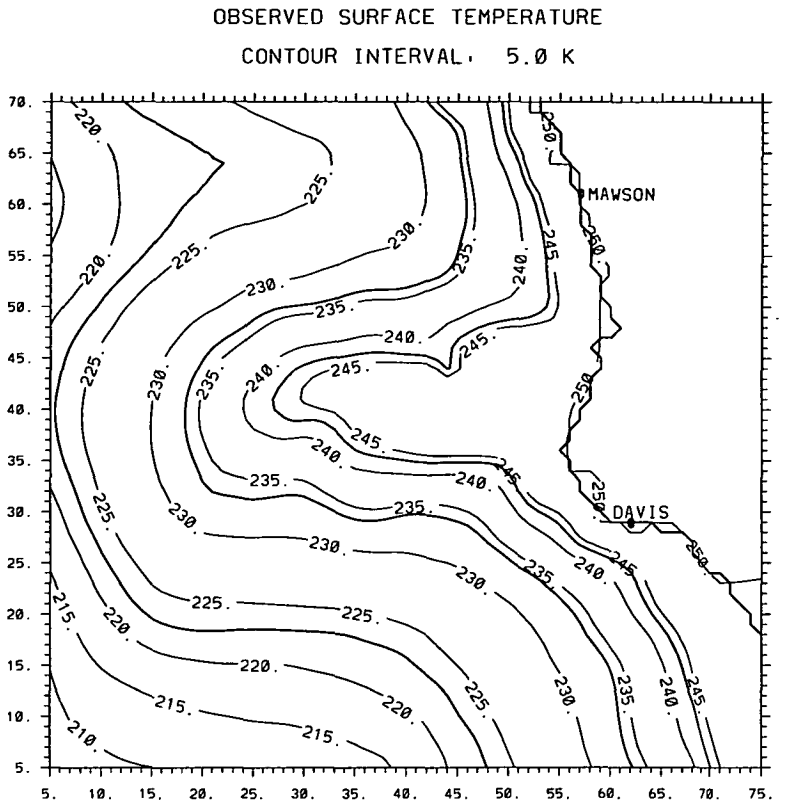

Figure 3.4: July surface firn temperatures, derived from observations of 10 metre depth firn temperatures.

Figure 3.12) is evident at this inland location also.

INVERSION

The mean winter (June-July-August) inversion pattern over Antarctica from Phillpot and Zillman (1970) is reproduced as Figure 2.2 in Chapter 2. The inversion specific to the region to be modelled is extracted, and shown in Figure 3.7. This is used for verifying July numerical modelling results in Chapter 6.

Discussions in Chapter 6 show that the interpolation of observed temperature inversion strengths does not allow details within the region of interest to be resolved, but numerical modelling results can resolve such details.

It should be noted that this is the winter mean inversion strength, and it can vary considerably. Depending on warm air advection, mixing, and longwave radiation interacting with clouds, the inversion can completely decay over plateau areas, or it can grow larger, as described in Chapter 2.

During summer, the inversion over the plateau regions is much weaker than

during winter. For example, Phillpot and Zillman (1970) showed that the mean winter inversion strength at Vostok was 24.6°C, but during January just 2.8°C.

Monthly mean values of the percentage occurrence, strength and depth of inversions at Mawson and Davis are shown in Figures 3.19 and 3.31 respectively.

CLOUD

Cloud amounts are largely unknown over Antarctica. There are difficulties observing cloud during winter, with extended periods of darkness, and durng blizzards, with visibility reduced due to blowing snow. Problems with cloud observations are discussed in more detail in Section 3.5.2.

There are relatively few stations over inland Antarctica, which means observations of cloud are sparse. There is a general decrease in cloud amount with increase in elevation. Monthly mean cloud amounts at Sovietskaya station during 1958 are shown in Figure 3.6.

Cloud amounts are discussed further in Section 6.6.3, Chapter 6.

WIND

Figure 3.5 shows monthly mean values of wind direction and wind speed at Sovietskaya station. The wind directions do not vary over a wide range. This is characteristic of the Antarctic plateau where strong inversions are present, as discussed in Chapter 2.

The predominant wind direction is close to 110°, about ESE. This shows that the air flows towards the Lambert Glacier, due to the orientation of the terrain slope; Sovietskaya station is located within the Lambert Glacier drainage basin, although far to the southeast, see Figure 4.2.

The wind speeds at Sovietskaya are a maximum during winter, from June to October. During this time of year, the air is colder and more dense, and the inversion is also stronger. With strong stratification of the inversion near the surface, stronger winds can blow close to the surface because the flow is relatively isolated from surface frictional effects.

Work by Parish (1982) (Figure 2.5) showed that there was likely mean surface air flow over part of the east Lambert Glacier Basin Region with a significant northerly component.

Numerical modelling of the Antarctic boundary layer for both summer and winter conditions, presented in Chapter 6, also produces surface winds with northerly components over the eastern side of the basin. These winds are verified using AWS data that were recorded during 1994, showing that the numerical model used here, and that used by Parish (1982), both function realistically.

RADIATION

Figure 3.8 compares global and net monthly mean radiation values at Sovietskaya and Mawson stations. Generally, global radiation is greater at Mawson than at Sovietskaya. The differences in latitude explain this. During December, (and possibly January, but values at Sovietskaya are not available), the monthly mean global radiation at Sovietskaya is greater than that at Mawson, because Mawson is further to the north and is also sheltered from solar radiation by the relatively high Antarctic land mass.

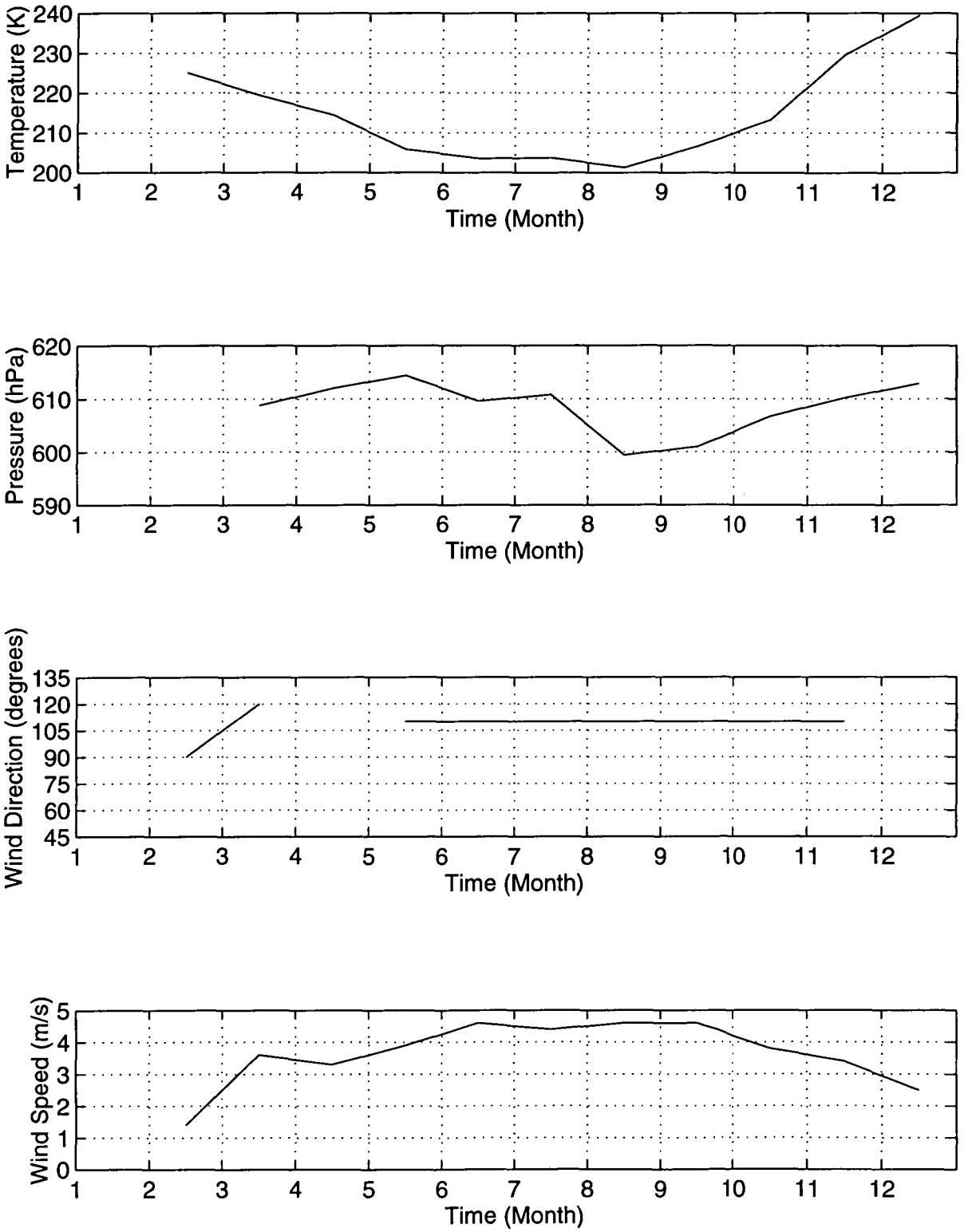

Figure 3.5: Monthly mean surface air temperatures, pressures, wind directions and wind speeds at Sovietskaya, 1958. No observations were made during the month of January, and, as shown by these figures, other data are also missing; surface pressures during February and wind directions during April.

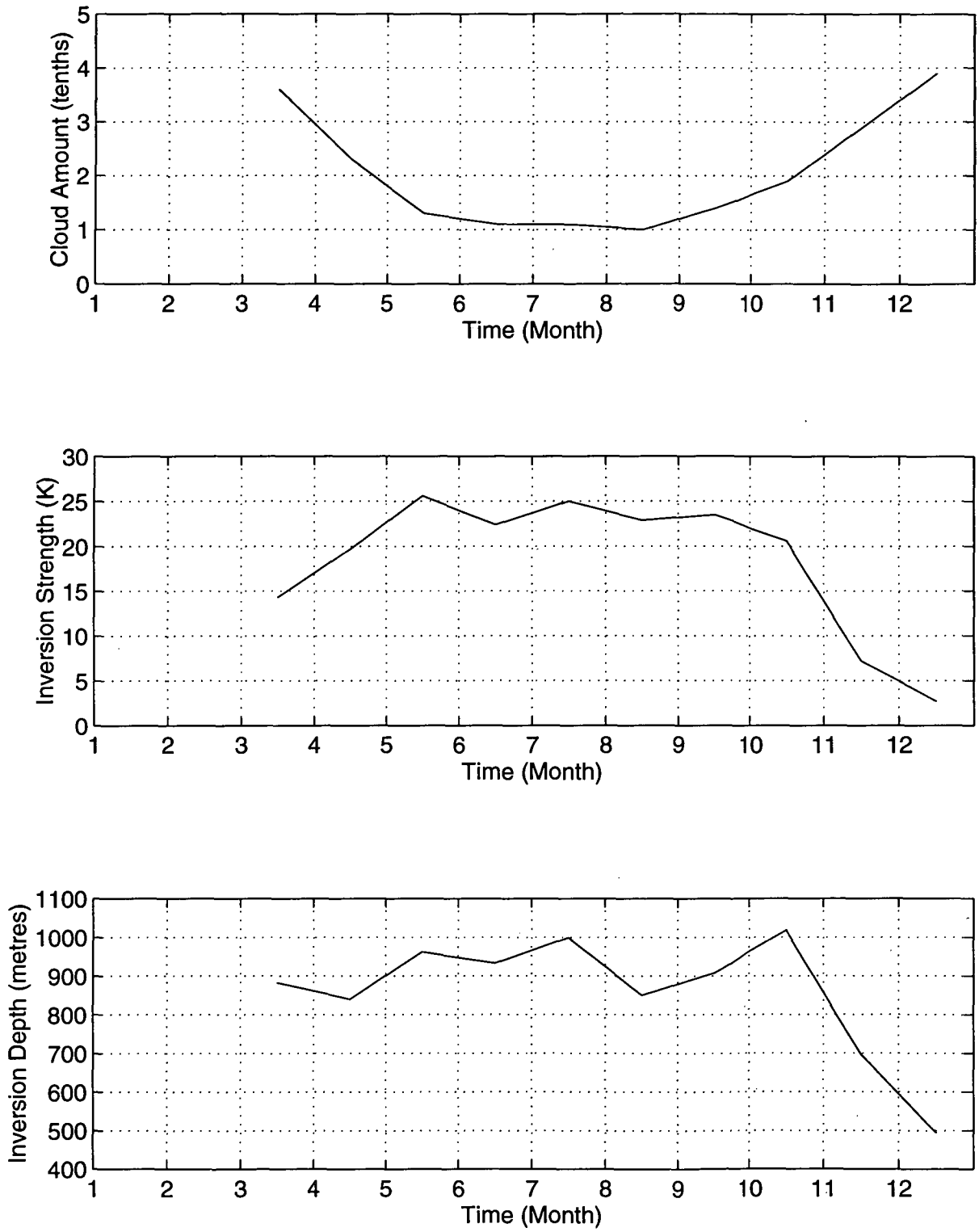

Figure 3.6: Monthly mean cloud amounts, inversion strengths and inversion depths at Sovietskaya, 1958. Observations of these parameters were not made during January and February.

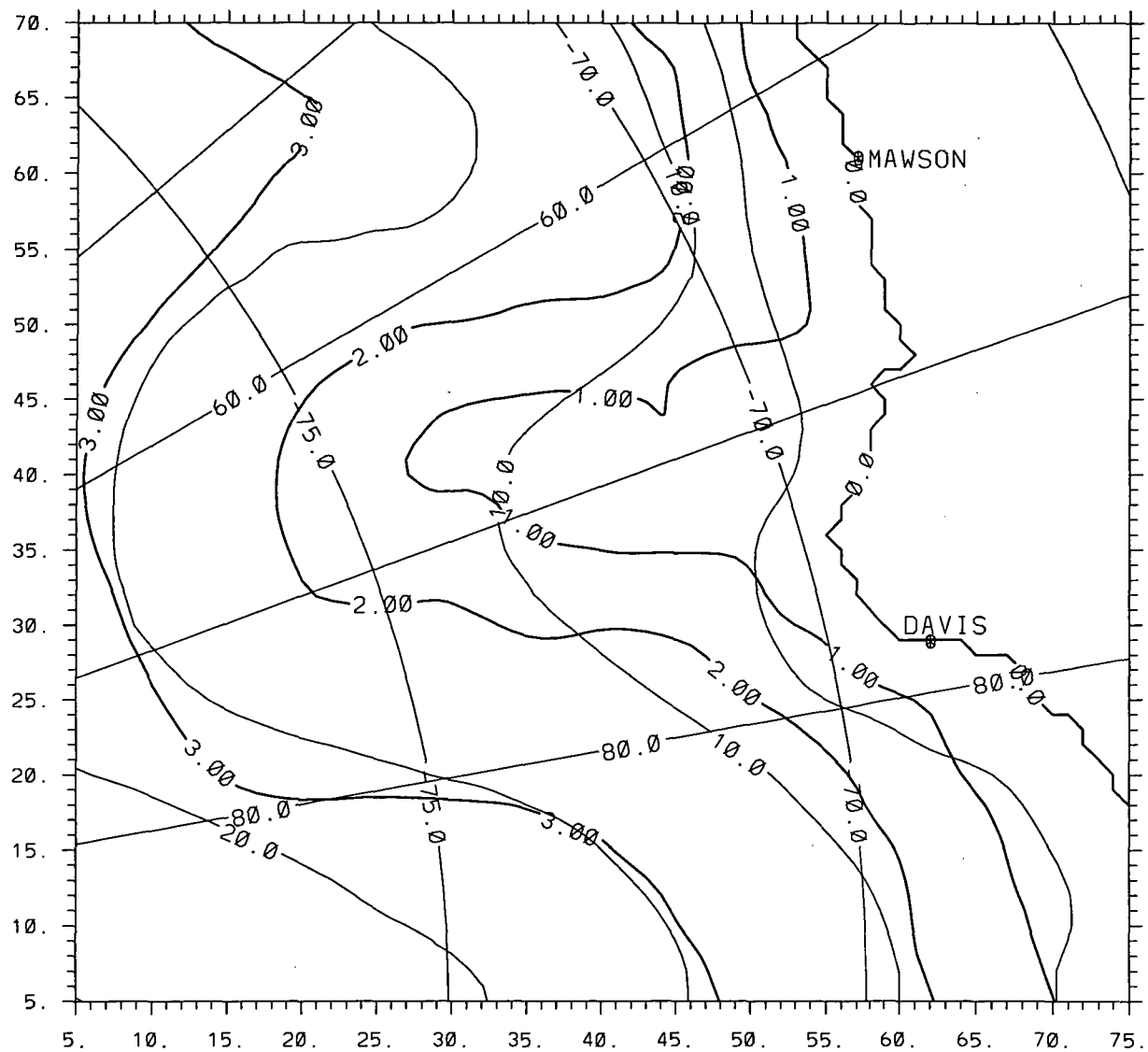

Figure 3.7: The mean winter inversion strength pattern over the Lambert Glacier Basin region, extracted from Phillpot and Zillman (1970) . (Thin) contour intervals are 5°C, and terrain elevation (thick) contour intervals are 1 kilometre. Latitudes and longitudes are also shown. The tick marks on the borders of this figure represent 20 kilometre spacings. The x- and y-coordinates are grid points corresponding to the grid used for numerical modelling of the atmosphere. This is explained in more detail in Chapter 4.

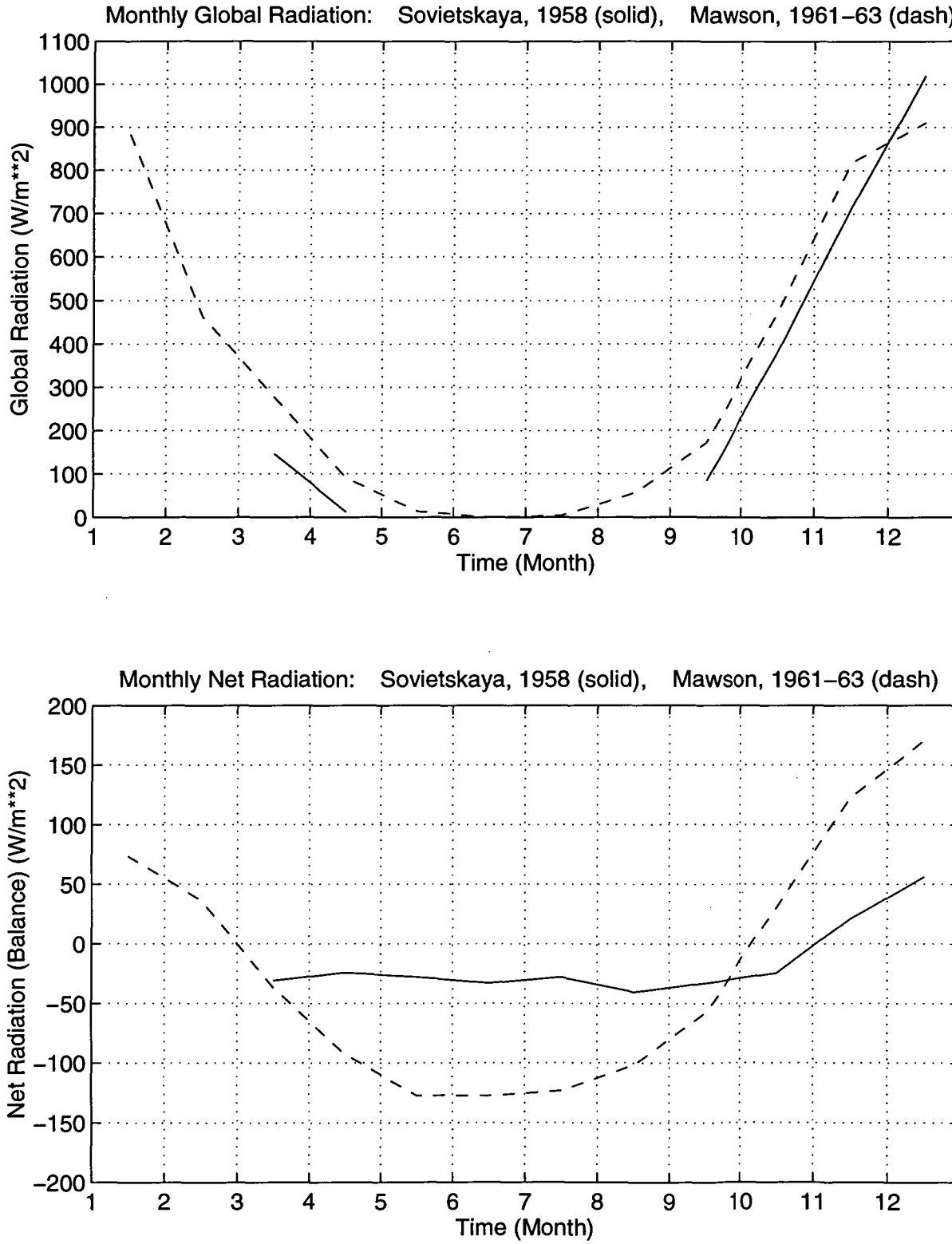

Figure 3.8: Comparison of monthly mean global and net radiation values at Sovietskaya (1958) (solid line) and Mawson (1961-63) (dash). The Sovietskaya data are from Dalrymple (1966) and the Mawson data are from Weller (1967) .

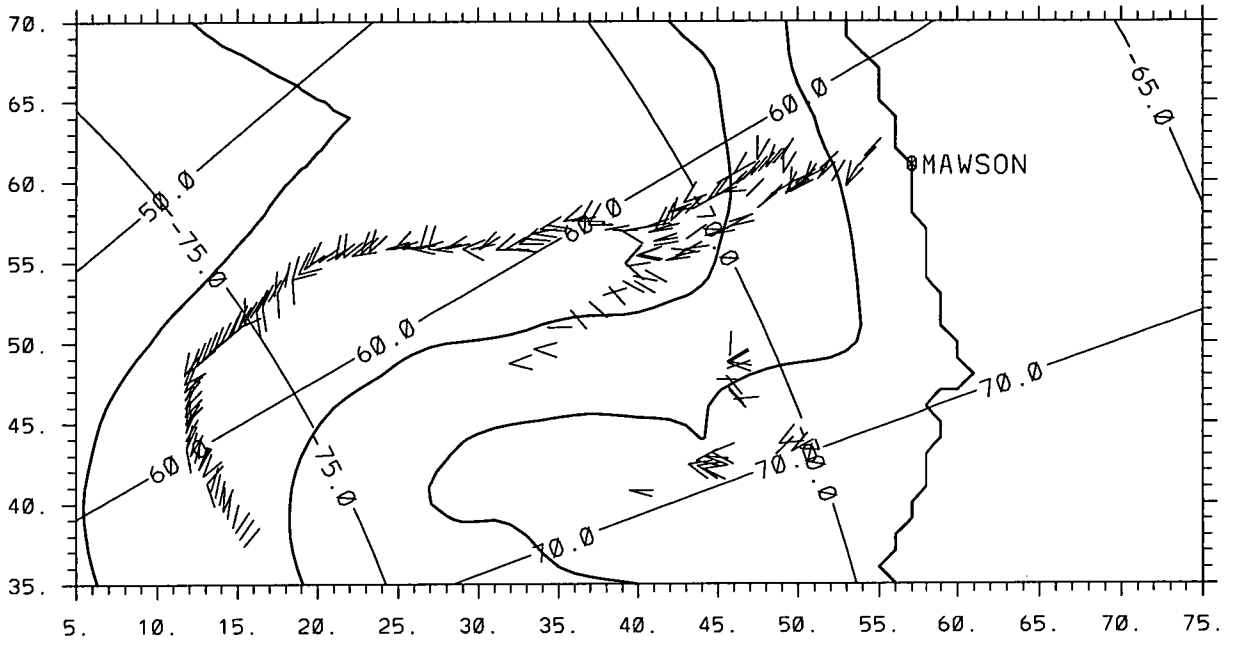

Figure 3.9: Sastrugi orientations south of Mawson, compiled from several sources: Allison and Higham (1993, traverse, personal communication), Allison (1993, observations from helicopter flights, personal communication), Mather (1960) and Mather (1962) . These data are compared with numerical modelling results in Chapter 6. The tick marks on the borders of this figure represent 20 kilometre spacings. The x- and y-coordinates are grid points corresponding to the grid used for numerical modelling of the atmosphere. This is explained in more detail in Chapter 4.

3.4 DEFINITIONS

Antarctic Upper Wind (AUW), Surface and Radiosonde data at Mawson and Davis are analysed in Sections 3.5 and 3.6 respectively. Also examined are relationships between different wind types (defined below) and corresponding values of meteorological parameters; temperature, pressure, wind direction, wind speed, visibility, total cloud amount, low cloud amount, specific humidity (mixing ratio) and lapse rate.

The period of measurement of these data varies between stations. Table 3.2 shows when data at each station are available.

The term "day" is used to refer to measurements of winds made at each station from 0600 to 1800 local time, and "night" refers to measurements made from 1800 to 0600 local time at each station.

The following terms are defined because they are used extensively as classification of wind types in the analyses throughout this chapter.

The term "katabatic" is defined as a wind that has a component of downslope flow (due to relatively dense air being acted upon by gravity) and also has a near-surface jet, such that the wind speed measured at the level nearest the surface is greater than the wind speed at the adjacent level above. Generally, the low-level wind maximum is in the lowest 100 metres of the atmosphere, but the AUW data set only has one measured level below about 370 metres, as shown by Table 3.3.

The analyses of "katabatic" winds (and related wind types: "katabatic-blizzard" and "katabatic-non-blizzard") are not carried out for Davis station because it is not situated on or at the base of sloping terrain and is therefore not subject to downslope air flow. Davis is in the Vestfold Hills and is approximately 10 kilometres north of the Sorsdal Glacier and approximately 25 kilometres west of the Ingrid Christensen Coast, the only nearby slope of significance. The terrain surrounding Davis consists of bare rock, lakes and fjords.

In contrast, Mawson is located at the foot of an ice slope, and such a lo-

cation can be considered typical in regard to katabatic winds and strong slope winds, comparable with other Antarctic locations such as Mirny, Casey, Dumont d'Urville, Port Martin and Cape Denison.

"Downslope" winds are those with a strong component of flow downslope, regardless of features such as a near-surface jet. "Katabatic" winds are a subset of these downslope winds.

"Upslope" winds may or may not possess a jet, as long as the flow is upslope. These are associated with weak anabatic effects during summer and with strong cyclonic winds that oppose the drainage flow at Mawson. "Upslope" and "downslope" wind occurrences add to give 100% for each month.

Blizzard winds usually refer to strong winds accompanied by blowing snow, but here, the term "blizzard" refers to wind speeds at the surface that equal or exceed 15 m/s, irrespective of whether blowing snow is observed.

"Calm" is defined to be when the wind at the lowest level of the profile has zero velocity.

"Katabatic-blizzard" (kat-blz) is defined as a katabatic jet that has a wind speed greater than or equal to 15 m/s.

"Katabatic-non-blizzard" (kat-non-blz) is defined as a katabatic jet that is below blizzard strength.

"Blizzard-non-katabatic" (blz-non-kat) is defined as a wind of blizzard strength that does not have the characteristic near-surface "katabatic" jet. This wind type may or may not flow downslope.

"Katabatic-blizzard" and "katabatic-non-blizzard" winds are mutually exclusive subsets of "katabatic" winds. Also, "katabatic-blizzard" and "blizzard-non-katabatic" winds are mutually exclusive subsets of "blizzard" winds.

In cases when "average" is referred to, the characteristics of the wind have not been used to place the wind in a category, and all valid data at the particular station are used.

Wind direction is abbreviated to "WD", and wind speed to "WS". Also, lapse

Wind type	Surface Wind Speed	Near-surface jet	Downslope flow
Katabatic	—	Y	Y
Blizzard	≥15m/s	N	N*
Calm	0	(N/A)	(N/A)
Kat-blz	≥15m/s	Y	Y
Kat-non-blz	<15m/s	Y	Y
Blz-non-kat	≥15m/s	N	N*

Table 3.4: Definition of wind types, used in analyses of data recorded at Mawson and Davis stations, throughout Section 3.5 and 3.6.
(N/A) denotes Not Applicable.
* These winds may or may not flow downslope; they are not defined using this criteria. See text of Section 3.4 for more information.

rate is abbreviated to either "Lapse" or "Lap". It is calculated as the negative of the change in temperature over the change in height; a stable atmosphere (inversion) has a negative lapse rate.

$$Lapserate = -\frac{\Delta T}{\Delta z} \tag{3.1}$$

3.5 COASTAL CLIMATE: MAWSON

The climatologies of Mawson and Davis presented here are based on the various wind types defined in Section 3.4. Instead of analysing only mean monthly values corresponding to the average wind, these more detailed analyses are useful for examining the characteristics of different types of surface winds.

The climatology of Mawson station is not specifically discussed, because it has been presented in the past, for example, Streten (1990) . Conclusions are drawn about the origins of winds and a picture of katabatic, blizzard and calm winds is developed. These analyses are expanded upon in Chapters 7 and 8, where surface winds are related to different synoptic conditions.

The climatology of Davis station is discussed briefly to demonstrate the differences between atmospheric conditions at this East Antarctic coastal station, that is not subject to katabatic winds, and a site such as Mawson, that is subject to frequent katabatic flow.

Complete analyses of winds at Mawson and Davis stations are presented in Dare (1995) .

The solid lines representing meteorological fields corresponding to "average" winds in Figures 3.11 to 3.18 can be regarded as the climatological values of these fields, while the other line styles (defined in each figure) represent the mean values of fields corresponding to the various wind types defined in Section 3.4.

3.5.1 WIND AT MAWSON

CHARACTERISTICS OF DIFFERENT WIND TYPES AT MAWSON

This discussion draws on the data plotted in Figures 3.11 to 3.18, which show the variations through the year of the monthly mean characteristics of the wind and related variables.

The mean pattern of surface air temperature (solid line, Figure 3.11 shows a minimum in August, corresponding to a period of thermal lag of $\pi/8$, (from the radiation flux), or about 6 or 7 weeks after the solar minimum in June. From

about April to September there are fairly steady mean monthly temperatures (within a range of 5°C), and during summer, December and January, the mean monthly temperatures are also fairly steady, but the intervening equinox periods show rapid changes in mean temperature from one month to the next.

Katabatic wind types are generally cooler than mean and blizzard wind types, with lower temperatures when the katabatic is weaker, as there is less turbulence and mixing and formation of waves and vertical advection are less likely. Blizzard winds have higher than average temperatures during winter but are slightly cooler during summer. Calm conditions allow enhanced cooling during winter but warming during summer; when air advection does not cause a disturbance, the temperature rises or falls according to the radiation conditions, primarily controlled by the solar input.

Blizzard winds are associated with lower pressures, linking them with cyclonic influences. This is shown to be the case for mean katabatic-blizzard winds also, suggesting that usually there is coupling of the cyclonic forcing with the near-surface jet when katabatic winds of blizzard strength are present.

Although blizzard winds are generally associated with lower pressures, the greatest wind speeds are likely to occur as a cyclone moves away to the east, and there is an increase in pressure, not a decrease.

Katabatic-non-blizzard winds show higher than average pressures; these are steady near-surface jets that form when anticyclones are present on the synoptic scale, as noted in Chapter 2. Calm conditions also show higher than average pressures; anticyclones (high pressure systems) characteristically have relatively low wind speeds, and therefore calm wind conditions are likely to occur. This also weakly suggests a relationship between katabatic winds and formation of calm periods. This relationship is explained in Chapter 7.

Katabatic mean monthly wind speeds are stronger than monthly mean wind speeds by only about 1 m/s. The monthly mean wind speeds of the blizzard are substantially stronger, Figure 3.14, almost double the average. Of course, because

blizzard winds were defined to be equal to 15 m/s and greater, the monthly mean speeds would be larger than the average, which is below this limit.

Blizzards winds can be divided into the subsets, katabatic-blizzard and blizzard-non-katabatic. These reveal in Figure 3.14B, that winds of blizzard strength associated with a near-surface jet are stronger than those without, when considering monthly means. Katabatic-blizzard winds only occur a relatively small percentage of the time (see Figure 3.10), but they are consistently the strongest wind type analysed here. Because blizzard winds can be generally associated with cyclonic activity, and not near-surface jets, these data suggest that although the blizzard-non-katabatic type wind is strong and due to cyclonic forcing, the coupling between the cyclonic forcing and a near-surface jet produces even stronger winds. Another explanation for these strong katabatic-blizzard winds is a good supply of negatively buoyant air upwind of Mawson.

Figure 3.11B shows that katabatic-blizzard winds cause warming during the winter months, and cooling during the summer months, but relative to the average, they are cooler than blizzard-non-katabatic winds. This supports Rusin (1961), who stated that winds flowing from the interior are the most severe due to their strength and low temperature, even though cyclonic winds may be stronger. However, the specific wind type analysed here, katabatic-blizzard, shows clearly that a wind of blizzard strength that is characterised by a near-surface jet is stronger than that forced by a cyclone alone, at Mawson.

Monthly mean visibilities are well differentiated depending on the type of wind, Figure 3.15. As noted in Chapter 2, the amount of snow transported depends on the supply of snow and on the strength of the wind. When a greater amount of snow is drifting or being blown, the visibility is reduced. There is a general fall in visibility during winter, but as explained in Section 3.5.2, this is probably partly due to the decrease in sunlight, which hampers observations.

The monthly mean specific humidity values, Figure 3.17, show similar patterns to those of total cloud amount, for the respective individual wind types. Kata-

batic and katabatic-non-blizzard winds are drier than average winds, but the katabatic-blizzard winds contain more moisture during the non-summer months. This may occur because there is moisture input from a nearby cyclone, or greater turbulence and mixing may cause moisture to be entrained from the relatively moist maritime air. A weaker, and more steady katabatic jet does not encourage such mixing and therefore flows from south of Mawson, preserving its low moisture characteristic.

The monthly mean lapse rates shown by Figure 3.18 show that the mean situation at Mawson is an unstable column of air. Positive values mean that there is thermal instability, and negative values represent inversions. There is a general increase in stability during the winter months. The most unstable column of air is associated with blizzard winds, again showing that most blizzards are related to cyclones. It is also expected that stronger winds cause more turbulence and mixing than do winds such as katabatic-non-blizzard, and therefore stronger winds inhibit inversion formation, meaning higher lapse rates. However, it is shown in Chapter 7 that this is not the mean situation observed; it varies with season and the type of wind.

These values are monthly means only; statistics related to inversions at Mawson are shown in Figure 3.19. Further investigations of winds and lapse rates are made in Chapter 7.

SUMMARY OF CHARACTERISTICS OF DIFFERENT WIND TYPES

Tables 3.5 to 3.7 summarise the broad seasonal (summer and winter) characteristics of the wind types, defined in Table 3.4, compared with mean conditions.

Blizzard winds are relatively warm and moist and are associated with cyclones that are situated to the northeast of Mawson station, directing air from ESE. The winds are strong and the corresponding cloud amounts are relatively larger. Blizzard-non-katabatic winds are largely influenced by cyclones, with air masses of even higher temperatures and humidities than shown for the blizzard wind

Wind type	Temperature		Pressure	
	Summer	Winter	Summer	Winter
Katabatic	−	−	0	0
Blizzard	0	+	−	−
Calm	+	−	+	+
Kat-blz	−	+	−	−
Kat-non-blz	−	−	+	+
Blz-non-kat	0	+	−	−

Table 3.5: Characteristics of wind types at Mawson, relative to values of parameters corresponding to the average of all winds, summarised from analyses shown in Figures 3.11 and 3.12. A negative (−) sign indicates that the meteorological parameter (corresponding to the wind type in question), is lower than the average value of that parameter for the season in question. For example, this table shows that temperatures recorded, during both summer and winter when katabatic winds are present at Mawson, are lower than the respective seasonal average temperatures. A positive (+) sign indicates a larger than average value.

type.

Katabatic winds bring cool, dry air from over the continent, approaching Mawson from SE. There are fewer clouds and the column of air at Mawson is more stable, thermally. Katabatic-non-blizzard winds are steady near-surface jets, characteristic of katabatic flow. The low wind speeds prevent substantial vertical mixing, which results in low air temperatures and humidities.

Katabatic-blizzard winds seem to be forced to some degree by cyclones, but they also possess some characteristics of the katabatic, apart from the presence of a near-surface jet. These winds may be produced from the coupling of katabatic flow and cyclonic forcing. Such a coupling can explain why this wind type is the strongest analysed here.

DIRECTION FREQUENCIES

The general circulation consists of predominantly westerly winds at 500 hPa throughout the year, except during the short summer period (December to January), when easterlies dominate, as the pressure gradient around the Antarctic

Wind type	Wind speed		Wind direction		Visibility	
	Summer	Winter	Summer	Winter	Summer	Winter
Katabatic	+	+	+	+	+	+
Blizzard	+	+	−	−	−	−
Calm	(N/A)	(N/A)	(N/A)	(N/A)	+	+
Kat-blz	+	+	−	−	−	−
Kat-non-blz	−	−	+	+	+	+
Blz-non-kat	+	+	−	−	−	−

Table 3.6: Characteristics of wind types at Mawson, relative to values of parameters corresponding to the average of all winds, summarised from analyses shown in Figures 3.13 to 3.15. A negative (−) sign indicates that the meteorological parameter (corresponding to the wind type in question), is lower than the average value of that parameter for the season in question. For example, this table shows that wind speeds recorded, during both summer and winter when katabatic-non-blizzard winds are present at Mawson, are lower than the respective seasonal average wind speeds. A positive (+) sign indicates a larger than average value.
(N/A) denotes Not Applicable.

Wind type	Total Cloud Amount		Specific Humidity		Lapse Rate	
	Summer	Winter	Summer	Winter	Summer	Winter
Katabatic	−	−	−	−	0	0
Blizzard	+	+	+	+	+	+
Calm	−	−	+	−	+	−
Kat-blz	+	+	−	+	−	+
Kat-non-blz	−	−	−	−	0	−
Blz-non-kat	+	+	+	+	+	+

Table 3.7: Characteristics of wind types at Mawson, relative to values of parameters corresponding to the average of all winds, summarised from analyses shown in Figures 3.16 to 3.18. A negative (−) sign indicates that the meteorological parameter (corresponding to the wind type in question), is lower than the average value of that parameter for the season in question. For example, this table shows that total cloud amounts recorded, during both summer and winter when katabatic winds are present at Mawson, are lower than the respective seasonal average total cloud amounts. A positive (+) sign indicates a larger than average value.

continent is reduced with increased solar radiation flux. These patterns are shown in Dare (1995), but for conciseness, only January and July monthly mean percentage occurrences of wind directions from the surface to 500 hPa at Mawson are included here, Figure 3.20.

During the summer months,the Ekman spiral is found to exist up to the 850 hPa level. The veering of wind direction from one level to the next is relatively small, and can be accounted for by influences of surface friction. It appears that there is are "direct" influences between consecutive levels, so that the most frequent wind directions at one level are similar to those at an adjacent level.

During the remainder of the year the pattern is less straight-forward. The structure of the atmosphere between the surface and 500 hPa differs from that observed during summer for three main reasons. Firstly, inversions are more common, and stronger, during winter and these influence the change in mean wind direction between levels. The surface wind regime can be somewhat isolated from the synoptic scale flow in the presence of an inversion, Loewe (1974), Lettau and Schwerdtfeger (1967).

Secondly, upwind of Mawson there exist stronger inversions than at the coast and there is stable stratification of the atmosphere relatively close to the surface (within the lowest 200 metres), and these characteristics allow near-surface katabatic jets to form. Such winds occur more often during the non-summer months, Figure 3.10 and, as noted in past literature (see Chapter 2), they occur independently of the synoptic forcing. Therefore, the relationship between surface and synoptic level winds is less significant when near-surface jets are present.

Throughout the year, the surface wind direction is close to southeast, a consequence of the underlying terrain, the importance of which has been discussed in Chapter 2. The third reason that the relationship between wind directions at different levels during winter is less clear than for during summer is that the general circulation of the upper air during winter has a significant westerly component. This means that a larger change in wind direction must occur between

the surface wind direction (largely influenced by terrain) and that at 500 hPa, during winter.

WIND SPEED PROFILES

Figure 3.21 shows mean January and July vertical profiles of wind speed at Mawson station. Mean "day" and "night" profiles are also shown. These are adequate for demonstrating general seasonal patterns, but complete analyses, for every month of the year, are included in Dare (1995) .

The resolution of the vertical sampling of the sondes, Table 3.3, is not enough to capture detail (such as a wind maximum) below 100 metres.

Diurnal variations occur during summer in the lower atmosphere, due to the radiation flux at the surface. Surface wind speeds are greatest during the night, when air is cool and dense and flows downslope under the effect of gravity. The winter profile does not show significant diurnal variations, but wind speeds at the surface and at 5000 metres are greater than in summer.

DIURNAL VARIATIONS OF TEMPERATURE, WIND DIRECTION AND SPEED

Summer (January) diurnal variations of temperature, wind speed and wind direction for Davis, Mawson, Sovietskaya stations and AWS LGB00, LGB10, LGB20 and LGB59 are shown in Chapter 6. During winter, variations of these parameters do not follow diurnal patterns, due to the absence of significant solar input. Analyses for all months are shown in Dare (1995) .

The general pattern of summer diurnal temperature variation at Mawson (and around coastal East Antarctica) is a maximum during the afternoon, and a minimum during the early morning hours, trailing the solar flux by about 3 hours; thermal lag of $\pi/8$, where π is the wavelength, 24 hours.

The changes in density that occur with temperature changes affect the downslope wind speed. Wind are strongest at around 0600 hours local time, and weakest around 1800 hours local time. Weaker winds are directed more across-slope than

stronger winds.

3.5.2 CLOUD AND VISIBILITY AT MAWSON

Cloud amounts depend on human observations, not on instrument measurements, (as in the case of temperature for example) and there is a lack of sunlight during much of the year, therefore clouds cannot always be observed with great accuracy.

During winter, there is not complete darkness 24 hours of every day at Mawson; the sun is very low on the horizon and the diurnal variation is close to insignificant in terms of heating, but significant in the light it provides for manual observations. It is thought that there is not a diurnal pattern of cloud amount, but due to the diurnal sunlight variation, less cloud is visible to the human eye when there is less light.

Moonlight is important for allowing clouds to be seen over Antarctica during winter, but it is not always present and during such times cloud observations can be hindered. Even given ideal viewing conditions, cloud observations can be subjective.

Vowinckel (1957) noted that the thin haze in the sky observed at high Antarctic latitudes makes it difficult to determine whether the cloud amount is 0 or 10 tenths.

The variation seen throughout the year is less suspect than the diurnal variation; during the winter months there is a decline in the cloud amounts observed, probably partly due to the lack of sunlight. However, the air is drier during winter than summer at Mawson, as shown by the mean monthly specific humidities in Figure 3.17 so less cloud may be expected. Also, the mean monthly pressure is highest during winter, Figure 3.12, meaning that cyclonic systems are less frequent and clouds that are associated with such depressions are not present.

Schwerdtfeger (1970) noted that blowing snow and lack of moonlight during winter nights cause problems in observing cloud cover amounts.

Strong winds and precipitation that occur with storms around coastal areas

can obscure the sky when the particles are lifted and blown by the wind, Wilson (1968). Reduction in visibility due to drifting snow at Mawson during gales was noted by Streten (1968a), but during the summer months this did not necessarily occur because there was not always a plentiful supply of snow. Figure 3.15 shows a decrease in visibility from summer to winter.

The frequency of occurrence of inversions at Mawson is much lower than for over the Antarctic plateau, as demonstrated by Figure 3.19. Mawson station is not located over a plateau region and the strength of inversions when present are relatively small, in comparision with those over the plateau. Levels from the surface up to 600 hPa were considered when the inversion statistics were computed from radiosonde data, but it was found that the mean depths of inversions, when present, at the coast were only around 750 metres.

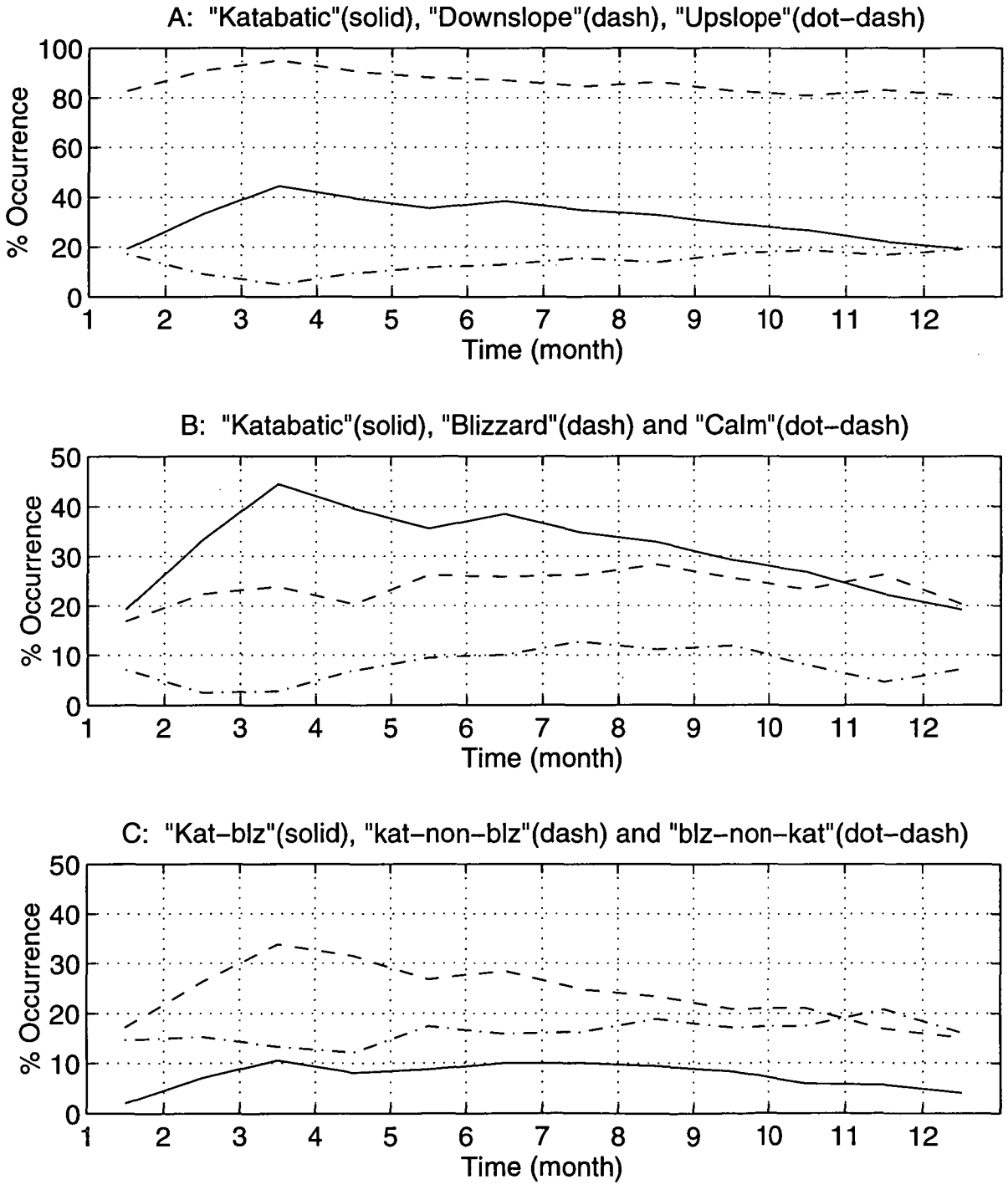

Figure 3.10: Monthly mean occurrences of winds at Mawson. A: katabatic and downslope, B: katabatic, blizzard and calm, C: katabatic-blizzard, katabatic-non-blizzard and blizzard-non-katabatic winds.

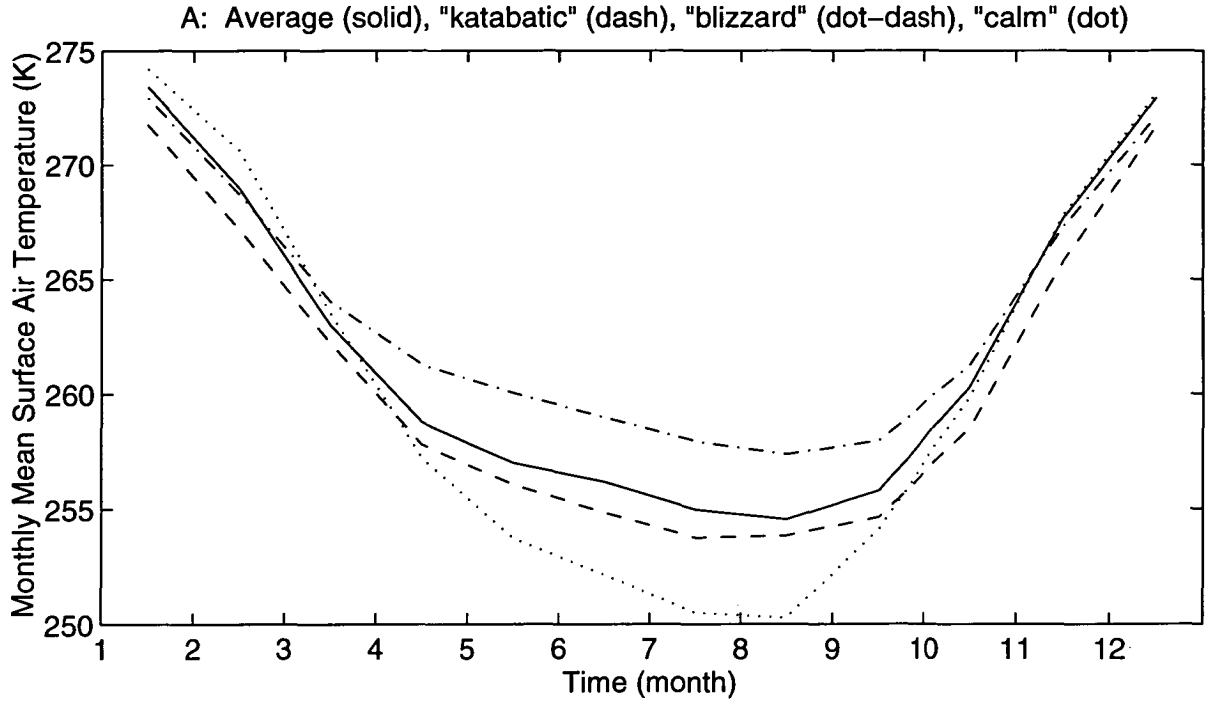

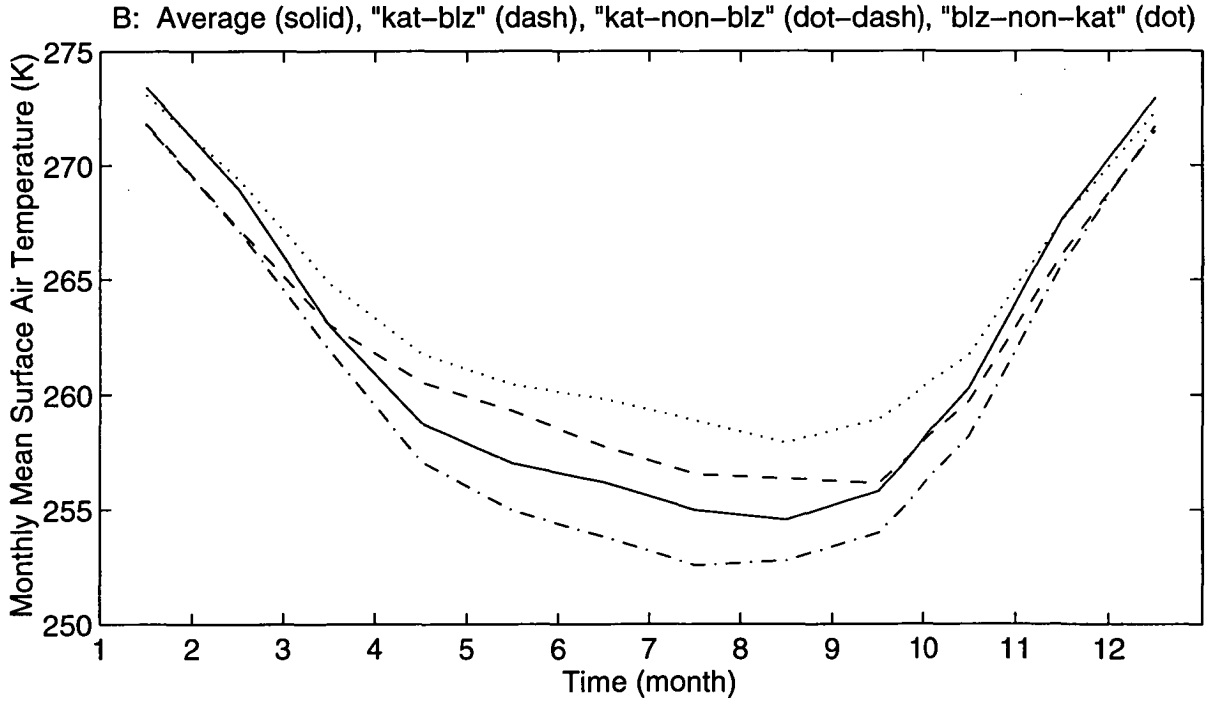

Figure 3.11: Monthly mean surface air temperatures at Mawson for A: average, katabatic, blizzard and calm winds, B: katabatic-blizzard, katabatic-non-blizzard and blizzard-non-katabatic winds. The average is plotted in both A and B to allow easy comparison between the wind types in each.

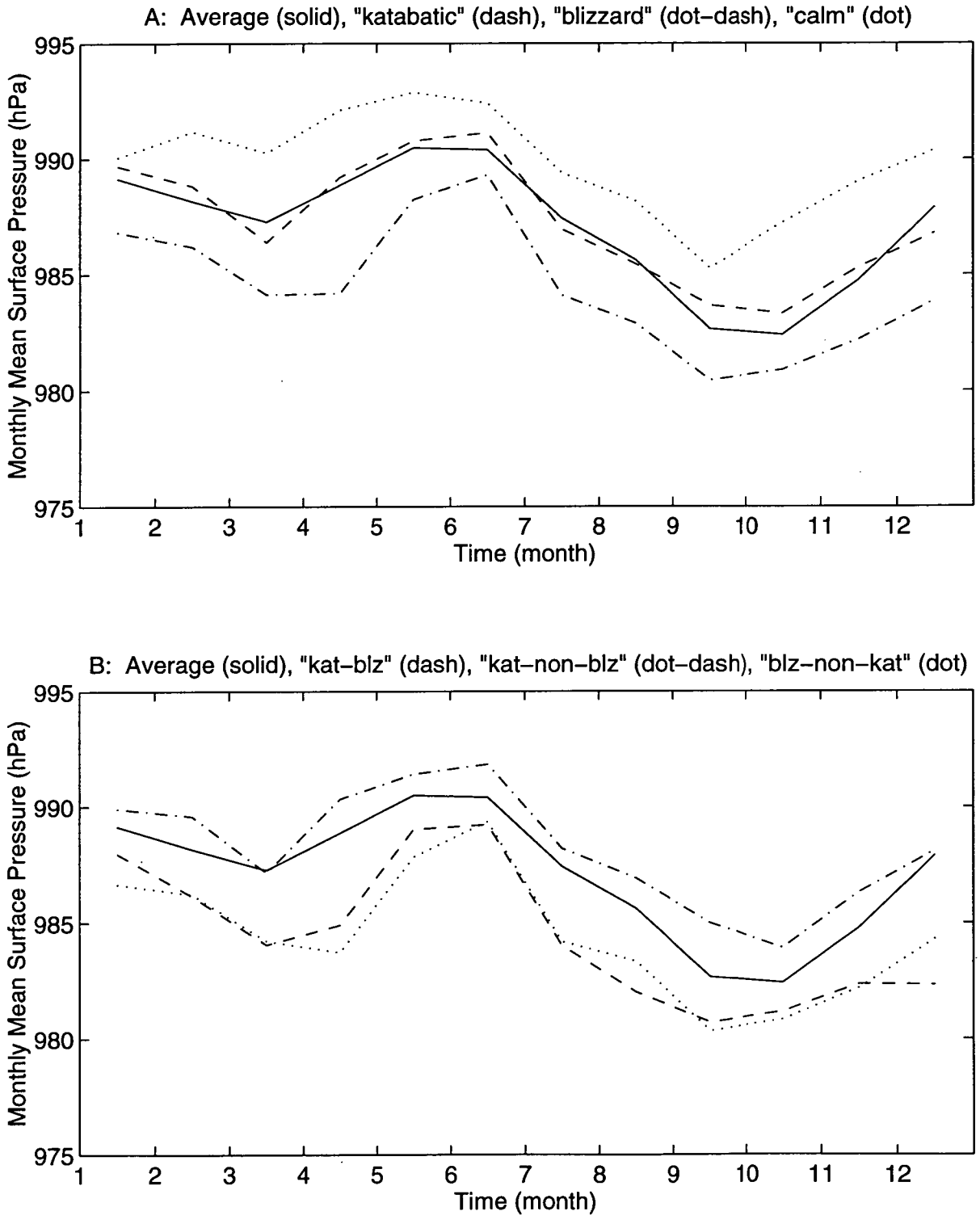

Figure 3.12: Monthly mean surface air pressure at Mawson for A: average, katabatic, blizzard and calm winds, B: katabatic-blizzard, katabatic-non-blizzard and blizzard-non-katabatic winds.

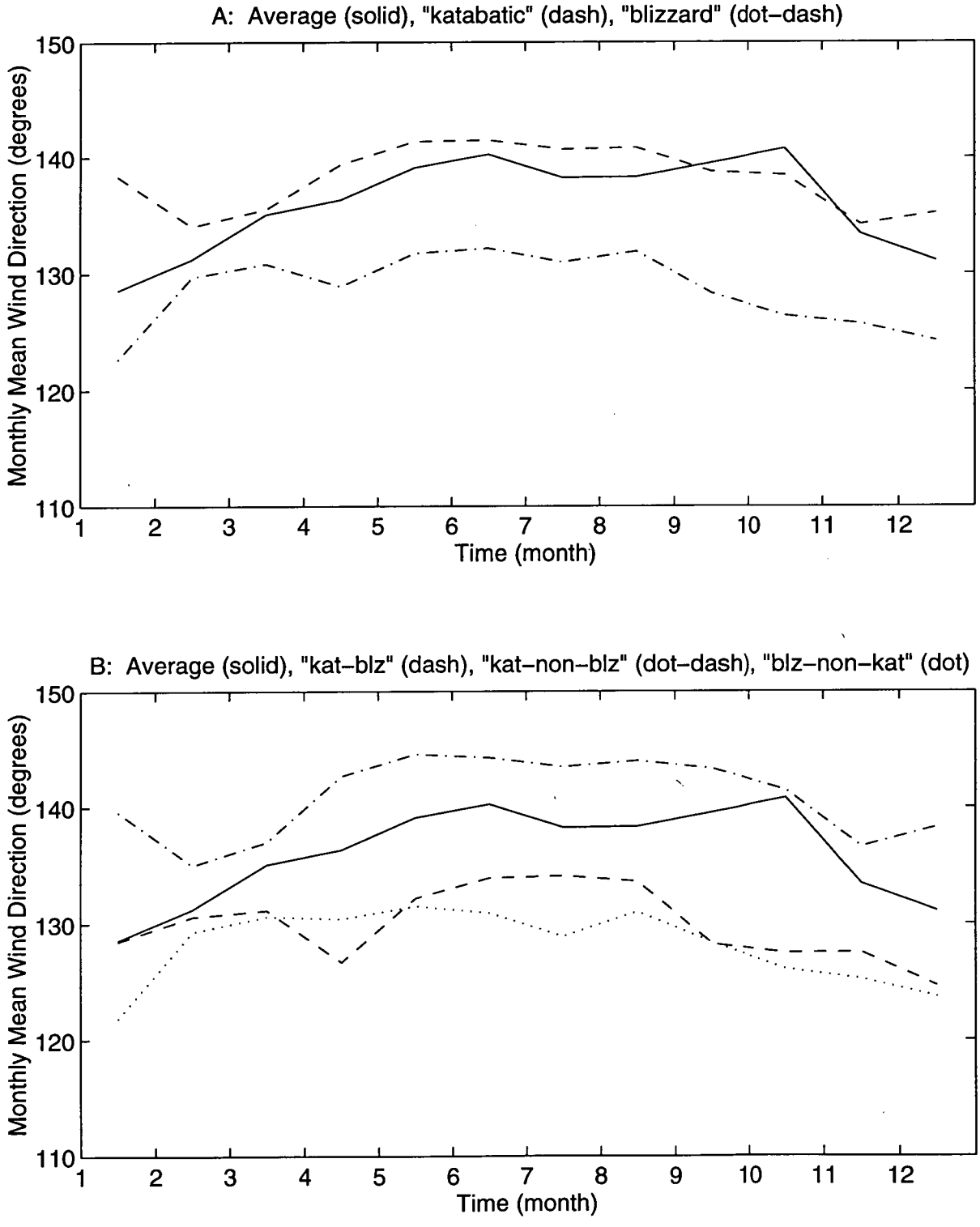

Figure 3.13: Monthly mean surface wind directions at Mawson for A: average, katabatic and blizzard winds, B: katabatic-blizzard, katabatic-non-blizzard and blizzard-non-katabatic winds.

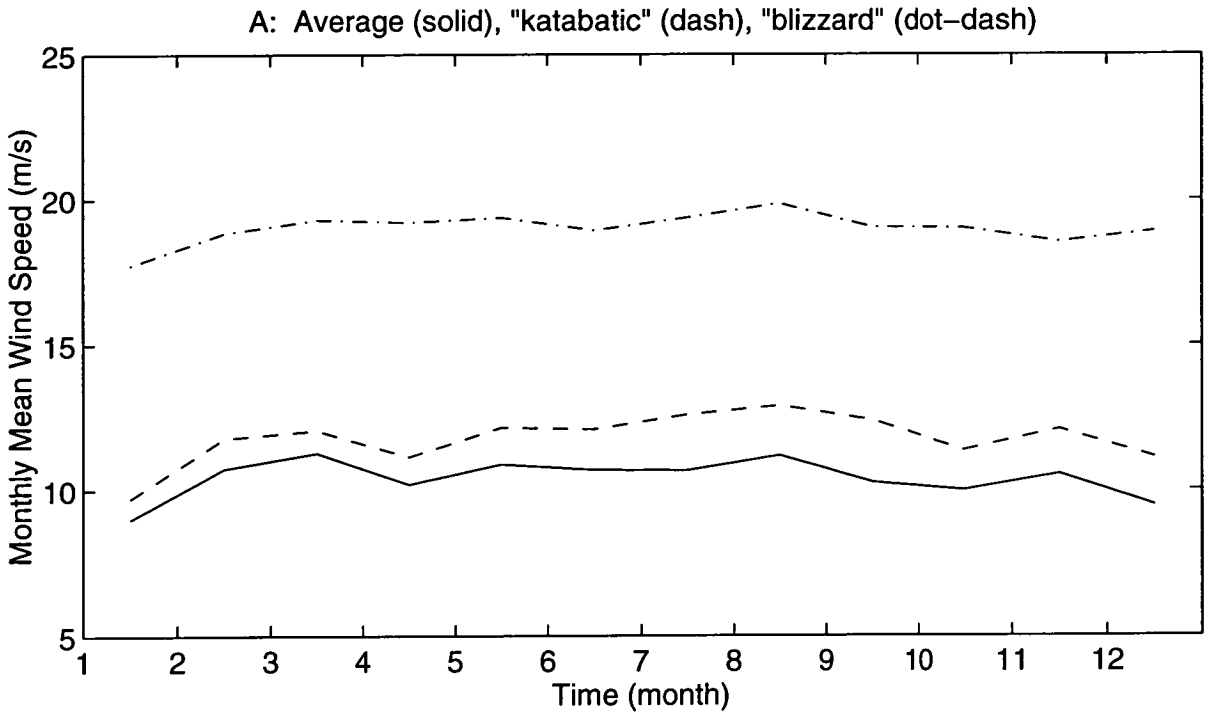

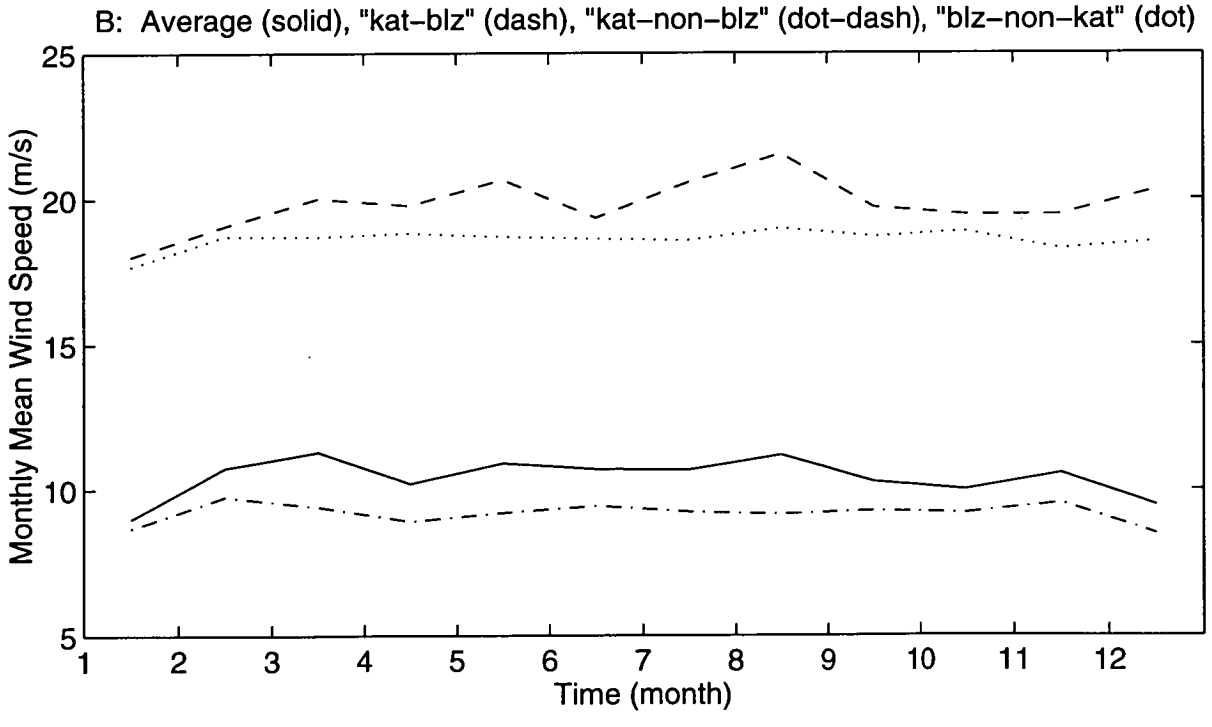

Figure 3.14: Monthly mean surface wind speeds at Mawson for A: average, katabatic and blizzard winds, B: katabatic-blizzard, katabatic-non-blizzard and blizzard-non-katabatic winds.

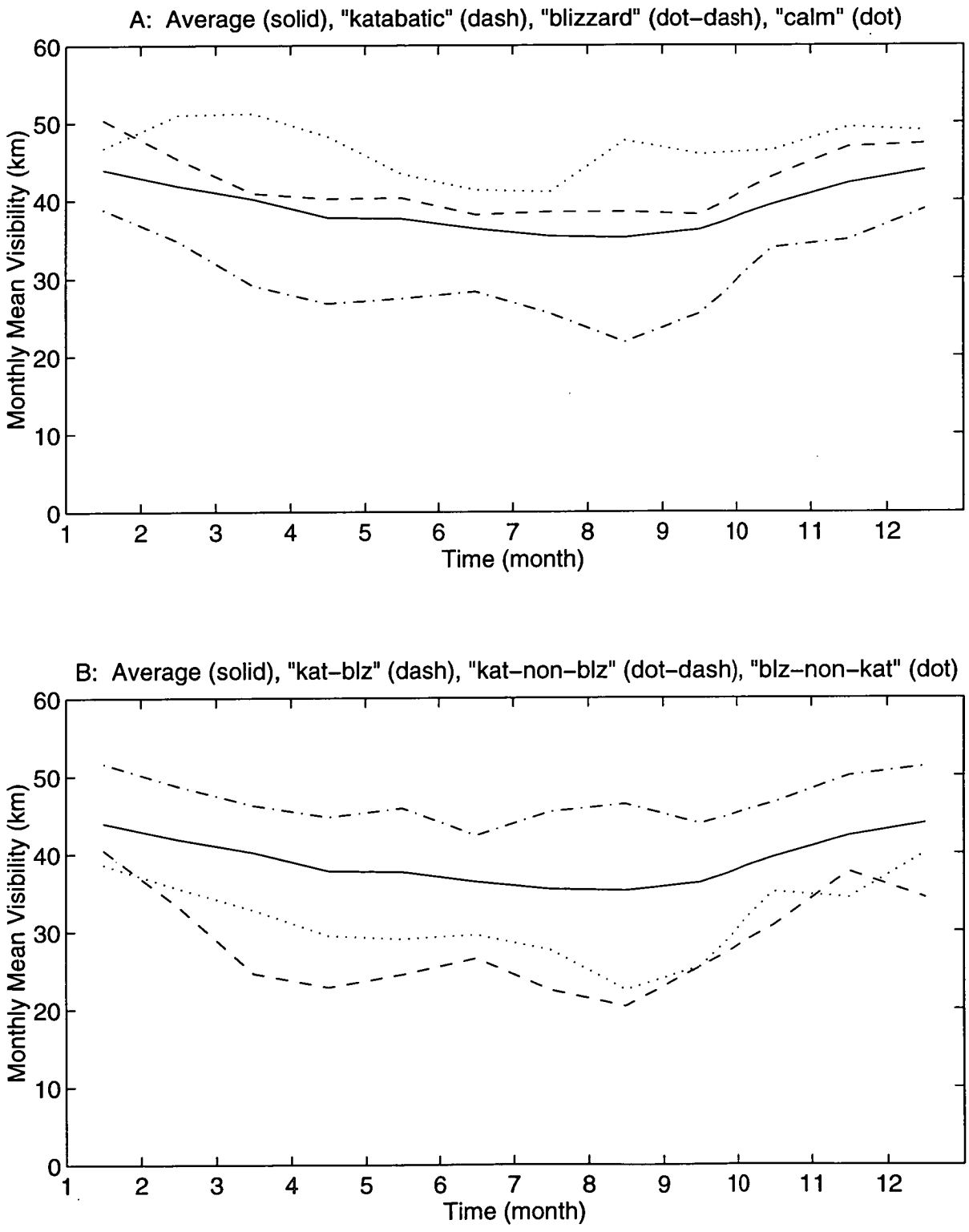

Figure 3.15: Monthly mean visibilities at Mawson for A: average, katabatic, blizzard and calm winds, B: katabatic-blizzard, katabatic-non-blizzard and blizzard-non-katabatic winds.

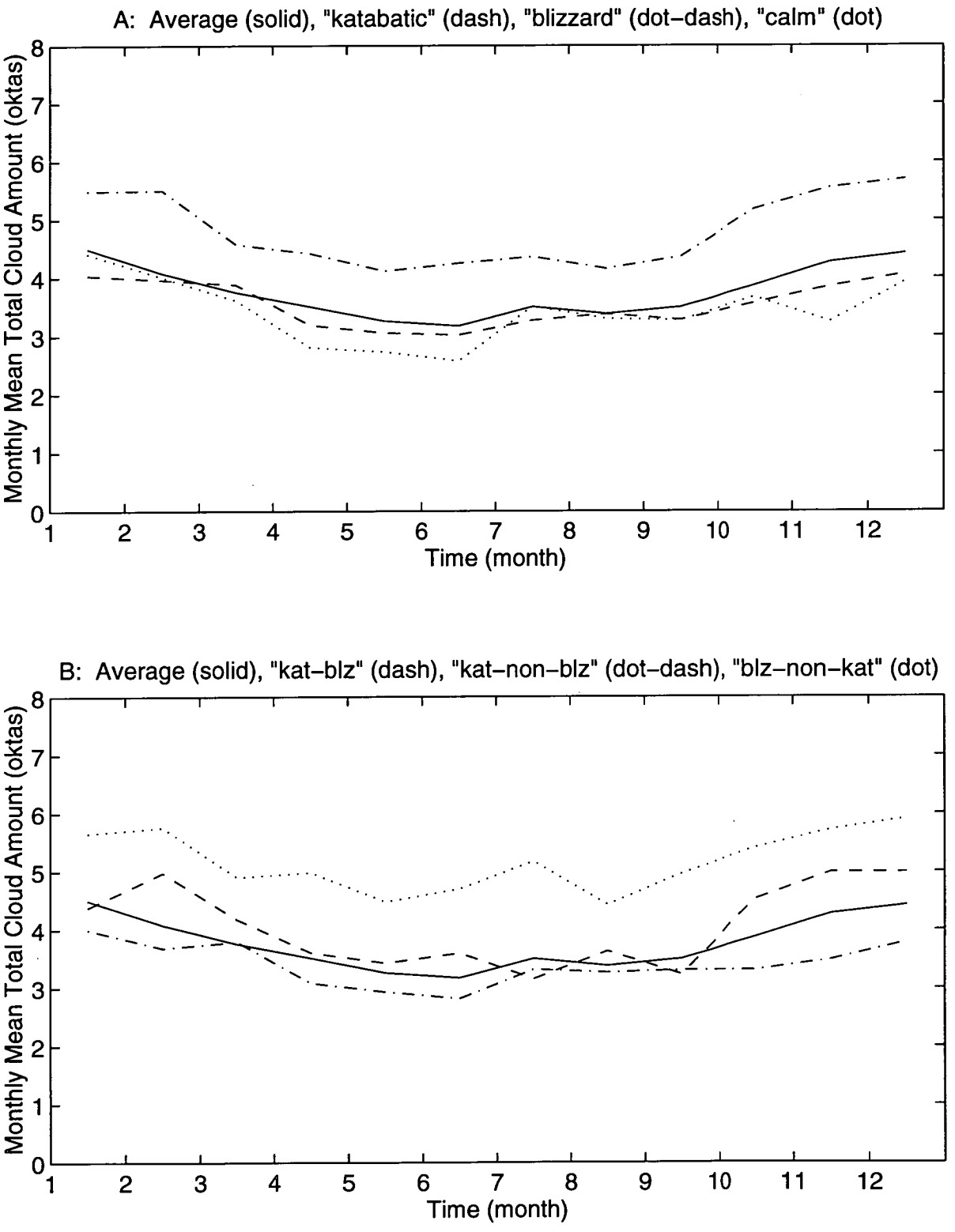

Figure 3.16: Monthly mean total cloud amounts at Mawson for A: average, katabatic, blizzard and calm winds, B: katabatic-blizzard, katabatic-non-blizzard and blizzard-non-katabatic winds.

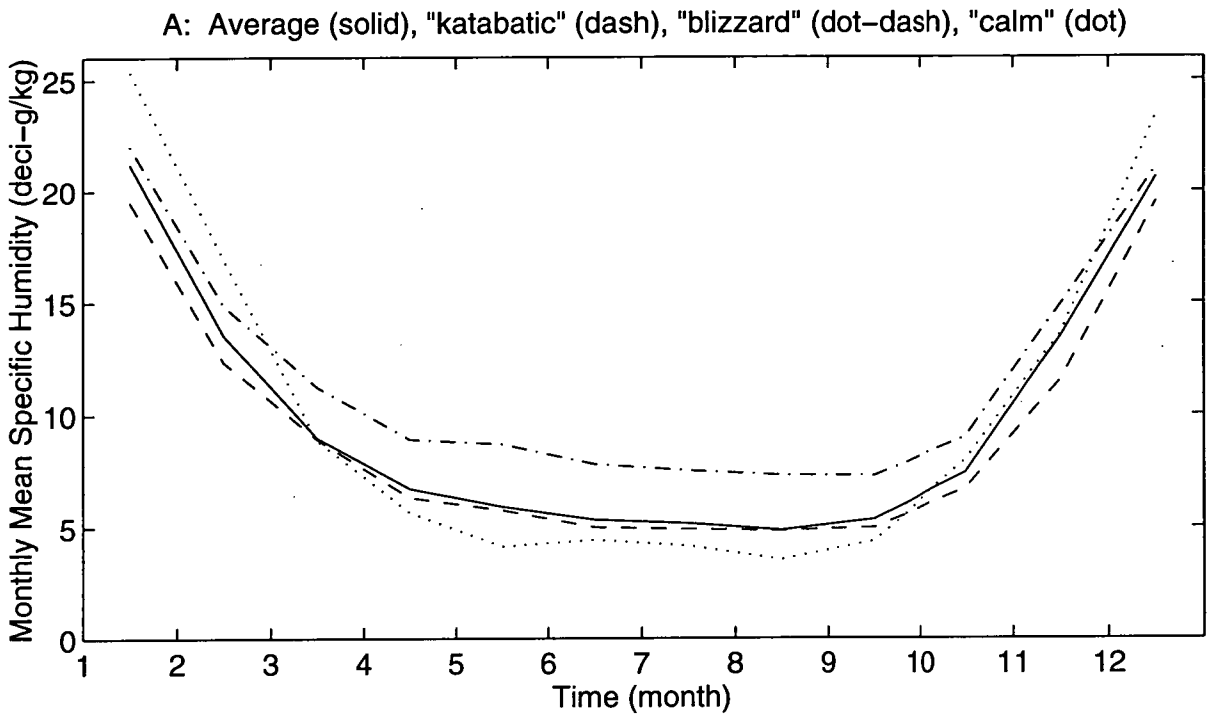

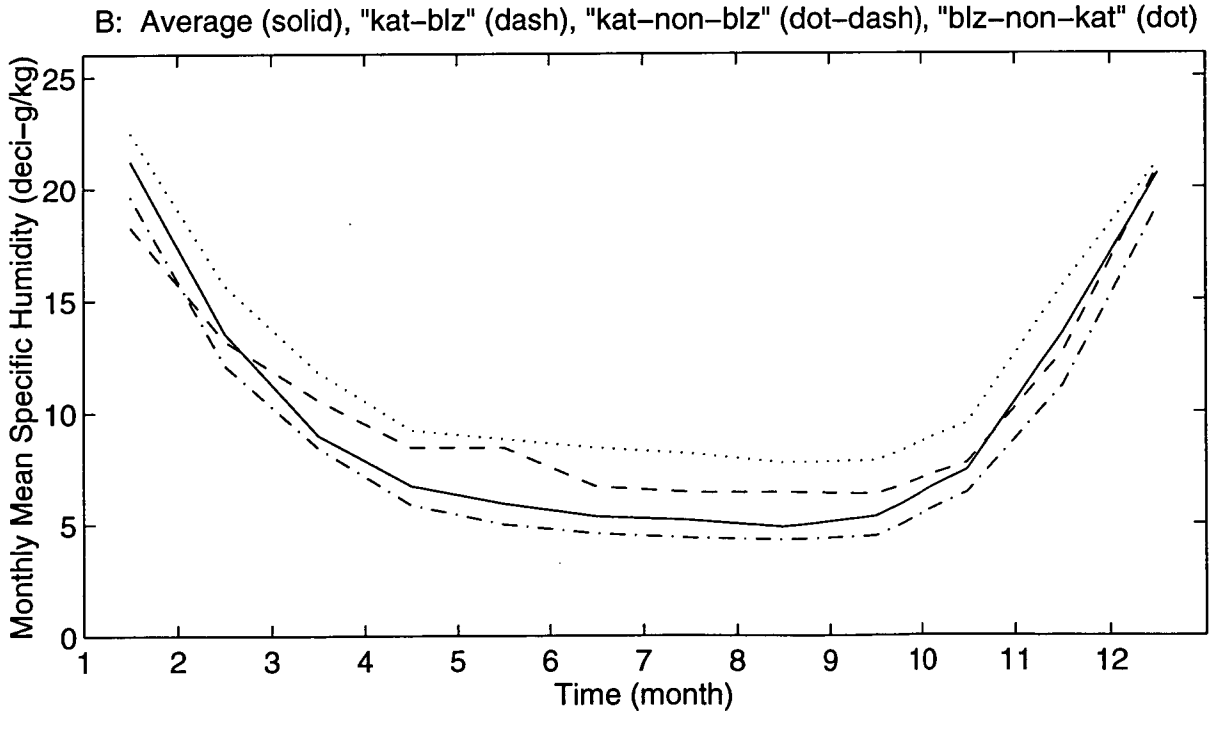

Figure 3.17: Monthly mean specific humidity at Mawson for A: average, katabatic, blizzard and calm winds, B: katabatic-blizzard, katabatic-non-blizzard and blizzard-non-katabatic winds.

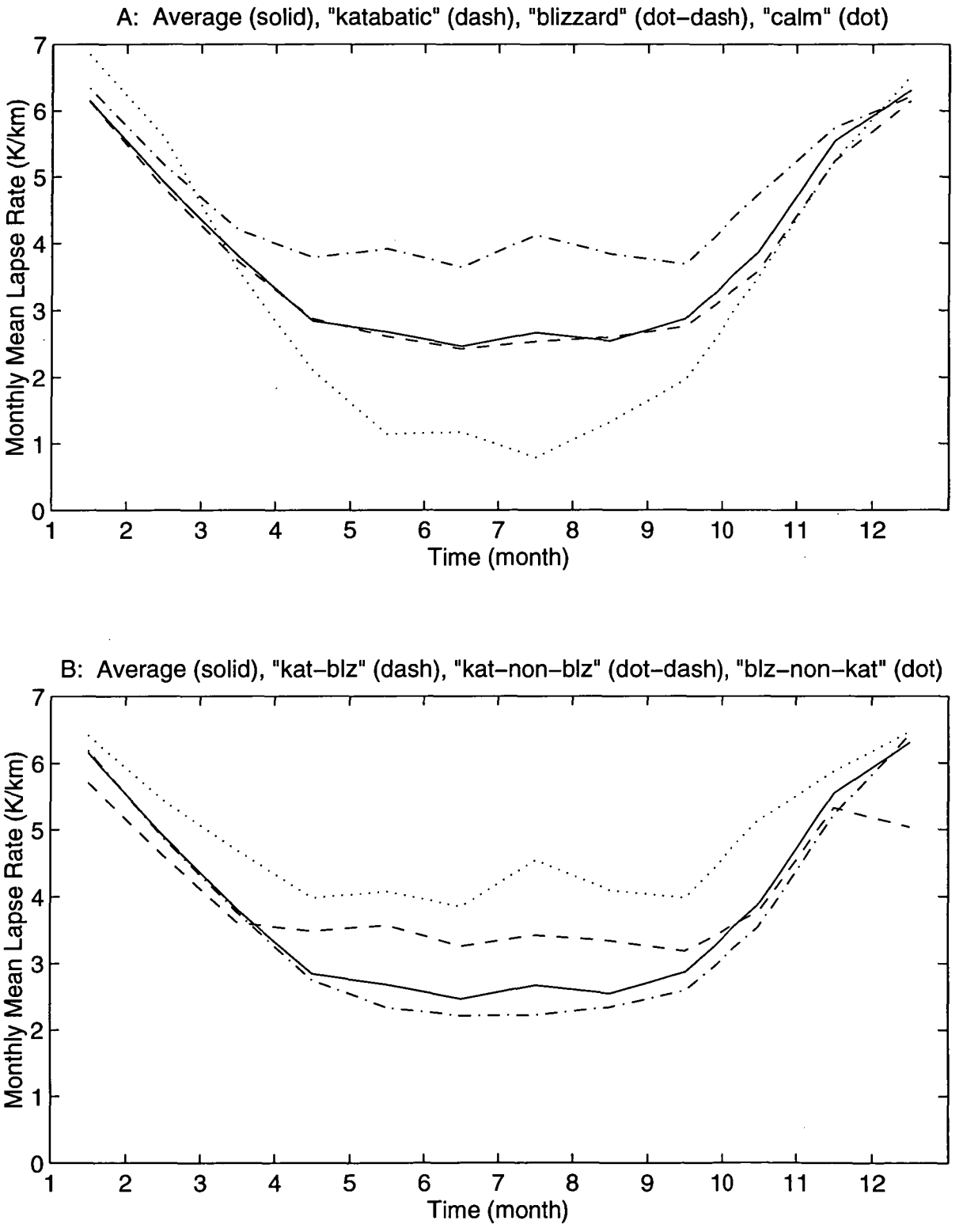

Figure 3.18: Monthly mean lapse rate at Mawson for A: average, katabatic, blizzard and calm winds, B: katabatic-blizzard, katabatic-non-blizzard and blizzard-non-katabatic winds.

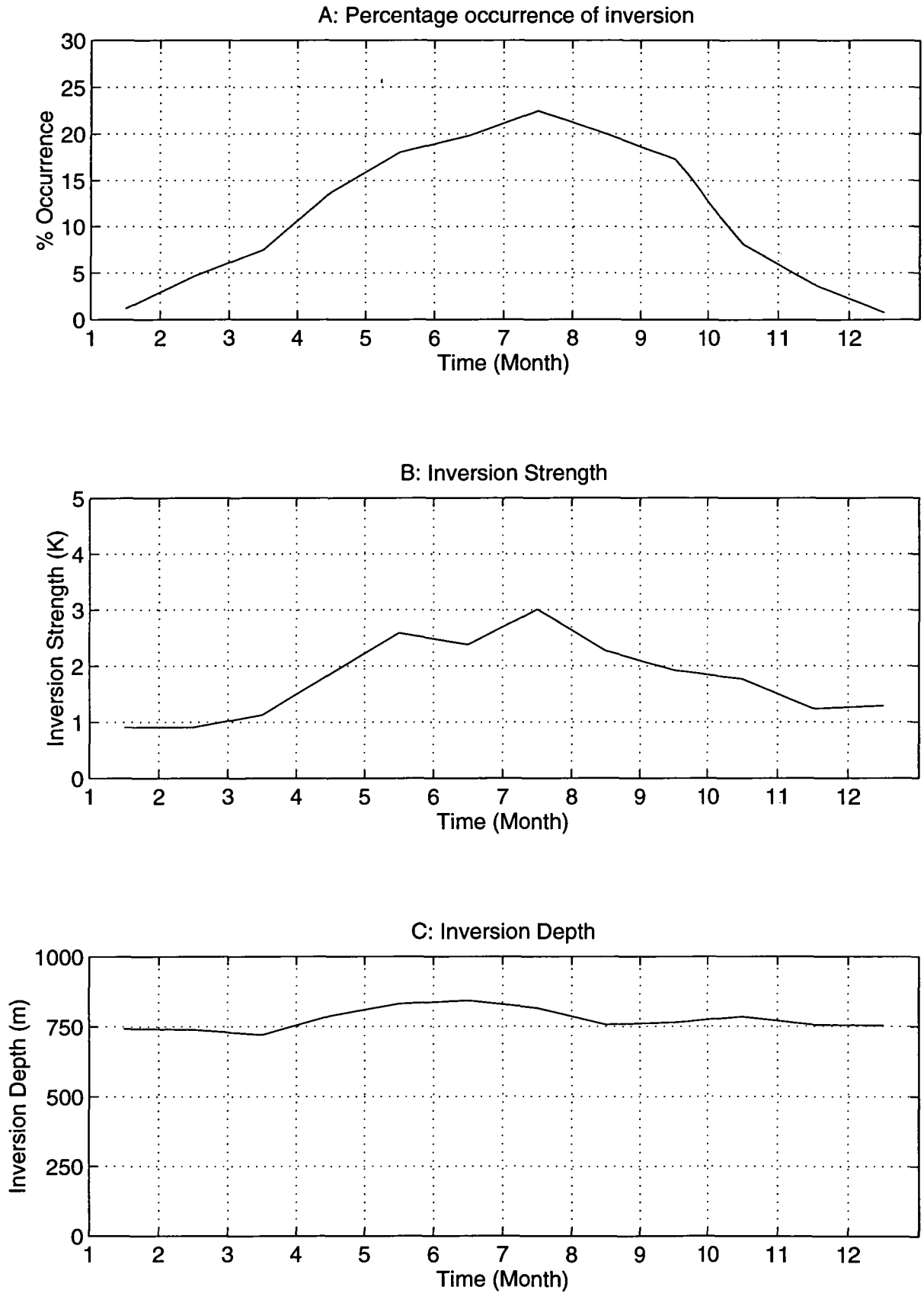

Figure 3.19: Monthly mean inversion parameters at Mawson. A: Percentage occurrence of inversion, B: Inversion strength when present, C: Inversion depth when present.

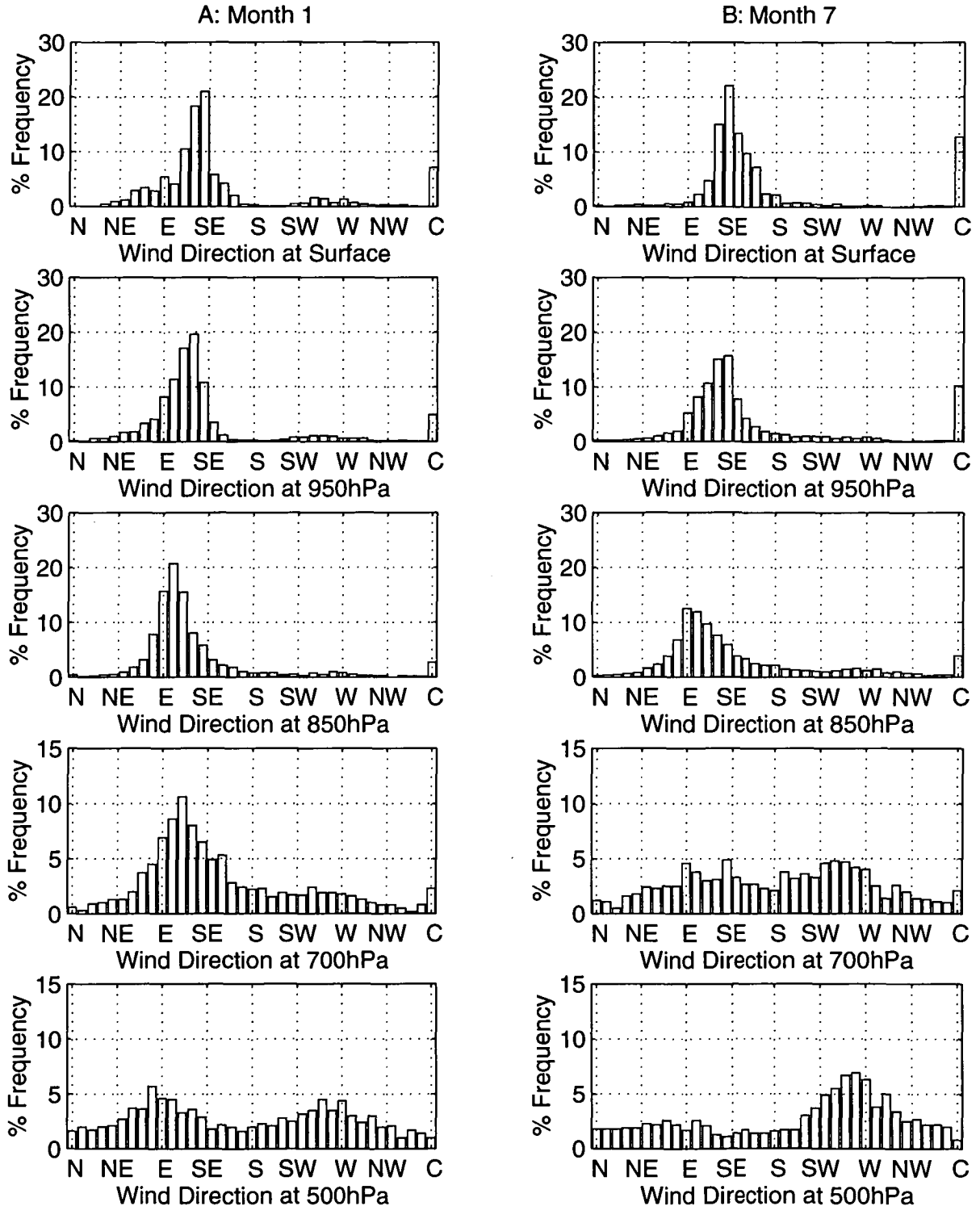

Figure 3.20: A: January, B: July percentage frequencies of wind directions at the surface, 950hPa, 850hPa, 700hPa and 500 hPa for average winds at Mawson.

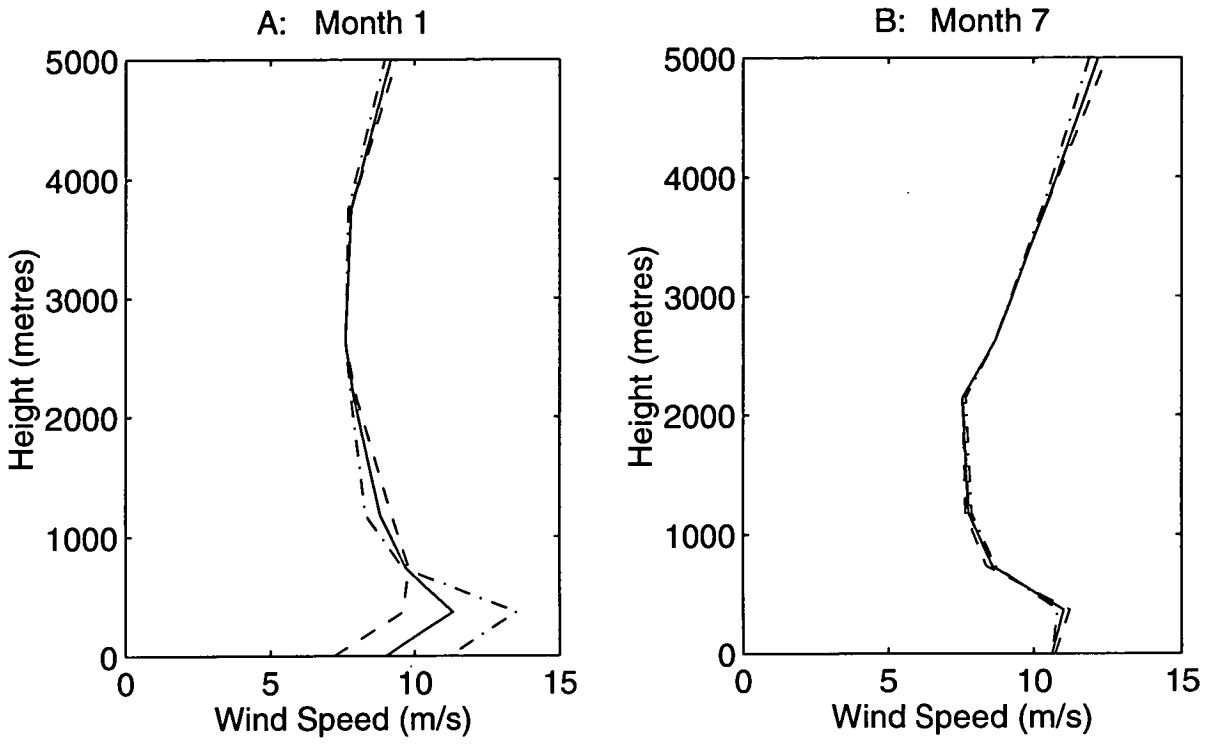

Figure 3.21: Monthly mean vertical wind speed profiles; daily mean (solid line), "day"(dash), "night"(dot-dash), A: January, B: July, at Mawson.

3.6 COASTAL CLIMATE: DAVIS

This section contains a brief discussion of the climate at Davis station. Characteristics of winds are compared with those at Mawson station. Further analyses, and numerical modelling, of weather at Mawson station are discussed in Chapters 7 and 8. Apart from references in Chapter 6, regarding verification of model results, the climate of Davis is not discussed beyond this section.

As noted in Chapter 2, Davis station is not subject to katabatic winds because it is situated several kilometres from the ice slope, and the immediate surroundings are comprised of rock and lakes, whereas Mawson is located at the base of an ice slope.

Throughout the year, the percentage occurrences of blizzards at Davis station are around 5%, substantially less frequent than at Mawson station, where percentage occurrences are 20 - 30%.

Mawson and Davis stations are subject to similar synoptic influences throughout the years; monthly mean surface pressures are shown in Figures 3.12 and 3.24. The strength of the 500 hPa level winds are also similar for Mawson and Davis during summer and winter respectively, Figures 3.21 and 3.33. However, there are some small differences in wind directions at the 500 hPa level, during winter, as shown by comparison between Figures 3.20 and 3.32.

Surface wind speeds at Mawson are greater than surface wind speeds at Davis by about 5m/s. These significant differences in monthly mean surface wind speeds between the two stations, despite similar synoptic forcings, show that the terrain has an important influence on surface winds.

The mean monthly strengths of blizzard winds at Davis are weaker than those at Mawson. This shows that the terrain has some effect, even when a cyclone is largely controlling the surface wind speed.

The percentage frequency occurrences of wind directions at the surface at Davis cover a wider range than those at Mawson. This is due to the terrain

Wind type	Temperature		Pressure	
	Summer	Winter	Summer	Winter
Blizzard	+	+	−	−
Calm	−	−	−	+

Table 3.8: Characteristics of wind types at Davis, relative to values of parameters corresponding to the average of all winds, summarised from analyses shown in Figures 3.23 and 3.24.
A negative (−) sign indicates that the meteorological parameter (corresponding to the wind type in question), is lower than the average value of that parameter for the season in question. For example, this table shows that temperatures recorded, during both summer and winter when calm conditions are present at Davis, are lower than the respective seasonal average temperatures. A positive (+) sign indicates a larger than average value.

Wind type	Wind speed		Wind direction		Visibility	
	Summer	Winter	Summer	Winter	Summer	Winter
Blizzard	+	+	−	−	−	−
Calm	(N/A)	(N/A)	(N/A)	(N/A)	−	+

Table 3.9: Characteristics of wind types at Davis, relative to values of parameters corresponding to the average of all winds, summarised from analyses shown in Figures 3.25 to 3.27.
A negative (−) sign indicates that the meteorological parameter (corresponding to the wind type in question), is lower than the average value of that parameter for the season in question. For example, this table shows that visibilities recorded, during both summer and winter when blizzard winds are present at Davis, are lower than the respective seasonal average temperatures. A positive (+) sign indicates a larger than average value.
(N/A) denotes Not Applicable.

surrounding Mawson that guides the air flow, but at Davis, the terrain is complex and does not have such an organised channelling effect.

As found with analyses in the previous section, blizzard winds are associated with cyclones offshore, and higher than average wind speeds, temperatures and relative humidities.

Tables 3.8 to 3.10 summarise characteristics of blizzard and calm wind conditions, relative to average (all wind) conditions, at Davis station.

Wind type	Total Cloud Amount		Specific Humidity		Lapse Rate	
	Summer	Winter	Summer	Winter	Summer	Winter
Blizzard	+	+	+	+	−	+
Calm	+	+	+	−	+	−

Table 3.10: Characteristics of wind types at Davis, relative to values of parameters corresponding to the average of all winds, summarised from analyses shown in Figures 3.28 to 3.30.
A negative (−) sign indicates that the meteorological parameter (corresponding to the wind type in question), is lower than the average value of that parameter for the season in question. For example, this table shows that visibilities recorded, during winter when calm conditions are present at Davis, are lower than the respective seasonal average temperatures. A positive (+) sign indicates a larger than average value.

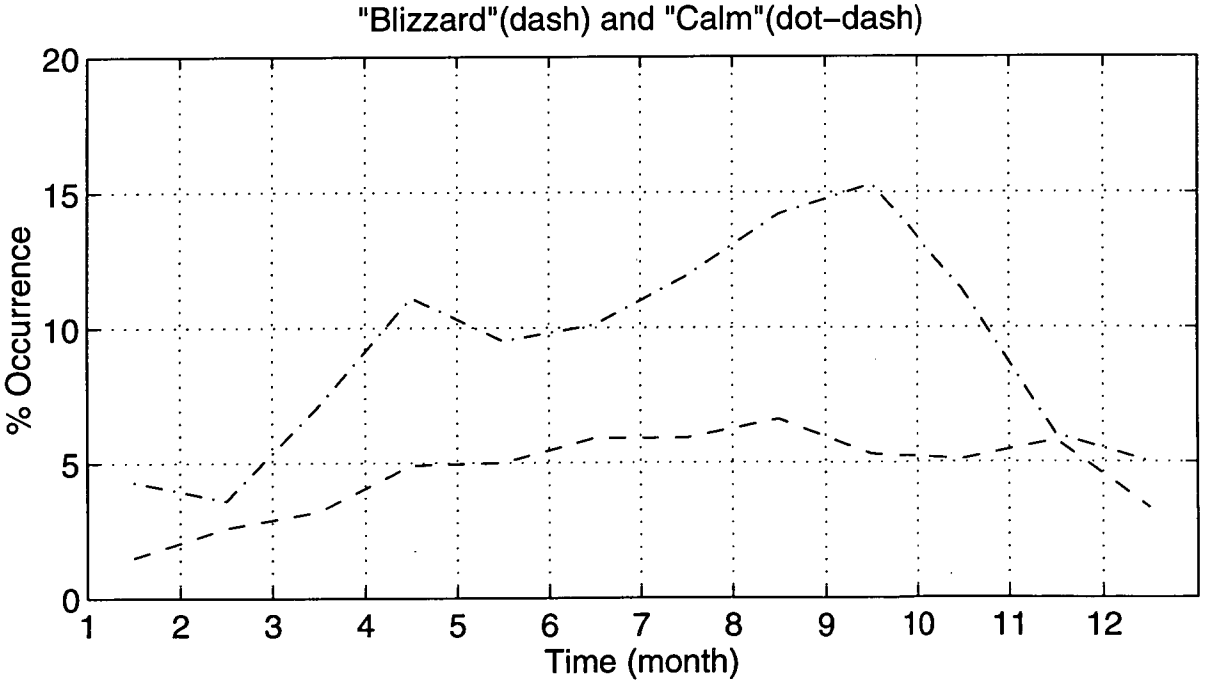

Figure 3.22: Monthly mean occurrences of blizzard winds and calm conditions at Davis.

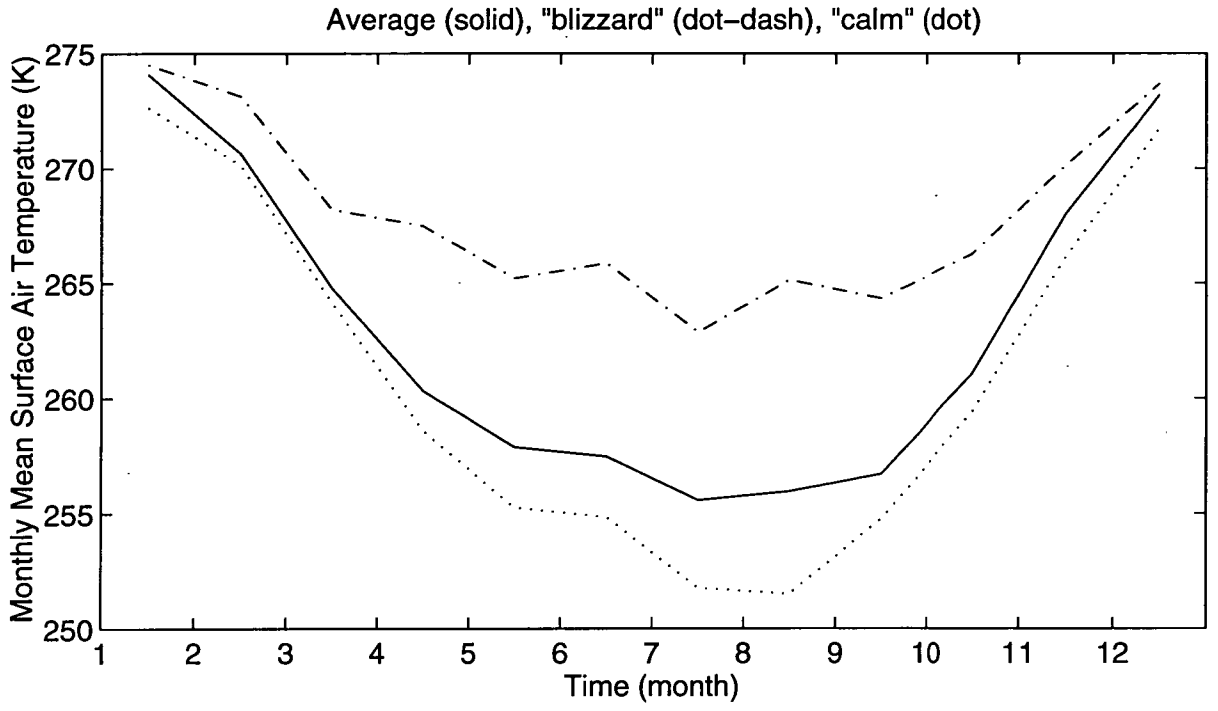

Figure 3.23: Monthly mean surface air temperatures at Davis for average, blizzard and calm winds.

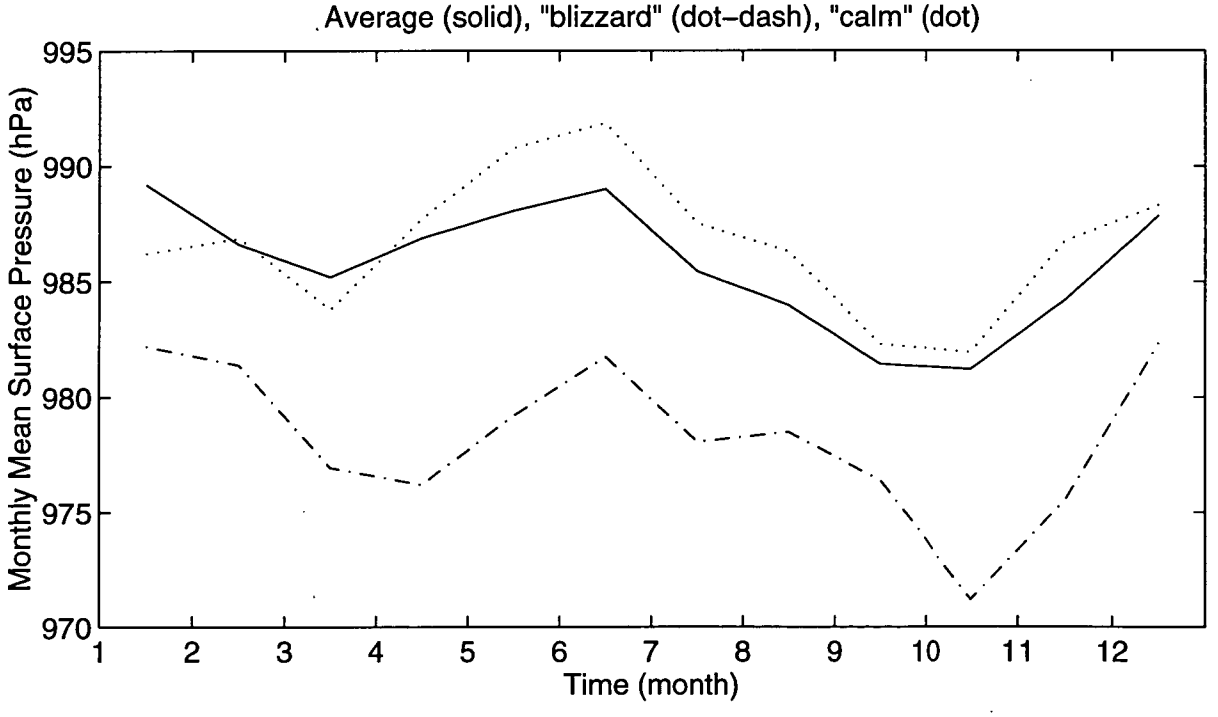

Figure 3.24: Monthly mean surface air pressures at Davis for average, blizzard and calm winds.

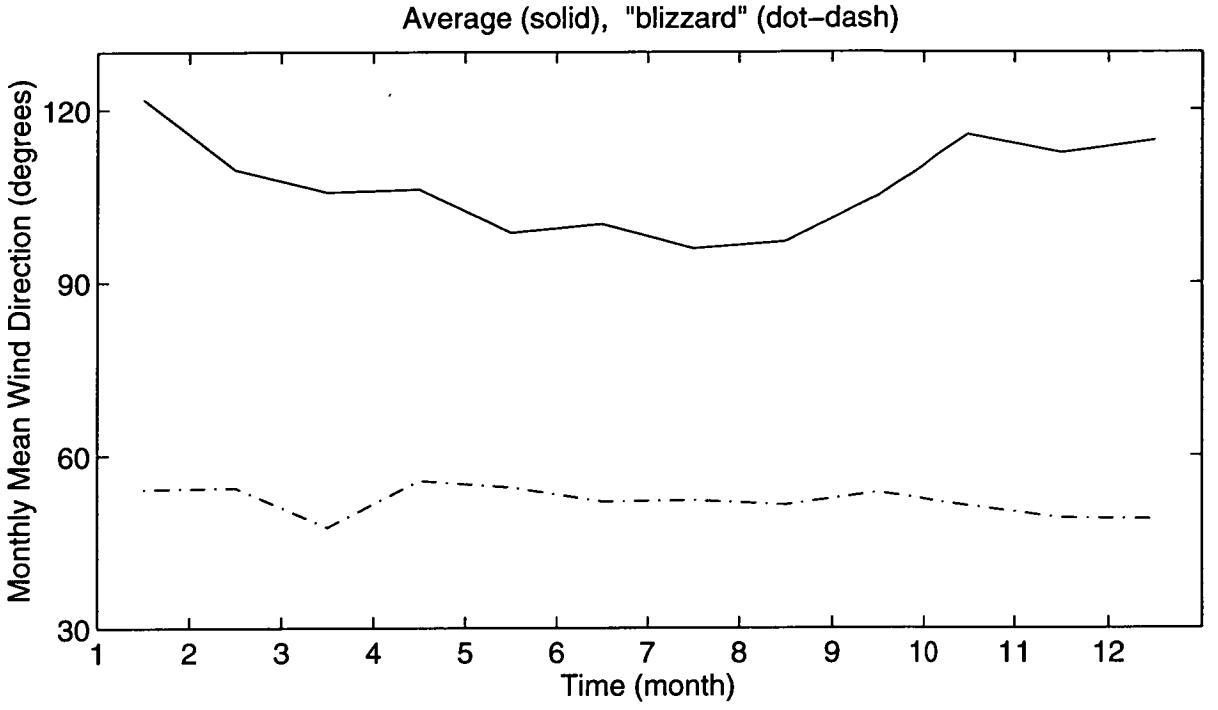

Figure 3.25: Monthly mean surface wind directions at Davis for average, blizzard and calm winds.

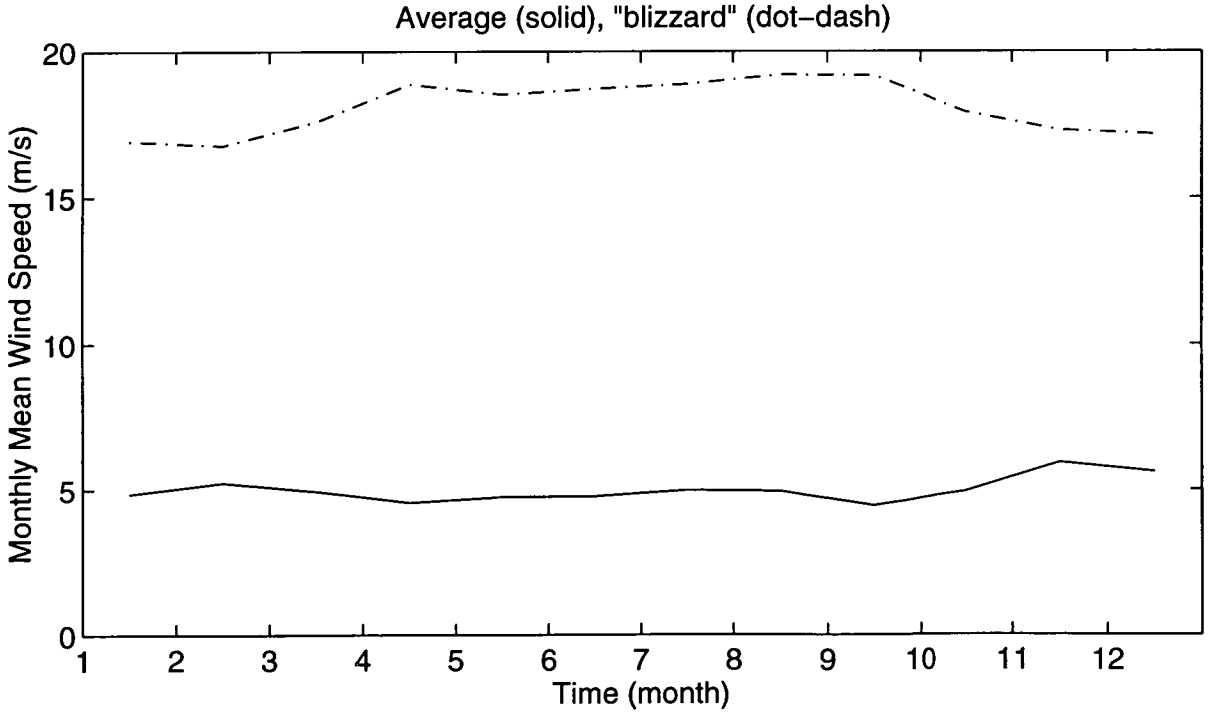

Figure 3.26: Monthly mean surface wind speeds at Davis for average, blizzard and calm winds.

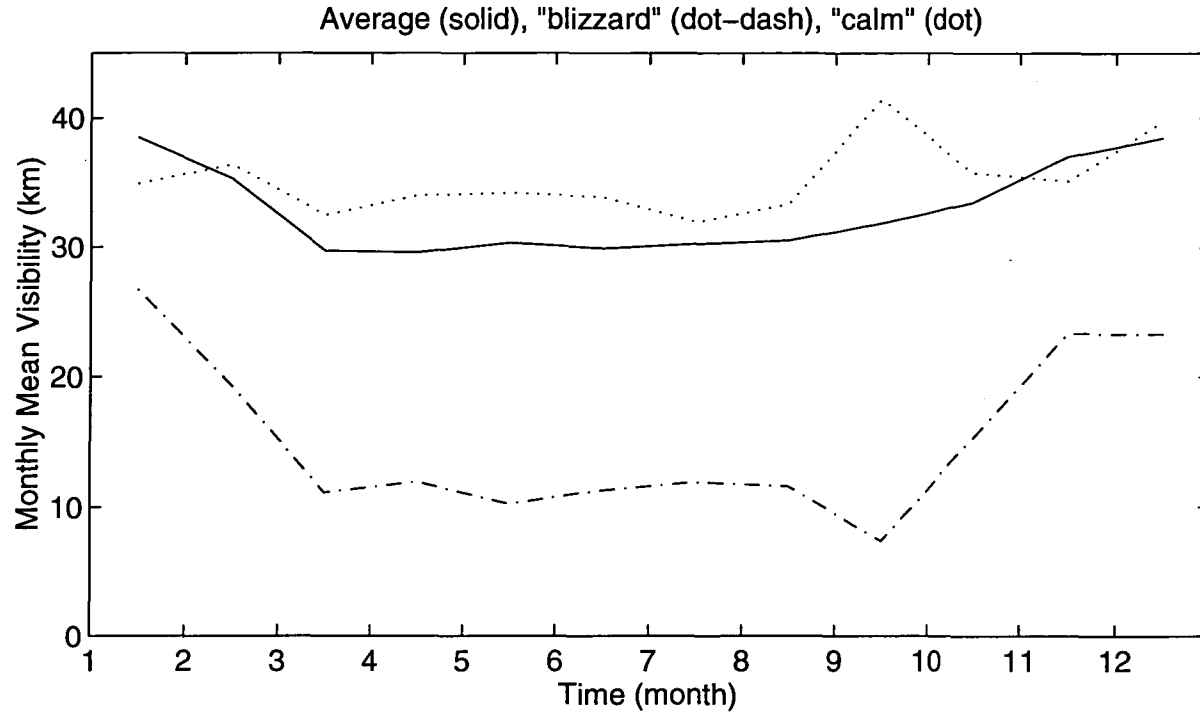

Figure 3.27: Monthly mean surface visibilities at Davis for average, blizzard and calm winds.

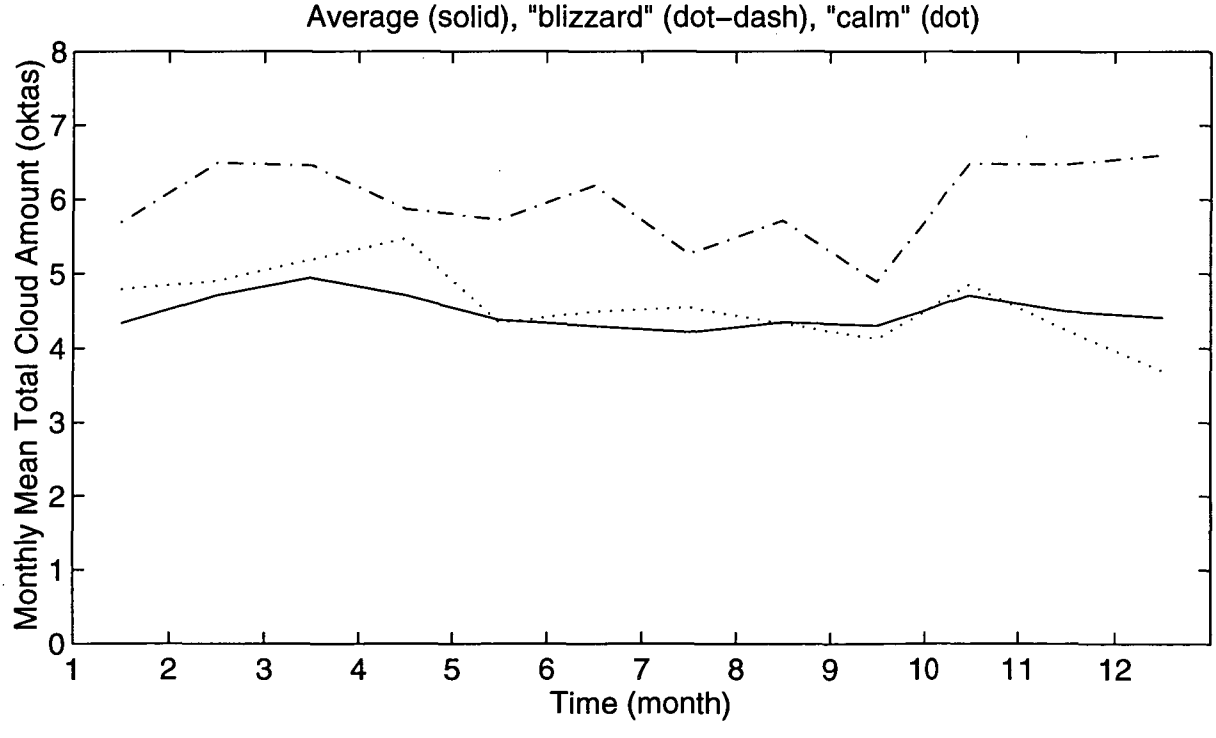

Figure 3.28: Monthly mean total cloud amounts at Davis for average, blizzard and calm winds.

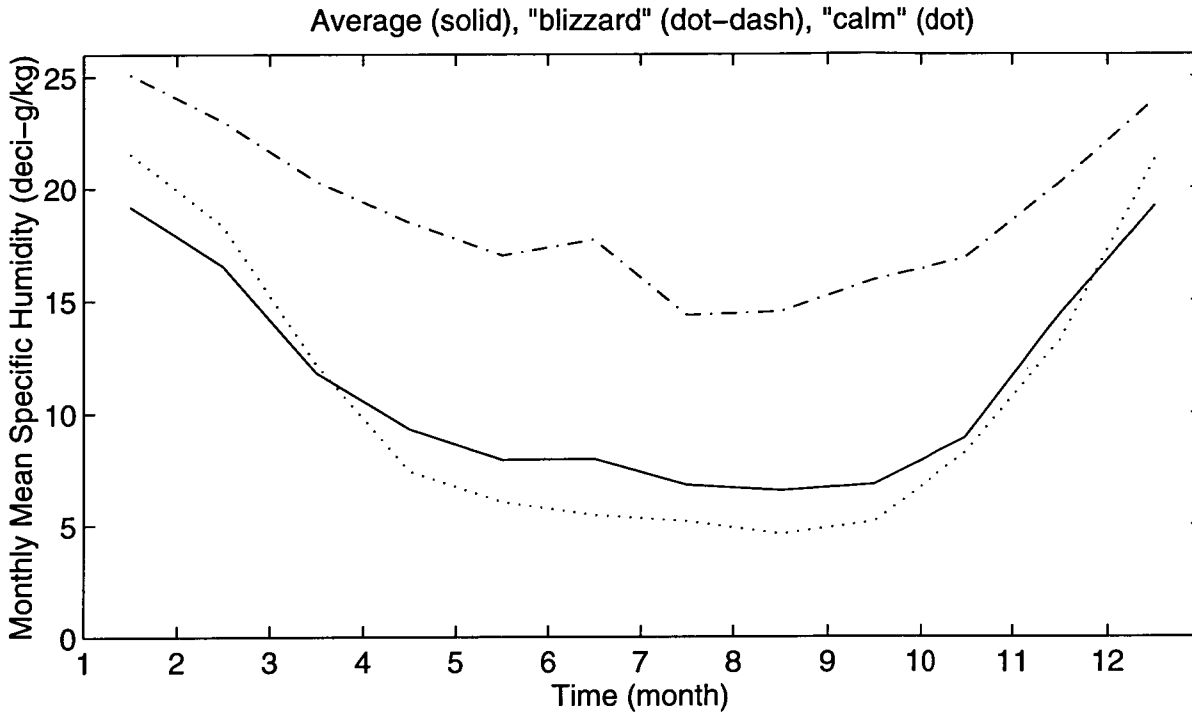

Figure 3.29: Monthly mean specific humidities at the surface at Davis for average, blizzard and calm winds.

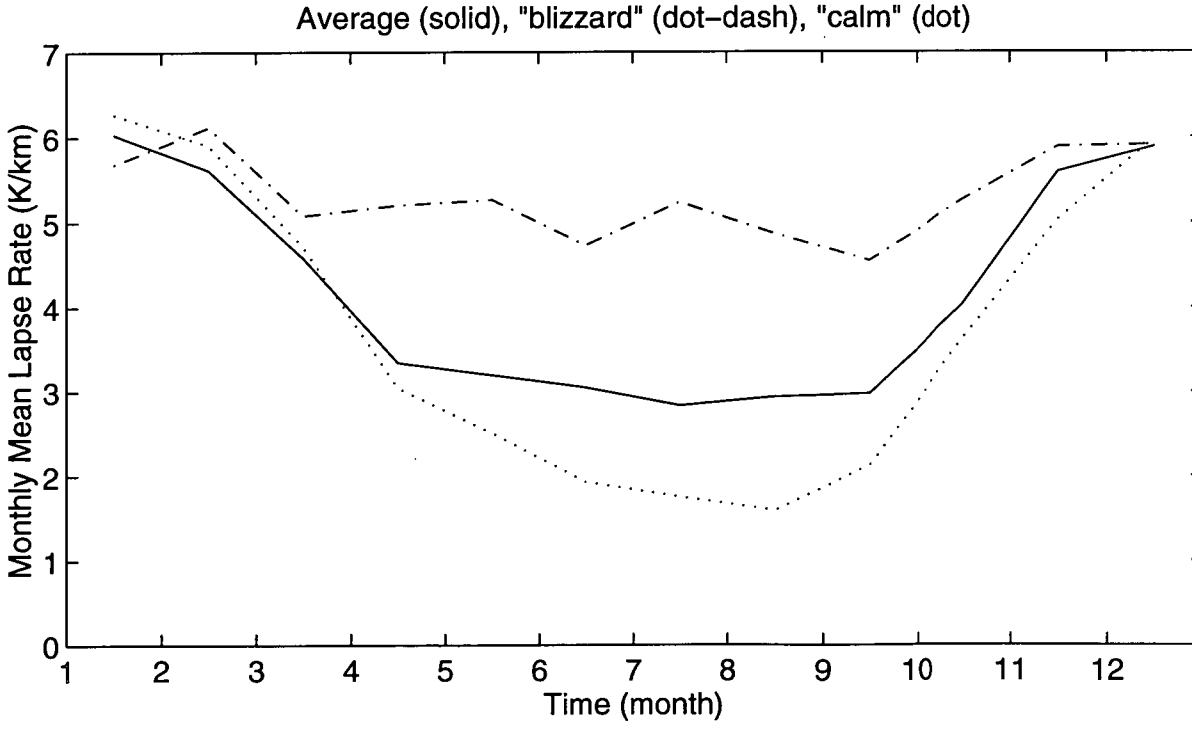

Figure 3.30: Monthly mean lapse rates at Davis for average, blizzard and calm winds.

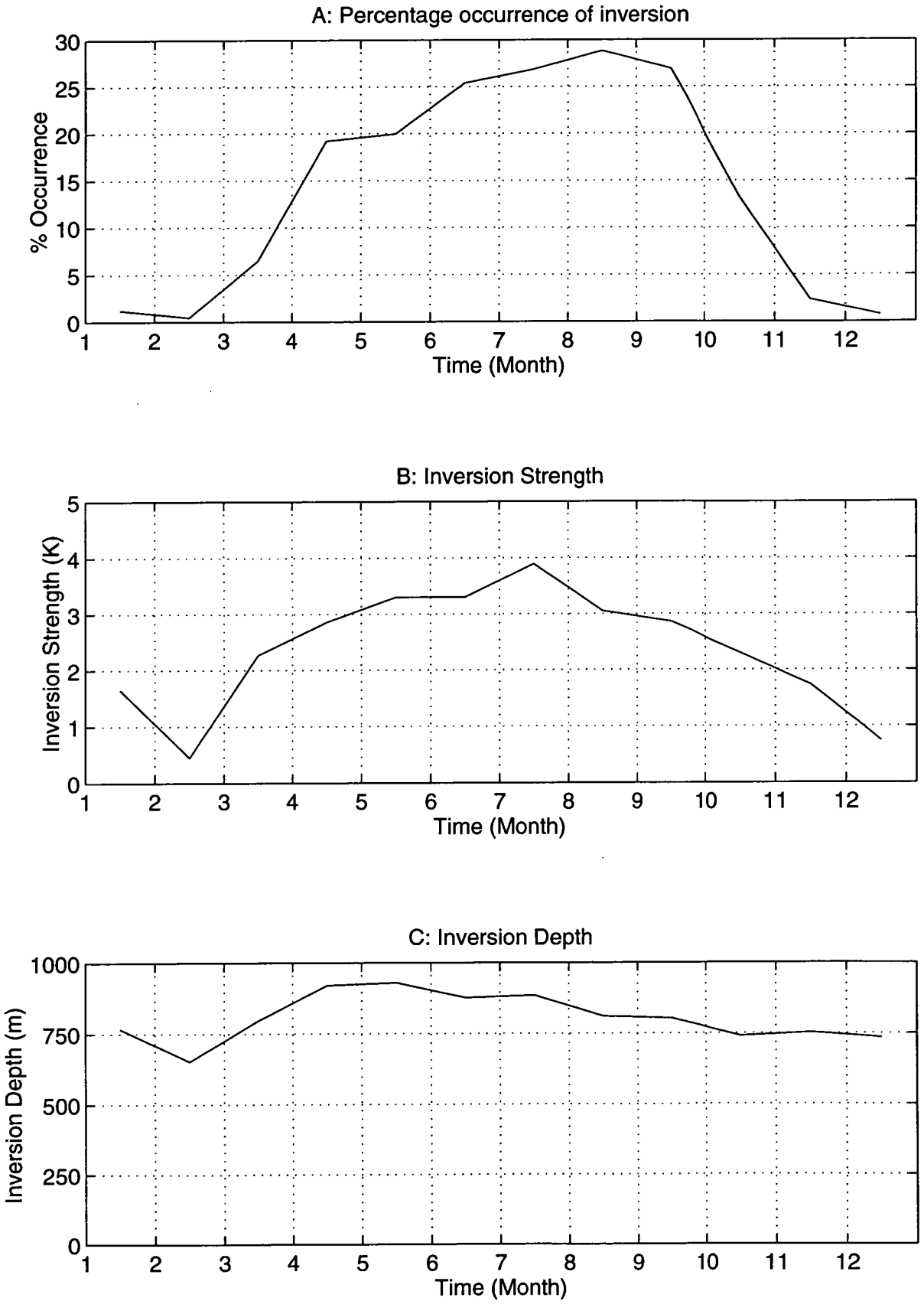

Figure 3.31: Monthly mean inversion parameters at Davis. A: Percentage occurrence of inversion, B: Inversion strength when present, C: Inversion depth when present.

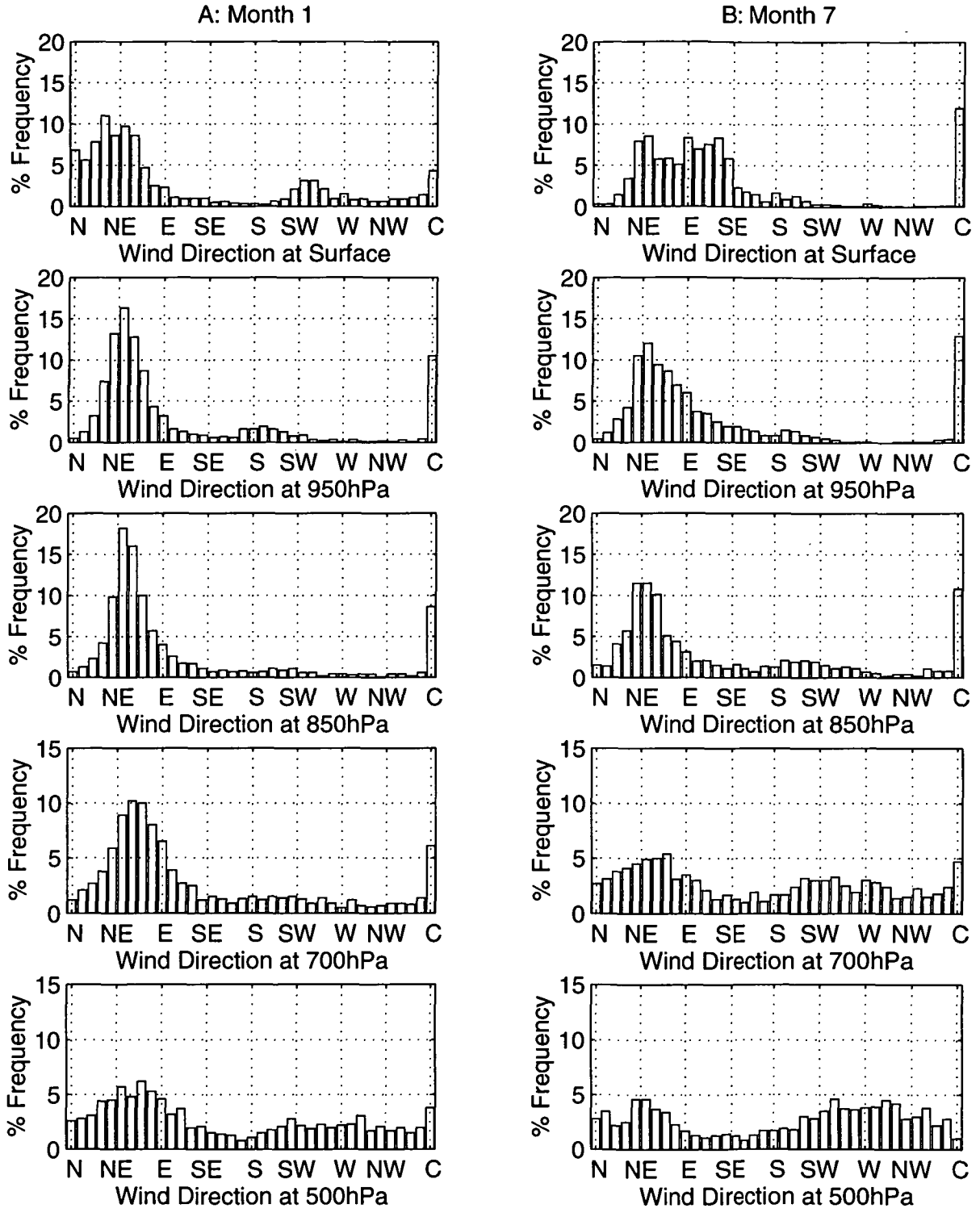

Figure 3.32: A: January, B: July percentage frequencies of wind directions at the surface, 950hPa, 850hPa, 700hPa and 500 hPa for average winds at Davis.

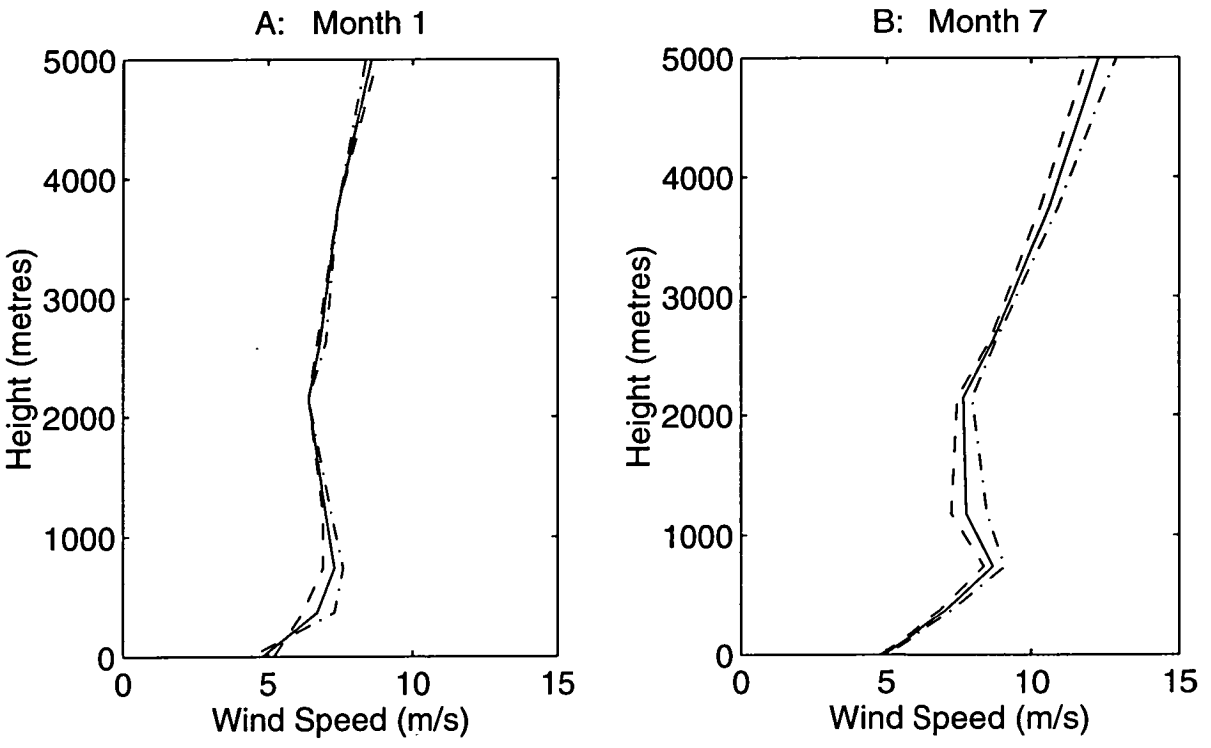

Figure 3.33: Monthly mean vertical wind speed profiles; daily mean (solid line), "day"(dash), "night"(dot-dash), A: January, B: July, at Davis.

3.7 CONCLUSION

The validity of establishing a reliable climatology over the Lambert Glacier Basin has been examined. Apart from Mawson and Davis stations, only small amounts of data have been collected throughout the region. Overall, the establishment of an accurate climatology over the Lambert Glacier Basin region is not possible at present because observations have only been made at a small number of locations, and only for very short periods of time, (less than 5 years at most stations). However, there are adequate data available to indicate general patterns of air flow and the thermal fields over the region.

A numerical model of the atmospheric boundary layer shall be introduced in the following chapter. With accurate parameterisations followed by verifications of results, the model, as a dynamic and thermodynamic system, should be able to "fill in gaps" in the meteorological fields over the Lambert Glacier Basin region, thereby clarifying the climatology of the region. The observations that are available can be used to verify the results of the numerical modelling. This is covered in Chapter 6.

There are many data available at Mawson and Davis stations. These have been processed to produce climatologies.

Mawson is a "katabatic wind site". In addition to a general climatology at Mawson station, several types of winds have been analysed and their individual characteristics discussed. These are expanded upon and used to further explain winds at Mawson in Chapters 7 and 8.

There is much literature discussing severe katabatic wind events, but such events are more the exception than the rule around the coast of East Antarctica. As explained in Section 2.3 of Chapter 2, Parish (1982) showed that it is not possible for there to be a constant supply of air along all of the Antarctic coast.

The inclusion of the climatology of winds at Davis is important because it is a station that is not subject to katabatic flow and so helps to present a true picture

of the climate of coastal Antarctica.

The numerical model will also be used to examine the synoptic forcings that lead to the various wind profiles that have been found to develop at Mawson. This should also contribute to the understanding of the "supply and demand" of air that may cause fluctuations in the flow at coastal locations, as noted by Schwerdtfeger and Mahrt (1968), Parish (1982), Parish (1988), and Schwerdtfeger (1984). This and other air motions in the region of interest are discussed in Chapters 6, 7 and 8.

Chapter 4

THE NUMERICAL MODEL AND DATA FOR INPUT

4.1 INTRODUCTION

This chapter contains a brief introduction to the numerical model that is used and the region of Antarctica to be modelled. Data that are used to initialise the model, for summer and winter runs, are presented.

Model test runs are conducted in Chapter 5, where several problems with parameterisations are solved.

Verification of modelling results and tuning of the model's surface energy balance are discussed in Chapter 6.

Mean January and mean July conditions, that are modelled, represent summer and winter respectively.

4.2 THE NUMERICAL MODEL

4.2.1 INTRODUCTION

The numerical model used is the CSU-Pielke atmospheric mesoscale model. It was developed during and prior to 1973 by Roger A. Pielke for use in studying sea breezes over South Florida, Pielke (1974). This was modified several times, resulting in the 1981 version, as described by Pielke and Martin (1981). This has been used extensively for non-Antarctic atmospheric modelling. It was also used successfully by vanMeurs and Allison (1989) for studying katabatic flow over a region of East Antarctica, south of Casey station and over Law Dome. This

version shall be used for the modelling throughout this project but with further modifications as described in this and following chapters.

vanMeurs and Allison (1989) initiated the model with weak geostrophic conditions, and winter flow was simulated by allowing an inversion to develop through radiative cooling of the surface. Wind directions were found to be in good agreement with sastrugi orientations. Along with three automatic weather stations, the model was used to infer the structure of the katabatic wind field south of Casey station.

The surface wind was said to be at least partially responsible for non-linear variations in the snow-fall accumulation and the non-adiabatic temperature relationship along parts of the 112°E traverse.

The 1981 version of the CSU-Pielke model, but not the "RAMS", is used because the aim is to produce climatologies, and also in later chapters to investigate relationships between synoptic and surface winds over the region, and the CSU-Pielke model was considered to be an effective and simple tool to achieve this. Subsequent results also show this to be the case. As shall be demonstrated throughout Chapters 5 and 6, the model required substantial modifications to function well over Antarctica, and it was expected that extensive modifications would also have been required of the RAMS code.

4.2.2 BASIC FEATURES OF THE CSU-PIELKE MODEL

The model is three-dimensional and uses a form of the primitive equations of motion written in terrain-following coordinates. The flow is assumed to be hydrostatic and incompressible. There is a detailed boundary layer parameterisation scheme that takes into account radiation and discriminates between land and water surfaces.

The model's atmosphere is divided into three vertical regions; an atmospheric planetary boundary layer (PBL), which contains a surface layer and above this an Ekman layer, and above the PBL is the "free" atmosphere, defined to be where

the gradient wind is present.

A typical conventional GCM used for climate studies during the 1980s contained around nine levels with one or two of these used to represent the PBL. The mesoscale model uses about nine levels to represent the boundary layer alone; the number varies depending on the depth of the PBL.

This model does not use lateral boundaries in the same manner as a GCM, where the left boundary equals the right boundary. The lateral boundaries of this model consist of linearly stretched grid spacings that cause dissipation and damping of energy. Without these, energy can be reflected back into the model grid and this disrupts the simulation, and errors in the calculated fields develop. The stretching of the grid spacings moves the lateral boundaries as far away from the region of interest as is practically possible. The final lateral grid spacings around the four sides of the grid set the gradient of meteorological fields equal to zero so that reflection back into the centre of the grid is inhibited. Erroneous accelerations are also reduced by defining the gradient of the topography to be zero across the lateral grid spacings.

There is no cloud forming scheme in the 1981 version of the CSU-Pielke model. The model evaporates water from the surface and there is absorption of both short- and long-wave radiation by water vapour, but there is no reflection of radiation by cloud droplets. Water vapour that is present in the model's atmosphere is advected with the flow. A simple representation of the effects of cloud on radiation is introduced to the model in Chapter 6.

A history of past modifications and examples of modelling shall be outlined in the remainder of this section to demonstrate the capabilities of the model. For more detailed information on the CSU-Pielke model, the reader is referred to Mahrer and Pielke (1977), Mahrer and Pielke (1978), Pielke and Martin (1981) and Pielke (1984), and other reports referenced in the following discussion.

4.2.3 HISTORICAL DEVELOPMENT OF THE CSU-PIELKE MODEL

The Pielke (1974) version of the model was three-dimensional and it was based on the primitive equations, with the hydrostatic assumption. Radiation effects and molecular diffusion of momentum, heat and moisture were neglected. The phase changes of water were not considered. At the upper boundary of the model's domain was a rigid material surface.

A two-dimensional version of the model was used by Pielke and Mahrer (1975) to study air flow over mountains. A terrain-following system was used. Initial accelerations, due to terrain, were reduced by using the scheme of Deaven (1974), in which the mountain used in the experiment was allowed to "grow" gradually during the first two hours of simulated time. In the 1981 version of the model, this method of avoiding computational instability that may develop due to initial accelerations caused by terrain, was not used.

At the initial time, before this growth of terrain, the shear stress, the Coriolis force and the pressure gradient force were assumed to be in balance. The 1981 version of the model does not assume this; these forces are balanced while inducing an Ekman spiral during initialisation, before the actual simulation begins.

The height of the boundary layer was determined by the technique proposed by Deardorff (1974). This allows the height to increase as a function of surface heat, momentum fluxes and mesoscale vertical motion. It also depended on the thermodynamic stability above the present height of the boundary layer.

The upper boundary of the model is called a material surface and it moves vertically in response to mass divergence and convergence beneath it; calculation by integration of the continuity equation from the ground surface to the top of the model's domain. Pielke and Mahrer (1975) showed that this "material surface" method resulted in more realistic results than those obtained when a "rigid lid" was used. The top six model levels, below the material surface, comprise an absorbing layer that damps vertically propagating waves

Mahrer and Pielke (1977) developed the model to a stage very close to the 1981 version. The model described was three-dimensional and based on primitive equations, with a hydrostatic assumption. Radiation effects were taken into account; heating and cooling at different levels in the atmosphere were included dependent on emissivities due to water vapour and carbon dioxide at each level. A surface energy balance was included that calculated the temperature of the surface dependent on incoming radiation, incoming and outgoing infrared radiation, and latent and sensible and soil heat fluxes at the surface. This balance was reached using a double-iteration (nested) technique, as described by Pielke (1984).

The surface layer momentum, heat and moisture fluxes were calculated based on the work of Businger (1973). The exchange coefficients within the Ekman region of the boundary layer were calculated using the formulations suggested by O'Brien (1970). The roughness length over water was calculated using the Clarke (1970) scheme. These boundary layer calculations were used in the original 1974 version of the model and through to the 1981 version. In the 1974 version, the boundary layer height was calculated using a scheme suggested by Deardorff (1972). The 1977 version used a scheme suggested by Deardorff (1974).

The major differences between the 1981 version of the model and that described by Mahrer and Pielke (1977) are that the 1977 version did not contain the upstream spline interpolation technique for advective terms, nor did it utilise the filter, by Paul Long. Also, the terrain was "grown" in the 1977 version and the effects of fluxes of heat and moisture at the surface were not included.

Mahrer and Pielke (1978) introduced to the model the technique of using upstream interpolation with a cubic spline for the advective terms. To carry out tests using this technique, a two-dimensional version of the model was used. The cubic splines were evaluated separately in the horizontal and the vertical. The 1981 three-dimensional version calculated the splines separately in the x, y and z dimensions. A filter suggested by Paul E. Long was adopted for use in the model

during these cubic spline experiments.

It was found that the cubic spline technique had superior accuracy over the basic linear differencing technique. Experiments with air flow over mountains, and sea and land breezes along flat coastlines showed this. Purnell (1976) had already shown the cubic spline technique to be extremely accurate in conserving both phase and amplitude, but this was not in relation to the CSU-Pielke model.

Pielke and Martin (1981) derived a new set of equations in a terrain following coordinate system that could be applied for use in the hydrostatic CSU-Pielke model, so that the use of terrain following coordinate systems that had been previously used, could be critically assessed. It was concluded that the terrain following coordinate system used previously, Pielke and Mahrer (1975), was appropiate for use in the model, but this is only correct when the hydrostatic assumption is exactly satisfied.

Pielke et al. (1983) used the model for predicting the spatial and temporal position of pollutants. Experiments were carried out in regions such as coastlines and irregular terrain, where there are few air monitoring stations. The results show that the model may be used in the future to improve knowledge of air pollution characteristics in regions where data are sparse. This is an important point in relation to the modelling of the Antarctic planetary boundary layer because one of the reasons for carrying out the modelling is to provide simulated and predicted meteorological fields, because observations are relatively sparse over the Antarctic continent.

Abbs (1986) used the CSU-Pielke model for studying sea breezes along a concave coastline; Port Phillip Bay, Australia. The model was shown to successfully simulate the sea breezes, as well as the formation of a mesoscale cyclonic eddy over the northern half of the bay. The model results agreed well qualitatively with the observations, but unfortunately the anemometer network was too sparse to perform a quantitative comparison. The model made it possible to explain features that were not explained from observations alone. This point also suggests

that the model would be very useful for use over Antarctica where observations are lacking.

Segal et al. (1988) carried out several experiments using the model in order to evaluate the possible impact of vegetative areas on typical thermally induced daytime mesoscale circulations. It was concluded that further study was required in order to obtain a good understanding of the influence of vegetation on mesoscale circulations. Also, incorporating vegetation characteristics into the model was found to require that the specification of surface characteristics be accurate because slightly incorrect specification led to significant simulation errors. Although not directly applicable to Antarctica, these results show the importance of correct representation of the ground surface within the model. Discussions are included in this and following chapters in regard to representation of the Antarctic surface.

4.3 REGION OF ANTARCTICA TO BE MODELLED

The atmospheric planetary boundary layer over the Amery-Lambert basin region of Antarctica outlined in Figure 4.1 is to be modelled. This area has not previously been the focus of high-resolution (grid spacings of 20 km) atmospheric modelling.

The topography used has been digitised from the polar stereographic maps of Drewry (1983). These projections mean that the distance scale is only strictly accurate at one latitude, at around 75°S, but as the topography is relatively unknown, minor distortions are acceptable.

The "bottom" edge of the box (in Figure 4.1) is aligned along the longitude of 90°E. The values at each corner of the box correspond to the grid points used in the modelling. The lowest values shown are five, and not one, because the lateral grid region over the first four grid spacings is taken into account, but this only has significance for the computational stability; it does not enhance the terrain definition. This is discussed in Section 4.2.

Figure 4.2 is the same area, with latitude and longitude values overlaid on terrain elevation contours. The negative values represent Southern Hemisphere

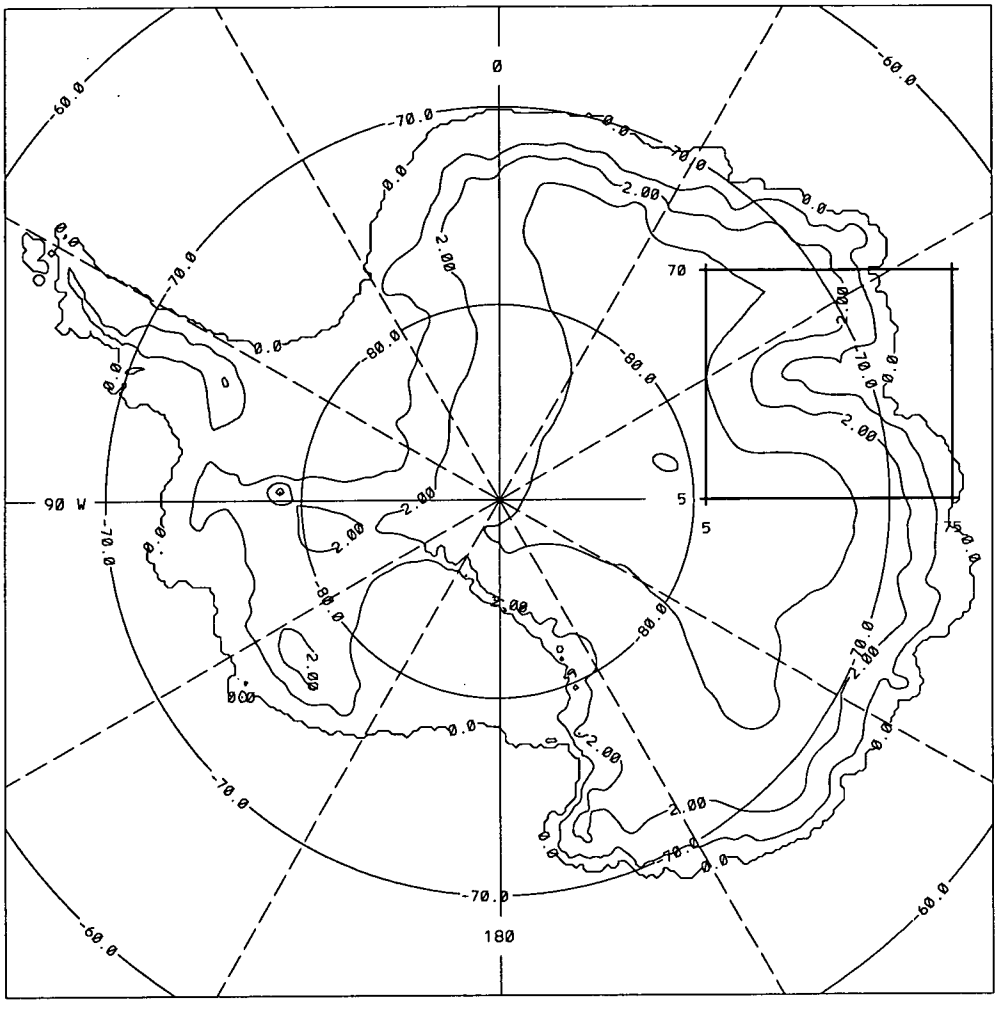

Figure 4.1: Antarctica, with the region to be modelled, shown in the box on the right of the figure; the Lambert Glacier Basin region, west of 90°E. Terrain elevation contour intervals are 1 kilometre.

latitudes at 5 degree intervals. The average latitude of this grid is -71.68°. The grid consists of 20 km grid spacings on a 80 x 74 grid. Four grid points around all four lateral boundaries are not shown in this plot because they are used for damping/absorption of energy that reaches the edge of the domain. The stretched grid spacings cover horizontal distances of 280 km around each of the four lateral boundaries; the "terrain" is flat in these regions, to promote damping. In effect, the grid used for actual meteorological modelling is 72 x 66. Most modelling results to be displayed in later chapters, with a horizontal aspect, will be of this format.

The locations of Mawson and Davis stations are also shown in Figure 4.2. Mawson and Davis have grid point coordinates of (57,61) and (62,29) respectively. Corresponding latitudes and longitudes are shown in Table 3.1.

Figure 4.3 is a mesh plot of the region to be modelled, as viewed from the north, looking approximately towards the south pole over the Lambert Glacier Basin region. This figure is informative in that each square in this plot represents a 20 x 20 km grid box and this is the actual topography used in the model. The four lateral grid spaces have the same (terrain height) value; zero-gradient conditions, as discussed earlier in this chapter.

Figures 4.1- 4.3 show the advantage of using a mesoscale model that operates at a relatively high-resolution; the terrain is well defined using 20 km grid spacings over this large area. It was noted in Chapter 2 that terrain has an important influence on surface winds in Antarctica. A grid that has spacings of 20 km has better definition of terrain heights than do spectral Atmospheric General Circulation Models (AGCM) of 21 or 31 waves.

Figure 4.4 is a representation of the slope of the topography overlaid on the topography elevations of 1 km interval. The slope at each grid point was calculated using the root of the sum of the squares of the slope along the x- and y-axes. The slope contour interval is 0.005 but the values shown on the contours are 10000 times larger than their true values, simply to help with the clarity of the plot.

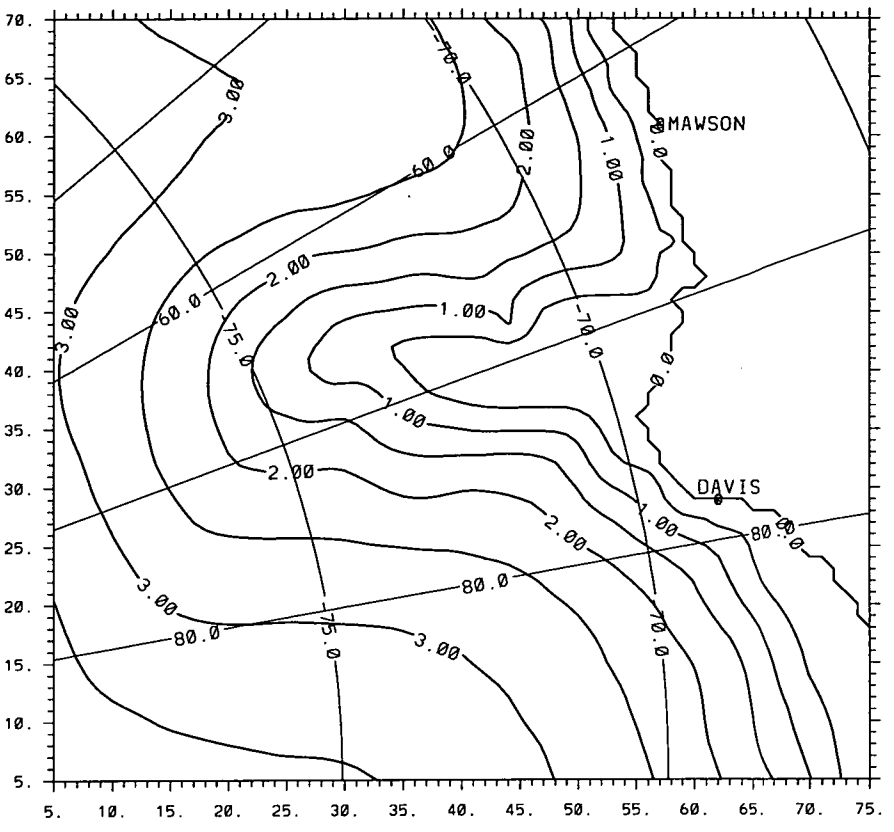

Figure 4.2: The model grid, with terrain elevation contours (intervals of 0.5 kilometre), latitudes, longitudes and locations of Mawson and Davis stations. Locations of other stations are shown in Table 3.1 and Figure 3.1, Chapter 3. Grid spacings are 20 kilometres.

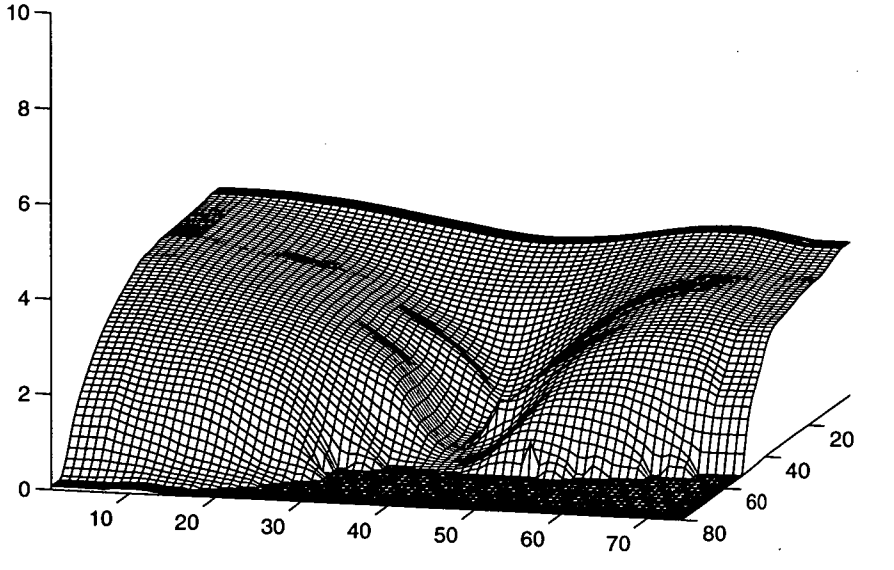

Figure 4.3: 3-D mesh plot of the 80 x 74 model grid, as viewed from over the sea to the north of the region, looking approximately towards the south pole.

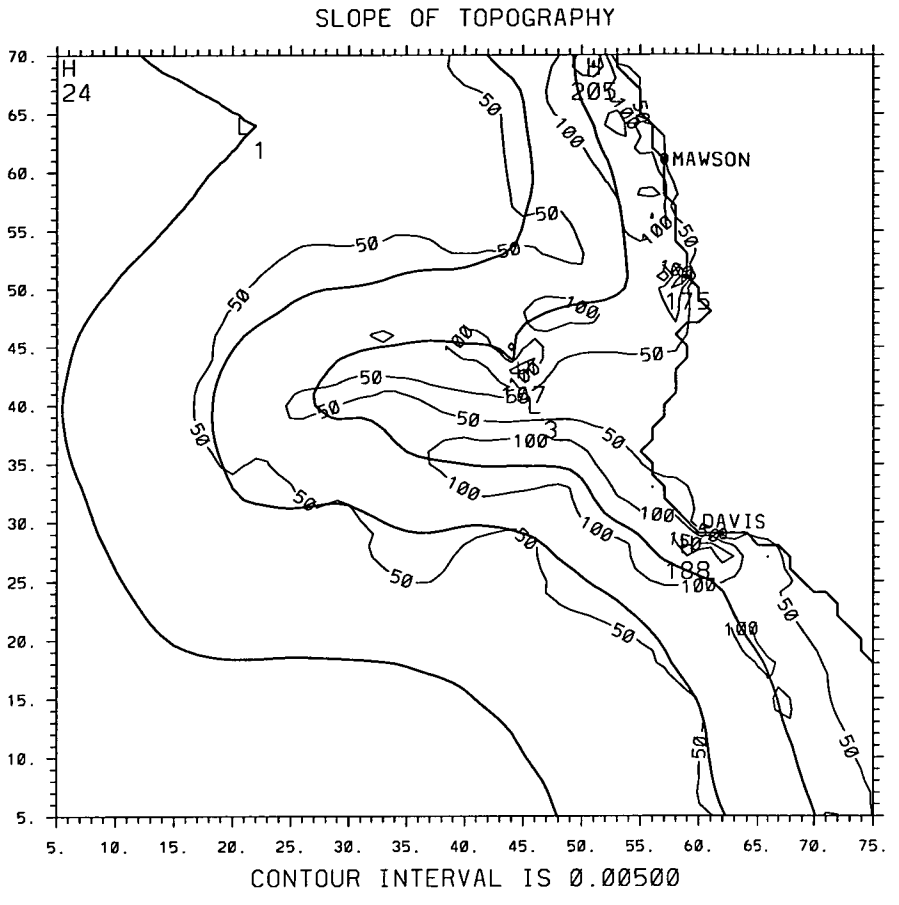

Figure 4.4: Terrain slope magnitudes for the model grid, shown by the thin contour curves, with units of $10x^{-4}$. The thick contours represent the terrain elevations, with intervals of 1 kilometre. Each tick mark on the x- and y-axes represent a 20 km interval.

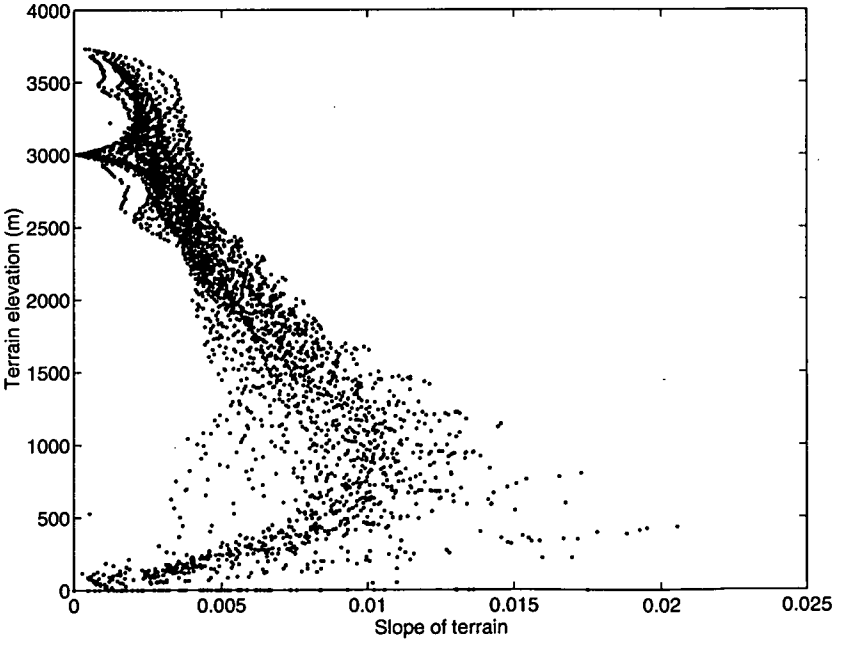

Figure 4.5: Scatter plot of Terrain slope versus Terrain elevation. For the region being considered here, 52% of the grid points are plateau points, and 19% are over the sea or sea ice region. The remaining points form escarpments and the Amery Ice Shelf.

At terrain elevations of about 2 km, the slope is 0.005, and there is a general increase towards the coast. There is a local high south of Davis and also at the Scullin Monolith, which is located on the coast between Mawson and Davis. This terrain feature can also be seen in Figure 4.3. The slope is also relatively high throughout the area south of Mawson, northern MacRobertson Land, where the Framnes Mountains are located.

Near the centre of the grid, there are contrasting terrain slope magnitudes, where the southern Amery Ice Shelf meets the Prince Charles Mountains. The slope from the mountains to the ice shelf is 0.0167 but the slope minimum over the ice shelf is only 0.0003 . A slope that has significance because of its effect on the inversion strength, and the subsequent influence on the parameterised PBL height is shown by the local low at around grid point (21,64). This is discussed in Sections 5.5 and 5.6 of Chapter 5.

Figure 4.5 is a further display of terrain elevation and the corresponding slopes. Although there is wide scatter, the general pattern shows that the greatest slopes are not at the coast but inland at elevations of about 200 - 1000 metres. However, the very steepest slopes are located at under 500 metres elevation near the coast. As covered in Chapter 2, Dalrymple (1966) defined the Antarctica plateau on the basis of slope. Points with slopes less than 1 degree (slopes less than 0.017455) and elevations greater than 2000 metres in East Antarctica are plateau points. For the region being considered here, 52% of the grid points are plateau points, and 19% are over the sea or sea ice region. The remaining points form escarpments and the Amery Ice Shelf.

4.4 MODEL TEST RUNS AND DATA

There were ten model runs conducted for this initial study using the 80 x 74 grid with 20 km grid spacings. The time step used was 60 seconds. The results from these ten runs are discussed in Chapter 5.

All of these runs were forced with a synoptic wind speed of 0.25 m/s, which

was considered to be of negligible strength, and the wind direction was approximately southerly. This small value was used so as to allow the development of the meteorological conditions within the boundary layer without significant disturbance from the synoptic scale pressure gradient. A synoptic wind speed of 0.25 m/s was used because it does not have a significant effect on the drainage flow development within the boundary layer; a totally flat pressure field led to computational disturbances within the model's numerics, an unfortunate property of the model used, but not one that is overly troublesome and was overcome simply.

This procedure is desirable for testing purposes; the results obtained from the runs in Chapter 5 are not simulations of actual weather events. After the adjustments to parameterisations are made and the corresponding justifications discussed, the resultant runs presented will represent mean boundary layer weather conditions that may occur under weak upper wind conditions in the region modelled. However, the upper wind has an important influence on the thermal fields and air flow at lower levels, as shown in later chapters.

The upper wind, the terrain and thermal fields are probably the three most important influences on the low level wind. The importance of thermal fields is demonstrated in Chapter 6. Terrain influences on surface winds are demonstrated by modelling results shown in Chapters 6 and 8. Upper wind fields and their relationships with low level winds are investigated in Chapters 7 and 8.

Considering that lack of data is often a problem with Antarctic research, the relatively large amount of meteorological data available from Mawson station is unusual. Observations covering a period of thirty-seven years are used to calculate mean values of meteorological parameters for use in these test runs. January and July conditions are modelled. The January data used was from years 1955 to 1991, and for July the period was 1954 to 1990. However, for the region to be modelled, shown by Figures 4.1 and 4.2, data are greatly lacking spatially, as was noted in Chapter 3.

Solar radiation input during the Antarctic polar night, as represented by the month of July, is negligible. This is demonstrated by a sensitivity test in Chapter 6. For January, there is a diurnal wave but the sun does not pass beneath the horizon. Because the region modelled is relatively large (compared with what might usually be termed as "mesoscale"), the solar radiation is not assumed to be constant over the entire domain. The numerical model has been adjusted so that the solar input is spatially-varying, depending upon the latitude.

The January test run used January 15 as the date on which to base the solar conditions. Runs were begun at local midnight, when the solar declination is at a minimum. This time was chosen because it synchronises the execution of modelling of the thermodynamics and the time when the real atmosphere's solar input is at a minimum and is about to increase. The January data that were used to calculate mean fields were divided into "day" and "night", defined from local hours 0600 to 1800 and 1800 to 0600 respectively. July runs were also begun at "midnight", but with no solar input the time of day is meaningless.

Radiosonde data measured at Mawson are shown in an interpolated form, for use as input to the model, in Table 4.1. Corresponding potential and sensible temperature profiles to a height of 1000 metres are plotted from these soundings in Figures 4.6 and 4.7, for January and July respectively. Inversions are not present for either mean January or mean July soundings at Mawson. The frequencies of inversions for each month at Mawson and Davis stations are shown in Chapter 3.

VERTICAL LEVELS IN THE MODEL

The vertical levels selected for use in the model are most highly concentrated towards the surface. The two levels closest to the surface are at heights of 4 and 8 metres (in preference to the more usual 5 and 10 metres), because this should provide a more convenient comparison with automatic weather station (AWS) data, which are measured at these levels. It is also convenient to define several model levels close to the surface in the manner shown in the left hand column of

Elevation (m)	Potential temperature (K)		Specific humidity (g/kg)	
	January	July	January	July
4	271.7	254.9	1.950	0.550
8	271.7	254.9	1.945	0.549
15	271.8	255.0	1.940	0.547
25	271.8	255.1	1.933	0.545
50	271.9	255.3	1.917	0.541
75	272.0	255.5	1.900	0.536
100	272.1	255.7	1.884	0.532
150	272.4	256.0	1.850	0.522
200	272.6	256.4	1.817	0.513
300	273.1	257.2	1.751	0.495
500	273.9	258.7	1.618	0.458
700	274.8	260.2	1.485	0.421
900	275.4	261.1	1.398	0.411
1200	275.9	262.4	1.304	0.398
1500	276.8	264.2	1.208	0.392
2000	278.9	268.3	1.058	0.386
2500	281.5	272.4	0.915	0.380
3000	284.1	275.1	0.779	0.331
3500	286.8	277.7	0.648	0.276
4000	289.4	279.9	0.530	0.235
4500	291.9	281.8	0.439	0.200
5000	294.4	283.7	0.347	0.167
5500	296.6	285.6	0.293	0.150
6000	298.6	287.5	0.254	0.134
6500	300.7	289.4	0.216	0.118
7500	305.8	294.0	0.167	0.096
9000	318.8	304.8	0.114	0.071

Table 4.1: Mean January "night" and mean July profiles of temperature and humidity at Mawson, computed from 32 years of radiosonde data.

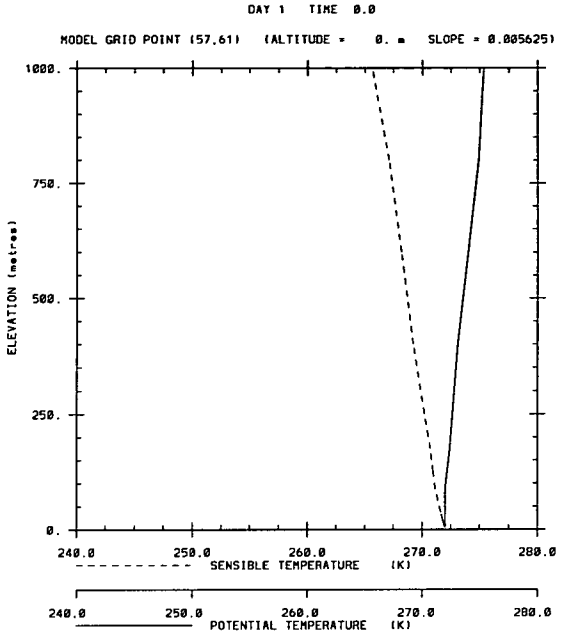

Figure 4.6: Mean January vertical profile of temperatures at Mawson, as used to initialise the model for summer runs.

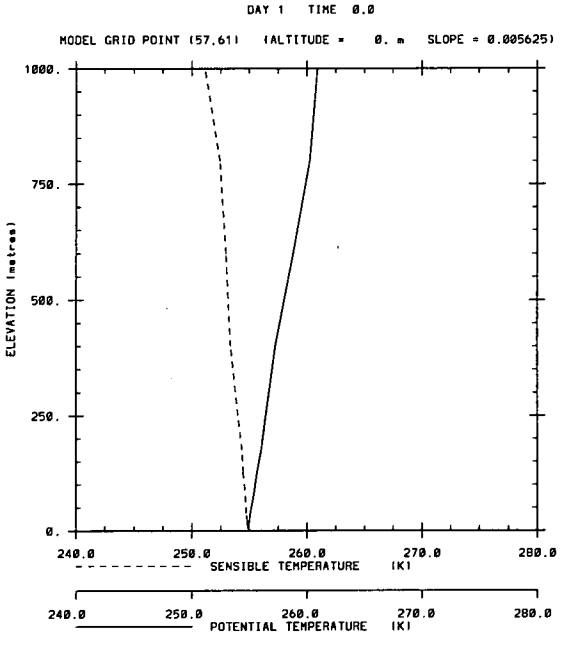

Figure 4.7: Mean July vertical profile of temperatures at Mawson, as used to initialise the model for winter runs.

Table 4.1 to capture details of surface air flow, particularly of the katabatic jet, which is of primary interest during this investigation. The levels are also defined at such heights to effectively model the logarithmic nature of change with height of parameters above the surface. The levels used are quite typical of those used in boundary layer models.

SURFACE PARAMETERS

Definition of surface parameters (density, thermal conductivity and specific heat capacity) within the numerical model are important. These three parameters define the diffusivity and this is very important in determining the heat balance of the surface layers and the air adjacent to the surface. The temperature of the surface and the air temperature depend on the heat balance, and therefore the definition of surface properties can affect the atmosphere's temperature profile, and the wind field. Results from model runs, in Chapter 5 and 6, demonstrate the sensitivity of the model's thermal fields to changes in these parameters.

The region to be modelled is large and contains several different surfaces; snow, ice, rock and ocean. However, the surface is mainly ice and snow, and has its properties set accordingly for these test runs. For the January case, the ocean is defined, but for the July run, the entire domain is assumed to be covered by ice and snow.

DENSITY OF THE SURFACE

Allison and Higham, (1993, personal communication) measured firn densities throughout MacRobertson Land, East Antarctica, while on traverse during the summer 1989/90. Measurements were made in the top 50 centimetres of the surface. One hundred and twenty-two measurements made at one hundred and five different locations yielded an average density of 399 kg m^{-3}. The most southern and northern extents of the traverse from which density measurements were used were 76°3′11″S and 68°44′58″S respectively. The longitudes covered were from 55°40′5″E to 64°39′0″E. Sastrugi orientations were also measured on

this traverse and are compared with modelling results in Chapter 6.

Measurements made on traverse in Wilkes Land, from Goodwin (1988), have been used to calculate a mean density value for this area. Only the measurements made closest to the surface at each location along the traverse were used. The traverse approximately followed the 69°S latitude. The most southern and northern sites were at latitudes 69°01′14″S and 68°35′35″S respectively. The longitudes covered were from 113°19′41″E to 130°48′26″E. The mean depth where these measurements were made was 11 centimetres. The mean density value was 412 kg m^{-3}. vanMeurs and Allison (1988) modelled the low level meteorological conditions south of Casey using a surface density value of 400 kg m^{-3}.

Density measurements of wind-packed snow, with a horizontal surface and located close to Mawson, were made by Weller (1968). The density value was 420 kg m^{-3}. This supports the use of the mean near-surface density values, obtained from Allison and Higham (1993, personal communication) and Goodwin (1988), over the entire model grid, despite the fact that they were obtained from measurements made at surface elevations greater than 1900 metres, and may have been expected to be unsuitable to represent the density of firn at low elevations.

Gallée and Schayes (1992) used a snow density value of 330 kg m^{-3}. This value is relatively low compared with the measurements discussed above because it was assumed that the coastal area that they modelled was covered by snow, which has a lower density than ice or an ice-snow mixture. The depth that the diurnal temperature wave was allowed to reach below the surface in their model was 15 cm, which shows that the values used from Goodwin (1988), at a mean depth of 11 cm, are representative of the region where thermal transfers occur, and not just the first few centimetres of the surface.

Somewhat to the other extreme, Weller (1968) measured densities of sea ice and of blue ice, that was inland at an elevation of 150 metres, 2 km from Mawson. All of these measurements were of ice, not of snow or snow and ice, and therefore the values are high compared with the other values quoted. From 40 samples,

the mean density of the ice was 880 kg m^{-3}.

There are many data available from measurements made at Antarctic stations and on traverses that provide density values for surface ice and snow. There is a little variability, but considering the sources mentioned above, a suitable value to use is 400 kg m^{-3} .

THERMAL CONDUCTIVITY OF THE SURFACE

From Schwerdtfeger (1963), and Budd (1966), the thermal conductivity of snow can be calculated from a theoretical relationship dependent on snow and ice densities and the thermal conductivity of ice, if the snow is of high enough density ($\geq$ 400 kg m^{-3}) to allow neglect of conductivity due to air. This relationship is given by equation 4.1 and was used to calculate the thermal conductivity of the surface to be used in the model.

$$k_s = \frac{2\rho_s}{3\rho_i - \rho_s} k_i \tag{4.1}$$

ρ_s is the density of the snow, ρ_i is the density of the ice, k_s is the thermal conductivity of the snow and k_i is the thermal conductivity of the ice.

The thermal conductivity of the ice surface varies also with temperature, as shown by Budd (1966). This is not examined until Chapter 6, where sensitivity model runs and some "fine tuning" are performed. The overall aims of the following two chapters are to find problems with the parameterisations used in the model and attempt to fix them.

Using Weller (1968) ice measurements at a location 2 kilometres inland from Mawson at an elevation of 150 metres, density, ρ_i = 880 kg m^{-3} and conductivity, k_i = 2.09 W m^{-1} K^{-1} , and the snow density discussed above, ρ_s = 412 kg m^{-3} , the thermal conductivity of the surface to be used in calculating the surface energy balance during numerical modelling is k_s = 0.819 W m^{-1} K^{-1} .

This conductivity value is suitable for use in the region to be modelled because it lies in the range of values quoted by Lee (1978) and Oke (1973) for old snow.

Run Name	Time of year	Density	Conductivity	Specific heat
R01	January	400 kg m^{-3}	0.819 W m^{-1} K^{-1}	2006.4 J kg^{-1} K^{-1}
R02	July	400 kg m^{-3}	0.819 W m^{-1} K^{-1}	2006.4 J kg^{-1} K^{-1}
R03	July	900 kg m^{-3}	2.510 W m^{-1} K^{-1}	2093.0 J kg^{-1} K^{-1}
R04	July	400 kg m^{-3}	0.250 W m^{-1} K^{-1}	1420.0 J kg^{-1} K^{-1}
R05-10	July	400 kg m^{-3}	0.819 W m^{-1} K^{-1}	2006.4 J kg^{-1} K^{-1}

Table 4.2: Surface parameters input to model runs R01 - R10. Surface diffusivities and other details about runs are shown in Table 5.1, Chapter 5.

The use of different surface properties and the effect this has on surface temperatures and surface based inversions is discussed in Chapters 5 and 6. There are related discussions throughout Chapter 6, particularly in Section 6.4.

SPECIFIC HEAT CAPACITY OF THE SURFACE

Another parameter to be used in defining the surface is the specific heat capacity, c_s. Unlike density and thermal conductivity, the specific heat capacity does not alter substantially between ice and snow. Gallée and Schayes (1992) used a value, c_s = 2000 J kg^{-1} K^{-1} . All snow and ice values from Lee (1978) and from Oke (1973) lie within a narrow range of 2090 to 2100 J kg^{-1} K^{-1} . vanMeurs and Allison (1988) used a value of 1420 J kg^{-1} K^{-1} , from Weller and Schwerdtfeger (1977). The specific heat capacity value to be used in this project is c_s = 2006 J kg^{-1} K^{-1} , from Weller (1968). This value is from blue ice near Mawson but is very close to that used by Gallée and Schayes (1992) for a snow covered surface, and also agrees well with Lee (1978) and Oke (1973).

Table 4.2 contains data used to define the surface properties in each of the test runs, R01 - R10. The results of these runs and the rationale for carrying them out are discussed further in Chapter 5.

SURFACE AERODYNAMIC ROUGHNESS

The surface roughness parameter, z_0 is given a value of 0.2 mm. This value is estimated from values given by Budd, Dingle and Radok (1966) for different surface types in Antarctica; hard smooth snow, $z_0 = 0.119$ mm; Dunes, barchans, sastrugi, $z_0 = 0.146$; Soft snow, $z_0 = 0.220$. Estimation is a suitable method to use because a weighted average could not be made, as the surface types are unknown over the region to be modelled.

SURFACE ALBEDO

The albedo value used is 0.75 . This is an estimate for the entire grid region, from albedo values given by Weller (1980) for three zones of Antarctica; Interior continental zone, $\alpha = 0.85$, Coastal ablation zone, $\alpha = 0.69$ and Coastal sea ice zone, $\alpha = 0.65$. Albedo is not a significant factor when modelling July conditions, because the incoming solar radiation is minor. For January period model runs, the sea region contains no sea ice and the temperature of the water does not vary during the course of a run. Therefore the albedo value corresponding to the Coastal sea ice zone is not relevant for these January and July test runs.

The representation of surface albedos used in the model are reviewed, and improved, when sensitivities of thermal fields to changes in albedo are examined in Chapter 6.

CORIOLIS

The Coriolis parameter depends on the latitude and is defined uniquely for each grid point. Although the Coriolis parameter does not vary a great amount with change in latitude for high latitude regions, as is being modelled, for two reasons it was considered useful to define Coriolis in this way, instead of using a mean value over the whole grid, as it was defined in the 1981 version of the model.

The first reason is that the region modelled, (see Section 4.3), is relatively larger than has been modelled in the past using this model, and therefore the

use of a constant Coriolis parameter over the entire grid becomes a less valid approximation. The second is that the Coriolis parameter should be accurately defined over Antarctica because the surface friction is very low and therefore Coriolis may have a relatively more important role to play in regards to influencing air flow near the surface than it would in other regions of the world.

However, it was found that there were only very minor changes to both wind fields and temperature fields when Coriolis was defined uniquely at each grid point instead of using a mean value over the whole model grid. Tests involving sensitivities to Coriolis are not investigated further.

TIME EVOLUTION OF SOLUTIONS

Following a 4 hour simulated period of "spin up", the model was integrated for 24 hours (model time), for July runs because this was when the solutions reached a steady state, which was possible because the synoptic forcing was constant and there were no significant diurnal variations. This knowledge was used to estimate the integration time required for January model runs, which was more difficult to observe due to the diurnal wave present in the solutions. Results from January modelling were extracted at integration times varying from 12 to 48 hours, depending on the time of day required. However, it was found for both January and July runs that the model reached an approximately steady state (when neglecting the diurnal variations) only about 2 hours following the "spin up" period.

Chapter 5

INITIAL NUMERICAL MODEL RUNS: PARAMETERISATION ADJUSTMENTS

5.1 INTRODUCTION

This chapter presents the first CSU-Pielke model runs carried out for the region of East Antarctica outlined in Figure 4.1, Chapter 4.

The aim of conducting these model runs is to produce data that may be examined so that problems or inaccuracies, relating to parameterisations of meteorological fields, can be found and remedied, before further simulations are carried out and discussed in later chapters. This is important because the numerical model has mainly been used in the mid-latitudes, (see Chapter 4), and it is desirable to test the performance of the model under Antarctic conditions.

The ten runs discussed in this chapter, listed in Table 5.1, were all forced with negligible synoptic winds, and were initialised with monthly mean data, discussed in Chapter 4.

The results of these initial runs revealed three problems. These were subsequently solved by adjusting the parameterisations of meteorological fields. Further improvements, by tuning the model, are discussed in Chapter 6.

There was a problem with the surface energy balance iteration scheme. Values were converging to solutions that were mathematically correct but nonsense in terms of surface temperature. This problem and the solution are discussed in

Section 5.2.

During summer, it is assumed that there is no ice present in the sea, but during winter, it is assumed to be covered completely with sea ice; polynyas and variations in open water fractions are not considered in this project.

The surface temperatures of the sea ice region that developed in July model runs were too low, compared with observed values. This problem must be fixed because the basis for realistic modelling of the Antarctic atmospheric boundary layer is the realistic definition of surface temperatures; air interacts with the surface and there are exchanges of heat and moisture. Inaccurate temperatures of the surface lead to inaccurate air temperatures in the boundary layer, which has an effect on the wind field. The problem of inaccurate surface temperatures is shown in Section 5.3.

The improvement in representation of the sea ice surface temperatures and the methods used to achieve this are dealt with in Section 5.4.

The performance and realism of the Deardorff (1974) scheme for parameterisation of Planetary Boundary Layer (PBL) heights were examined. Although accurate overall, a problem was found in model runs that were defined with July (Antarctic polar night) conditions. Over small terrain slopes, with low wind speeds, significant cooling of the firn (ice and snow) surface can occur due to loss of long-wave radiation. Strong inversions develop and the result is the parameterisation of extremely low (about 5 metres) PBL heights.

Other meteorological fields appeared reasonable with regard to the initial conditions, but as these depend to some degree on the PBL heights that are used at each grid point during each time step of a model run, they may not be as accurate as can be achieved using a PBL parameterisation scheme that is more suited to conditions of weak wind and very strong inversion, that occur over regions of the Antarctic plateau during winter.

Section 5.5 questions the realism of modelled PBL height values and also discusses numerical problems that arise from small PBL depths. Possible ways

Run	Month	Firn Diffusivity	Sea/ice	PBL depth scheme
R01	January	0.9 x 10^{-6} m^2s^{-1}	sea*	D
R02	July	0.9 x 10^{-6} m^2s^{-1}	sea ice**	D
R03	July	1.3 x 10^{-6} m^2s^{-1}	sea ice**	D
R04	July	0.4 x 10^{-6} m^2s^{-1}	sea ice**	D
R05	July	0.9 x 10^{-6} m^2s^{-1}	sea ice***	D
R06	July	0.9 x 10^{-6} m^2s^{-1}	sea ice †	D
R07	July	0.9 x 10^{-6} m^2s^{-1}	sea ice ‡	D
R08	July	0.9 x 10^{-6} m^2s^{-1}	sea ice*	D
R09	July	0.9 x 10^{-6} m^2s^{-1}	sea ice*	A
R10	July	0.9 x 10^{-6} m^2s^{-1}	sea ice*	D & A

Table 5.1: Descriptions of model runs conducted in this chapter.
* Prescribed surface temperature,
** Sea ice temperatures calculated using the surface energy balance scheme that is used over the continent, as noted in Chapter 4 and on Section 5.2,
*** Sea ice temperatures substituted from the temperature of the nearest land point,
† Sea ice 25 cm thick, (25 levels, each of 1 cm thickness),
‡ Sea ice 1 m thick, (25 levels, each of 4 cm thickness).

to improve the scheme are discussed and a minor change is made and tested in Section 5.6 .

Conclusions are drawn in Section 5.6 .

5.2 THE SURFACE ENERGY BALANCE ITERATION SCHEME

The surface energy balance equation, containing terms that represent incoming short-wave(less reflected), incoming long-wave radiation, latent and sensible heat fluxes, soil heat flux and outgoing long-wave radiation, was balanced at each time step for each grid box using the Newton-Raphson iteration method. Discussed below, this is also described by Mahrer and Pielke (1977) and Pielke (1984).

$$R_{SHORT} + R_{LONG} + \rho L u_* q_* + \rho c_p u_* \theta_* - \rho_s c_s K_s \left.\frac{\partial T}{\partial z}\right|_G - \sigma T_G^4 = 0 \qquad (5.1)$$

where R_{SHORT} : short-wave radiation (less reflected due to albedo), at the surface,

R_{LONG} : long-wave radiation (incoming), at the surface,

$\rho L u_* q_*$: latent heat flux,

$\rho c_p u_* \theta_*$: sensible heat flux,

$\rho_s c_s K_s \left.\frac{\partial T}{\partial z}\right|_G$: soil heat flux, where $\left|_G\right.$ denotes this quantity to be at the surface,

σT_G^4 : long-wave radiation (outgoing),

c_p : specific heat at constant pressure,

c_s : specific heat of soil,

K_s : soil heat diffusivity,

L : latent heat,

q_* : surface friction humidity,

u_* : surface friction velocity,

ρ : density,

ρ_s : surface density,

θ_* : surface friction (potential) temperature.

In Equation 5.1, θ_* and T_G are both unknown. The heat balance equation is solved by expressing θ_* in terms of T_G. The terms u_*, q_*, ψ_1 and ψ_2 are assumed to be constant:

$$\theta_* = k_0(\theta(1) - T_G(\frac{P_{00}}{P_G})^{\frac{R}{c_p}})/[0.74(ln\frac{z}{z_0} - \psi_2) + 0.0962(\frac{u_* z_0}{\nu})^{0.45}] \qquad (5.2)$$

where P_{00} : reference pressure,

P_G : surface pressure,

R : gas constant for dry air,

z : height above surface,

z_0 : surface roughness parameter,

ν : kinematic viscosity of the air,

ψ : surface layer parameter, shown in detail by Mahrer and Pielke (1977).

The surface roughness parameter, z_0, was input, as noted in Chapter 4, as a value of 0.2 mm. Over water, it was calculated using the scheme of Clarke (1970):

$$z_0 = 0.032u_*^2/g \tag{5.3}$$

with the condition that $z_0 \geq 0.0015$ cm.

The surface energy balance equation is solved for surface temperature using the Newton-Raphson method:

$$T_G^{\tau+1} = T_G^{\tau} - \frac{F(T_G)}{F'(T_G)} \tag{5.4}$$

where $T_G^{\tau+1}$: land surface temperature at the next step in the iteration,

T_G^{τ} : land surface temperature at the present step,

$F(T_G)$: sum of the terms on the left hand side of Equation 5.1,

$F'(T_G)$: derivative of $F(T_G)$ for the present value of the land surface temperature.

The term on the right in the denominator of Equation 5.2 is added to the surface layer equation of Businger (1973), (discussed by Mahrer and Pielke (1977)), because these formulae require temperature and specific humidity at z_0 rather than at the surface. Equàtions 5.5 and 5.6 show $\theta(z_0)$ and $q(z_0)$ expressed as functions of u_* and θ_*, and u_* and q_*, respectively from the work of Zilitinkevich (1970).

$$\theta(z_0) = \theta_G + 0.0962\frac{\theta_*}{k_0}\left(\frac{u_* z_0}{\nu}\right)^{0.45} \tag{5.5}$$

$$q(z_0) = q_G + 0.0962\frac{q_*}{k_0}\left(\frac{u_* z_0}{\nu}\right)^{0.45} \tag{5.6}$$

The derivative of $F(T_G)$ can then be expressed as shown in Equation 5.7:

$$F'(T_G) = ((\rho c_p u_* k_0)/[0.74(ln\frac{z}{z_0} - \psi_2) + 0.0962(\frac{u_* z_0}{\nu})^{0.45}])(\frac{P_{00}}{P_G})^{\frac{R}{c_p}}) - \frac{\rho_s c_s K_s}{\Delta z_G} - 4\sigma T_G^3 \quad (5.7)$$

The iteration process is complete when fifty iteration steps have been carried out or when the value of $F(T_G)$, the left hand side of Equation 5.1, is found to be less than 10^{-5} Wm^{-2}, and therefore relatively close to the right hand side, zero.

Tests of the model with the surface defined to be soil, as that in the mid-latitude region of Melbourne, Australia, and used in modelling by Abbs (1986), did not result in problems due to use of this iteration scheme. However, when the ground surface inside the model was defined to be firn, a problem was revealed.

There are multiple roots that the iteration technique may converge towards, or possibly it may not converge. The solution is sensitive to the initial values used. The definition of the firn surface in the model meant that a different set of surface parameters was used (compared to that for Australia). It was found that very small changes in surface parameters could cause convergence to unrealistic values, such as a negative absolute temperature.

It was not acceptable to simply check for this possibility and adjust the surface temperature because the components of the surface energy balance equation would then not be balanced in respect to one another for that specific grid box. This problem was solved by checking for unrealistic values once a root had been converged upon, adjusting the initial conditions by a very small amount (if the result was unrealistic) and then re-iterating. This was repeated until the root found was an acceptable value. It was essentially a problem of high-sensitivity to initial conditions.

5.3 COMPARISON BETWEEN MODELLED AND OBSERVED SURFACE TEMPERATURES

JANUARY

The differences between modelled and observed surface temperatures for January are shown in Figure 5.1. The temperatures differ slightly from those generated by the mean January runs in Chapter 6, where the model is tuned and results are verified using observations.

The initial temperature sounding at Mawson station did not define the presence of an inversion. After a period of 24 hours simulated time, the vertical stratification of the air did not vary significantly. This is the expected result because under January radiation conditions, the temperatures may vary throughout the day but there should be only minor changes from day to day at the same location for the same local hour.

For mesoscale modelling of July Antarctic conditions, the scenario is different; other than the sea, there is not a major heat source because the sun is below the horizon. Therefore the surface temperatures can fall due to radiational cooling that is not compensated for by solar input. In reality, heating can also occur for other reasons, such as poleward advection of warm air associated with the large scale circulation, and adiabatic subsidence of air that moves poleward at higher levels in the troposphere.

Weller (1968) noted that there was no inversion present at Mawson. However, analyses presented in Chapter 3 show that weak inversions are sometimes present at this station. Although possibly more relevant to winter conditions, Ball (1957) mentioned the relatively tranquil and well mixed layer of air over the sea. More realistic synoptic wind speeds are used in modelling in Chapter 6, which affect the winds strengths over the sea to the north of the continent.

Although cyclones are not represented in this model, it is important that the area of sea and sea ice is represented realistically so that it does not interfere with the meteorological conditions occurring over the continent and at the coast.

No problems with parameterisations were found in the results of January test run R01. The differences between modelled and observed surface temperatures are discussed further in Chapter 6. The results from July test run R02 show two problems.

JULY

Model generated surface temperatures from the mean July run, have a problem over the sea ice area. The differences between modelled and observed surface firn temperatures are shown in Figure 5.2. The modelled temperatures over the sea ice are very low, compared with observations.

Realistic values for sea ice surface temperatures during July are about 253 to 254 K. The temperature varies depending on the open water fraction, but these values can be considered accurate. Simmonds and Budd (1991) presented AGCM modelling results of average surface temperatures of sea ice for various open water fractions for the month of July. For no open water, the average surface temperature of the sea ice was 253.9 K. Weller (1968) measured sea ice surface temperatures one kilometre from Mawson and found the July average to be 253.5 K.

Weller (1968) provided valuable measurements of conducted heat fluxes at upper and lower boundaries of sea ice. Half-monthly values for the period mid-June to mid-November all showed that the fluxes were from sea water towards the sea ice and from the sea ice to the atmosphere.

In test run R02, the thermal regime of the sea ice was parameterised in the same manner as ice over the continent. This method is not acceptable because it allows the sea ice to cool in the same manner as an ice shelf not significantly affected by winds and thick enough to prevent significant heat transfer from the sea underneath.

Figure 5.3 shows the presence of a strong inversion over the sea ice. This is not realistic and has been generated in test run R02 due to the unrealistically

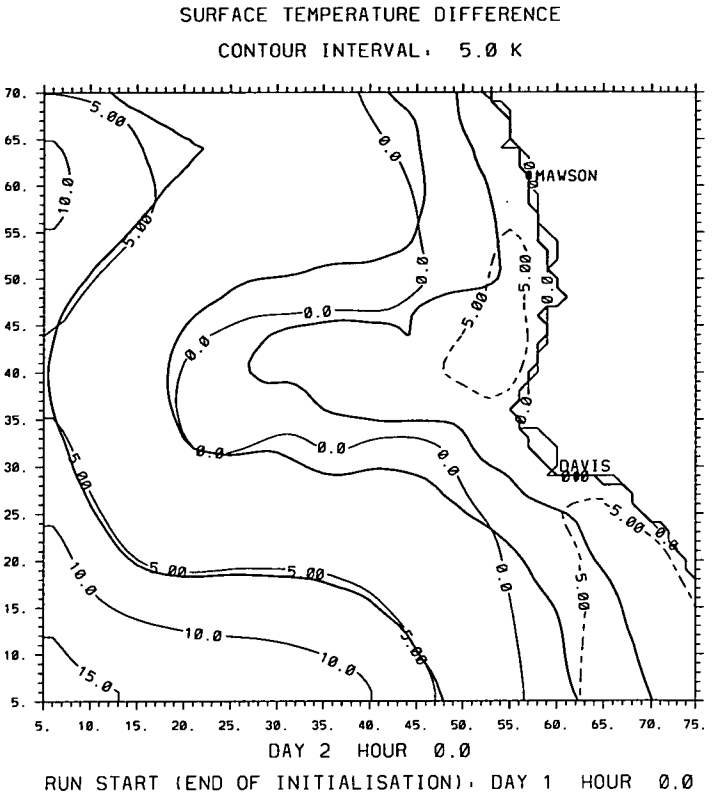

Figure 5.1: January modelled surface firn temperatures, from model run R01, less observed values.

low sea ice surface temperatures.

Weller (1968) stated that the stratification of the air over the sea ice is neutral or close to neutral and that "...proper inversions due to radiational cooling of the surface did not develop, since there was always a constant large heat supply to the surface from the sea water below." These observations were made over the sea ice one kilometre from Mawson.

It is therefore necessary to parameterise the thermal regime of the sea ice in a different manner to that used for the surface of the continent. Before this change is made, two runs are carried out to test the sensitivity of the modelled surface temperature to changes in surface properties.

SENSITIVITY TEST: SURFACE DIFFUSIVITY

The surface diffusivities shown in Table 5.1 represent Antarctic surfaces, but the range of values is relatively large. The effect of using different values to those used in runs R01 and R02 is examined.

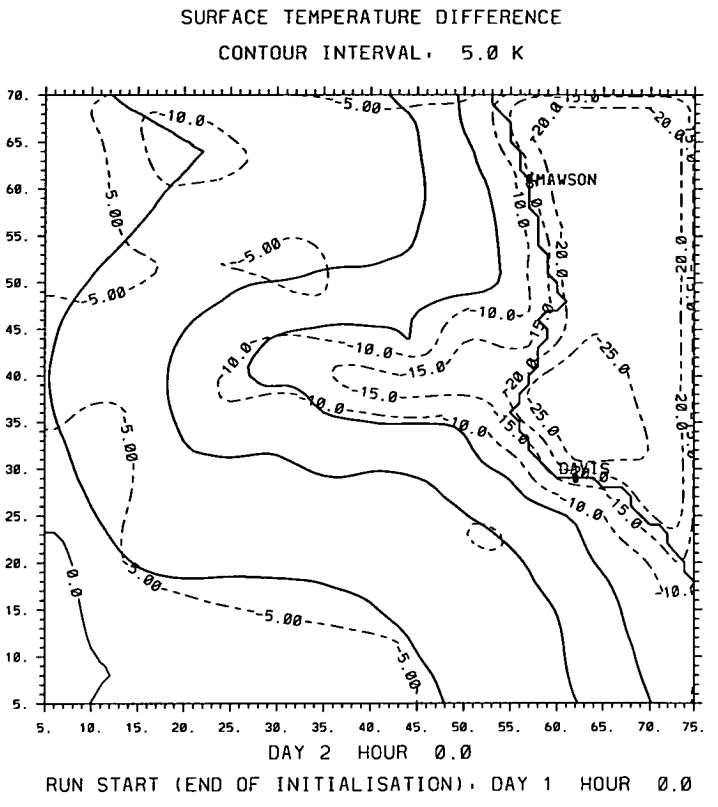

Figure 5.2: July modelled surface firn temperatures, from model run R02, less observed values.

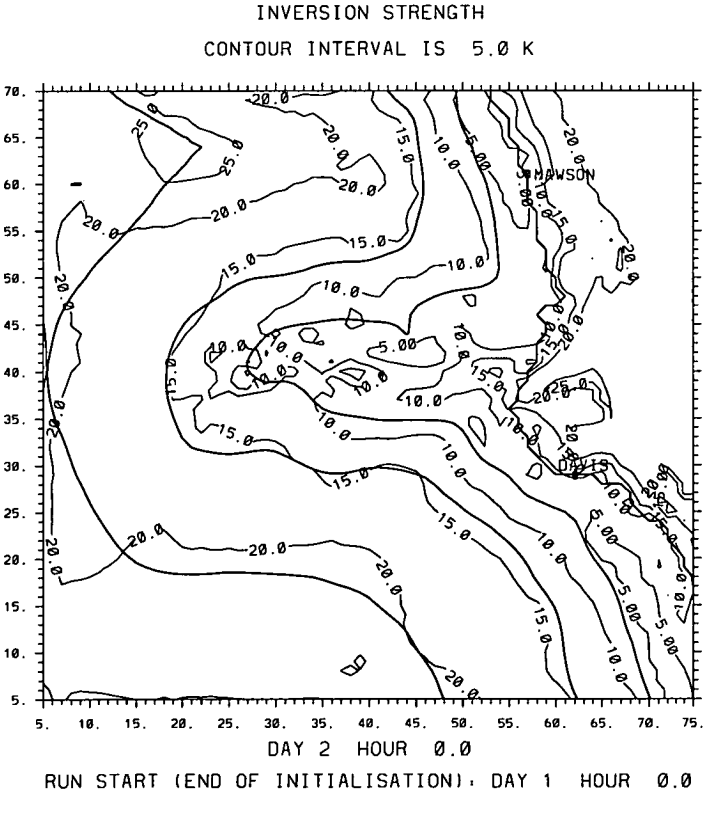

Figure 5.3: July modelled inversion strength, from model run R02.

The following two test runs, R03 and R04, are both initialised with mean July conditions, but they differ from R02 in the surface diffusivities that are used. Run R03 defines the surface to be pure ice, while R04 defines the surface to be the same as that used by vanMeurs and Allison (1988). Corresponding diffusivities are shown in Table 5.1. These changes to surface thermal properties demonstrate the importance of accurate definition of surface parameters. These runs also show the effect of surface properties on the surface temperature and the inversion strength.

Other model parameters are constant between runs, so the surface diffusivities used cause run R03 should inhibit surface cooling and inversion formation, while R04 should encourage surface cooling and inversion formation. Because the surface properties used in test runs R01 and R02 have generated realistic surface temperatures over the continent, the results of runs R03 and R04 are of most interest over the sea ice region.

Figure 5.4 from test run R03, show that the high surface diffusivity value that was used inhibits surface cooling significantly. The surface temperatures are generally about 10 K higher than those produced by test run R02. However, the differences between surface temperatures modelled in run R03 and the observed mean July surface temperatures are largest over the sea ice region, despite the decrease in differences. This supports the conclusion reached previously, that the thermal regime of the sea ice region should not be handled the same way as the land firn surface. It is not plausible to adjust the surface properties so that the diffusivity is high enough to prevent the sea ice region cooling too much, because this prevents the land surfaces cooling to realistic temperatures.

In Chapter 6, sensitivity tests are conducted to examine the changes in surface diffusivity that occur with changes in temperature of the firn surface.

As expected, the surface temperatures generated by run R04 are lower than those produced from runs R02 and R03, due to the higher surface diffusivity value used. The differences shown in Figure 5.5 show that the surface temperatures are

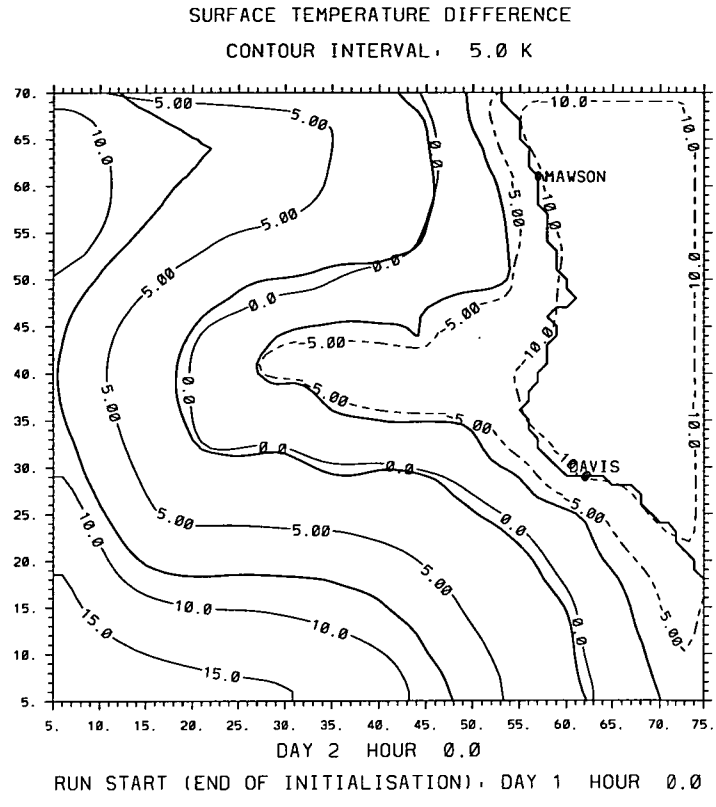

Figure 5.4: July modelled surface firn temperatures, from model run R03, less observed values.

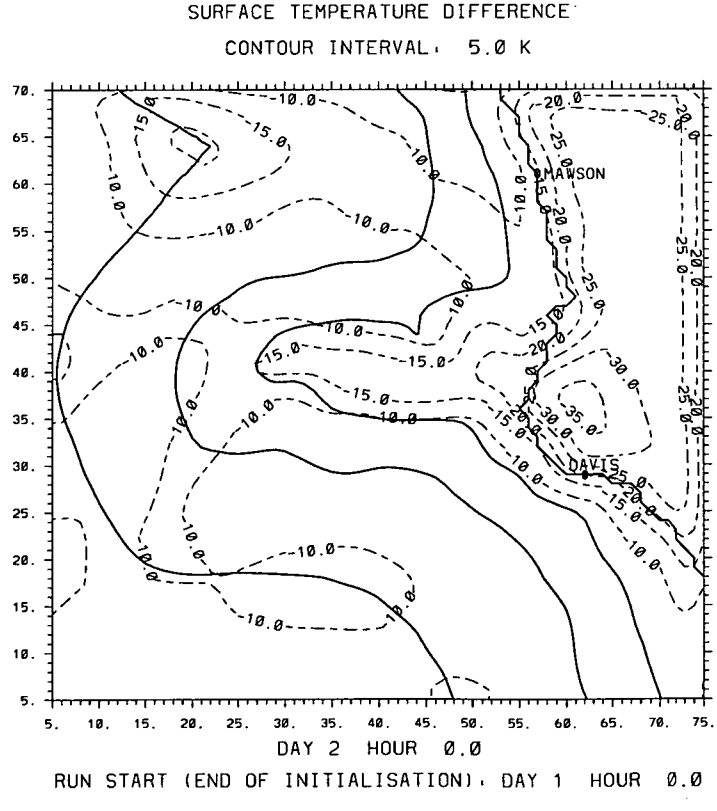

Figure 5.5: July modelled surface firn temperatures, from model run R04, less observed values.

significantly lower than the observed mean July surface temperatures.

It is concluded that the definitions of the surface parameters are important because they directly influence the surface temperatures depending on the value of thermal diffusion. The surface parameters play an important part in the energy balance between the surface, the lower layers of the firn and the atmosphere. The slope of the terrain and the ability for the surface to cool are important factors for inversion formation.

The results from model runs R03 and R04 also support the use of those surface parameters defined in run R02, except for over the sea ice region. Runs R05 to R08 are used to test adjustments to the representation of sea ice temperatures, and these are discussed in the following section.

5.4 IMPROVED REPRESENTATION OF SEA ICE SURFACE TEMPERATURES

It was found in the previous section that winter simulations produced sea ice surface temperatures that were significantly lower than observed values. These led to the formation of unrealistically strong temperature inversions over the sea ice region.

Several methods of defining the temperature of the sea ice were tested. The first involved finding the nearest coastal grid point to each sea ice grid point and substituting the surface temperature value from the coast into the particular sea ice grid point. This method was used in run R05.

Figure 5.6 shows that this method is not satisfactory because it does not take into account the relatively warm sea ice temperatures that exist due to heat transfer from the underlying sea water. Also, the heat flux from the sea surface (in areas of open water), to the atmosphere, is not considered, in even an approximate form, when this method is used.

The mesoscale model does not define warm air advection from lower latitudes, as an AGCM does. The aims of this project are primarily concerned with the

boundary layer air flow over continental Antarctica. Sea ice surface temperatures influence air flow near the coast and it is therefore necessary to define them realistically.

Test run R06 simulated thermal transfers in sea ice of thickness 25 centimetres. This small thickness was used as an initial test. The sea ice was divided into 25 vertical levels of 1 centimetre thickness each and the lowest level was set to a constant temperature of 271.3 K, which is marginally lower than freezing point of sea water, (-1.8°C = 271.4 K).

Sea ice temperatures that resulted were fairly realistic, as shown by Figure 5.7. However, Mellor (1960) showed that the sea ice thickness for July near Mawson and Davis is very close to 1 metre.

Test run R07 used a sea ice thickness of 1 metre with 25 levels each of 4 centimetres thickness. Despite the promising result from run R06, the resulting surface temperatures of the sea ice after 24 hours of simulation were unrealistically low, as shown by Figure 5.8. This can be explained by Weller (1968) measurements of heat transfers through sea ice. A thermal wave travelling through the sea ice near Mawson had a period of 50 days during July, August and September of one year. This means that a period of one or two days (as modelled here), is too short to establish realistic temperatures throughout sea ice of thickness 1 metre or greater using thermal transfers.

One possible solution is to initially define the temperatures of the sea ice at each level. However, for ice of realistic July thickness, about 1 metre, the changes to sea ice surface temperatures due to thermal transfers are not significant over periods of 24 or 48 hours, when mean conditions are being considered. It is therefore better to apply realistic surface temperature values to the sea ice instead of modelling the heat transfers. Model run R08 used this method and the results are shown in Figures 5.9 to 5.10. The sea ice region has a surface temperature of 253.9 K, (from Simmonds and Budd (1991)), applied to it, but the continental surface temperatures are computed at each time step for each grid box using the

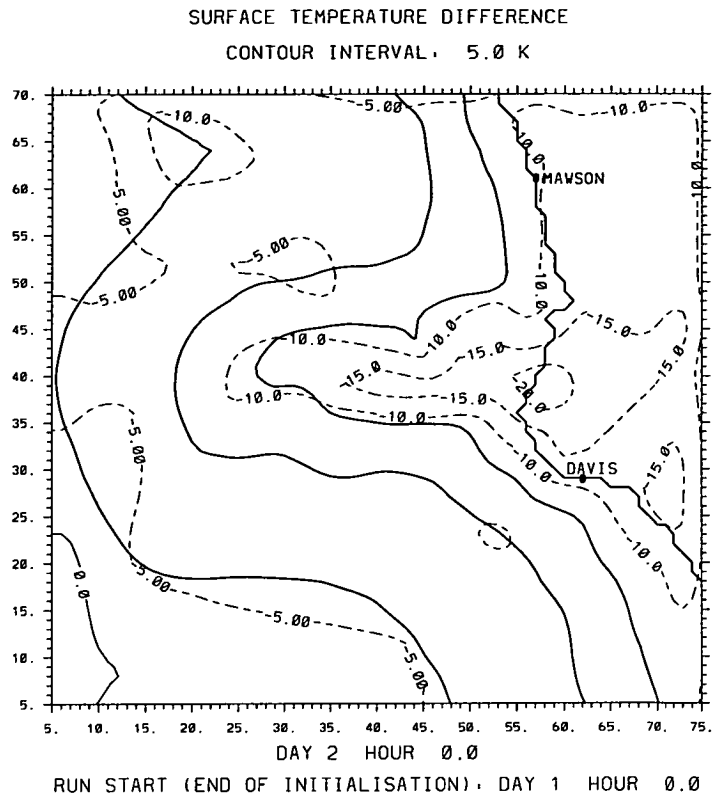

Figure 5.6: July modelled surface firn temperatures, from model run R05, less observed values.

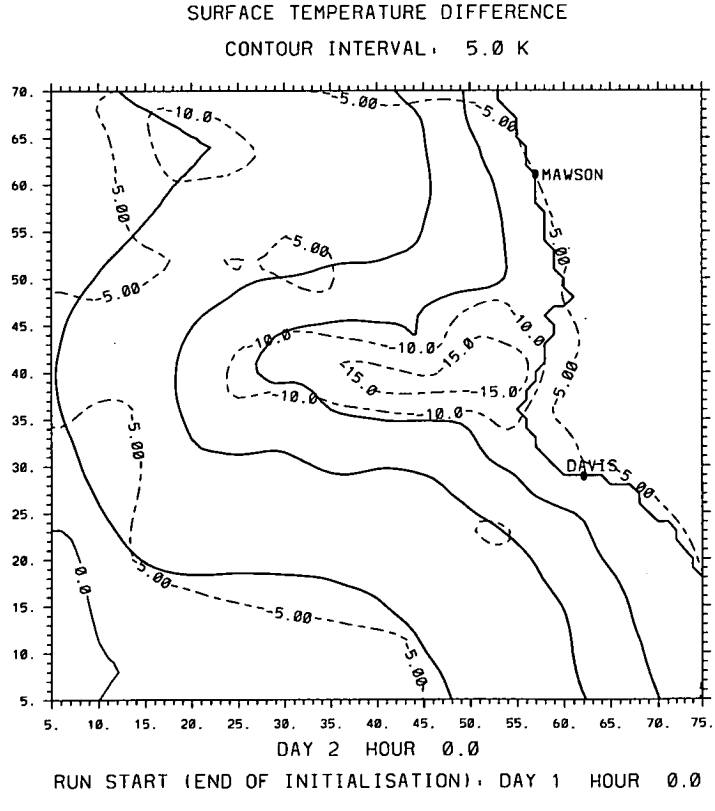

Figure 5.7: July modelled surface firn temperatures, from model run R06, less observed values.

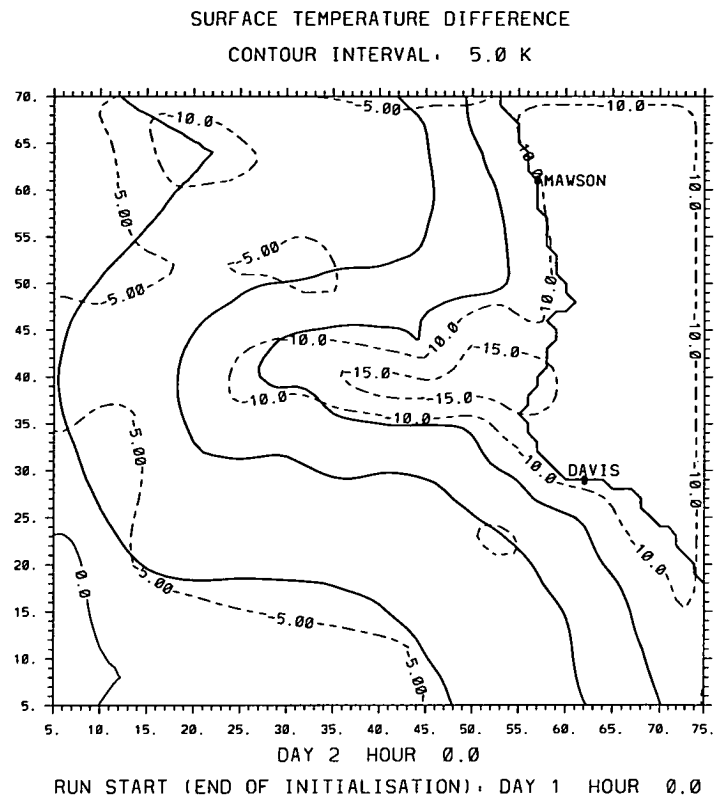

Figure 5.8: July modelled surface firn temperatures, from model run R07, less observed values.

surface energy balance scheme, as noted in Chapter 4.

The surface temperatures are fairly realistic over the continent, and are further improved in Chapter 6.

The inversion strengths, shown in Figure 5.10, show that there is a very strong inversion in the vicinity of grid point (20,63). This is due to the small slope of the terrain. A problem with parameterisation of PBL heights when strong inversions are present is discussed in the following section.

Strong inversions also occur near the boundaries of the grid. These occur because the four lateral grid spacings around each side of the grid have no slope (in terms of terrain), from one point to the next for reasons of computational stability, as previously discussed in Chapter 4. The only disadvantage of using this method for removing potential computational instabilities is that the "terrain" of these lateral regions is flat and therefore the inversion is able to increase in strength because the winds are of insufficient strength to generate mixing. This

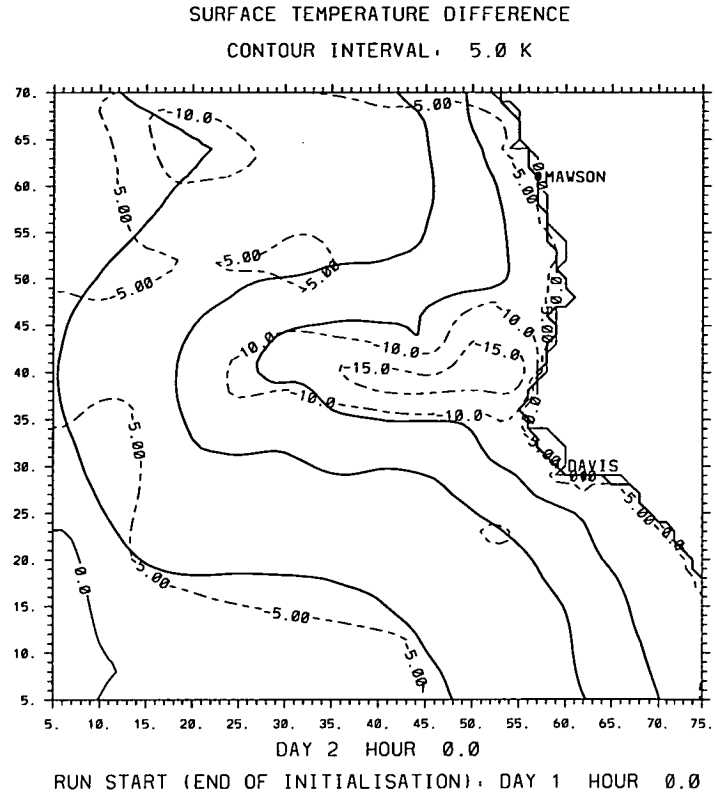

Figure 5.9: July modelled surface firn temperatures, from model run R08, less observed values.

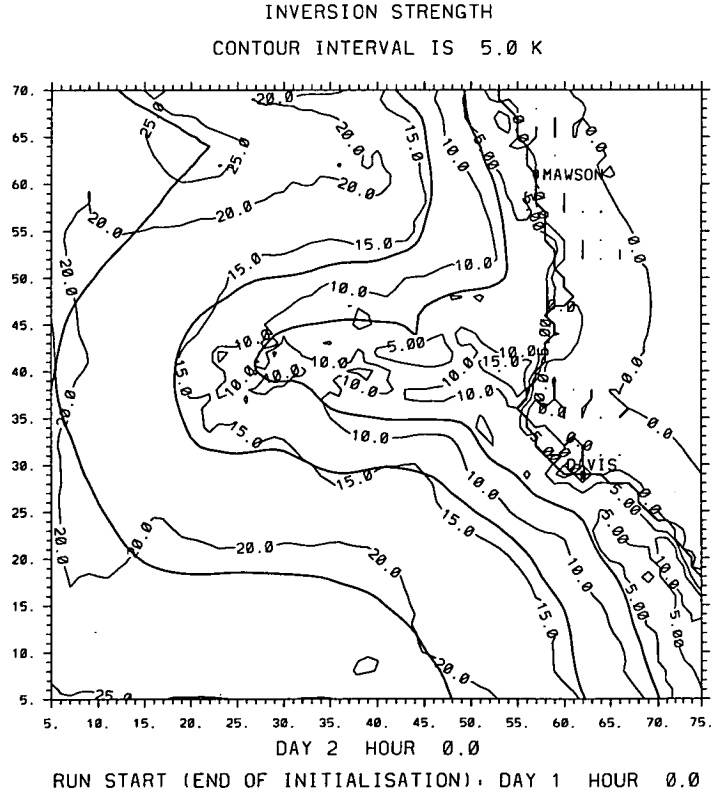

Figure 5.10: July modelled inversion strength, from model run R08.

is not a problem in terms of how well the model functions, but over the four or five neighbouring grid spacings there can be some advection from the lateral grid point regions and this results in the unusually strong inversion, as shown by Figure 5.10 in the bottom left hand corner, where the 25 K contour approximately follows the edge of the grid. This "edge-effect" does not cause problems and the region of interest is a significant distance away from the boundaries in any case.

The absence of a significant inversion over the sea ice region has been shown to depend upon the accurate definition of surface parameters. Gallée and Schayes (1992) used a thermal diffusivity of 0.27 x 10^{-6} m^2 s^{-1} for the snow surface in their modelling. The comparison of the three test runs R02, R03 and R04 showed that the surface diffusivity of 0.4 x 10^{-6} m^2 s^{-1}, used in R04, was too low because it allowed the surface to cool too much and the inversion strengths subsequently became too large. Although the ground surface temperatures of the CSU-Pielke model and the Gallée and Schayes (1992) model are predicted using different schemes, the surface diffusivity is a real parameter that does not alter depending on what parameterisation scheme is used. The inversion strength presented by Gallée and Schayes (1992) is too strong over the region seaward from the coast. This may influence the dynamics of the katabatic wind that they modelled.

5.5 USE OF DEARDORFF SCHEME OVER ANTARCTIC INTERIOR

This section discusses observations and model-generated results, so that the problems relating to PBL prediction and their likely causes may be examined.

The problems with the Deardorff (1974) PBL parameterisation scheme for use in the Antarctic atmosphere fall into two categories.

The first involves the realism of the PBL height that is predicted by the Deardorff (1974) scheme, which is the scheme present in the 1981 version of the CSU-Pielke model, used in this project, (see Chapter 4). The difficulty with examining the realism of the values produced is that there is little real data available with which they may be compared.

The second category is to do with computational problems that arise when the PBL height falls to a low level.

5.5.1 REALISM OF LOW PBL HEIGHTS

The realism of the modelled thermal fields has been discussed earlier in this chapter. The wind field shall be specifically covered in more detail in later chapters; the aim here is to examine the PBL heights. Figure 5.13 is an xy-plot of PBL height contours over the model domain, as produced from run R08. Around the coastal regions the PBL heights are in the order of hundreds of metres and there are several maxima present where there is convergence of air. (Wind fields are modelled in the following chapter using real wind data instead of the negligible upper wind that was applied to runs R01 - R10 in this chapter, that was done for purposes of testing modelled thermal fields and parameterisation schemes).

Far inland, with grid point coordinates (29,63), there is a minimum in the PBL height, with a value of 5.96 metres. The realism of such a low value is questioned. There are no atmospheric sounding data available for the area near this point. Use of data from coastal stations are not suitable because the atmospheric temperature and wind field structures vary greatly between these environments. Use

must be made of data that are available from inland stations where conditions are similar. The terrain slope at grid point (29,63) is 0.0007, significantly less than coastal regions but the same order of magnitude to those at inland stations, such as Vostok (terrian slope: 0.0011), Sovietskaya (terrain slope: 0.0015) and Amundsen-Scott (terrain slope: 0.0018). However the slope at grid point (29,63) is very low, even for the plateau region. Due to the differences in elevations, synoptic and local meteorological conditions and distances from the coast at these locations, atmospheric data that are available can only be used as a very approximate guide to what may occur at the real location that is modelled for grid point (29,63). The terrain slope at and near grid point (29,63) is anomalously low, as shown by Figure 4.4, in Chapter 4.

The discussion below is based on the assumption that the height of the planetary boundary layer and the inversion depth are proportional over inland areas of Antarctica. The validity of this assumption is then discussed.

Monthly mean depths and strengths of surface inversions were tabulated by Wilson (1968) for Antarctic inland stations. The stations were Vostok, South Pole (Amundsen-Scott), Sovietskaya, Pionerskaya and Byrd.

As there were only four years of data presented, this collection would be inadequate for establishing a good climatology of monthly mean inversion depths and strengths for these locations, but there are enough data to indicate realistic magnitudes for inland areas of Antarctica.

In terms of terrain, data from Amundsen-Scott should be suitable because the altitude of this station (2800 metres) is relatively close to that at point (29,63) (2971 metres) and the terrain slopes of these two locations are also similar. However, as noted above, other factors differ to such a degree as to not allow the atmospheric environment at one location to be applied to the other. Sovietskaya is the closest station to the region of interest and is located at 78°24'S, 87°32'E, which corresponds to model grid point (10,7). This is hundreds of kilometres away from grid point (29,63) and again demonstrates the sparseness of data coverage

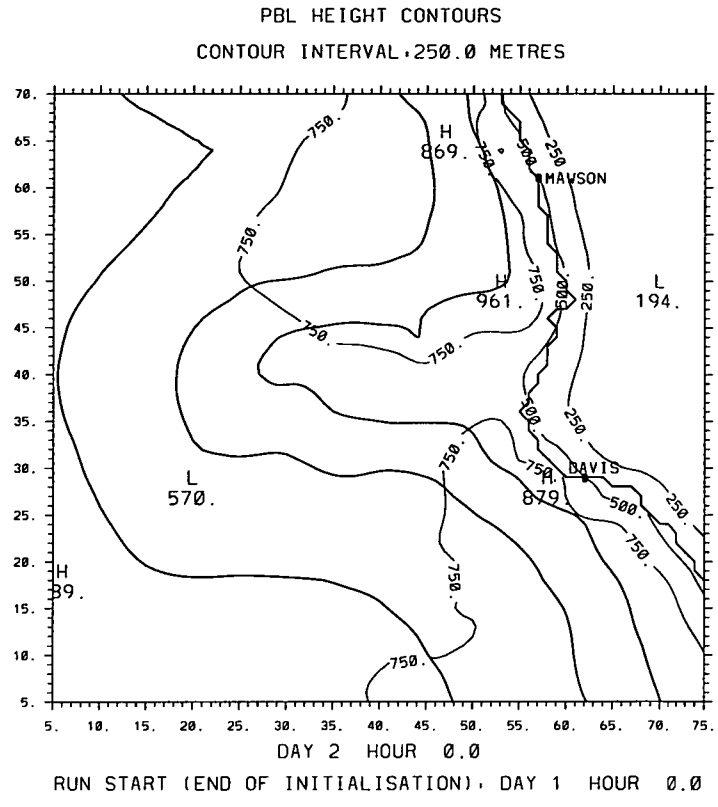

Figure 5.11: January modelled PBL depth, as predicted using the Deardorff (1974) scheme, from model run R01.

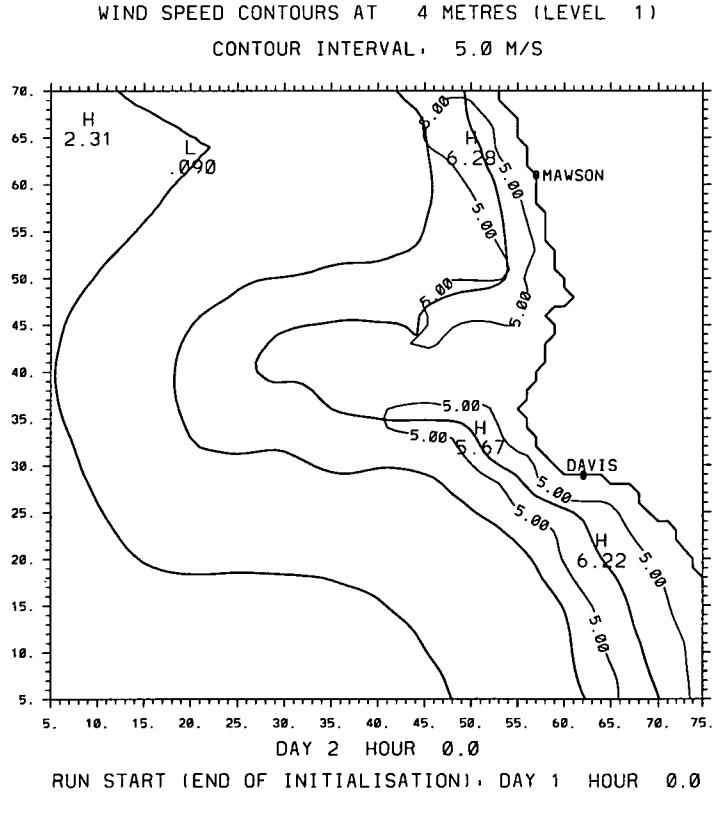

Figure 5.12: January modelled surface wind speeds, from model run R01.

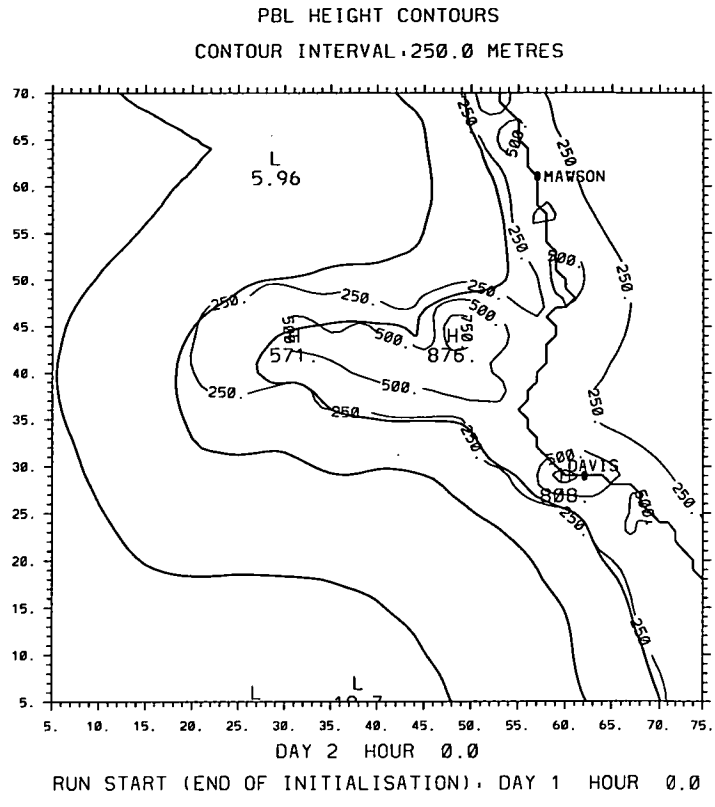

Figure 5.13: July modelled PBL depth, as predicted using the Deardorff (1974) scheme, from model run R08, following the correction to the unrealistically low surface temperatures of the sea ice.

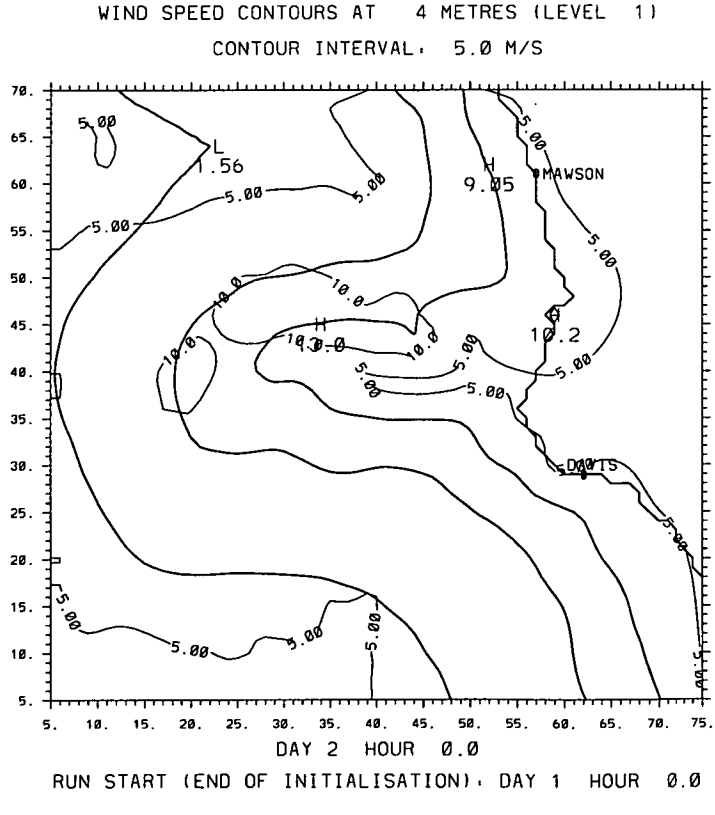

Figure 5.14: July modelled surface wind speeds, from model run R08, following the correction to the unrealistically low surface temperatures of the sea ice.

over Antarctica, previously discussed in Chapter 3.

Although the Antarctic winter spans more than three months, data for the months June, July and August shall be used to determine PBL heights of realistic magnitudes. Over the years 1957 to 1961, the five plateau stations measured a mean "winter" PBL height of 735 metres. The minimum monthly mean PBL depth of any station was 485 metres at Byrd and the maximum monthly mean depth of any station was 1118 metres at Vostok.

The general trends of both inversion depths and inversion strengths at the inland plateau stations documented by Wilson (1968) show larger values during winter than summer. This suggests that the use of a scheme that was primarily designed to parameterise the height of a heated PBL, such as Deardorff (1974), would function less well over the Antarctic interior.

Figure 5.15 is a plot of the vertical temperature profile at model grid point (29,63), generated by July model run R08. The depth of the inversion is 250 metres, with the lowest region having the greatest temperature gradient. This low level feature was documented by both Dalrymple (1966) and Wilson (1968).

The realism of the inversion strength over the model grid has been confirmed by Phillpot and Zillman (1970), but the anomalously strong inversion at, and surrounding, grid point (29,63) is due to the small slope at this location, shown by Figure 4.4.

The modelled inversion depth of 250 metres has a value of about half of those depth values measured at Amundsen-Scott station for three winter months. This is a good result because model run R08 was initialised with a mean July air temperature profile, that did not contain a significant inversion because it was extrapolated over the entire model grid from the sounding at Mawson. To achieve such a result after 24 hours of simulated time shows that the physics within the model are operating well. This is confirmed by the vertical temperature profile at the same location after 48 hours of simulated time, shown by Figure 5.16, which has an inversion depth of 400 metres.

However, the differences in inversion depth and strength between 24 and 48 hours of simulated time, are minor, Figures 5.15 and 5.16 respectively. The main feature is the intense inversion near the surface, which suggests that the height of the PBL may be around 100 metres.

Bromwich (1976) made precise recordings of boundary layer depths over the Wilkes Ice Cap, (Law Dome near Casey station), East Antarctica, using a tethered kite with attached sensor. The mean observed depth of the cold air layer was 99.7 metres, which supports the modelled temperature profiles, but shows that a parameterised PBL depth of 5.96 metres not realistic.

Because the model grid point (29,63) did not correspond to the specific region and atmosphere around any of the five plateau stations noted above, the inversion depth measurements cannot be used as a strict verification, but only as an indication of the realism of values produced from modelling a different region. It is concluded that the modelled inversion depths and inversion strengths are accurate, because they are in agreement with those observed at other locations over the Antarctic plateau, as described by Wilson (1968).

Continuing the assumption that the inversion depth and PBL height are proportional, the mean values, although at different locations, show that the inversion depth produced by the model at grid point (29,63) is realistic but that the PBL height produced by the Deardorff (1974) scheme is unrealistic.

This assumption is now discussed. In the study of the inversion layer over the Antarctic plateau, by Miller (1974), it was stated that there is no obvious reason why the inversion scale height and the Ekman layer scale height should even be proportional.

Lettau and Schwerdtfeger (1967) and Schwerdtfeger and Mahrt (1968) discussed features of ground based temperature inversions of inland Antarctica. Their work was discussed Chapter 2. Data from Byrd station that were discussed showed that the surface winds were affected to a large degree by the inversion, which suggests that the inversion is an important phenomenon in isolating the

atmosphere near the surface from that above. This is some support for the PBL height and the depth of strong inversions over the Antarctic interior being of similar magnitude, in this case, because the PBL is a region where air is affected by ground frictional effects, but above such a region there is free flow which is representative of geostrophic flow.

Because the work by Lettau and Schwerdtfeger (1967) had essentially the same result whether the 750 mb level (approximately 500 metres above the surface at Byrd station) or the 700 mb level (approximately 1000 metres above the surface at Byrd station) was used to represent the free flow indicates that at this location for the five winter periods 1961-1965, that the PBL height was no higher than 500 metres. If it were higher than 500 metres some difference would be expected between the result found using the two levels because of changes in wind direction due to Ekman spiralling and also possible upper-level turbulence that was discussed by Manins and Sawford (1979a). Although not from the same years, inversion depths listed by Wilson (1968), for Byrd station for the years 1958-1961 for the same months of the year as used in the study by Lettau and Schwerdtfeger (1967), had a mean value of 578 metres. This also supports the case for depths of Antarctic inland inversions and PBL heights having similar magnitudes.

Arya (1988) noted that the top of nocturnal boundary layers coincide with the nose of wind speed profiles but this is only about half of the depth of the inversions that are present. However, these conclusions were arrived at from measurements taken from a tall tower in Texas, USA and from the Wangara experiment conducted in south-eastern Australia.

Zeman (1979) made the point that a nocturnal boundary layer may disappear entirely. The mechanism behind this is the suppression of turbulence by buoyancy forces at night, and with less turbulence the PBL height decreases. From this fall in PBL depth, mean shear may increase and turbulence can be generated. From the results of Lettau and Schwerdtfeger (1967) and Schwerdtfeger and Mahrt (1968), this is unlikely to occur over the Antarctic interior.

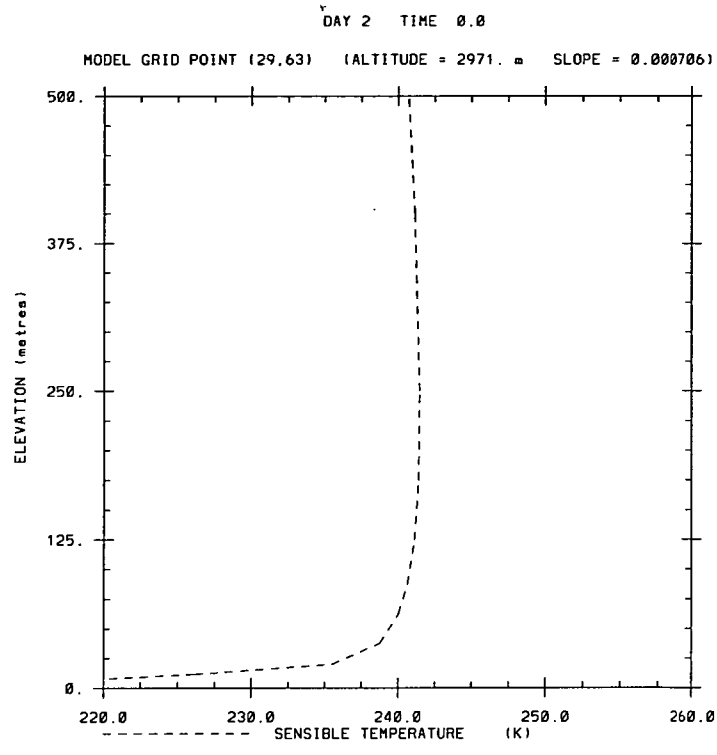

Figure 5.15: July run R08 temperature profile at (29,63) after 24 hours modelling

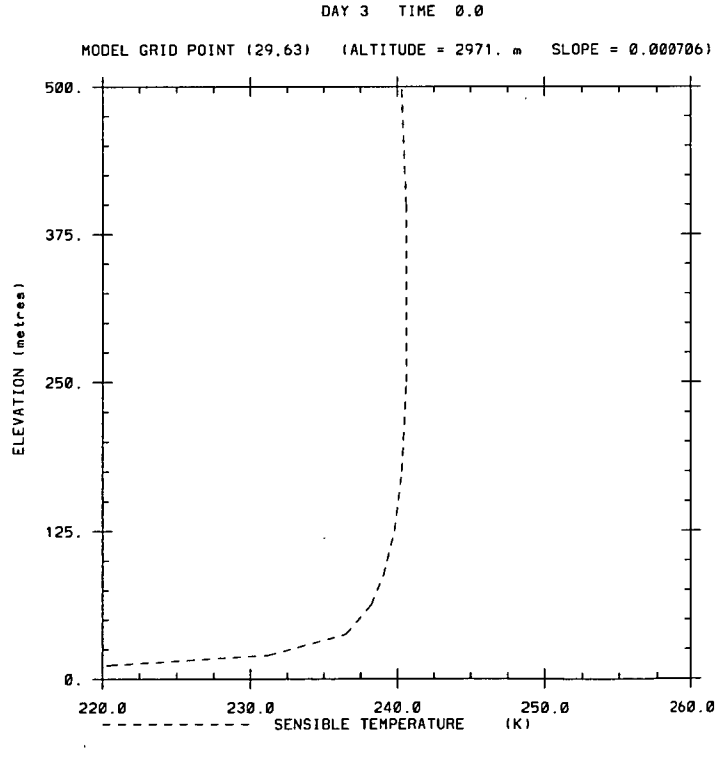

Figure 5.16: July run R08 temperature profile at (29,63) after 48 hours modelling

Given a situation of strong vertical stratification that may be exist through a strong inversion of the Antarctic interior with weak air flow and little turbulence, the PBL height could decrease. In this region during the polar night, there is no disturbance from convective activity, unlike in the sea ice area where polynyas can develop. (This is not relevant to the result of the modelling presented here; polynyas are not simulated in this numerical model, although they can be prescribed).

Other instabilities that can arise are caused by friction or by synoptic development. During these model runs, the synoptic gradient is kept at a constant value. The inland of Antarctica is quite resistant to penetration by cyclones because of the strong inversion during winter; with a well stratified atmosphere, cold air and good drainage from the Antarctic interior, cyclones would need to move up relatively steep slopes, cover distances of hundreds of kilometres and overcome opposing low level winds, before reaching a plateau region. In addition to these "obstacles", there is the lack of a heat source to maintain the vortex. Terrain elevation is also a factor, because the vertical extents of cyclones varies. Those with greater vertical extent may be partially dissipated but can continue to pass over the inland regions of Antarctica at higher levels, around 500 hPa. Shallower vortices, however, are almost totally prevented from penetrating the interior of the continent.

Turbulence caused by friction could exist in a very low region of the atmosphere, even with strong vertical stratification; there is friction/turbulence above and below a katabatic jet. The katabatic is able to flow in the region where there is less turbulence, which is the well stratified region. Using this argument and the presence of the intense inversion shown at grid point (29,63) in Figures 5.15 and 5.16, a PBL height as low as about 50 metres may be justified.

However, this argument depends on the PBL being supported or defined by turbulence alone. There is another approach. The property of the strong inversion to isolate the atmosphere close to the surface from that above has been noted

previously in Chapter 2. This suggests that such a property may define the boundary layer because it is able to separate the meteorological regime next to the surface from the free atmosphere overhead.

More clearly, Arya (1988) defines a boundary layer as the region where there are significant exchanges of momentum, heat or mass between the surface and the atmosphere. For development and maintainence of the strong inversions over the Antarctic plateau, there must be significant exchanges of heat. Applying this specifically to the particular inversion shown in Figure 5.16, the PBL height could be approximately 100 metres, even though the total inversion depth is greater, extending to 400 metres.

In conclusion, considering all these arguments, the PBL height value of 5.96 metres produced by the Deardorff (1974) scheme within the CSU-Pielke model at grid point (29,63) is unrealistic. The inversion depth at the same grid point is a good result. A realistic PBL height, under the modelled polar night conditions of run R08, for this grid point is a value of between about 100 and 400 metres. The depth depends on whether the total inversion is considered, (up to around 400 metres), or whether the most intense region of the inversion is considered, (up to around 100 metres).

5.5.2 COMPUTATIONAL PROBLEMS OF THE NUMERICAL MODEL CAUSED BY LOW PBL HEIGHTS

With the great strength of inversions over the interior of Antarctica, Phillpot and Zillman (1970), and the large vertical temperature gradient within the lowest 50 metres of the inversion, a prediction of PBL height is difficult to make. The results of the four model runs carried out in this test show that the Deardorff (1974) scheme has a significant dependence on the lapse rate. Derived from Wangara data, it has been shown in previous studies to be a good tool under "mild" conditions of non-polar regions, but in Antarctica a problem has been found. When an inversion develops, the Deardorff PBL height tends to decrease.

The very strong inversions over the Antarctic interior therefore cause the PBL height predicted by Deardorff's scheme to fall to very low values. The Deardorff scheme depends on heat fluxes to grow, and the intense temperature inversions over the Antarctic plateau prevent this growth.

There are two different types of computational problems that arise from low PBL heights within the model. The first concerns numerical stability. The other is to do with the realism of the wind field that is allowed to develop.

Analysis of data produced by model test run R08 showed that when the PBL height fell to very low values, computational instabilities could develop. These involved the disturbance of the surface energy balance. This is related to the second type of computational problem.

In this version of the CSU-Pielke model, the PBL height is not just a set of values that may be of interest in itself, because within the model, the PBL height is important because it is used to separate the winds of the Ekman spiral from those in the "free" atmosphere. If the PBL height is very low, the Ekman spiral is practically non-existent within the modelled atmosphere. Besides considerations of realism, this is a problem because this version of the CSU-Pielke model operates under the assumption that within the PBL is an Ekman layer and a surface layer, (defined in Chapter 4). When the heights of these three layers are close together and near the surface, numerical instabilities can develop which upset the surface energy balance. This is a property of the model, not of the real atmosphere.

Low PBL heights can prevent there being an adequate number of vertical levels within the model for use in calculating gradients; the lowest two levels are defined at heights of 4 and 8 metres, as shown in Table 4.1, Chapter 4. Therefore, a PBL height of 5.96 metres would disturb computations.

Therefore, even if the realism that was discussed in the previous section is ignored and only the numerics of the modelling are considered, it is not acceptable to allow the PBL height to fall too low. It would be more productive to set a minimum limit on the PBL height than allow it to decrease to a height that

causes computational problems. The following section discusses a minor change to the PBL height parameterisation.

5.6 MODIFICATION OF PBL PARAMETERISATION

Following the results from test run R08, two runs were conducted for testing of PBL height parameterisation schemes. The Deardorff (1974) scheme was used in R08 and problems were found over areas where the terrain slopes were small.

Small terrain slopes allowed the inversion to become very strong and the PBL height that was parameterised was small, as it tended to follow the height of the intense low level inversion, that exists within the lowest 50 metres of the atmosphere over plateau regions, instead of the height of the total inversion, which has a mean height of hundreds of metres, during winter. The strong inversion prevented growth of the PBL using Deardorff (1974) scheme because the scheme parameterised the growth of a PBL that was heated and a decrease in the PBL when an inversion formed overnight. In reference to a mid-latitude region, Pielke and Mahrer (1975) commented that the Deardorff (1974) scheme was useful only during the day and a new PBL developed closer to the ground at night, with the decay of turbulence and cooling due to longwave radiation.

These test runs have not found there to be a problem with the work of Deardorff (1974) because the parameterisation depended upon data from the Wangara Experiment and mid-latitude conditions, with heating during the day and cooling at night. However, the PBL height parameterisation scheme is not suitable for use in the drastically different meteorological conditions over the Antarctic plateau.

Previous to the work of Deardorff (1974), Equation 5.8, Pielke (1974) parameterised the height of the PBL within the model using the Equation 5.9, that is only suitable for neutrally stratified air.

$$\frac{\partial H}{\partial t} = -u\frac{\partial H}{\partial x} - v\frac{\partial H}{\partial y} + w_H^* + \frac{1.8(w_*^3 + 1.1u_*^3 - 3.3u_*^2 f H)}{g\frac{H^2}{\theta}\frac{\partial \theta^+}{\partial z^*} + 9w_*^2 + 7.2u_*^2} \tag{5.8}$$

with $w_* = [\frac{-g}{\theta} u_* theta_* H]^{1/3}$ for $\theta_* \leq 0$,

$w_* = 0$ for $\theta_* > 0$,

where f : Coriolis parameter,

g : acceleration due to gravity,

H : PBL height,

x, y, z : cartesian coordinates,

u, v, w : velocities respective to cartesian coordinates,

θ^+ : potential temperature immediately above the PBL.

$$H = \frac{0.25u_*}{f} \tag{5.9}$$

Parish (1984) used a similar equation for parameterising the height of a stable PBL. Equation 5.10 was used to determine the PBL height for modelling of katabatic flow over Antarctica.

$$H = \frac{0.2u_*}{f} \tag{5.10}$$

Equation 5.11, from Arya (1981), has a similar form to Equations 5.9 and 5.10, used by authors in the 1970s and 1980s. It was computed from a best-fitted regression line from observations of an "extremely stable" atmosphere. These observations were made during winter at Cabauw in the Netherlands. This formula may be applied to the atmosphere over Antarctica because strong inversions are present, meaning that the atmosphere is very stable.

Equation 5.11 is useful because it contains a constant that prevents the PBL height falling below the height of 85.1 metres. This is an acceptable value because the mean height observed by Bromwich (1976) over Law Dome, East Antarctica, was 99.7 metres. This means that it is a realistic value, and also prevents the occurrence of computational problems described previously.

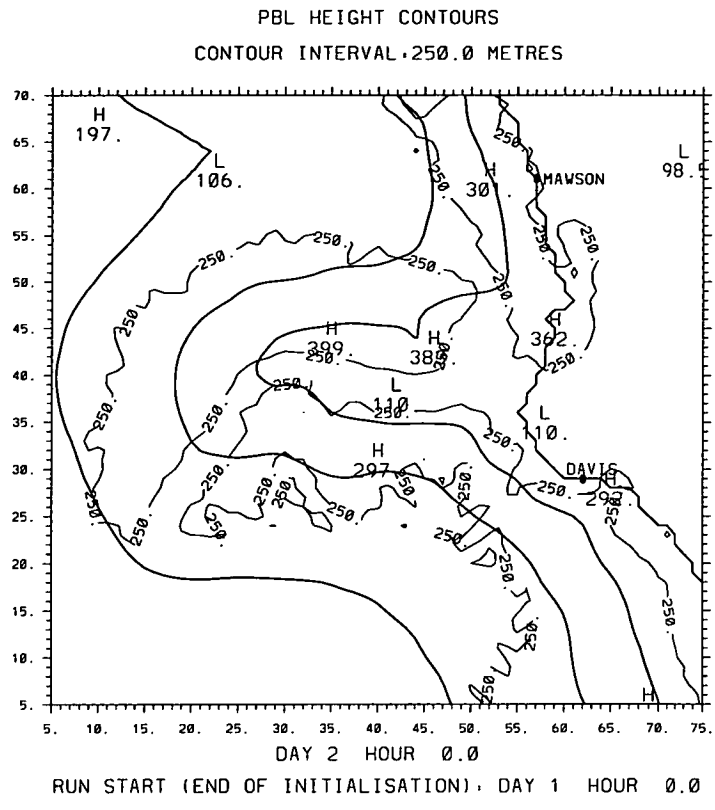

Figure 5.17: July modelled PBL depth, from model run R09, as predicted using the Arya (1981) "extremely stable" atmosphere formula to compute PBL heights, as shown by Equation 5.11.

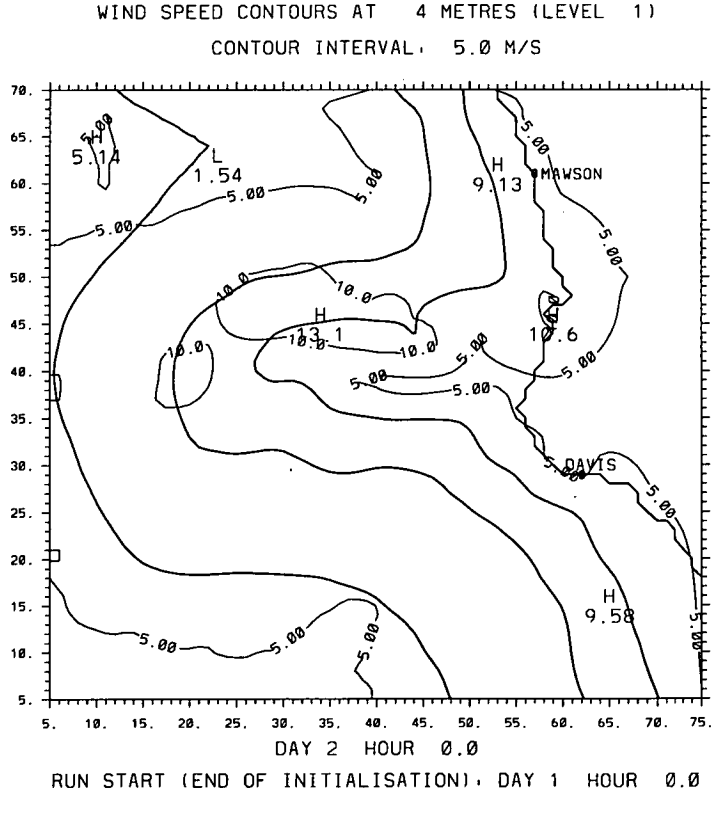

Figure 5.18: July modelled surface wind speeds, from model run R09, that used the Arya (1981) "extremely stable" atmosphere formula to compute PBL heights, as shown by Equation 5.11.

This scheme is tested in runs R09 and R10. This equation was used as the sole scheme in test run R09 but this approach is not suitable because the stratification of the atmosphere was not extremely stable over the entire model grid.

Test run R10 utilises a combination of the Arya (1981) and the Deardorff (1974) schemes. The Deardorff formula is used at each grid point, at each time step, but when the predicted PBL height falls below that computed using the Arya formula, the Arya value is substituted.

Values were computed at each time step using both schemes, but the Arya scheme was substituted for the Deardorff scheme when the values computed using Deardorff fell below those computed using Arya. Inconsistencies did not occur because the Deardorff values were not allowed to fall below Arya values in any case; the Arya values were essentially a lower limit for the PBL height. The Arya values were found to be substituted for Deardorff only when the inversion strengths were above 20 C, which is justified because the Arya scheme is for an "extremely stable" atmosphere.

$$H = 85.1 + \frac{0.089 u_*}{f} \tag{5.11}$$

The CSU-Pielke model set a minimum limit on the value of $u_* = 2$ cm.

Figure 5.11 shows the PBL height contours calculated using the Deardorff (1974) scheme for run R01, a mean January thermal field. There were no problems with the scheme during this summer test run, but R08, a July run, showed that over a plateau area, the PBL height was unrealistically low, as shown by Figure 5.13 in the region of grid point (29,63).

Test run R09 differed from R08 by the use of the Arya (1981) scheme instead of the Deardorff (1974) scheme for parameterisation of PBL heights. This removed the problem of very low PBL heights over the plateau, but did not respond adequately to the neutrally stratified air flow in coastal regions, Figure 5.17. Comparisons between Figures 5.11 and 5.17 show that much detail is lost when

the Deardorff scheme is not used.

Figure 5.19 shows the resultant PBL heights when the Deardorff (1974) scheme is used except for regions of extreme stability, generated from run R10. A minimum is still present in the PBL height field at around grid point (29,63), but it is not low enough to cause numerical instabilities.

The results of the combined schemes are good. This method of PBL height parameterisation is used for all runs in following chapters.

Figures 5.12, 5.14, 5.20 and 5.20 are plots of the wind speed contours at 4 metres above the surface from runs R01, R08, R09 and R10 respectively. The minima at around grid point (29,63) on each of these figures reflects the small slope in this area, as shown by Figure 4.4. The low wind speeds allow inversions to develop, which links the terrain slope, wind speed and thermal stability of the atmosphere.

Comparing these four figures, the lowest wind speed was produced by the summer run R01, Figure 5.12, but the PBL height did not fall to extremely low levels, Figures 5.11. This is because the atmosphere is warmer during summer than winter and the inversion did not develop to such strengths.

The three winter runs, R08 - R10, were identical except for the scheme used to determine the PBL height. The minor differences in the surface wind speed patterns between these runs show that the modification to PBL height parameterisation has not significantly disturbed the surface wind fields.

To generalise, the wind speed increases as the terrain slope increases, and this causes increased turbulent mixing, which prevents inversion formation. This generalisation does not take into account other effects, such as the change in surface temperature throughout the model domain.

Ten numerical model runs were conducted to examine the numerical model's performance over Antarctica. These tests were found to be valuable because they revealed three problems in regard to parameterisation of meteorological fields within the model.

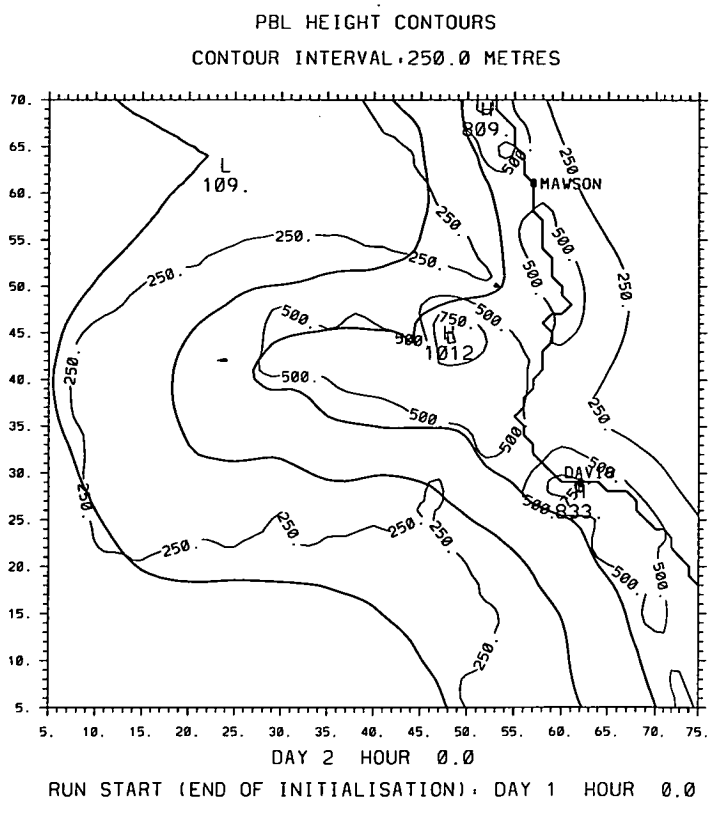

Figure 5.19: July modelled PBL depth, from model run R10, that used a combination of the Deardorff (1974) PBL height parameterisation scheme and the Arya (1981) "extremely stable" atmosphere formula to compute PBL heights. This is discussed further in Section 5.6.

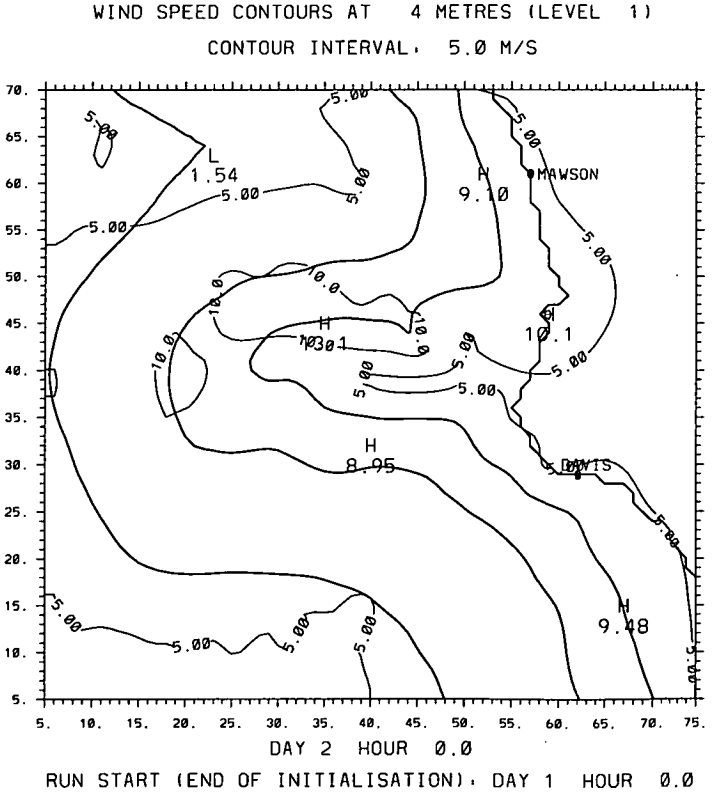

Figure 5.20: July modelled surface wind speeds, from model run R10, that used a combination of the Deardorff (1974) PBL height parameterisation scheme and the Arya (1981) "extremely stable" atmosphere formula to compute PBL heights. This is discussed further in Section 5.6.

The iteration scheme used in the surface energy balance was improved to avoid convergence to unrealistic values.

Winter surface temperatures of the sea ice region were prescribed (253.9 K), to avoid the model computing unrealistically low values during winter simulations. This occurred because the "terrain" of the sea ice region is flat and the weak synoptic forcing used for the test runs throughout this chapter did not cause adequate transfer of momentum to lower levels and subsequent mixing of air near the surface. Cooling of the surface occurred due to loss of long-wave radiation, and strong inversions were able to form, and these were also unrealistic for the sea ice region.

The strong temperature inversions, (typically 20 - 25 K), that occur over the plateau of Antarctica during winter, caused the PBL height, predicted using the Deardorff (1974) scheme, to fall to very low values (about 6 metres). Such values were unrealistic and also disrupted the computations within the boundary layer. This problem was solved by introducing the Arya (1981) PBL height parameterisation, for "extremely stable" atmospheres. Tests showed that the combination of these two schemes produced the best results.

The use of the correct physics in a parameterisation scheme is of as much importance to the precision of the numerical model, as the use of accurate input data, and computing power.

Further improvements, by tuning the model, are discussed in Chapter 6.

Chapter 6

JANUARY AND JULY MONTHLY MEAN RUNS

6.1 INTRODUCTION

There are important interactions between the dynamic and the thermal fields in the atmospheric boundary layer. These were discussed in Chapter 2 and also observed in Chapter 5, in reference to low wind speeds allowing very strong inversions to develop, due to lack of vertical mixing of air.

Surface wind fields that appear to be fairly realistic may be produced by adjusting the synoptic level wind speeds and directions but neglecting thermal fields. This does not guarantee realistic thermal fields, and the synoptic winds that are adjusted without reasonable justification may also be unrealistic.

The method used to produce realistic surface wind fields is to firstly introduce a realistic synoptic level wind field. Monthly mean synoptic wind fields are suitable forcings for numerical modelling of monthly mean boundary layer conditions. The second step is to adjust parameters involved in the determination of the model's thermal fields, so as to produce realistic thermal fields using realistic values for parameters such as surface and cloud albedos, surface albedos, cloud amounts and surface conductivities. Following these adjustments, the synoptic wind fields and the thermal fields of the boundary layer are correctly "tuned", and it is expected that the corresponding surface wind field that results will also be realistic.

The monthly mean synoptic forcings used in this chapter will "smear" the pressure field, neglecting the effects of intense storms, and also calmer conditions, but

these forcings were only used to establish mean summer and winter climatological runs over the region. In Chapter 8, cyclonic forcings and other pressure patterns are considered.

In summary, once the synoptic forcing and the surface thermal parameters are correct, low level winds flow as the system attempts to reach a balanced state.

Section 6.2 demonstrates the sensitivity of the model's thermal fields to variations in the synoptic wind field forcing. Spatially-varying wind fields, interpolated from SHANAL data, are used.

Several adjustments to surface parameters are made in order to find the most suitable values; over Antarctica, these values are relatively unknown in many areas. Even when fairly realistic values are known, it is reasonable to "tune" the fields further within the remaining uncertainty, using available information as a guide. Parameters that are adjusted are listed below.

Surface albedos are adjusted from a single value over the entire model grid to be spatially-varying. This takes into account changes from the sea ice zone to the plateau regions, as listed by Weller (1980). Changes in surface albedo fields and the model's sensitivity to these changes is discussed in Section 6.3.

Surface thermal parameters, conductivity and specific heat capacity (and therefore diffusivity), are tested for their influence on the model's thermal fields. This discussion is in Section 6.4

In near-coastal regions of East Antarctica, the surface can consist of blue ice instead of firn. This may be important in regards to measurements of surface temperatures, because these areas are near occupied stations, and observations are made and expedition activities are carried out here, but blue ice regions are not representative of the majority of East Antarctica. There is also the problem of how best to represent surfaces of Antarctica within the numerical model so as to achieve a reasonably good match between observed and modelled surface temperature fields. These questions are addressed in Section 6.5.

Short-wave and long-wave radiation forcings due to clouds are introduced to

Run	Month	Description
R11	January	Spatially-varying upper wind, from SHANAL data
R12	July	Spatially-varying upper wind, from SHANAL data
R13	January	Surface albedo=0.85
R14	January	Spatially-varying albedo
R15	July	Change in diffusivity; for lower temperatures
R16	July	Spatially- and temporally-varying diffusivity
R17	July	Blue ice included in coastal regions
R18	January	Test LW_{OUT} adjustments from Weller (1967)
R19	July	Test LW_{OUT} adjustments from Weller (1967)
R20	July	Inclusion of cloud; improved radiation balance
R21	July	Total albedo=1; sensitivity demonstration
R22	January	Inclusion of cloud; improved radiation balance

Table 6.1: Descriptions of model runs conducted in this chapter.

the model's energy balance. These changes consist of estimating the influences of cloud albedo and cloud amount on incoming short-wave radiation and the blocking of outgoing long-wave radiation. These experiments are discussed in Section 6.6.

Following the various steps used to "tune" the numerical model's thermal fields, further observations are used to verify that the model is functioning correctly. These data include sastrugi orientations, from several sources, and Automatic Weather Station (AWS) data. The model's performance is discussed in Section 6.7.

January and July climatologies for the Lambert Glacier Basin region, as generated by the numerical model, are presented in Section 6.8.

6.2 SENSITIVITY OF THERMAL FIELDS TO SYNOPTIC WINDS

The model test runs conducted throughout Chapter 5 used upper winds of negligible strength (0.25 m/s), so as to allow development of thermal fields without specific synoptic forcing. This also allowed "pure" katabatic flow to form, not related to a particular synoptic pattern. However, these winds of negligible strength are unsuitable for establishing monthly mean conditions in the boundary layer.

As shall be shown by runs R11 and R12, when winds of more realistic strength and direction are used, changes occur in the thermal fields (due to different amounts of mixing) as well as in the wind fields (due to transfer of momentum from the synoptic level to levels within the boundary layer). This is an accurate method to use because over the large area modelled, the synoptic wind fields vary; the winds over a single station are not representative of the entire region.

The model was modified to allow forcing by a spatially-varying synoptic wind field. The wind fields used in runs R11 and R12 are shown in Figures 7.22 and 7.36 respectively, in Chapter 8. These are mean January and July fields calculated from almost 20 years of SHANAL data.

The modelled mean July thermal field, that results from using this wind field as the synoptic forcing, shows an improvement in the match with observed data; compare Figure 6.2 with Figure 5.9.

However, a significant improvement is not found for the January case; compare Figure 6.1 with Figure 5.1. Tuning of other parameters in following sections improves the accuracy of the mean January simulation.

For July (run R12), surface temperatures have increased by about 5 K throughout the region modelled, compared with run R08. These changes are due to increased vertical mixing, caused by the increased synoptic wind strengths. Increased mixing makes less difference during January because the temperature

inversions are weaker and therefore the differences in air temperatures between the surface and the atmosphere above are less.

The monthly mean January and July SHANAL 700 hPa level winds used in runs R11 and R12 respectively shall be used as the "standard" synoptic forcings for the remainder of runs carried out in this chapter. However, comparison between AUW and SHANAL data above Mawson suggest that the SHANAL-derived synoptic fields underestimate the wind speed. Problems with the SHANAL data are discussed in Chapter 7.

6.3 ADJUSTMENTS TO SURFACE ALBEDO

An albedo value of 0.75 was used for runs R01 to R12. This is too low for the plateau regions of Antarctica. A run to test the sensitivity of the model's thermal fields to a change in albedo was conducted. January mean conditions were used, as in run R11, but albedo was set to 0.85, closer to values that are suitable for the Antarctic plateau. The month of January is modelled because there is plentiful incoming short-wave radiation with which to test the importance of albedo. This run was labelled R13.

Figure 6.3 shows the difference in surface temperature fields generated by runs R11 and R13. Over the plateau region, temperature drops of 5 K are evident, corresponding to changes in albedo from 0.75 to 0.85 . Surface temperatures appear to be less sensitive to albedo nearer to the coast. This is due in part to the effect of the open water during January (the month modelled in these runs), which contributes heat to the atmosphere that is then mixed, and consequently, air and surface temperatures in the vicinity of the coast are prevented from decreasing by large amounts. It is concluded that albedo has a significant influence on the model's thermal fields.

Also, the values of albedo shown in Table 6.2 cover a larger range than those used in runs R11 and R13. Therefore, differences in the numerical model's thermal fields, when realistic values are used throughout the entire model domain, are

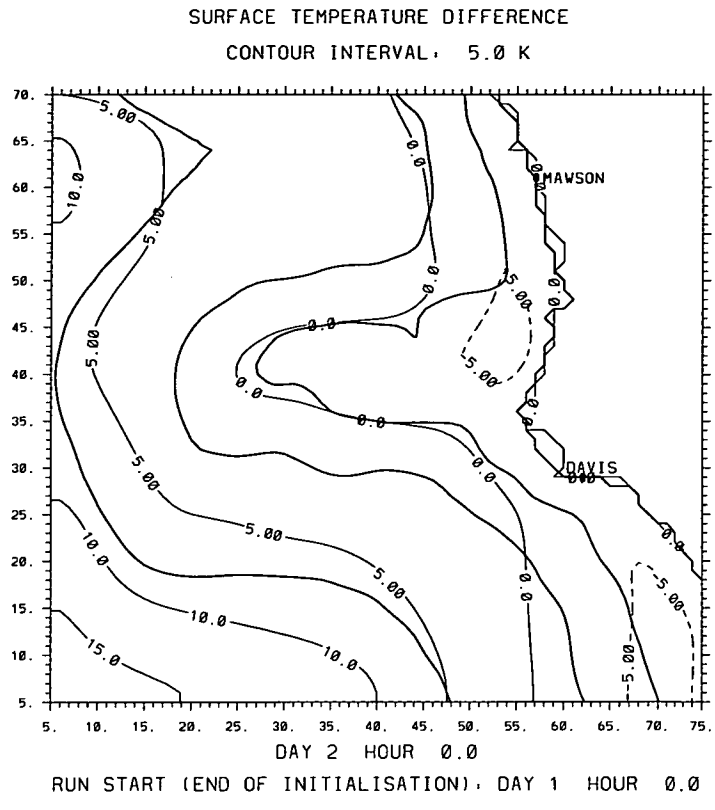

Figure 6.1: Surface temperatures produced by model run R11 (spatially-varying upper winds, January) less the January observed values.

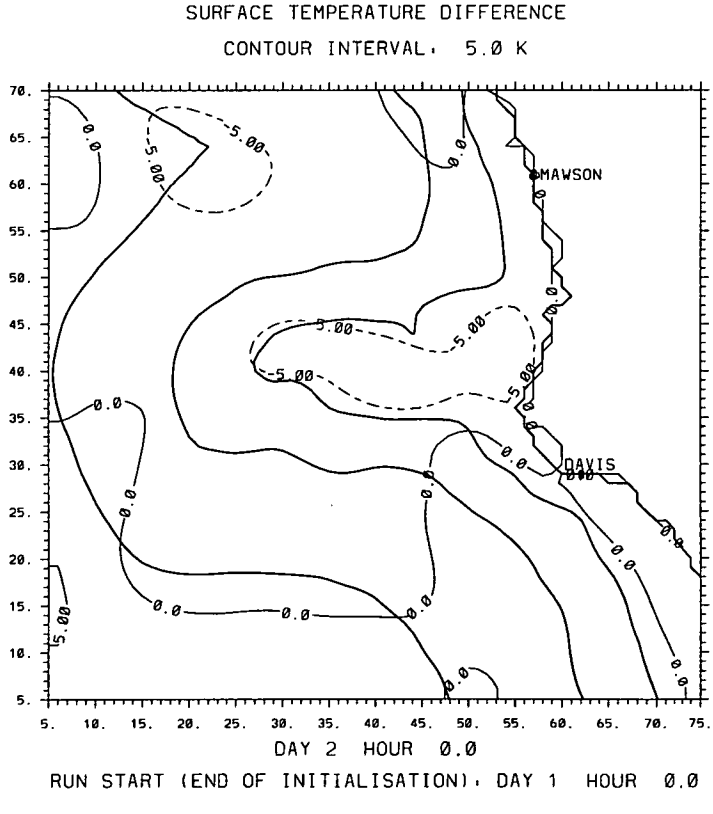

Figure 6.2: Surface temperatures produced by model run R12 (spatially-varying upper winds, July) less the July observed values.

Region	Albedo
Interior continental	85
Coastal ablation	69
Coastal sea ice zone	65
Inner pack ice, concentration $\geq$85%	75
Outer pack ice, 85% > concentration $\geq$15%	54

Table 6.2: Albedos in various regions of Antarctica, from Weller (1980).

likely to be even more significant than those shown in Figure 6.3.

Another change is made to the numerical model; instead of a single value for the entire grid, albedo is defined to be spatially-varying. Values from Weller (1980) are used to define the albedos, as follows.

Below 500 metres terrain elevation, near the coast, albedo = 0.75, above 2000 metres terrain elevation (plateau), albedo = 0.85 . The remaining regions are steady progressions between these two values, depending on the mean terrain elevation of each grid box. These values are used in run R14.

Streten (1962) noted that some Antarctic snow surfaces can have albedos as high as 0.90 , but it is unclear which regions of the grid can be represented by these values, or if such values occur in "patches", instead of throughout large areas consistently. Therefore, the albedos are defined using values from Weller (1980). However, it is important to be aware that some regions may have values significantly ($\geq$5%) higher than those decided upon for run R14.

Figure 6.4 shows that the improved representation of albedos used in run R14 led to a better match between observed and modelled surface temperatures than was found from previous runs. However, there remain some regions of the grid that still require correction, in regard to surface temperatures. These improvements are attempted in the following sections.

This spatially-varying albedo data set shall be used for all runs that follow.

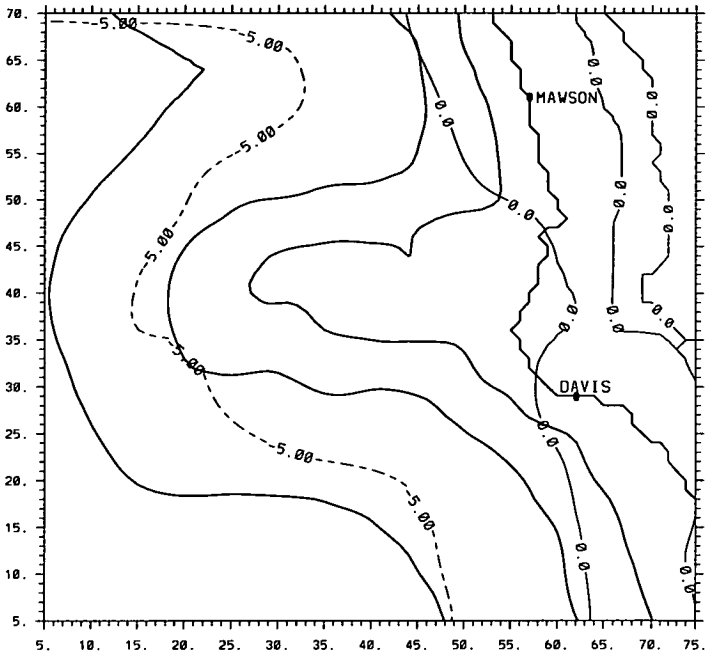

Figure 6.3: Surface temperature differences: model run R13 (albedo = 0.85, mean January) less model run R11.

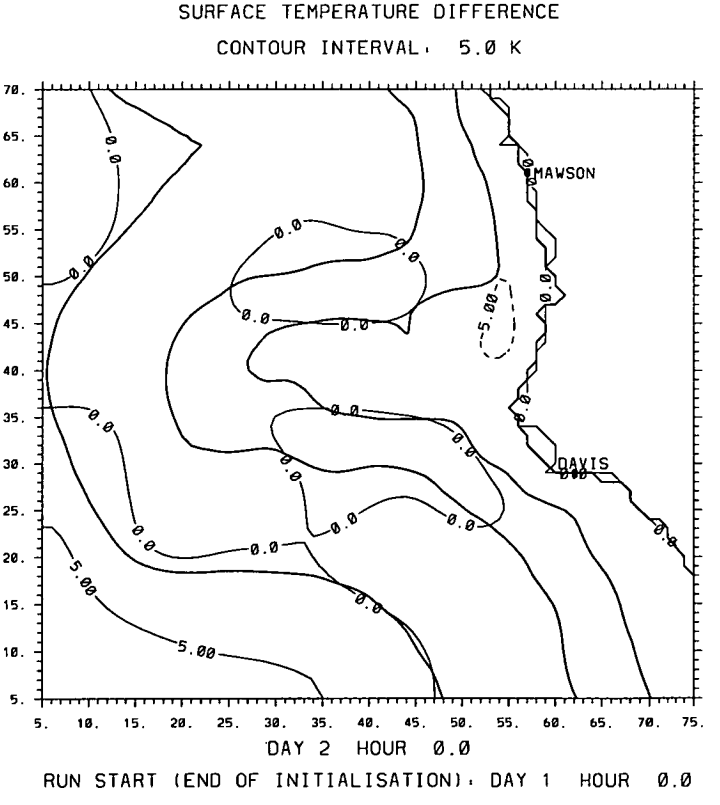

Figure 6.4: Surface temperatures produced by model run R14 (spatially-varying albedo, mean January) less the January observed values.

6.4 SENSITIVITY OF THERMAL FIELDS TO SURFACE DIFFUSIVITY

Conductivity and specific heat capacity of the firn vary with changes in temperature, as shown by Budd (1969). Depending on the relative changes in these two parameters, the diffusivity of the firn may also vary, because it is proportional to the ratio of conductivity to heat capacity.

An experiment is conducted with the numerical model by adjusting these parameters to values that correspond to the lower firn temperatures, instead of the "default" values that are based on 0 C. This is examined in run R15. Monthly mean July conditions are used because lower surface temperatures are observed during this month than during January. Lower temperatures mean greater departures of surface conductivity and specific heat capacity values from their respective "defaults". If the numerical model's thermal fields are significantly sensitive to changes in these surface parameters, they should be evident in this July run.

Figure 6.5 shows that differences in surface temperatures between runs R12 and R15 are very minor when conductivity and specific heat capacity are adjusted to those values corresponding to lower firn temperatures. It is concluded that changes in surface thermal parameters do not have a significant effect on surface temperature, even when July (low) temperatures are taken into account. Even less significant effects are expected during warmer periods of the year, such as January.

Despite these small effects, it was decided to proceed with another sensitivity test, because the surface energy balance is a very integral part of the numerical model and a high level of precision in calculating surface temperatures is desirable.

Differences in firn temperatures between plateau and coastal regions are greater during winter than summer. Therefore, the use of spatially-constant surface conductivities and specific heat capacities result in a greater loss of precision during July.

Following run R15, the model's surface energy balance is adjusted so that the conductivity and specific heat capacity are calculated at each grid point during every time step, with changes dependent on the temperature from the previous time step. The time step used was 60 seconds, so the use of the temperature from the previous time step is not a significant loss of precision, and this method is expected to be an improvement over the previous method of using constant values for these two parameters for every grid point throughout the period of a model run. These adjustments were tested in run R16.

Figure 6.6 shows differences between modelled (from run R16) and observed surface temperatures. The use of spatially- and temporally-varying surface conductivities and heat capacities had some effect on the surface temperatures (compare with Figure 6.2 in the vicinity of grid point (20,65), for example). Overall however, the changes are relatively small considering uncertainties in the observed data or compared with significant changes brought about by alterations to surface albedos, which are still not highly accurate. Despite the use of spatially-varying surface albedo data, the values used in the model are estimations largely dependent on terrain elevation and the values quoted in Table 6.2.

Over the Amery Ice Shelf, (central area of grid - between Mawson and Davis), there is still a problem with modelled surface temperatures that are too low. The interactive scheme for surface thermal parameters only makes significant changes to parameterisation of surface temperatures when the temperatures are quite low, such as over the plateau during winter. Although the modelled temperatures are low over the Amery Ice Shelf, they are not low enough to cause changes in surface conductivities and specific heat capacities that are significant enough to correct the problem.

This method of interactively calculating surface thermal parameters for each grid box at each time step is used for the remainder of numerical modelling in this report, although it is not vital to the model's accuracy.

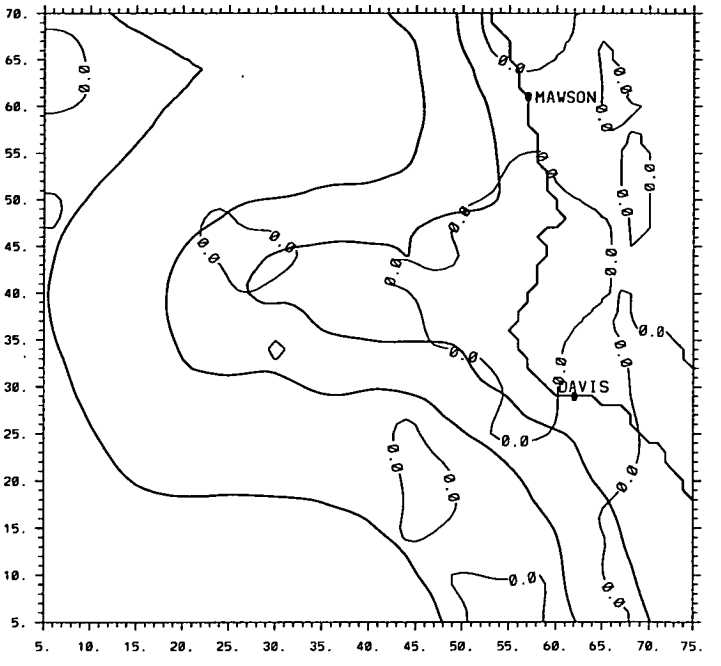

Figure 6.5: Surface temperature differences: model run R15 (mean July, surface diffusivity corresponding to a winter firn temperatures) less model run R12 (mean July, surface diffusivity corresponding to 0 C).

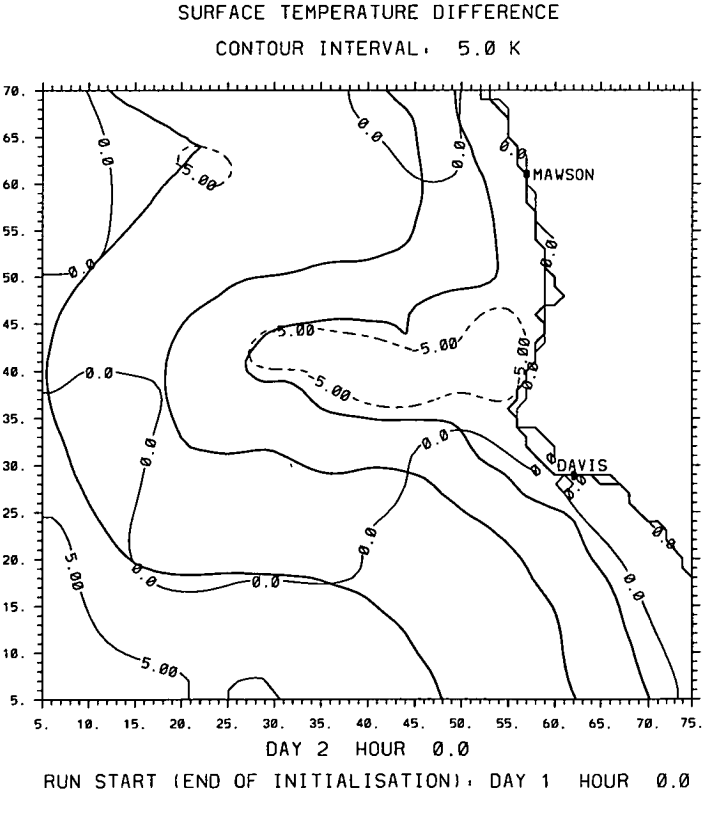

Figure 6.6: Surface temperatures produced by model run R16 (mean July, spatial and temporal varying diffusivities, calculated at each grid box at each time step, depending on surface temperature) less the July observed values.

6.5 REPRESENTATION OF BLUE ICE SURFACES

As noted by several authors (see Chapter 2), there are areas of blue ice short distances inland, due to the strong winds over these slopes that remove the loose snow, and increase evaporation (sublimation) rates. As these areas are those nearest to areas inhabited by humans (coastal), surface temperatures are measured in this region but may be misleading to the overall picture of surface temperatures because much of East Antarctica consists of firn (snow and ice) surface, not blue ice. When these data are used to interpolate or extrapolate (depending on what other data are available), the difference in temperature between blue ice and firn can lead to incorrect values in surface temperature data sets, particularly if few data are available over the plateau and the values near the coast are weighted relatively heavily.

A model run (R17) was conducted to test the influence of blue ice regions on the model's surface temperatures. Blue ice was represented in the model by altering the surface thermal parameters, including the density, resulting in a diffusivity of 1.2×10^{-6} $m^2 s^{-1}$, compared with firn diffusivity values of around 0.9×10^{-6} $m^2 s^{-1}$. Data for calculation of blue ice diffusivity is from Weller (1968).

Blue ice regions were defined along the coastline, at elevations below 700 metres. Although not considered in this test, blue ice regions are also observed over the Lambert Glacier, (centre of the model grid), as are melt pools. These features are not represented here. The difference between this modelled surface temperature data and observations is shown by Figure 6.7. The temperatures in the coastal regions do not alter significantly, and they already closely matched the results from model run R16.

Comparing with Figure 6.6, there is a large improvement over the central region of the grid from run R16 to R17. However, it is not justified to include blue ice continuously throughout this region because accumulations are high in parts of this area and strong winds are not always present to remove loose snow,

as is the case near Mawson where there is a high frequency of strong surface winds. The presence of blue ice is somewhat justifed near the coast, but as the results show, it is not a necessary inclusion.

Experiments with blue ice representation are no longer pursued. Solutions to surface temperature differences between modelled and observed data are sought in the following section.

In terms of "tuning" the model so that its thermal fields correspond well with the observed data, there is a potential problem because if the real data set is not correct, the model can not be correctly adjusted. This problem is not due to the measurements in the blue ice regions alone; it is also due to the lack of measurements throughout the entire Lambert Glacier Basin. To partly overcome this problem, the inversion strength is also used for the verification, but the compilation of inversion strength field relied upon interpolation over large areas, Phillpot and Zillman (1970). However, the use of two different fields to verify modelling results increases one's confidence in the performance of the numerical model.

6.6 REPRESENTATION OF CLOUD RADIATION FORCING

6.6.1 INTRODUCTION

Chapter 5 was concerned with correcting several problems in parameterisation schemes used in the numerical model.

In this chapter, up to this stage, improvements have been made to the representation of parameters that influence the model's thermal fields. The result is that mean January and July surface temperature fields have improved in comparison with observed values.

The task that remains is to further improve the match between modelled and observed temperatures. A potentially major effect on the thermal fields, that is absent in the model, is that of radiation forcing due to clouds.

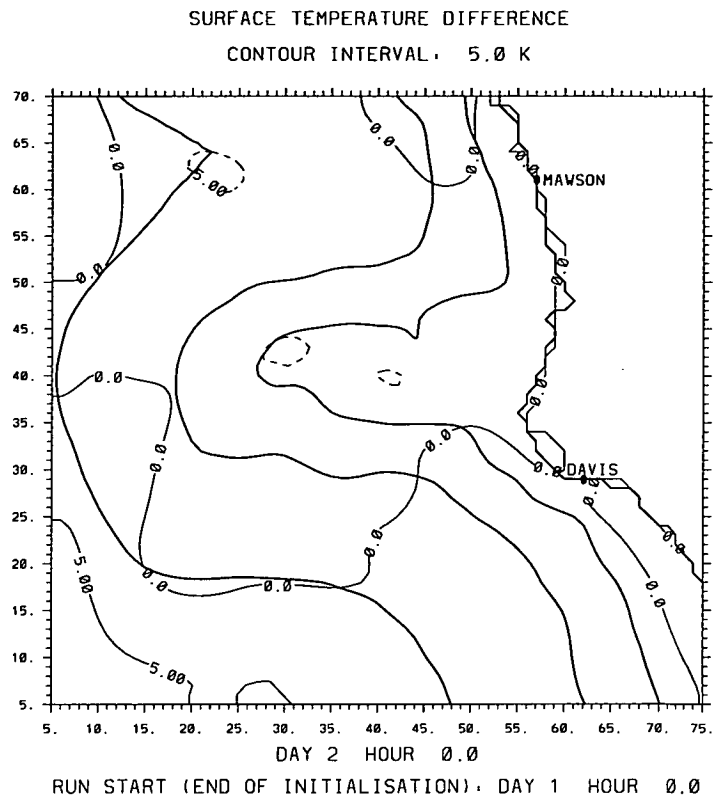

Figure 6.7: Surface temperatures produced by model run R17 (mean July, with blue ice areas along the coast), less the July observed values.

Because other parameters have been examined and their representations improved, it is concluded that differences between modelled and observed surface temperatures are due to the lack of representation of cloud radiative forcing in the numerical model. It is therefore required that short- and long-wave radiation terms within the surface energy balance equation be tuned to acount for the presence of clouds in the real atmosphere that are not simulated in the numerical model.

6.6.2 PARAMETERISATION OF CLOUD INFLUENCES ON RADIATION

As noted in Chapter 4, the numerical model used does not include cloud parameterisation or effects due to cloud. The aim here is not to parameterise cloud formation and precipitation but rather to represent the influence of clouds on radiation.

Rather than introduce clouds into the numerical model, simple representations

were made of cloud radiative properties. Cloud formation and precipitation processes were ignored. For each grid box, the surface energy balance was adjusted so that the influences of cloud albedo and cloud amounts on incoming short-wave radiation were taken into account. Also, the outgoing long-wave radiation was adjusted to allow smaller fractions to escape to space.

Absorption and emission by carbon dioxide and water vapour are taken into account in the 1981 version of the CSU-Pielke model. Although these are still present in the model, the cloud radiation effects that are added are based in the energy balance of the surface, not at levels where clouds are present in reality.

The cloud albedo used was estimated using an equation given by Ramanathan et al. (1983), reproduced here as Equation 6.1. The values obtained agreed well with values quoted by Arking and Childs (1985). The albedos were then adjusted depending on the cloud fraction for each model grid box.

$$\alpha = \frac{C_i}{C_i + \rho} \tag{6.1}$$

where, α is the albedo,

ρ is the cosine of the zenith angle,

$C_i = 0.6$ for low clouds,

$C_i = 0.3$ for middle clouds,

$C_i = 0.15$ for high clouds.

The cloud amounts and their effects at different levels are unknown over much of Antarctica, so a single albedo value is calculated to represent all the cloud levels. C_i=0.5 was chosen as a reasonable value to use; this may seem a higher than necessary value, but only a single level, not several levels, of cloud are taken into account, so it is therefore not an over-estimation. The cloud albedo was applied to the incoming solar radiation. The solar radiation input was therefore reduced by both cloud and surface (firn) albedos.

6.6.3 ESTIMATING CLOUD AMOUNTS OVER THE REGION OF INTEREST

Over Antarctica cloud amounts are not well known. The effects of clouds on radiation are also not well known, but Stone, Dutton and DeLuisi (1989) provide important information: observations suggest that cloudiness over the Antarctic Plateau contributes to surface heating. However, this depends also on the optical depth and cloud amount.

In contrast, both January and July modelling results up to this stage, (Figures 6.4 and 6.6 respectively), show that cooling is required over high plateau areas and warming is required over the Amery Ice Shelf region near the coast. In terms of what cloud types may be expected in these different regions, it appears that the tuning of the numerical model has progressed well. Near the coast, where moist maritime air masses are present, thicker clouds can form, to block outgoing long-wave radiation and therefore prevent cooling. Over the Antarctic interior, where there is much less moisture, thin haze-like clouds may be present to partially reflect incoming short-wave radiation but not substantially absorb outgoing long-wave radiation, and therefore cooling via long-wave radiation loss can occur. However, it is known that the radiative forcing by clouds is complex and the aim here is relatively simple, to make small adjustments to the surface energy balance to compensate for the absence of clouds in the model.

As noted by Vowinckel (1957), over the Antarctic interior it was difficult to determine whether the thin haze observed should be recorded as a cloud amount of 0 or 10 tenths. Miller (1974) stated that due to its remoteness and elevation, the Antarctic plateau is only infrequently subjected to intense cyclones that are present in coastal regions. Therefore, it may be reasonably concluded that clouds present over the plateau are quite thin and not efficient at preventing loss of long-wave radiation to space, except those that infrequently occur, associated with cyclones that penetrate the Antarctic interior.

From Streten (1962), one reason that Antarctica is cold is that there is a lack

of cloud over most of the continent and so outgoing long-wave radiation is not blocked and therefore escapes to space. This and the previous evidence suggest that the model should not be warm over the plateau regions in comparison with observations because clouds are not represented and therefore long-wave radiation should be able to escape and cooling should occur. Because other parameters have been corrected and tuned in the numerical model, it is concluded that thin haze-like clouds should be included in the model with the property of being quite efficient at reflecting incoming solar radiation, but not blocking outgoing long-wave radiation.

An important point to make at this stage is that a "radiation paradox" exists of surfaces of high albedo, such as the Antarctic plateau. This feature is described by Ambach (1974) and by Wendler (1986); the short-wave radiation budget decreases with cloudiness but the long-wave budget increases. For an albedo value of about 0.4, the all-wave radiation budget decreases as the cloud amount increases, but for an albedo of about 0.8, the all-wave radiation budget can actually increase with increases in cloud amount. This means that the conclusion reached previously, following tuning of cloud radiative forcing, regarding the clouds over the interior having little effect on long-wave radiation, is not correct.

However, this does not insubstantiate the tuning carried out; the effect of clouds on the long wave radiation appears to be underestimated by the model because the monthly mean temperature profile used to initialise the model must already include effects of clouds that were present. The model was used to investigate air flow over a limited area for a limited time period and does not include a "spin-up" period of many days, or months, over the entire globe, that is required by general circulation models to achieve realism of air mass properties and radiative transfers. The inclusion of cloud radiative forcing was for tuning purposes and did not model the radiative transfers over a high albedo surface, as described by Ambach (1974) and Wendler (1986).

Table 6.3 shows that there is a substantial reduction in total cloud amount

Station	Monthly mean total cloud amount (oktas)	
	Summer (December)	Winter (July)
Davis	4.41	4.22
Mawson	4.42	3.50
Sovietskaya	3.12	0.88

Table 6.3: Summer and winter cloud amounts at Davis, Mawson and Sovietskaya stations. December (instead of January) is used to represent summer because observations from Sovietskaya station were not available, but they were available at Davis and Mawson for all months of the year.

from coastal regions to the plateau during winter. This trend is also evident during summer but to a lesser degree.

In coastal regions, the relationship between clouds and surface heating is complicated by increases in cloud amount related to cyclones located offshore because such systems often advect relatively warmer air into the region. This advection causes changes in temperature apart from any temperature changes caused by the blocking of outgoing long-wave radiation by clouds. With temperature changes due to advection, it becomes more difficult to resolve the relationship between cloud, long-wave radiation and surface temperature. Solving this problem is not relevant to the goal of tuning the model's radiation balance. There is adequate information to perform tuning, in terms of introducing the effects of cloud on short- and long-wave radiation forcing.

There is difficulty in determining cloud amounts and optical properties using satellite data over snow. Over the region of interest, there are no reliable observations of cloud between Mawson, Plateau, Sovietskaya and Davis stations.

A general pattern of cloud amount was assumed, with decreases away from the coast, and with increases in terrain elevations. Adjustments were made to cloud amounts so as to "tune" the model's radiation balance and produce a realistic match between modelled and observed thermal fields. The cloud amounts used in the model varied depending on terrain; grid points over higher terrain were

assigned lower cloud amounts.

6.6.4 RELATING CLOUD AMOUNT TO LONG-WAVE RADIATION

Initial estimates of the effects of mean monthly cloud amounts in blocking long-wave radiation at Mawson are made from data given by Weller (1967). If a linear scale is used between long-wave radiation flux values corresponding to clear (0 oktas) and overcast (8 oktas) sky conditions, the outgoing long-wave fractions for any cloud amounts over Mawson can be computed. The use of a linear scale is not likely to allow highly accurate values to be calculated, but approximate estimates can be made.

As the numerical model does not include clouds, it can be assumed that it approximates clear sky conditions, (0 oktas). The outgoing long-wave radiation fraction for monthly mean cloud cover is therefore estimated, from data in Table 6.4, as:

$\frac{57.82}{96.14} \approx 0.6$

The same method is used to estimate the outgoing long-wave radiation fraction for July as was for January, from data in Table 6.5:

$\frac{53.64}{89.87} \approx 0.6$

This is the same fraction as found for January, even though the monthly mean total cloud amounts and the outgoing long-wave flux values differed substantially.

These outgoing long-wave radiation fractions mean that it is justified to remove 40% of the outgoing long-wave radiation that is calculated at each time step for use in the surface energy balance equation, in the vicinity of Mawson, for both January and July monthly mean model runs.

This is a relatively large percentage change in comparison with changes made in tuning of other parameters. (For example, albedos were tuned by about 0 - 15% maximum). The model is tested with these values for January and July mean conditions, in runs R18 and R19 respectively. At this stage, cloud albedos

January	
Total Cloud Amount (oktas)	Long-wave Out (Wm^{-2})
8	28.56
0	96.14
4.5 *	57.82

Table 6.4: Observations at Mawson from Weller (1967) of outgoing long-wave radiation net flux from the snow surface on clear days (0 oktas) and overcast days (8 oktas), monthly means for January. The monthly mean total cloud amount at Mawson was 4.5 oktas; this was used to calculate the monthly mean outgoing long-wave value by using a linear scale between clear and overcast sky conditions.
* Monthly mean January cloud amount at Mawson.

July	
Total Cloud Amount (oktas)	Long-wave Out (Wm^{-2})
8	7.66
0	89.87
3.5 *	53.64

Table 6.5: Observations at Mawson from Weller (1967) of outgoing long-wave radiation net flux from the snow surface on clear days (0 oktas) and overcast days (8 oktas), monthly means for July. The monthly mean total cloud amount at Mawson was 3.5 oktas; this was used to calculate the monthly mean outgoing long-wave value by using a linear scale between clear and overcast sky conditions.
* Monthly mean July cloud amount at Mawson.

are not taken into account.

6.6.5 TUNING OF CLOUD RADIATIVE FORCING

Differences between model-generated and observed surface temperatures for the January (R18) and July (R19) runs, that used the estimated fraction of 0.6 to reduce the amount of long-wave radiation lost, are given by Figures 6.8 and 6.9 respectively. For both runs there is an inadequate amount of cooling throughout the model grid. The greatest temperature increases occur away from the coast, with increased terrain elevations. This pattern has occurred because the long-wave fraction was adjusted for every grid box, but as noted in Section 6.6.3, there

are reductions in cloud amount as remoteness from the coast and terrain heights increase. It is therefore necessary to take these variations into account.

For January, the high temperatures may be partially reduced when cloud albedos are taken into account. For July, this is not the case because the amount of incoming short-wave radiation is quite minor. This means that the long-wave fraction used is too small and must be increased so that more long-wave radiation may escape to space. As previously noted, an adjustment of 40% was quite large and it is desirable, if possible, to alter parameters by only small percentages so as to "tune" them, not change them substantially.

Following trial-and-error experiments, not shown here, the amount of long-wave radiation allowed to escape to space was estimated, dependent on terrain elevation, so that an improved match was found between modelled and observed thermal fields for July monthly mean conditions, run R20. Surface temperature differences and inversion strength differences are shown by Figures 6.10 and 6.11 respectively. The match between modelled and observed data could be further improved, but as the observed values are not highly accurate, (as discussed in Chapter 4), the results of run R20 are satisfactory.

Outgoing long-wave radiation fractions that were used in run R20 are listed in the right hand column of Table 6.6. Higher fractions mean less cloud is blocking the escape of long-wave radiation to space.

Model run R21 was used to examine the importance of solar radiation input during July. The total albedo was defined to be 1, so that all short-wave radiation was reflected. Differences in surface temperatures between runs R21 and R20 are shown in Figure 6.12. It is concluded that the solar input during July is not significant because the surface temperatures generated by runs R20 and R21 have negligible differences.

Trial-and-error experiments, not shown here, were also carried out for mean January conditions. These experiments were complicated by the need to find a realistic balance between the long-wave fractions and cloud albedo, whereas

Terrain elevation (m)	Outgoing long-wave fraction	
	January	July
0 - 1000	0.88	0.85
1000 - 2000	0.91	0.91
2000 - 3000	0.92	0.92
3000 +	0.99	0.99

Table 6.6: Outgoing long-wave radiation fractions used in model runs R22 (January) and R20 (July). For terrain elevations of above 3000 metres, most outgoing long-wave radiation is allowed to escape to space.

in the July runs the cloud albedo was not a significant factor because the solar input was minor. It is for this reason that July tuning was carried out before the January.

Differences between modelled and observed surface temperatures from the resultant mean January model run, R22, with realistically balanced long-wave blockings and cloud albedos, are shown in Figure 6.13.

Results from mean January, R22, and July, R20, runs are also well supported by other sets of observed data, as discussed in Section 6.7.

Outgoing long-wave radiation fractions that were used in run R22 are listed in the left hand column of Table 6.6.

Cloud albedos contributed an approximate increase in total (surface + cloud) albedo of about 5%. Surface albedos are discussed in Section 6.3, with values varying from 0.75 at the coast to 0.85 over the plateau.

The "radiation paradox" was not explicitly modelled and therefore, the values shown in Table 6.6 are the result of tuning only, not direct representations of cloud radiative forcing.

These runs have demonstrated that with small adjustments to the radiation balance, the differences between modelled and observed surface temperatures are reduced.

The initial estimates of adjustments to long-wave radiation, using data from Weller (1967), justified reductions of up to 40%, (estimates from ratios in Tables 6.4 and 6.5), in the amounts of long-wave radiation allowed to escape to space during both January and July.

The final values used, as shown in Table 6.6, allow substantially less long-wave radiation to escape to space, than first estimated using data from Weller (1967). This is a useful result because it means that the model's radiation balance has been altered by no more than 15%, (in Table 6.6, this value corresponds to the 0.85 fraction for July at terrain elevations up to 1000 metres). Small adjustments are more desirable because the aim of this chapter was to tune the model, not alter the radiation scheme substantially.

It is important to note that the radiation was tuned for monthly mean conditions but if different synoptic situations were used as the forcing, or different vertical temperature profiles were used to initialise the model, the modelled and observed data would probably not match as well for the long-wave fractions listed in Table 6.6.

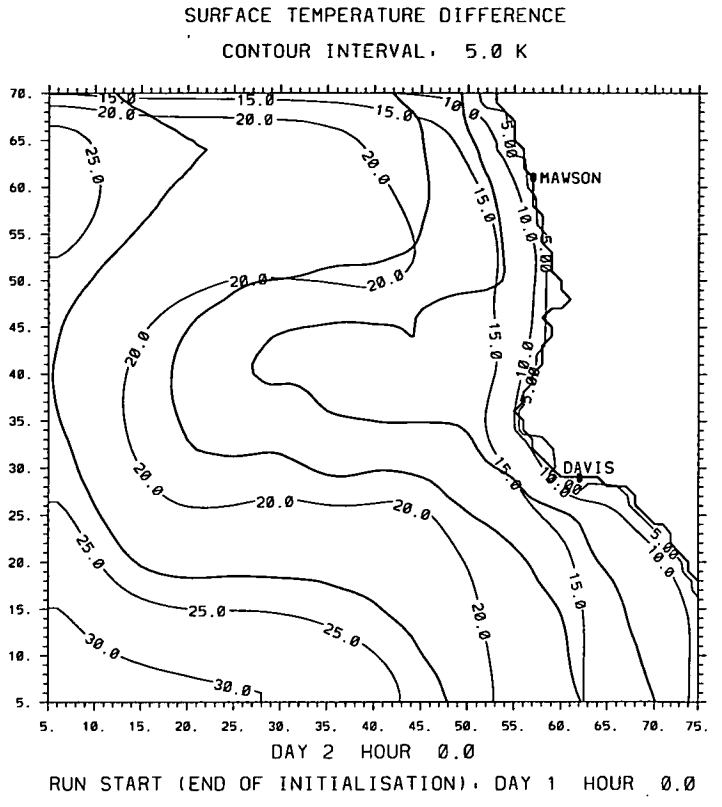

Figure 6.8: Surface temperatures produced by model run R18 (mean January run with outgoing long-wave radiation test, with fractions estimated from Weller (1967)), less the January observed values.

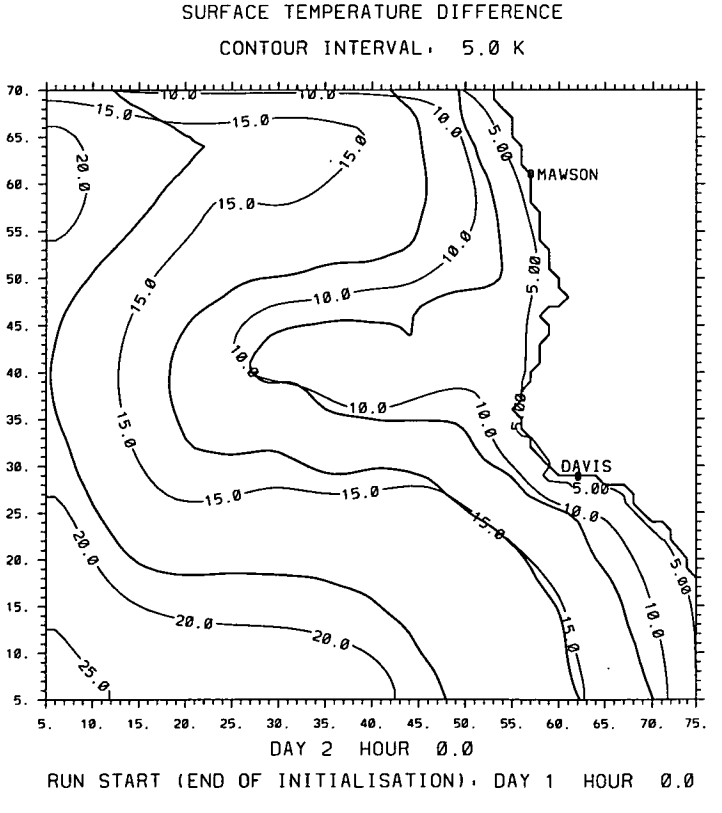

Figure 6.9: Surface temperatures produced by model run R19 (mean July run with outgoing long-wave radiation test, with fractions estimated from Weller (1967)), less the July observed values.

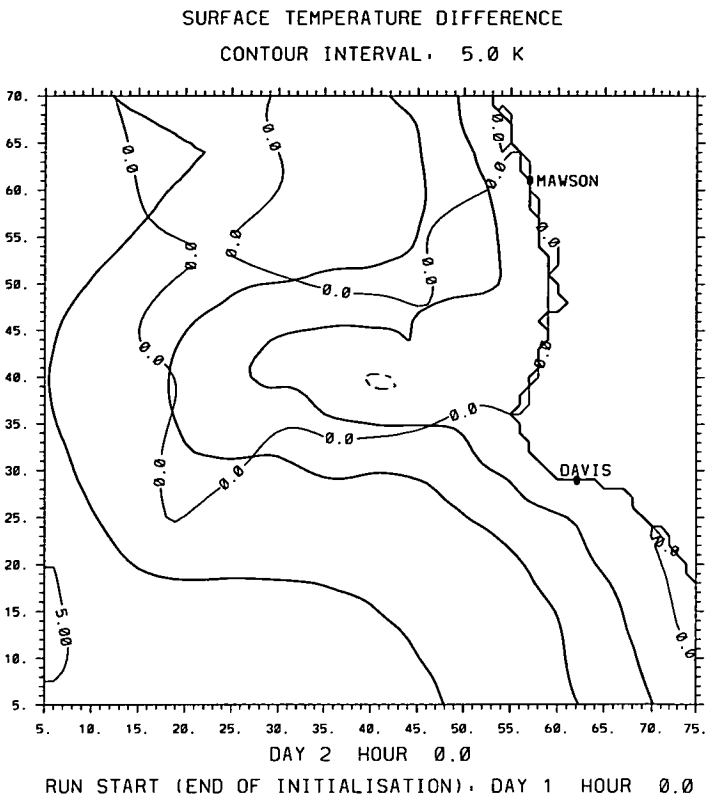

Figure 6.10: Surface temperatures produced by model run R20 (mean July run with improved radiation balance, following trial-and-error test runs using different cloud amounts), less the July observed values.

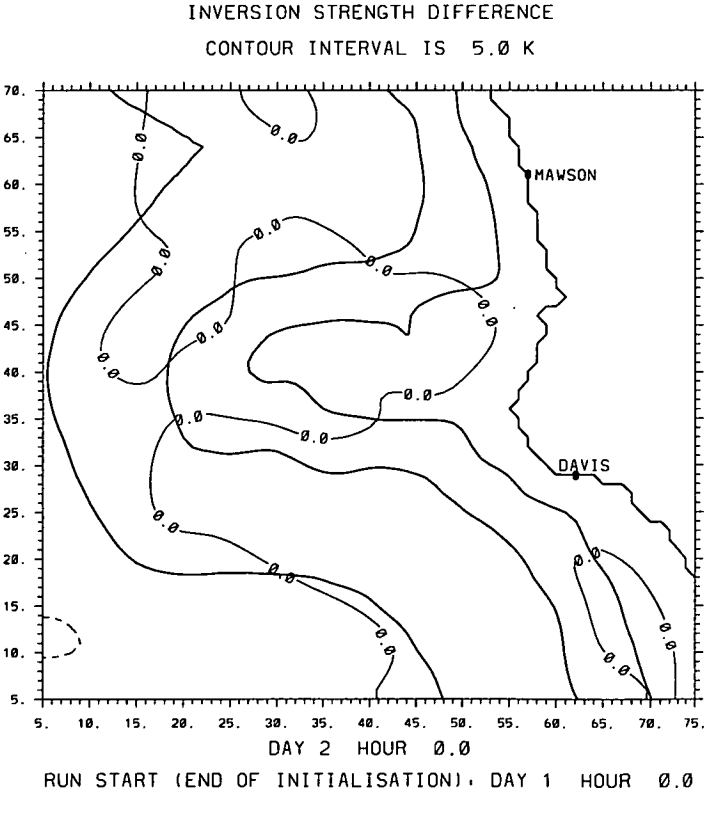

Figure 6.11: Inversion strengths produced by model run R20 (mean July run with improved radiation balance, following trial-and-error test runs using different cloud amounts), less the July observed values.

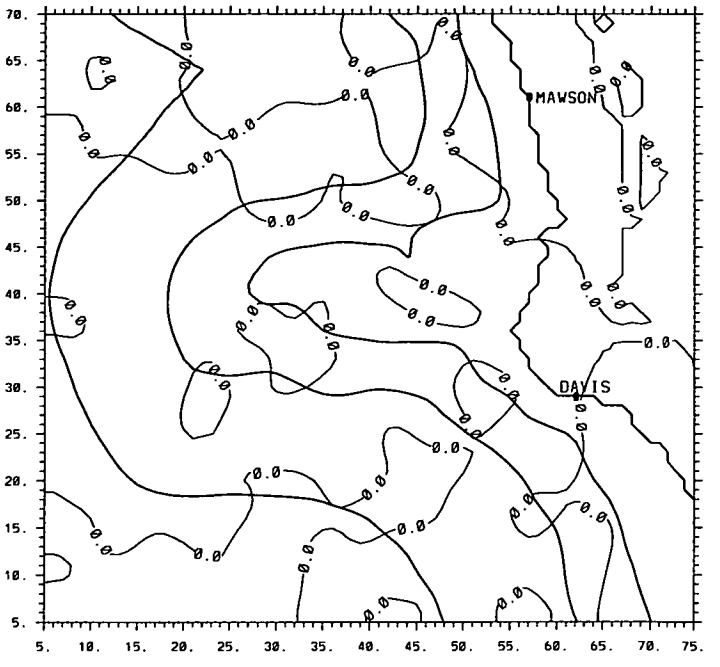

Figure 6.12: Surface temperature differences: model run R21 (mean July with albedo=1, no solar input), less model run R20 (mean July run, with the realistic, negligible solar input).

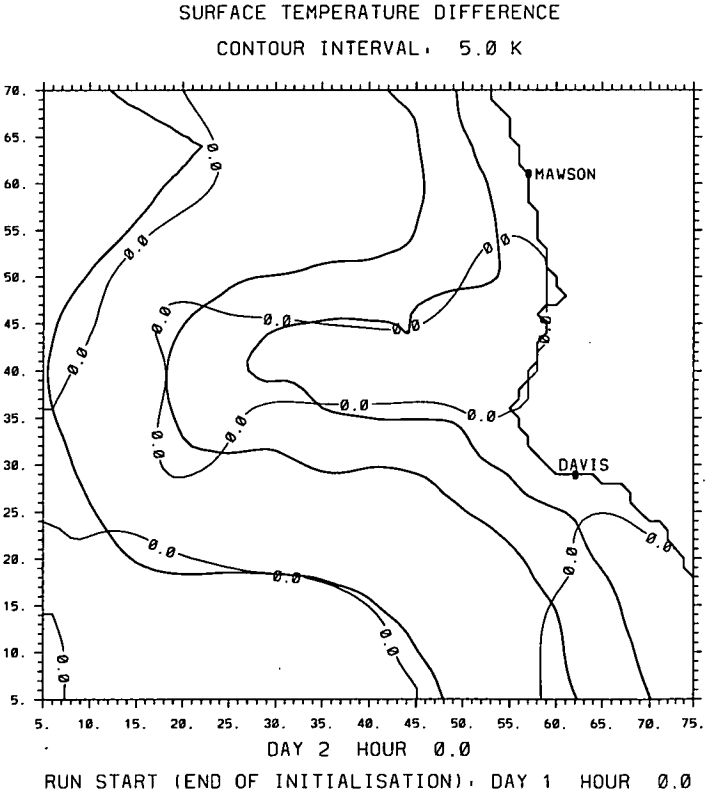

Figure 6.13: Surface temperatures produced by model run R22 (mean January run with improved radiation balance, following trial-and-error test runs using different cloud amounts), less the January observed values.

6.7 VERIFICATION OF MODEL-GENERATED FIELDS

6.7.1 INTRODUCTION

This section is concerned with verifying model-generated fields. The following section discusses the climatology of the region using numerical modelling results. There is some overlap between these two sections, as both discuss mean January and July modelling results.

Verifications of firn surface temperatures for mean January and July model runs were made successfully in Section 6.6. A reasonably good match was also found between observed and modelled July inversion strengths.

6.7.2 MONTHLY MEAN FIELDS

The next step in verifying the model-generated fields is to examine January and July monthly mean temperatures, wind speeds and wind directions at various locations; Davis and Mawson stations, automatic weather stations LGB00, LGB10, LGB20, LGB59 and Sovietskaya station.

Inland/plateau locations are likely to produce a better match between modelled and observed data than at locations near the coast. There are fewer terrain discontinuities over the plateau and therefore the representation of terrain within the model, using 20 km grid spacings, is better. It is more difficult to represent steep slopes and mountains using 20 km grid spacings than it is to represent the relatively featureless and small ice slopes of the plateau.

SURFACE TEMPERATURE

Table 6.7 contains monthly mean surface air temperatures, comparing observed and modelled data. There is a good match during January for all stations.

The July values suggest that over the inland areas, the model is producing temperatures that are too high, but the coastal regions are correct. This is an important observation because it was shown in Figures 6.10 and 6.11 that the numerical model's thermal fields were accurate. Differences between data sets

Location	Monthly mean surface air temperature (K)					
	January			July		
	Observed	R(O) †	Modelled (R22)	Observed	R(O) †	Modelled (R20)
Davis	274.1	2.2	272.3	255.6	6.9	255.1
Mawson	273.4	2.4	272.4	255.0	5.9	254.1
LGB00	257.4	3.4	258.1	236.1	6.7	243.4
LGB10	251.1	3.7	249.1	224.7	6.0	233.8
LGB20	248.9	3.8	246.5	(N/A)	(N/A)	230.2
LGB59	248.3	3.1	249.5	233.1	6.4	234.0
Sovietskaya	232.3*	(N/A)	234.6	203.8	(N/A)	216.4

Table 6.7: Comparison of observed and modelled monthly mean surface air temperatures at Davis, Mawson, automatic weather stations (LGB00, LGB10, LGB20, LGB59) and Sovietskaya.
* Average of December and February monthly means because January not available.
† R(O) denotes RMS Deviation from observed values.
(N/A) denotes Not Available.

demonstrate the difficulty of correctly tuning the model, because the accuracy of the observations is questioned.

Apart from the match between observed and modelled data, the progression of temperatures from coastal to inland locations demonstrates the accuracy of the model's thermal fields, particularly during January.

SURFACE WIND SPEED

Table 6.8 contains monthly mean surface wind speeds, comparing observed and modelled data. There is a good match during both January and July at most locations. Mawson station is the significant exception.

Surface wind speeds at Mawson station are too low during both January and July. These differences between observed and modelled values can be attributed to the poor representation of terrain slope within the model around coastal regions where terrain is quite steep. This problem is present despite the use of (relatively high resolution) 20 km grid spacings.

Another cause of low wind speeds at Mawson, within the numerical model, is the inhibition of the transfer of momentum from the synoptic to surface level.

Location	Monthly mean surface wind speed (m/s)					
	January			July		
	Observed	R(O) †	Modelled (R22)	Observed	R(O) †	Modelled (R20)
Davis	5.0	3.4	5.1	5.0	5.0	4.9
Mawson	9.1	6.1	5.6	11.7	7.6	4.1
LGB00	8.9	3.2	8.3	10.6	3.8	11.2
LGB10	(N/A)	(N/A)	5.4	(N/A)	(N/A)	7.0
LGB20	5.9	2.5	5.5	(N/A)	(N/A)	6.8
LGB59	8.3	2.5	8.4	11.2	3.8	10.9
Sovietskaya	3.0*	(N/A)	5.6	4.4	(N/A)	4.8

Table 6.8: Comparison of observed and modelled monthly mean surface wind speeds at Davis, Mawson, automatic weather stations (LGB00, LGB10, LGB20, LGB59) and Sovietskaya.
* Average of December and March monthly means because January not available, and February values questionable.
† R(O) denotes RMS Deviation from observed values.
(N/A) denotes Not Available.

This is examined in Chapter 8.

The main cause of weaker winds during winter than summer, instead of the reverse, as observed, is the poor representation of the synoptic forcing; this is particularly so during winter, as shown in Chapter 7, where inaccuracies were found in the SHANAL data. For Mawson station only, modelling in Chapter 8 shows greater realism near the surface due to more realistic synoptic wind speeds.

Sovietskaya mean January wind speed was not available; the average of mean December and mean February wind speeds were used to substitute for this missing value. This could be why the observed and modelled wind speeds do not match well. As Sovietskaya station was located over the plateau and the modelled and observed values at another plateau station, LGB20 are in good agreement, and the modelled wind speed at LGB20 and Sovietskaya are similar, it is reasonable to assume that the value used as the Sovietskaya mean January observed wind speed is incorrect.

From the available January and July data, it is concluded that the wind speeds

produced by the model are generally realistic over the plateau regions. Comparison of wind speed data at Davis show that the model is also producing realistic wind speeds at the coast, but the above comparison at Mawson shows that there are exceptions.

SURFACE WIND DIRECTION

Table 6.9 contains monthly mean surface wind directions, comparing observed and modelled data. There are generally good agreements between modelled and observed values.

The small value (108.3° compared with 135°) of the modelled wind direction at Mawson during January shows that there is more cross-slope flow (from east to west) than observed. This probably occurs because the slope is not adequately steep, as noted above, and the air not dense enough to force air drainage closer to the fall line, (an angle of about 135°). During January, with more heating than during winter, the winds can turn cross-slope and even weak anabatics have been observed in reality.

Station LGB00 has significant differences between observed and modelled wind directions for both January and July. The means of the wind directions observed are not reliable because only two years of data were used, not enough to compile an accurate climatological wind direction. The January value was averaged from two years of mean monthly values ((207°+172°)/2 = 189.5°) and the July value was also averaged from two years of mean monthly values, ((192°+158°)/2 = 175°). With such large annual variations in observed data, the differences between observed and modelled values are acceptable.

Important features to note are the north-easterly mean wind directions at station LGB59, during both summer and winter. Surface winds with northerly components over East Antarctica are unusual, because the surface flow generally consists of southerly drainage flow towards the sea.

The surface wind directions generated by the numerical model are in reasonable

Location	Monthly mean surface wind direction (°)					
	January			July		
	Observed	R(O) †	Modelled (R22)	Observed	R(O) †	Modelled (R20)
Davis	45*	5.5	55.8	90*	2.7	92.1
Mawson	135*	2.6	108.3	135*	2.4	131.3
LGB00	189.5	111.0	136.0	175	44.9	150.5
LGB10	192	32.3	188.1	186	(N/A)	199.1
LGB20	192.5	24.7	193.3	(N/A)	(N/A)	201.2
LGB59	44	9.9	58.4	49	16.1	78.7
Sovietskaya	90**	(N/A)	100.7	110	(N/A)	108.1

Table 6.9: Comparison of observed and modelled monthly mean surface wind directions at Davis, Mawson, automatic weather stations (LGB00, LGB10, LGB20, LGB59) and Sovietskaya.
* Estimated using percentage frequency distributions of wind directions instead of computing mean wind direction.
** February monthly mean used because January and December not available.
† R(O) denotes RMS Deviation from observed values.
(N/A) denotes Not Available.

agreement with the observed values. The differences can be attributed to the poor representation of terrain elevations in the vicinity of LGB59. There had been no observations in this area between terrain elevations of 1500 metres and 3500 metres, until the ANARE traverse of the 1993/94 summer, when LGB59 was installed.

The mean January "day" and "night" modelled surface wind fields are shown in Figures 6.25 and 6.27. These show that the drainage flow, from the east into the Lambert Glacier Basin, and turning due to Coriolis, led to the north-easterly surface flow, in the vicinity of LGB59, represented by grid point (35,25).

6.7.3 SASTRUGI ORIENTATIONS

Sastrugi snow dunes, formed by accumulation of snow, line up parallel with the surface wind direction.

Apart from the firn surface temperature and the mean winter inversion strength data sets, that were used previously for verification of modelling results (see Section 6.6), the sastrugi orientation data are useful because they cover large areas.

This somewhat contrasts the monthly mean values discussed above, that only took into account six grid points from the thousands that comprise the model grid.

The surface wind directions generated using mean January model run R22 are tested for realism using observed sastrugi orientations where available. Results from only the January run can be tested because the sastrugi orientations were measured during summer, the time of year when Antarctica is most accessible.

There are several reasons why there could be differences between sastrugi orientations and model-generated wind directions. It was noted by Mather (1962) that at a single location in Antarctica there may be quite different orientations of sastrugi, dependent on the recent history of the wind over the region. The mean January model run R22 did not take into account variations in synoptic forcing with time and therefore the variations observed in sastrugi orientations are unlikely to be reproduced by the January mean synoptic forcing used. The major variations in wind direction with time that were modelled were due to the diurnal cycle.

Sastrugi require the presence of loose snow and winds strong enough to cause drift of snow so that the sastrugi can be formed. The formation of sastrugi due to loose snow and strong winds associated with a cyclone are not taken into account by the model because the mean January synoptic conditions are applied. This means that cyclonic vortices and movement of cyclones were not modelled, but in reality the presence of such a system does affect winds and the movement of snow.

The synoptic conditions present during the periods when sastrugi orientations were recorded are unlikely to match the mean January synoptic forcing used in run R22. Therefore the sastrugi orientations are likely to differ from the modelled wind directions even if the variations in sastrugi orientation due to the recent history of the local wind could be neglected.

Local terrain features that may have influenced sastrugi formation and ori-

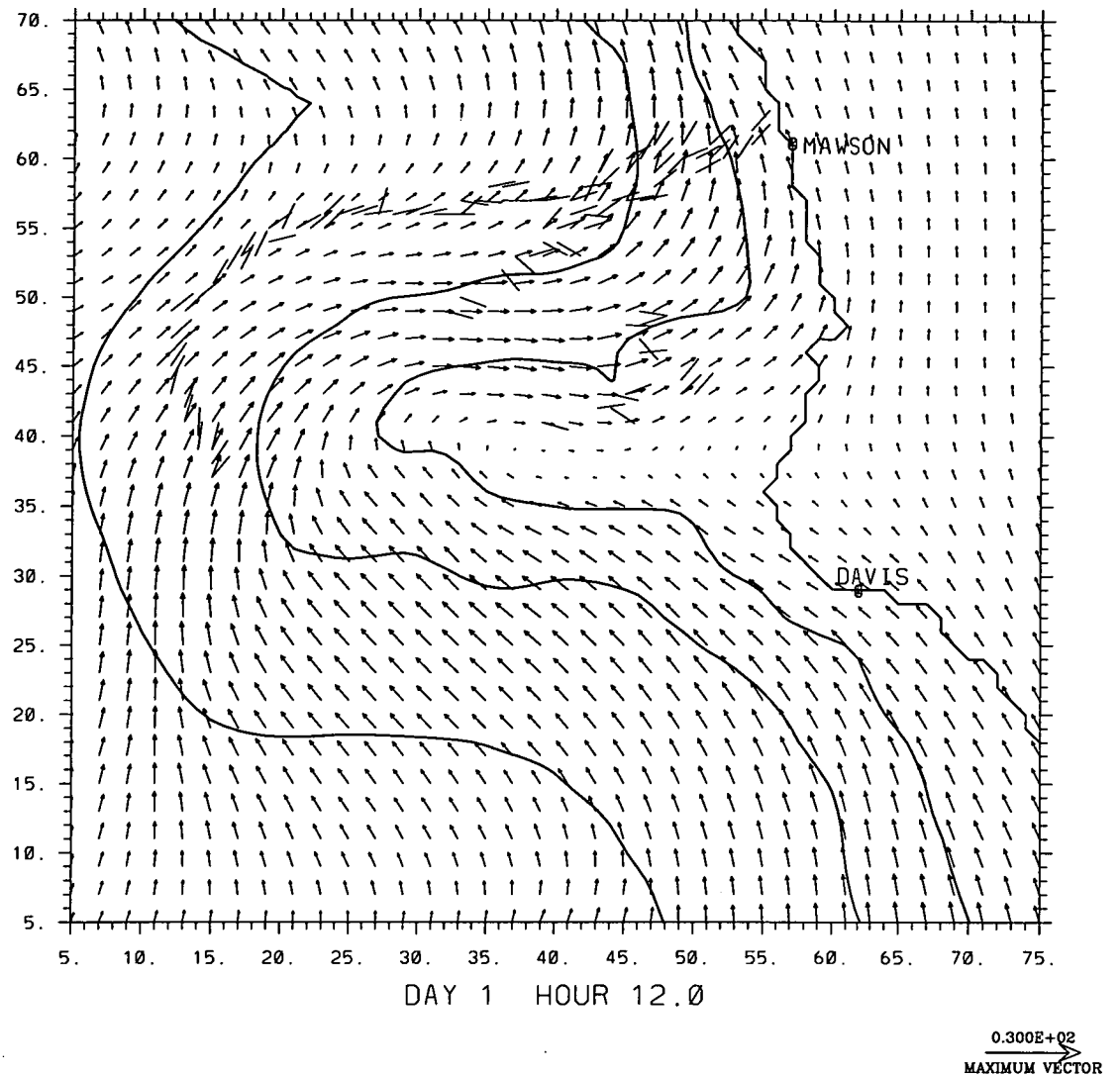

Figure 6.14: Comparison between sastrugi orientations and modelled surface wind directions from run R22 (January mean) at midday.

entations were not taken into account because the model used horizontal grid spacings of 20 km. This resolution is too coarse to resolve local terrain features that may be important. Although the modelling carried out was high resolution compared with many other atmospheric models, details such as the peaks of the Prince Charles Mountains and Framnes Mountains were not included.

The sastrugi orientations were measured at many locations along traverse routes. Because the model used horizontal grid spacings of 20 km, sastrugi patterns may be some distance from the nearest model grid point where a wind direction is computed. Therefore, sastrugi orientations and modelled wind directions that are compared may actually be several kilometres apart.

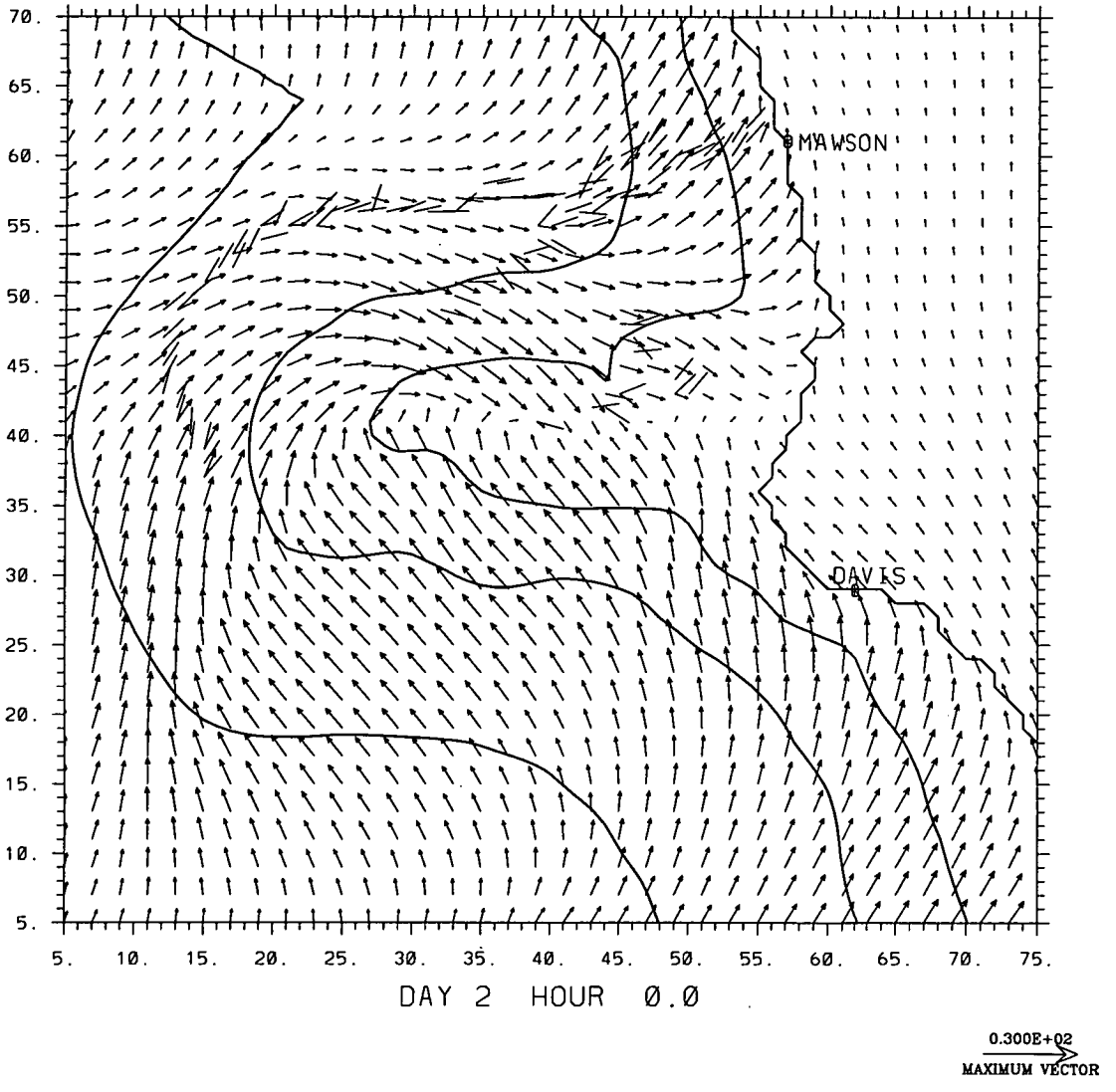

Figure 6.15: Comparison between sastrugi orientations and modelled surface wind directions from run R22 (January mean) at midnight.

If it is assumed that the sastrugi orientations measured are representative of mean January surface wind directions, differences between modelled wind directions and sastrugi orientations may be due to inaccuracies in the synoptic wind field used in model run R22. The synoptic wind field was compiled from SHANAL data. Inaccuracies in the SHANAL data are discussed in Chapter 7.

Wind directions were output from the numerical model every three simulated hours. To account for diurnal variations, eight sets of wind directions that were output (accounting for a modelled period of 24 hours) were compared with the sastrugi orientation data. The best matches between modelled and observed data, at grid points that had corresponding sastrugi orientation data available, were recorded.

Figures 6.14 and 6.15 show comparisons between modelled surface wind vectors and sastrugi orientations, at midday and midnight respectively. Note the diurnal variation in wind directions that allows some points to match sastrugi orientations at one time of day but not at the other.

From using 103 grid points at which to compare modelled wind directions and those inferred from sastrugi orientations, the result was a RMSE of 16.4°. This is a good result and again demonstrates the acccuracy of the numerical model.

6.7.4 JANUARY DIURNAL VARIATIONS

SURFACE TEMPERATURE

Figure 6.16 shows mean January modelled and observed diurnal surface air temperature waves at several stations.

At Davis, the modelled temperatures are lower than observed values by 2 - 3 K but the diurnal patterns are similar. At Mawson the observed and modelled temperatures are similar, but from 09 to 21 hours local time, the model is too cool by about 2 K.

At LGB00, there are small differences throughout the day but there is good general agreement between modelled and observed temperatures and diurnal vari-

ations.

The increase in the amplitude of the diurnal temperature wave in both observed and modelled data occurs as distance inland from the coast becomes greater. Although the temperatures do not match exactly, the diurnal variations are generally well simulated by the model.

Although data for stations LGB10 and LGB20 show good agreements between observed and modelled temperatures from around midday to 15 hours local time, the modelled temperatures over the plateau are around 3 K below the observed values.

The accuracy of the model's thermal fields could be improved beyond the tuning carried out previously, but as the majority of observed and modelled data (shown previously through this section and Section 6.6) agree within reasonable limits, mean January run R22 and mean July run R20 are satisfactory representations of monthly climatological conditions.

SURFACE WIND SPEED

Figure 6.17 shows mean January modelled and observed diurnal surface wind speed waves at several stations. There are two main reasons that there are mismatches between modelled and observed values.

The first is demonstrated by Figure 6.17B that shows data for Mawson station. There is a good match between the diurnal patterns of modelled and observed wind speeds, but the modelled values are significantly less than those observed. This is due to poor representation of the magnitude of the local terrain slope at Mawson station within the model.

The second reason concerns the characteristic minima in modelled wind speeds during mid to late afternoon.

At Mawson, this pattern occurs in reality. When the surface and surface air are heated more, with the sun higher in the sky, the density of air is reduced and therefore downslope flow due to gravity is reduced.

At stations LGB00 and LGB20, and at Davis to a lesser degree, the observed surface wind speeds do not exhibit minima during the afternoon. This may be due in part to the smaller terrain slopes at these locations that cause the change in air density to have relatively little effect on the wind speed.

The main cause of the non-existence of wind speed minima during the afternoon was explained by Loewe (1974). When the air temperature reaches a maximum during this period of the day, there is a corresponding reduction in the inversion strength. The weakening of the inversion allows increased transfer of momentum from the synoptic to surface levels, and therefore decreases in wind speed do not occur.

The modelled temperatures were found to be about 3 K below observed values at some locations. This may cause the inversion to be too strong, which in turn prevents transfer of momentum from the synoptic scale to the surface.

SURFACE WIND DIRECTION

Figure 6.18 shows mean January modelled and observed diurnal surface wind direction waves at several stations.

Generally there are good agreements between modelled and observed surface wind directions. At Mawson station, the wind speeds did not match, but the wind direction match is quite acceptable, that suggests the terrain slope within the model is not steep enough but the fall line is correctly orientated.

There are some significant differences at LGB00. This may be due to the inter-annual variability observed at this site, as noted in Section 6.7.2. Maintaining automatic weather stations closer to the coast can be a problem because of the high snow accumulation rates; approximately 1 metre accumulation per year occurs at the site of LGB00 and therefore the sensors operate at levels closer to the surface and are eventually buried.

LGB10 and LGB20 show good matches between modelled and observed surface wind directions. The regions where agreements are found are quite different; the

model performs well considering the changes in meteorological regimes from the coastal to plateau regions, even though there are not exact matches between modelled and observed data.

6.7.5 CONCLUSION

Following Section 6.6, it was found that the thermal fields generated by the model matched observed firn surface temperatures and inversion strengths. However, these data sets were created using interpolations over large areas and the accuracy of these observations can be questioned. Therefore, the tuning of the model's thermal fields is difficult without accurate observations.

This verification section has shown that the model generated fields are generally in agreement with observations but following the tuning in Section 6.6, that relied upon observations that were not highly accurate, there are some differences between modelled and "observed" fields, (based on limited observations), as discussed throughout Section 6.7.

It is concluded that the present mean January and July model runs (R22 and R20 respectively) are acceptable representations of monthly mean conditions. Although there are not exact matches between modelled and observed data at all points examined, the model does produce complete sets of data throughout the region in time and in space, and features are produced that are not revealed by the relatively "smooth" observed and interpolated data sets. Presentations of meteorological fields generated by these model runs are made in the following section.

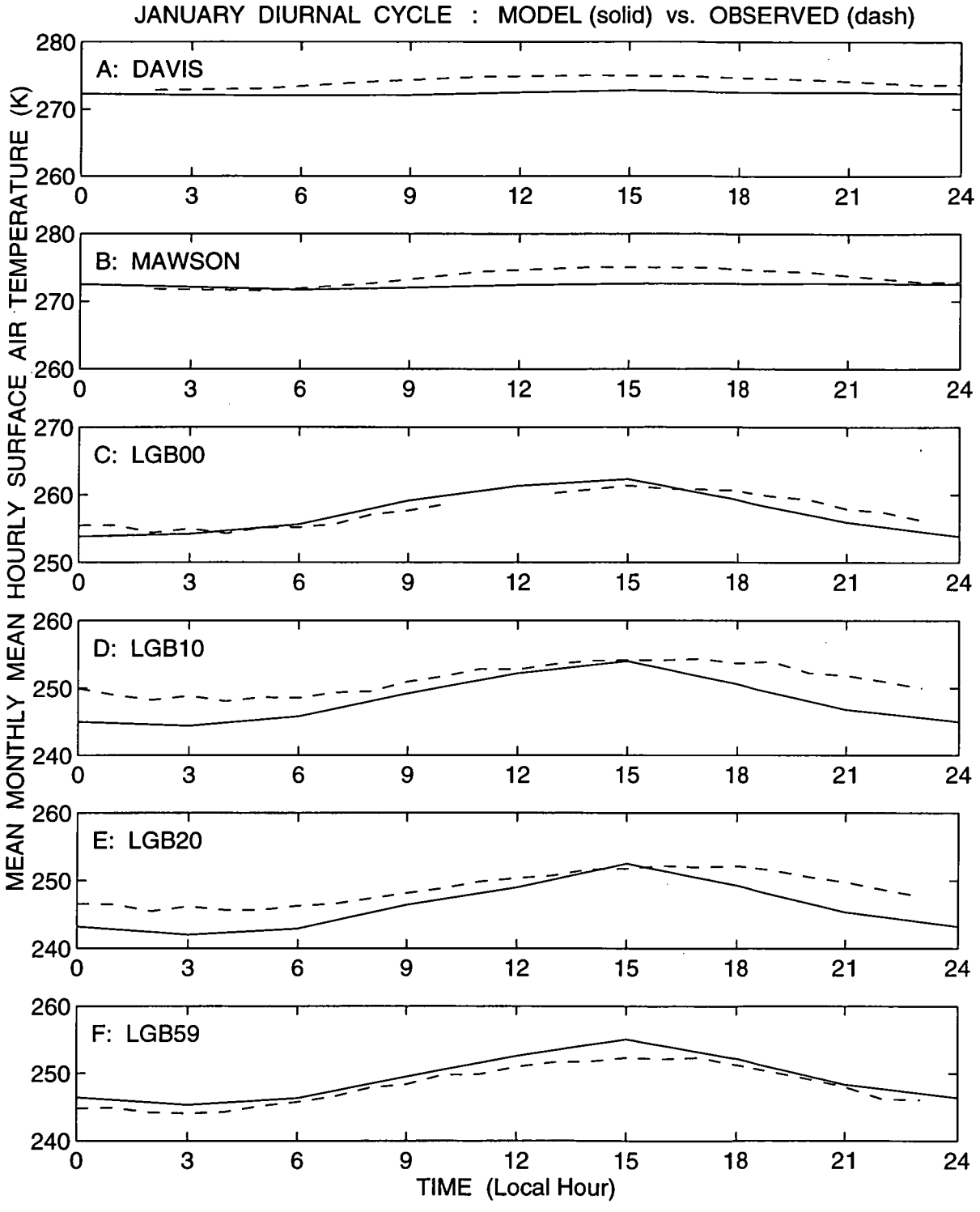

Figure 6.16: Comparison between modelled (solid line) and observed (dash line) January mean hourly surface air temperatures at locations throughout the Lambert Glacier Basin region; A: Davis, B: Mawson, C: AWS LGB00, D: AWS LGB10, E: AWS LGB20, F: AWS LGB59. Note that the temperature range varies from figures A to F, showing that the match between modelled and observed values is reasonably good from coastal to plateau regions but the diurnal patterns do not exactly match for all stations.

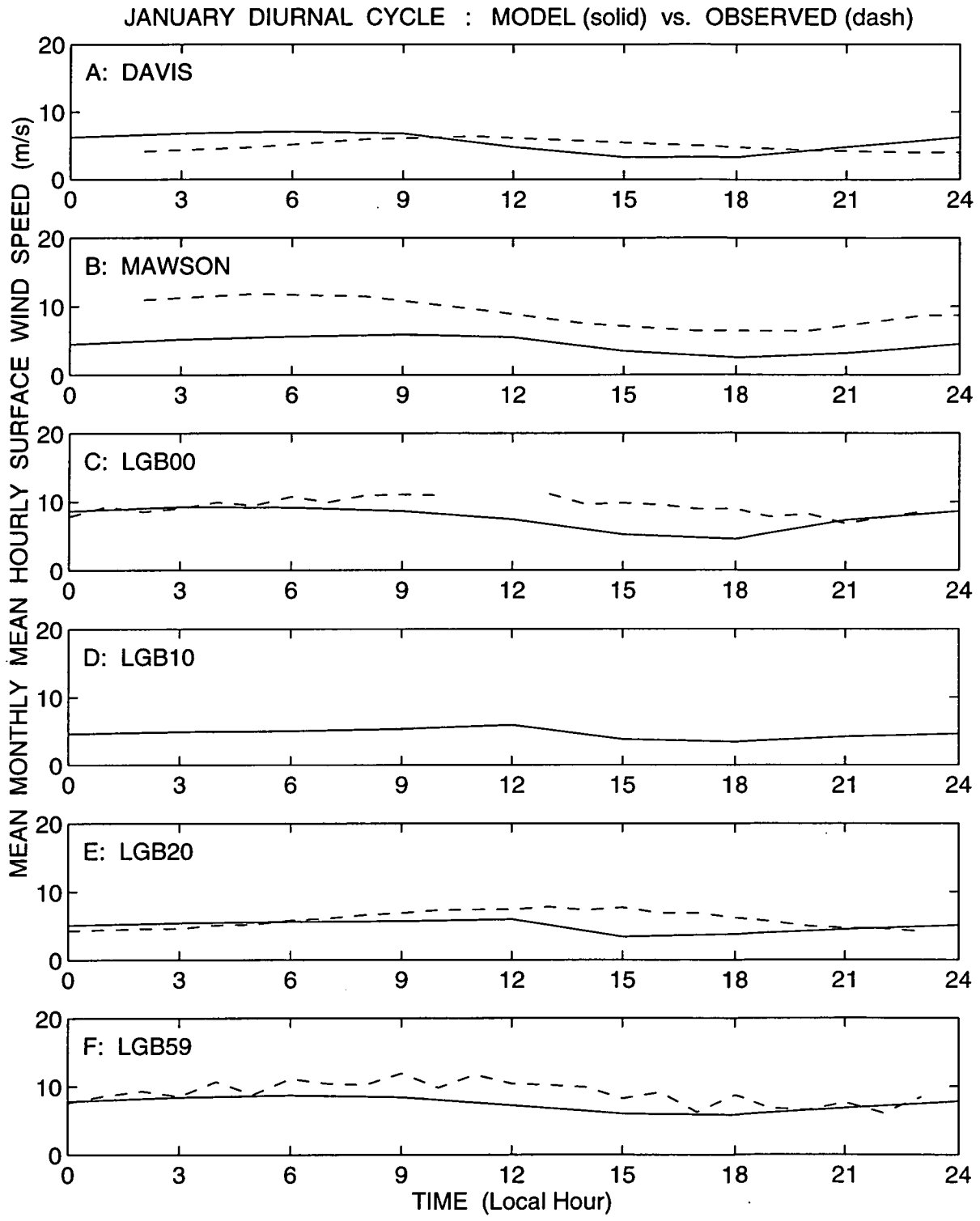

Figure 6.17: Comparison between modelled (solid line) and observed (dash line) January mean hourly surface wind speeds at locations throughout the Lambert Glacier Basin region; A: Davis, B: Mawson, C: AWS LGB00, D: AWS LGB10, E: AWS LGB20, F: AWS LGB59.

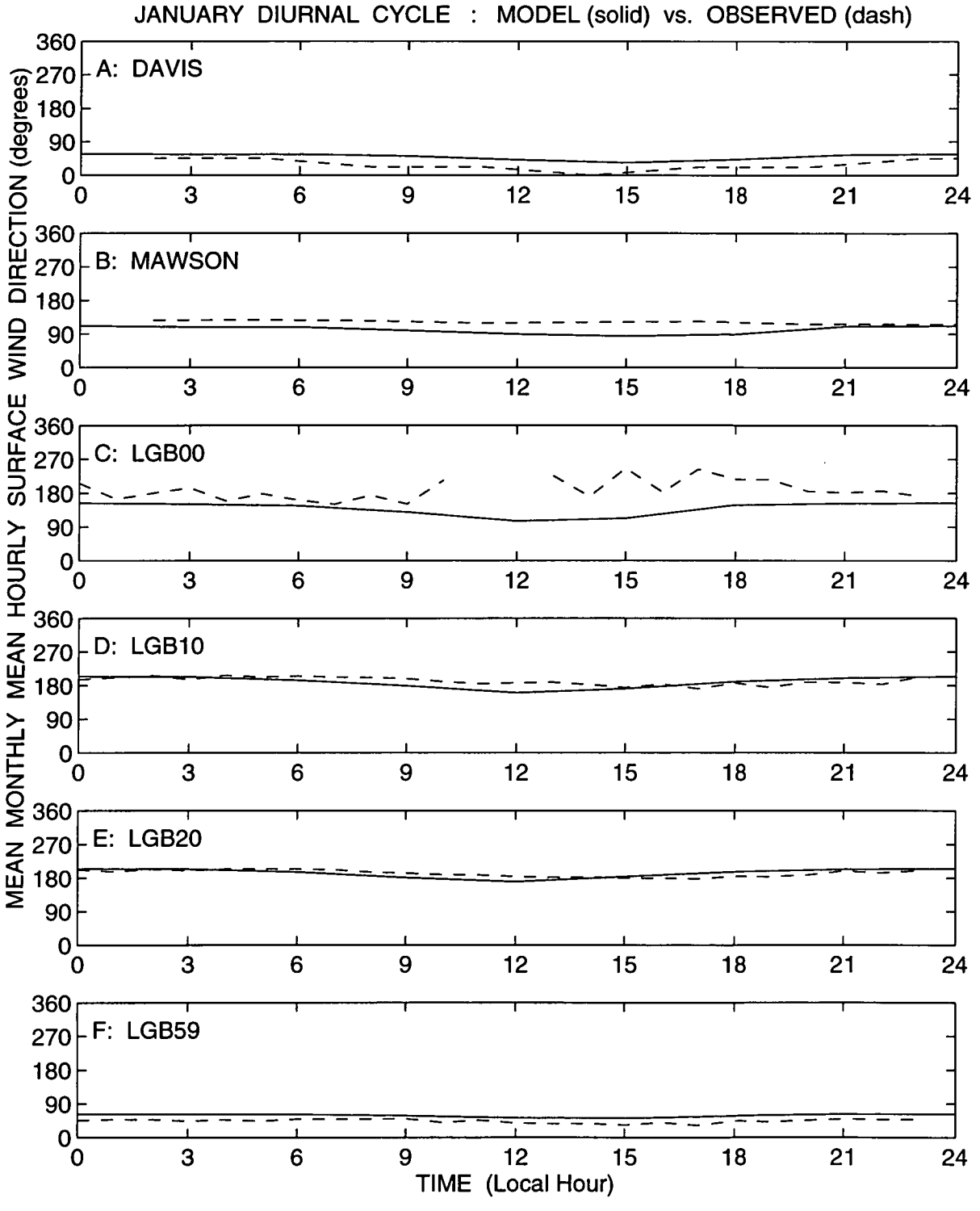

Figure 6.18: Comparison between modelled (solid line) and observed (dash line) January mean hourly surface wind directions at locations throughout the Lambert Glacier Basin region; A: Davis, B: Mawson, C: AWS LGB00, D: AWS LGB10, E: AWS LGB20, F: AWS LGB59.

6.8 CLIMATOLOGY OVER THE LAMBERT GLACIER BASIN

6.8.1 THERMAL FIELDS

Figures 6.19 and 6.20 show firn surface temperatures produced by mean January model run R22 for midday and midnight respectively. There are strong relationships between surface temperatures and terrain elevations. At midnight, there is a strong horizontal gradient of surface temperatures at the coast because the sea surface temperatures are constant in space and time (as defined in the numerical model), but the continental surface temperatures vary, cooling at night.

The differences in firn surface temperatures between midnight and midday are given by Figure 6.21. Negative (dashed) contours show that temperatures are lower at midnight than midday. Diurnal variations near the coast are about 5 K and over the continent the variations are approximately 10 K.

Firn surface temperature differences between mean July run R20 and mean January run R22 are shown by Figure 6.22. Mean summer conditions are represented by values calculated by the January model run for 6 PM local time. As there is no diurnal signal present during July, any time following the model reaching approximate equilibrium is suitable representation of mean winter conditions; temperatures computed for "midnight", 24 hours after the end of the "spin-up", were used. The negative (dashed) contours mean that temperatures are lower during July than January. Over most of the region the July surface temperatures are 15 - 20 K lower than during January, with greater differences present over the inland. The -15 K contour around the boundary of the figure is a boundary effect of the numerical model, not significant in terms of the thermal fields.

Figure 6.23 is a display of firn surface temperatures as produced by mean July model run R20. When compared with the surface firn temperatures produced from mean January run R22, in Figures 6.19 and 6.20, the July contours indicate increased continentality and relatively less dependence on terrain elevation. Nu-

merical modelling has shown features that sparse observations and interpolations did not show.

Inversion strengths produced by mean July model run R20 are shown by Figure 6.24. There are relationships between terrain elevation and inversion strength, but also additional features not shown by the mean July inversion produced from observations and interpolation by Phillpot and Zillman (1970). In the centre of the grid, where there is a zone of significant convergence (see Figure 6.32), the inversion strength varies significantly over short distances, probably due to the high wind speeds causing mixing of air from different levels and also due to the infeed of air with different temperatures from different locations, to the east, south and west.

6.8.2 WIND FIELDS

Modelled surface wind directions were verified using several different sets of data at grid points where observations were available. It is therefore reasonable to assume that the model-generated wind field over the entire grid is in generally good agreement with the true wind field, because it was produced using a consistent set of rules.

Surface (8 metres height) wind vectors and surface wind streamlines generated by mean January model run R22 for midday are shown in Figures 6.25 and 6.26 respectively.

The numerical modelling carried out used horizontal grid spacings of 20 km, but for purposes of clarity, the vectors that are plotted are separated by 2 grid spacings (40 km) in both the x- and y-dimensions. Streamlines that are plotted do not represent trajectories but rather the air flow over the region at one time.

There are significant cross-slope flows throughout the region. The area of negative relative vorticity (clockwise rotation) at grid point (40,39) is forced by the north-easterly and south-westerly flows draining into the Lambert Glacier basin from opposite sides. This circulation is not driven by a source of heat, but

is rather a product of winds flowing from approximately opposite directions into the same region.

Winds from the east of the basin are significantly affected by the underlying topography, that causes convergence of air over the Lambert Glacier - Prince Charles Mountains region. This convergence is more pronounced at midnight; Figures 6.27 and 6.28. Over this region there is significant mixing of air because the winds are directed more downslope at night and this results in opposing flows in the vicinity of the Lambert Glacier.

The mean January midnight surface air flow approaches Mawson from the southeast, but the midday winds were closer to easterly flow.

The winds at the coast are easterly due to Coriolis turning as the air flows downslope from the interior. These winds continue in this direction because the mean summer flow over the sea is also easterly.

Vector differences between mean January midnight and midday surface winds are shown by Figure 6.29. The main difference is that downslope flow (perpendicular to terrain elevation contours) is more pronounced at night, particularly over the steeper terrain slopes below heights of about 2000 metres.

During the night, the easterly surface winds over the sea are weaker than during the day; this must be due to the influence of terrain on continental outflow because the synoptic wind was constant throughout the period of the model run. The following discussion may partly explain the reduced easterly surface flow over the sea, because there is retardation of outflow over the Amery Ice Shelf towards the sea during January at night.

Over the Lambert Glacier - Amery Ice Shelf region, southerly flow is somewhat retarded at night during January because the increased downslope flow causes opposition of air flow from the east and west. Wind speeds from the eastern side of the basin (north-easterly winds) increased by a greater amount (see Figure 6.35) than those flowing from the south or west, and thus, southerly flow towards the sea is retarded.

Wind speed increases from January to July do not occur with the same patterns as found from January midday to midnight. The seasonal change (see Figure 6.36) shows increases in wind speeds on the western side of the basin during winter. The result of this is that southerly continental outflow over the Amery Ice Shelf is enhanced during July, Figure 6.30. As with the seasonal temperature differences, January run 6 PM local time is used to represent mean summer conditions.

This figure also shows that mean July downslope flow is greater over the steep terrain near the coast than it is during January. Over the sea, westerlies dominate; westerly surface winds in this region during July are stronger than the easterlies during January.

Surface winds produced by mean July run R20 are shown in Figure 6.31 and 6.32. The flow is downslope with turning to the left (as observed when facing downslope) due to the Coriolis effect. Air converges over the Lambert Glacier basin from the east, south and west. This pattern of air flow leads to high wind speeds in the vicinity of Lambert Glacier, as shown by Figure 6.37. Wind speeds of this magnitude are not usual so far from near-coastal regions, where steep terrain causes strong downslope flow. The pattern of terrain that causes convergence is responsible for the supply of air and high wind speed value in this region.

Figure 6.31 shows that there is dissipation and change in direction of surface winds short distances north of the coast for mean July conditions. These changes in direction are shown clearly by Figure 6.32 in the vicinities of Mawson and Davis stations. Between these two locations, outflow from over the Amery Ice Shelf is not disturbed to such an extent in terms of wind direction but wind speeds dissipate away from the continent.

The outflow along the coasts near Mawson and Davis may not simply be dissipating with increased distance from the continent because during July the mean flow over the seaice is westerly, that means the easterly/south-easterly

continental outflow is opposed. As a consequence, reductions in wind speed occur around 20 - 60 km offshore. At greater distances seaward of the coast, the July westerlies dominate because the continental outflow is no longer driven by terrain. This explains the substantial changes in wind direction short distances offshore; Figure 6.32.

These patterns are less likely to occur during January because the continental outflow is generally easterly as it is during July, but the monthly mean flow over the ocean to the north is also easterly during January. Therefore, the wind directions are not in opposition, Figures 6.26 and 6.28.

The modelled surface wind speeds for January and July are weaker at Mawson than observed, but the values at Davis match observations well, as discussed explained in Section 6.7.2. The general patterns of surface winds speeds shown by Figures 6.33, 6.34 and 6.37 are in agreement with observations; the strongest winds are some distance inland, with winds at the coast being weaker and plateau winds also weaker.

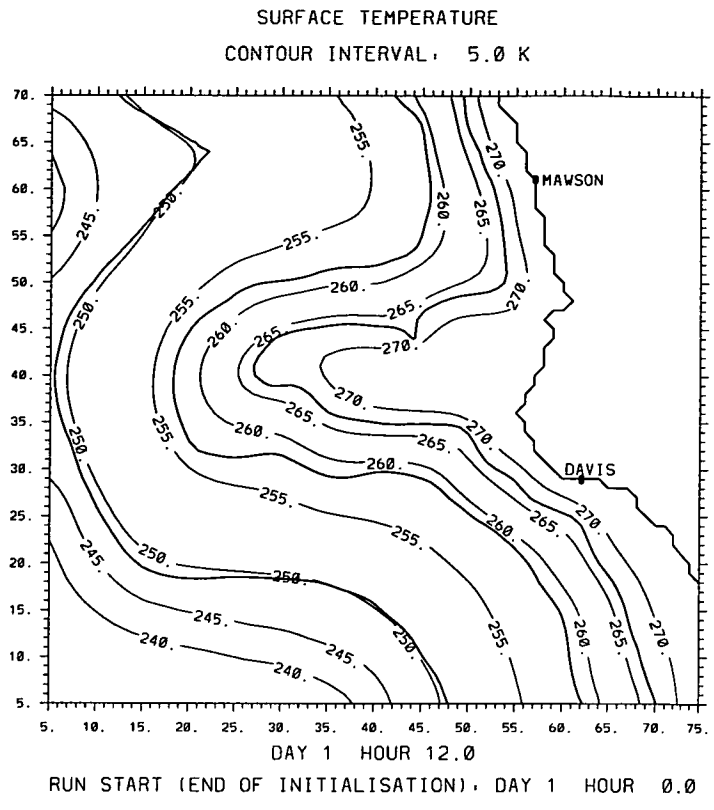

Figure 6.19: Firn surface temperatures as produced by mean January model run R22 at midday.

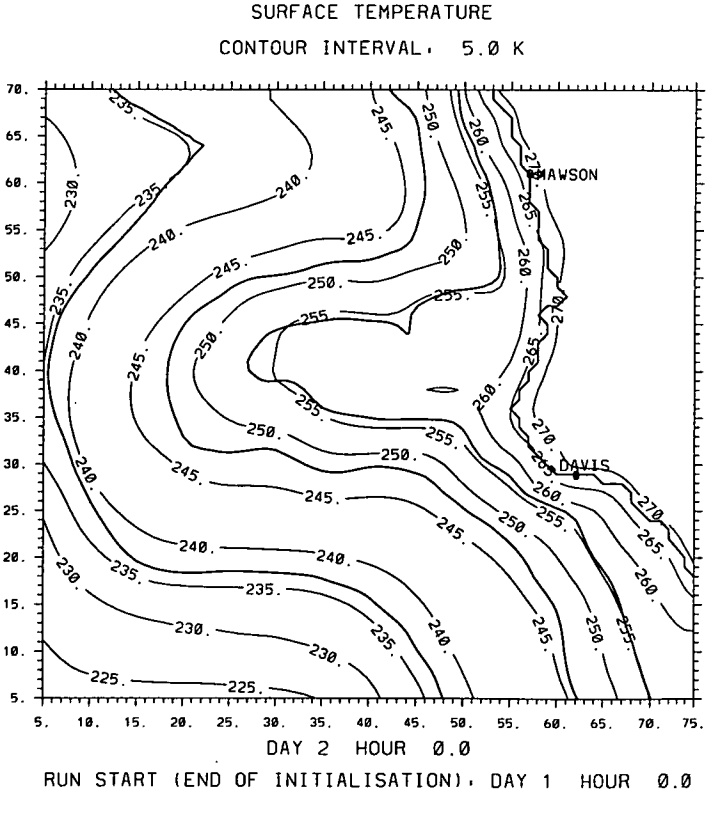

Figure 6.20: Firn surface temperatures as produced by mean January model run R22 at midnight.

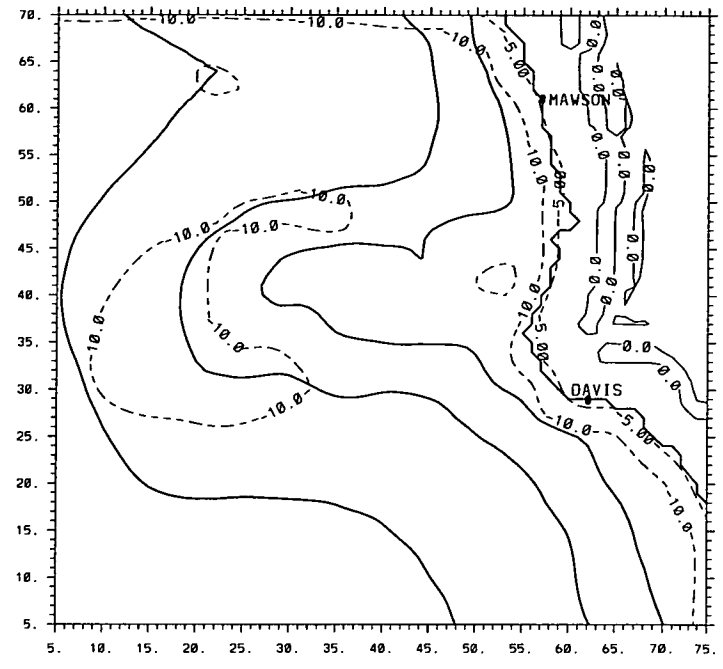

Figure 6.21: Difference in firn surface temperatures between midnight and midday, as produced by mean January model run R22, with negative values showing the presence of lower temperatures at midnight than midday.

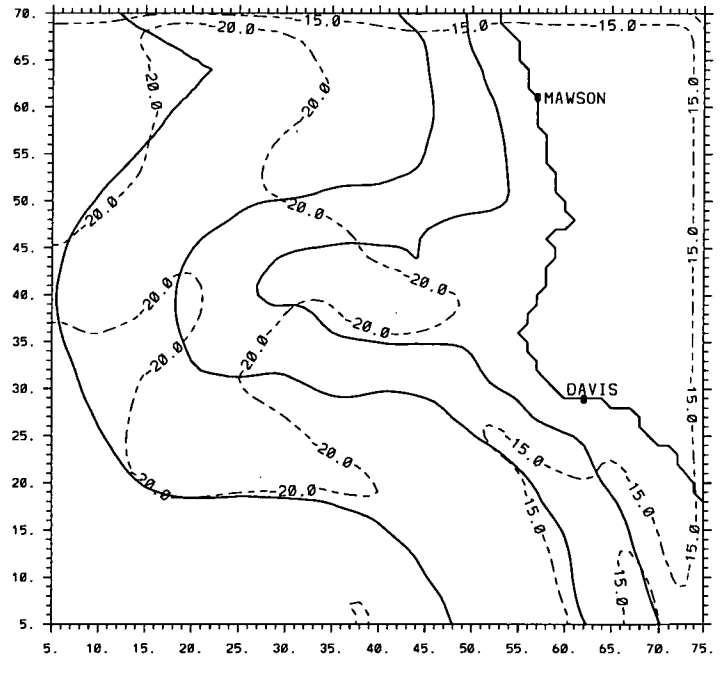

Figure 6.22: Difference in firn surface temperatures between mean July run R20 and mean January run R22, with negative values showing the presence of lower temperatures during July than January. The -15 contour around the boundary of the figure is not significant in terms of the thermal fields; it is a boundary effect of the numerical model.

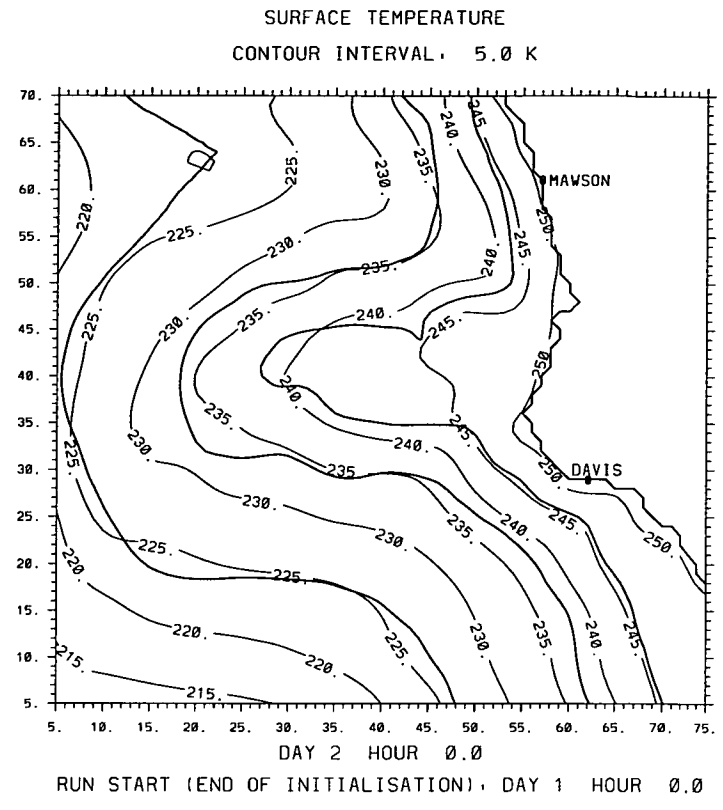

Figure 6.23: Firn surface temperatures as produced by mean July model run R20.

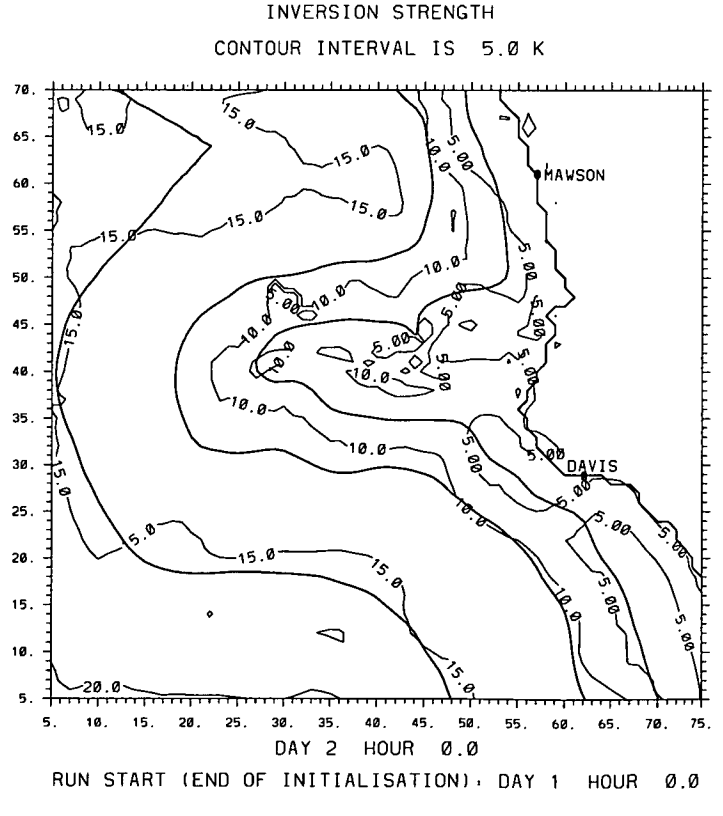

Figure 6.24: Inversion strength as produced by mean July model run R20.

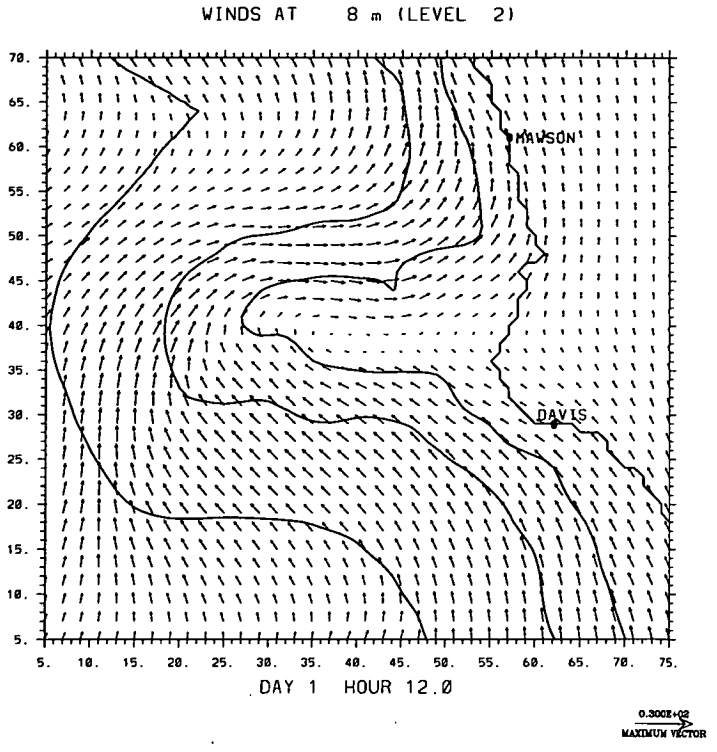

Figure 6.25: Surface (8 metres height) wind vectors as produced by mean January run R22 for midday. The numerical modelling carried out used horizontal grid spacings of 20 km, but for purposes of clarity, vectors plotted here are separated by 2 grid spacings (40 km) in both the x- and y-dimensions.

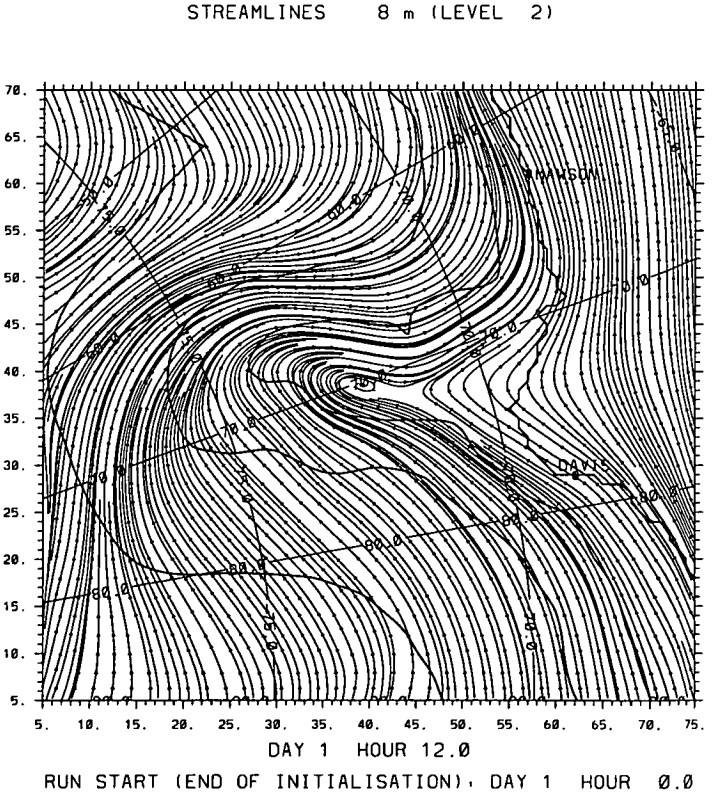

Figure 6.26: Surface (8 metres height) streamlines as produced by mean January run R22 for midday. These lines do not represent trajectories but rather the air flow over the region at one time.

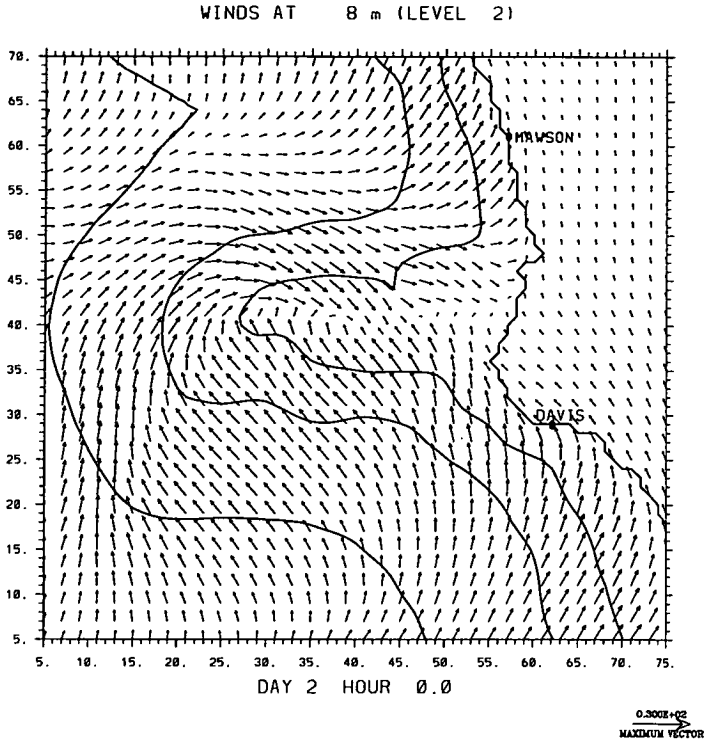

Figure 6.27: Surface (8 metres height) wind vectors as produced by mean January run R22 for midnight. The numerical modelling carried out used horizontal grid spacings of 20 km, but for purposes of clarity, vectors plotted here are separated by 2 grid spacings (40 km) in both the x- and y-dimensions.

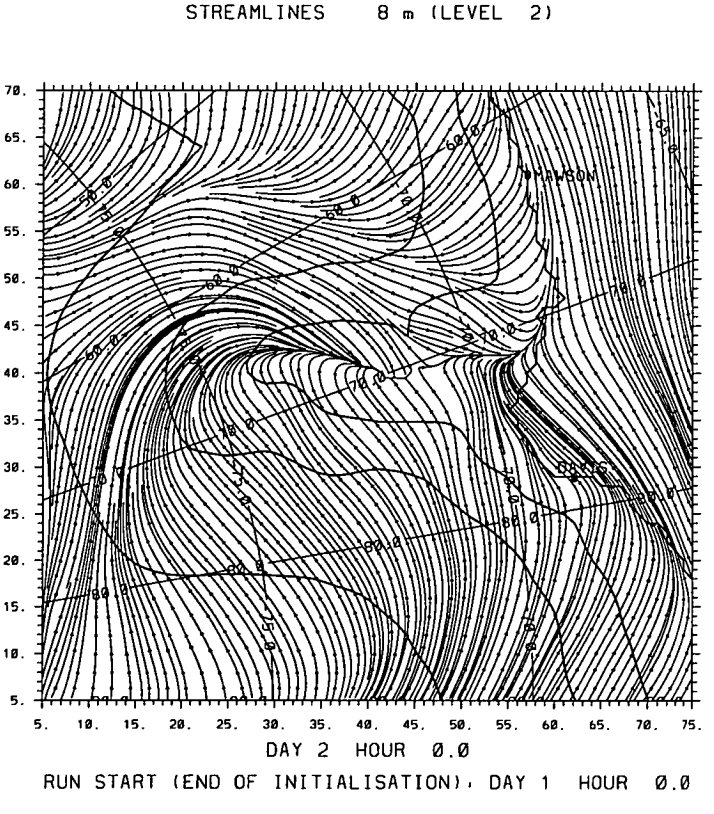

Figure 6.28: Surface (8 metres height) streamlines as produced by mean January run R22 for midnight. These lines do not represent trajectories but rather the air flow over the region at one time.

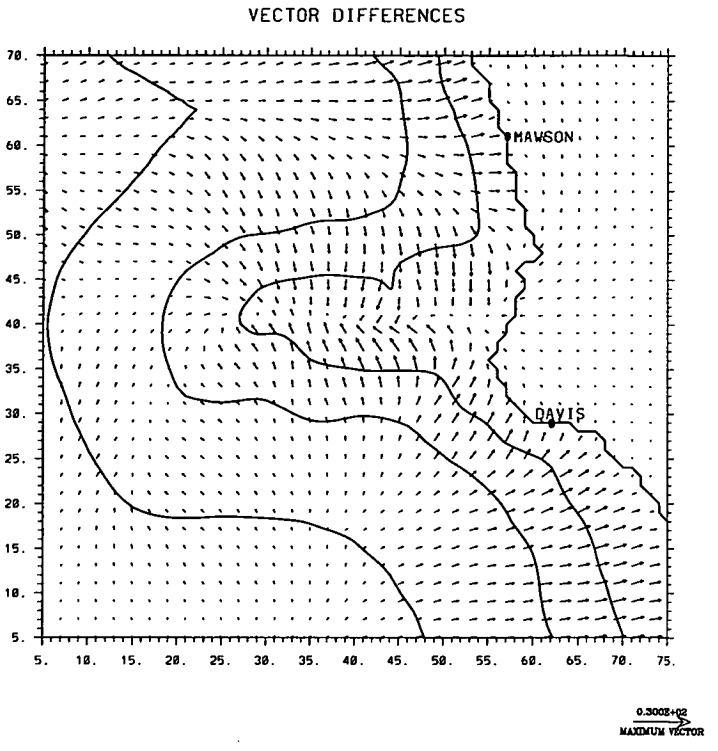

Figure 6.29: Difference in surface (8 metres height) wind vectors between midnight and midday, as produced by mean January model run R22. Midnight surface winds have greater downhill components of flow than those at midday.

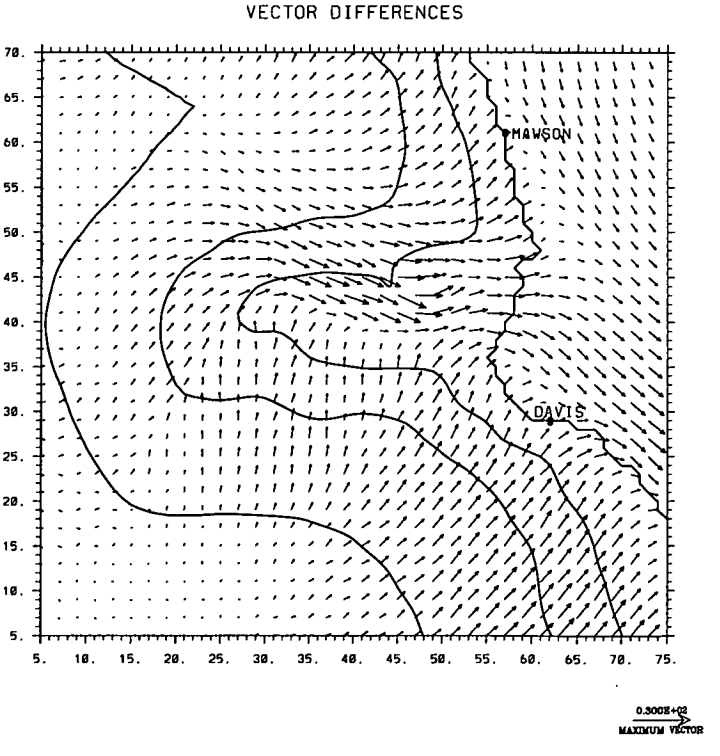

Figure 6.30: Difference in surface (8 metres height) wind vectors between mean July run R20 and mean January run R22. Downhill flow is more significant during July, as is the flow from over the Lambert Glacier towards the sea.

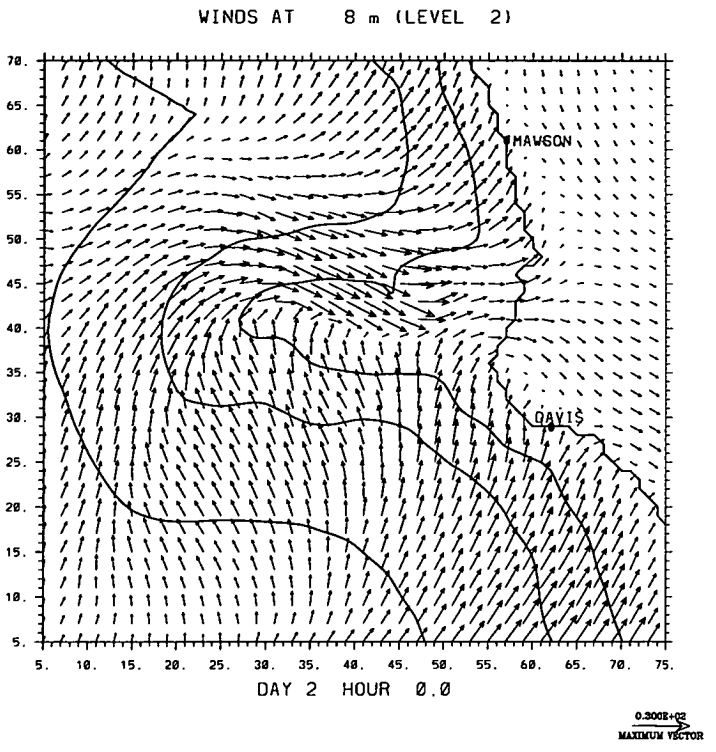

Figure 6.31: Surface (8 metres height) wind vectors as produced by mean July run R20. The numerical modelling carried out used horizontal grid spacings of 20 km, but for purposes of clarity, vectors plotted here are separated by 2 grid spacings (40 km) in both the x- and y-dimensions.

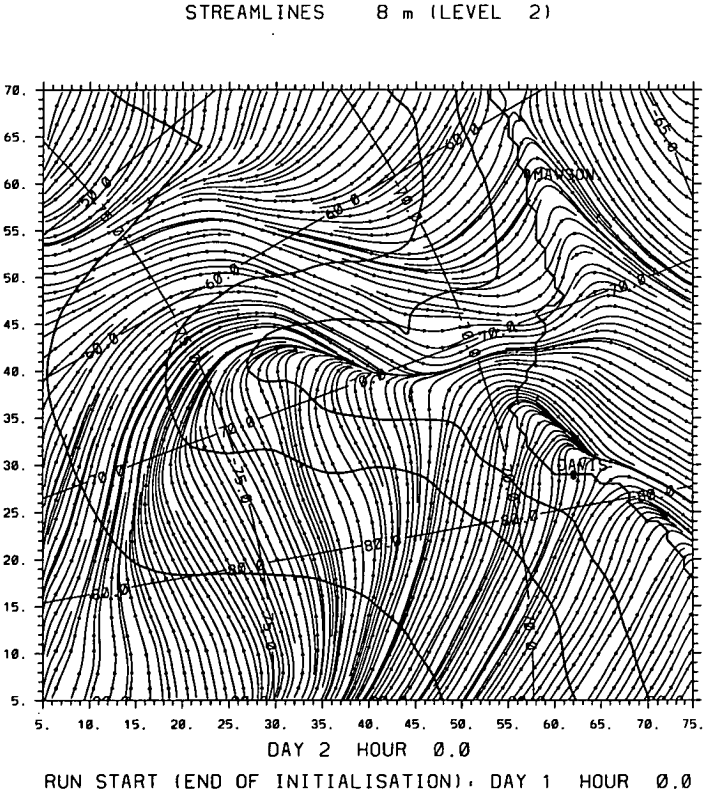

Figure 6.32: Surface (8 metres height) streamlines as produced by mean July run R20. These lines do not represent trajectories but rather the air flow over the region at one time.

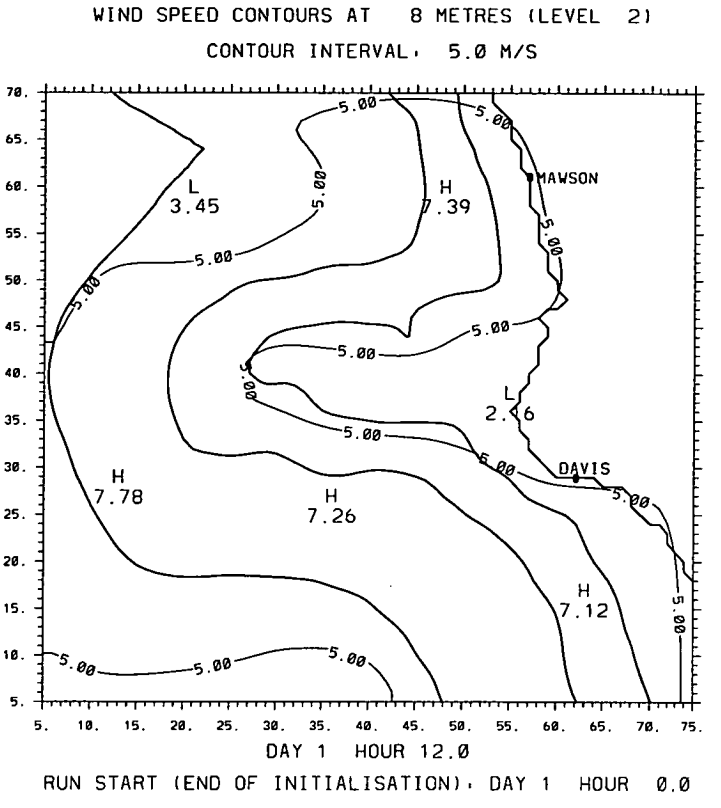

Figure 6.33: Surface (8 metres height) wind speeds produced by mean January run R22 for midday.

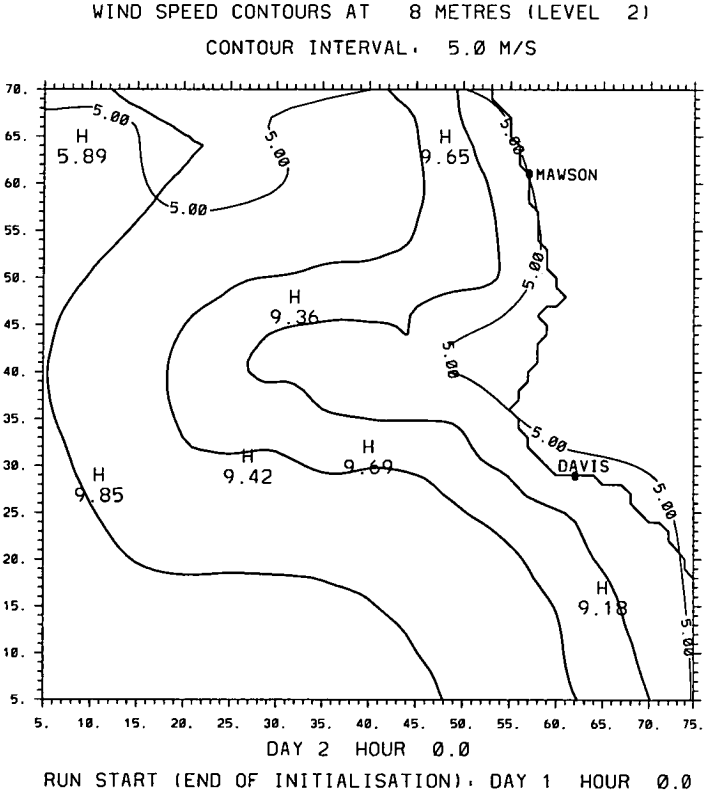

Figure 6.34: Surface (8 metres height) wind speeds produced by mean January run R22 for midnight.

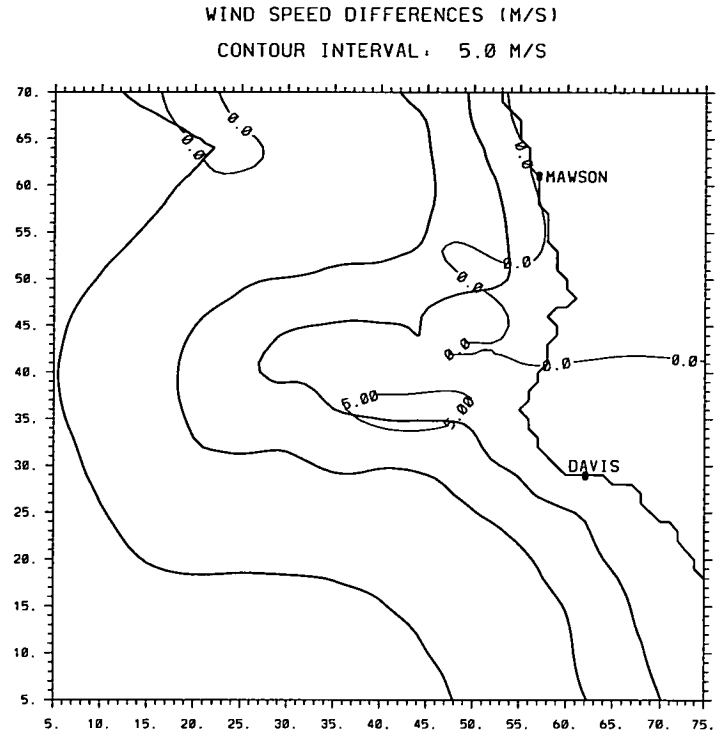

Figure 6.35: Difference in surface (8 metres height) wind speeds between midnight and midday, as produced by mean January model run R22.

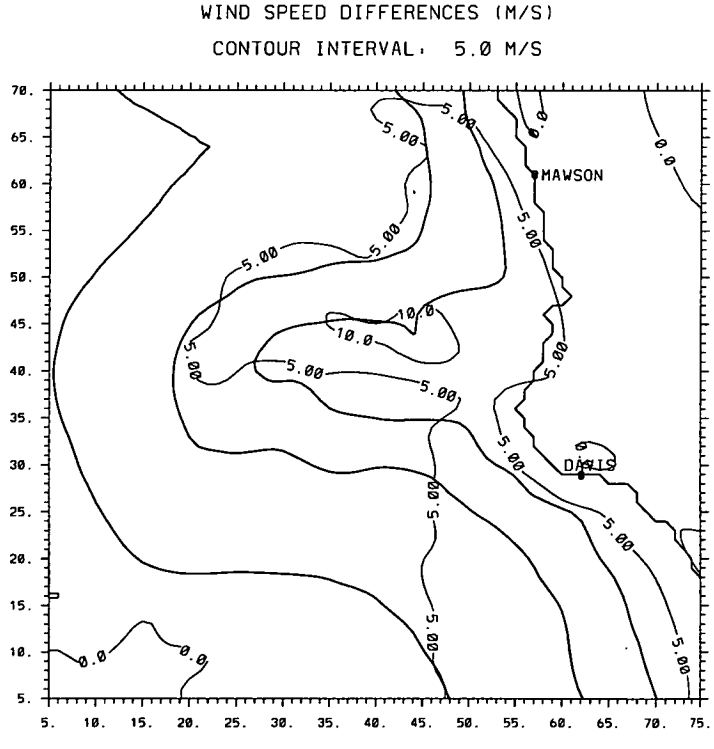

Figure 6.36: Difference in surface (8 metres height) wind speeds between mean July run R20 and mean January run R22, with positive values showing that winds are stronger during July than January. The region with greatest differences in wind speeds is the western side of the Lambert Glacier valley, where significant convergence of air occurs. Generally, the differences are confined to the areas with greatest terrain slope, below about 2000 metres.

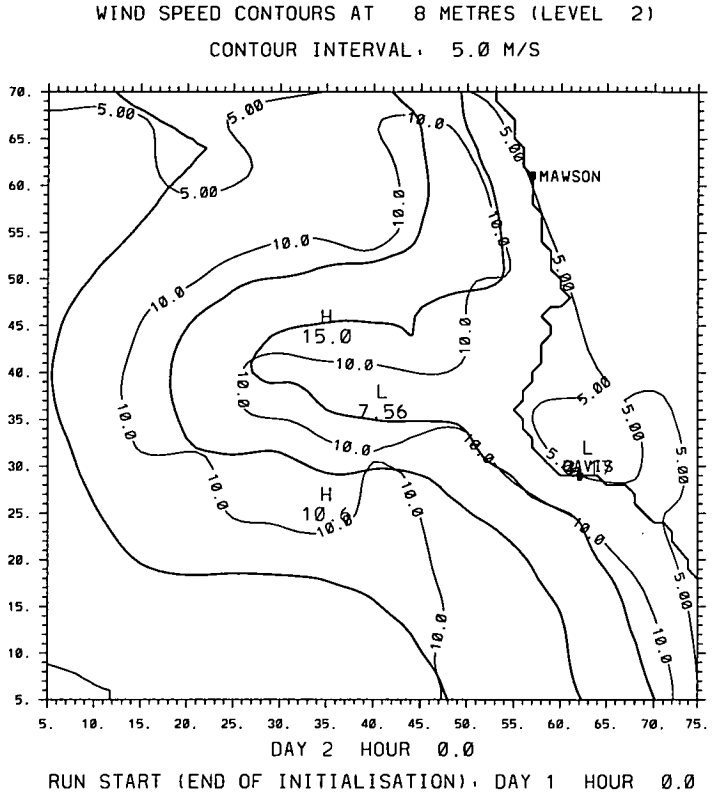

Figure 6.37: Surface (8 metres height) wind speeds produced by mean July run R20.

6.9 CONCLUSION

Problems with parameterisation schemes used in the numerical model were overcome previously in Chapter 5.

In this chapter, improvements in the match between the model's thermal fields and observations were made by tuning several parameters; a realistic spatially-varying synoptic wind field was introduced, spatially-varying surface albedos were tested, sensitivity experiments were made for variance of surface diffusivity with changes in temperature and simple parameterisations of cloud radiative forcing were introduced. Following these changes, good agreements were found between modelled and observed surface temperatures and modelled and observed winter inversion strengths.

Additional sources of data were used to further test the accuracy of the model-generated meteorological fields. It was found that the model was performing well but the definition of the terrain slopes in the vicinity of Mawson may be retarding the downslope flow within the model, resulting in wind speeds that are too low. Other minor differences between modelled and observed fields were discussed.

The mean January and mean July model runs were considered to provide useful information, particularly the surface wind direction fields that were found to match observed values when monthly mean data, sastrugi orientations or diurnal variations were considered.

Model-generated fields were used to construct a climatology of surface winds and thermal patterns over the region of interest.

Chapter 7

INFLUENCE OF SYNOPTIC SYSTEMS ON SURFACE WINDS AT MAWSON

7.1 INTRODUCTION

This chapter contains analyses of winds at Mawson that expand on the climatology presented in Chapter 3. The primary aim was to investigate the relationship between the surface and synoptic winds. The study was limited to the months of January and July, considered to be representative of summer and winter Antarctic weather conditions respectively.

Vertical profiles of January and July mean monthly wind speeds are presented for the wind types defined in Chapter 3. Progressing from these, vertical wind speed profiles of katabatic and non-katabatic winds were compared for different surface wind speeds. These investigations of the structure of the atmosphere help to reveal the relationship between surface and upper level (700 hPa to 500 hPa) winds and how momentum may be transferred from the upper levels to the surface. Analyses of lapse rates versus wind speeds were also carried out; these reveal the thermal stability regimes that accompany different wind types and speeds at Mawson.

The influence of synoptic winds on surface winds was examined and discussed using January and July meteorological data collected at Mawson. Data sets used and periods of measurements are discussed in Chapter 3. Corresponding

SHANAL wind fields are discussed in Chapter 6).

Following these analyses, the mesoscale model is utilised in the following chapter to construct the wind and thermal fields over the Lambert Glacier region while under the synoptic forcing patterns corresponding to several of the wind types for January and July.

The wind types referred to throughout this chapter have been defined in Section 3.4 of Chapter 3. Additional wind types are defined below.

"Non-katabatic" winds are those that do not possess a near-surface jet as a feature; they may or may not flow downslope. These winds are comprised of all remaining winds that do not fit into the "katabatic" category, defined in Chapter 3.

"Enhanced-katabatic-A" winds are those that have a near-surface jet and flow downslope, the same as the "katabatic" type, but the jet must be enhanced up to the 850 hPa level such that the wind speed at that height is greater than 5 m/s. "Enhanced-katabatic-B" winds require the presence of a katabatic jet and wind speed greater than 5 m/s at the 850 hPa level but the jet is not necessarily continuous up to this level. "Enhanced-katabatic-A" type winds are a subset of "Enhanced-katabatic-B" winds. These definitions are based on the descriptions given by Phillpot (1989) .

7.2 ANALYSES OF WIND PROFILES

7.2.1 JANUARY AND JULY WIND DIRECTION PROFILES

It is important to note that mean values of wind direction can be misleading; later in this chapter, frequencies of wind directions are presented. These show more clearly what the "mean" wind directions represent.

Figure 7.1 shows that all wind directions are close to south-easterly due to the influence of the underlying terrain. For both January and July, the upper wind direction profiles, corresponding to katabatic and calm upper wind, show similarities. Blizzard winds show upper wind directions that correspond with a

depression located to the north-east of Mawson.

Wind directions plotted in Figures 7.1B & D show that katabatic-non-blizzard winds have upper air forcings similar to katabatic and calm winds, while blizzard-non-katabatic winds have forcings similar to blizzard winds. The mean upper wind direction corresponding to the katabatic-blizzard wind type suggests that there may be forcings that can cause both blizzard and katabatic conditions at the surface. However, this forcing is somewhat unclear from these data; further discussions follow in this chapter.

7.2.2 JANUARY AND JULY WIND SPEED PROFILES

During July, the upper wind speeds for different wind types are very similar and are not useful for determining the wind type or the wind speed at the surface. Upper wind directions are probably more valuable than wind speeds in regard to examining the influence that synoptic winds have on surface winds.

The separation of upper wind speeds for each wind type is clearer during January. Calm and katabatic upper forcings are similar, with significant differences only below the 1000 metre level.

At around 400 metres above the surface, the blizzard-non-katabatic is much stronger than the katabatic-blizzard wind, but at the surface, the katabatic-blizzard wind is slightly the stronger.

7.2.3 JANUARY AND JULY KATABATIC WIND PROFILES

Figure 7.3A shows that a relatively narrow range of January upper wind speeds (within about 5 m/s) can result in a large range of surface wind speeds (1-14 m/s), for katabatic wind profiles. For July, Figure 7.5A, a similar comparison between upper and surface wind speeds is found but the July upper wind speeds are generally stronger than the January values by about 5 m/s, for the same surface wind speeds (1-14 m/s). The differences between these two figures show that there is less efficient transfer of momentum from the upper levels towards the surface during July, for katabatic winds.

For the katabatic surface wind speeds 15-24 m/s, the January vertical profiles are less well defined than for the lower wind speeds, Figure 7.3B. However, for the same wind speeds, the July profiles exhibit shapes that are characteristic of katabatics, 7.5B.

For katabatics with surface wind speeds equal to and greater than 25 m/s, the July profiles do not show consistent patterns above about 1000 metres, Figure 7.6A. In the lowest 1000 metres the near-surface jet is quite pronounced, with local minima at the level immediately above the surface.

As the surface wind speed increases during July, the jet is better defined and the level above the surface exhibits a local minimum. This demonstrates the important influence of "local" surface winds on a katabatic near-surface jet; the synoptic wind is also important but probably to a lesser degree, as momentum transfer from higher levels towards the surface does not occur efficiently and the stronger katabatic jets are relatively shallow, appearing to "undercut" the atmosphere, somewhat like a cold front, Figure 7.6A.

Figures 7.4B and 7.6B show that katabatic winds occur more often and are stronger during July than during January.

7.2.4 JANUARY AND JULY NON-KATABATIC WIND PROFILES

Wind profiles categorised as "non-katabatic", Figures 7.7 to 7.10, generally show the presence of a low level jet (about 400 metres height) for both January and July. Therefore, wind profiles at Mawson consist mostly of katabatic or low level jets.

During January, stronger wind speeds at the upper levels generally result in stronger surface wind speeds. This is not a general occurrence during July, particularly for surface wind speeds below 15 m/s, Figure 7.9A. Therefore, the upper wind speed is less important in determining the surface wind speed during July.

Figures 7.8B and 7.10B show that non-katabatic winds occur more often during January, but calms are recorded more frequently during July.

7.2.5 JANUARY AND JULY LAPSE RATES

Lapse rates plotted in Figure 7.11 were measured between the surface and a height of about 2600 metres, giving an indication of the lower atmosphere's (thermal) stability at Mawson. In Figure 7.12, lapse rates were measured from the surface to a height of about 740 metres, more representative of the near-surface flow than of the lowest two kilometres of the atmosphere.

For both katabatic and non-katabatic winds, the change in lapse rate as wind speed increases does not show a consistent trend, particularly when wind speeds are above blizzard strength. However, for January, the highest wind speeds on each figure suggest that stabilities decrease as wind speed increases. Below 15 m/s some basic relationships are found for the two wind types for January and July.

During January non-katabatic winds below about 5 m/s show a slight decrease in stability with increase in wind speed. Otherwise, increases in stability are accompanied by increases in wind speed for both non-katabatic and katabatic winds, up to blizzard strength, Figures 7.11A and B, 7.12A and B. For January, the same general relationships between wind speed and lapse rate do not vary when the lapse rates are calculated at different levels.

For the lowest 2600 metres of the atmosphere during July, increases in wind speed for katabatic and non-katabatic wind types are generally accompanied by reductions in stability. However, at wind speeds greater than about 15-20 m/s the relationship becomes less clear.

Lapse rates calculated in the lowest 740 metres of the atmosphere during July do not reveal any consistent trend for wind speed increase for katabatic winds. Figure 7.12C shows that very high wind speeds (29 and 33 m/s) do not necessarily correspond to reductions in thermal stability of the column of air over Mawson. For both of these values, inversions are present between the surface and 740 metres, although they are weak.

The general understanding of relations between inversions and wind speeds was that low wind speed conditions allowed inversions to form and then wind speeds can increase due to the inversion's strong stable vertical stratification. The higher wind speeds then cause increased turbulence and mixing and the inversion strength is reduced. The preceding paragraph and the monthly mean values presented here contradict this basic understanding. In regard to Mirny station, also a katabatic wind site, Rusin (1961) made a statement that is also contradictory of these basic mechanisms: "It is also difficult to explain why surface inversions persist even when gravitational winds reach hurricane force."

For non-katabatic winds, there is a general decrease in stability as wind speeds increase up to 6 m/s. Further increases in wind speed are accompanied by general increases in stability, but this trend again becomes less well defined as wind speeds reach blizzard strength and stronger.

Approximate relationships are summarising as follows: wind speed increases during January are accompanied by increases in thermal stability, but during July increases in wind speed correspond to reductions in stability.

Rusin (1961) noted that "temperature inversion in the boundary layer always accompanies katabatic conditions," but Figures 7.11 and 7.12 show that this is not the rule for Mawson station for either January or July.

7.2.6 ENHANCED KATABATIC WINDS

The low percentage occurrence of enhanced-katabatic A type winds at Mawson, Figure 7.13, shows that katabatic winds usually occur as low level jets, not as jets that are vertically enhanced, extending to levels as high as 850 hPa.

The enhanced-katabatic B type wind occurs more often at Mawson, and with increased frequency during the non-summer months, but the values are low enough to show that katabatic jets do not usually occur with accompanying strong ($\gg$5 m/s) winds aloft.

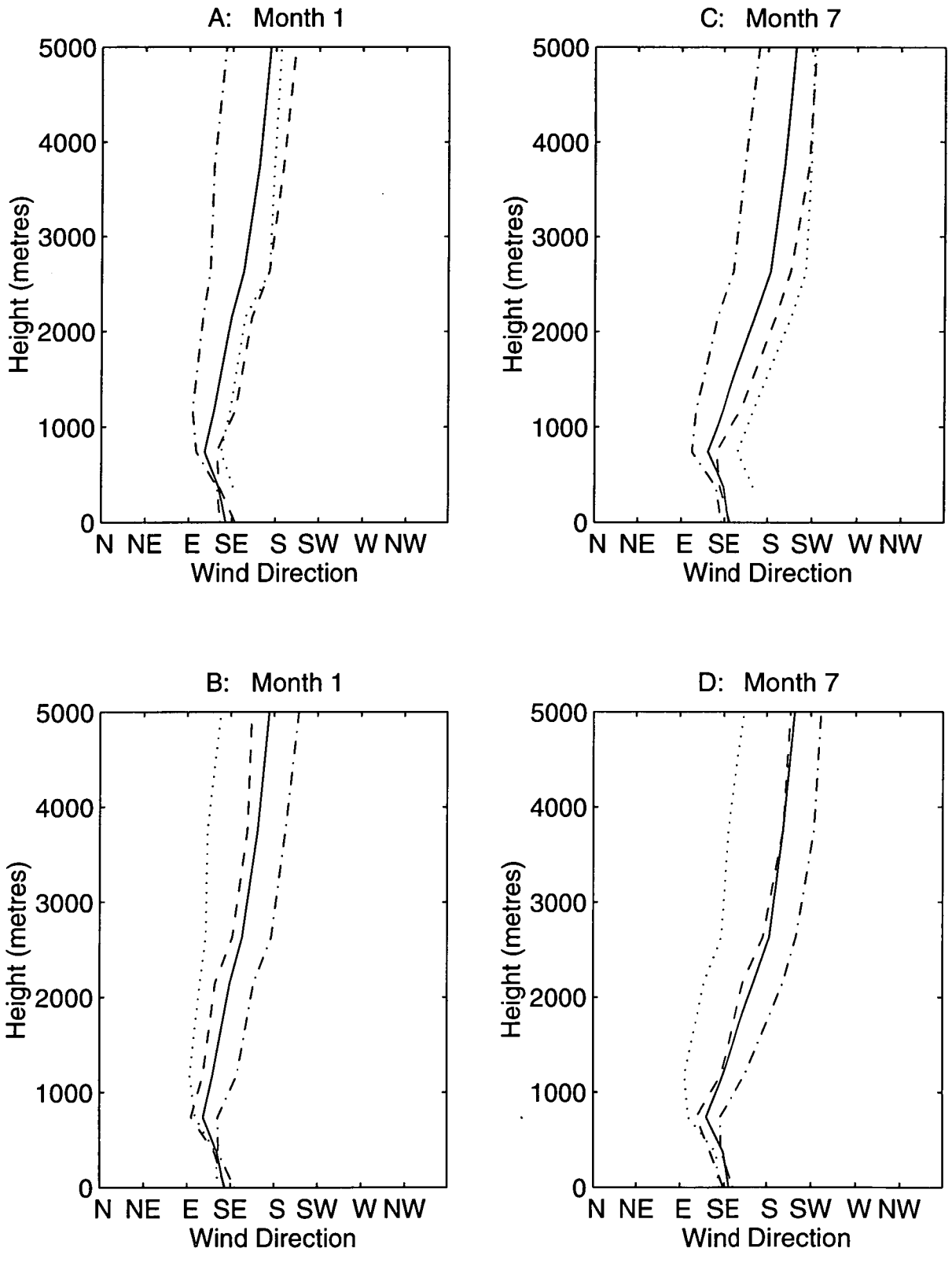

Figure 7.1: January and July monthly mean wind direction profiles for different wind types. A & C: Average(solid), katabatic(dash), blizzard(dot-dash), calm(dot), B & D: Average(solid), katabatic-blizzard(dash), katabatic-non-blizzard(dot-dash), blizzard-non-katabatic(dot). Average wind profiles for each month are plotted on all figures to allow easy comparison between the various wind types for each month.

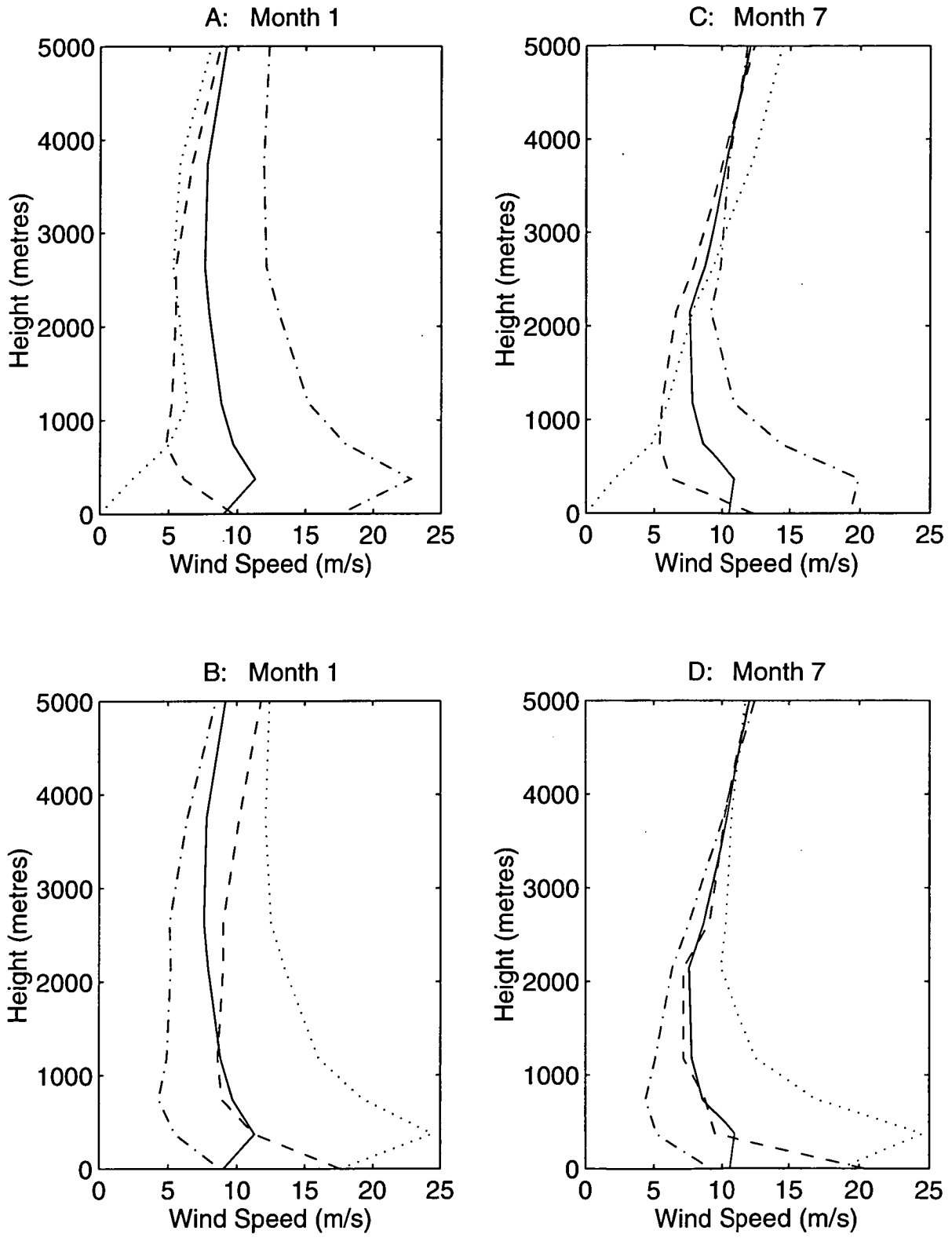

Figure 7.2: January and July monthly mean wind speed profiles for different wind types. A & C: Average(solid), katabatic(dash), blizzard(dot-dash), calm(dot), B & D: Average(solid), katabatic-blizzard(dash), katabatic-non-blizzard(dot-dash), blizzard-non-katabatic(dot). Average wind profiles for each month are plotted on all figures to allow easy comparison between the various wind types for each month.

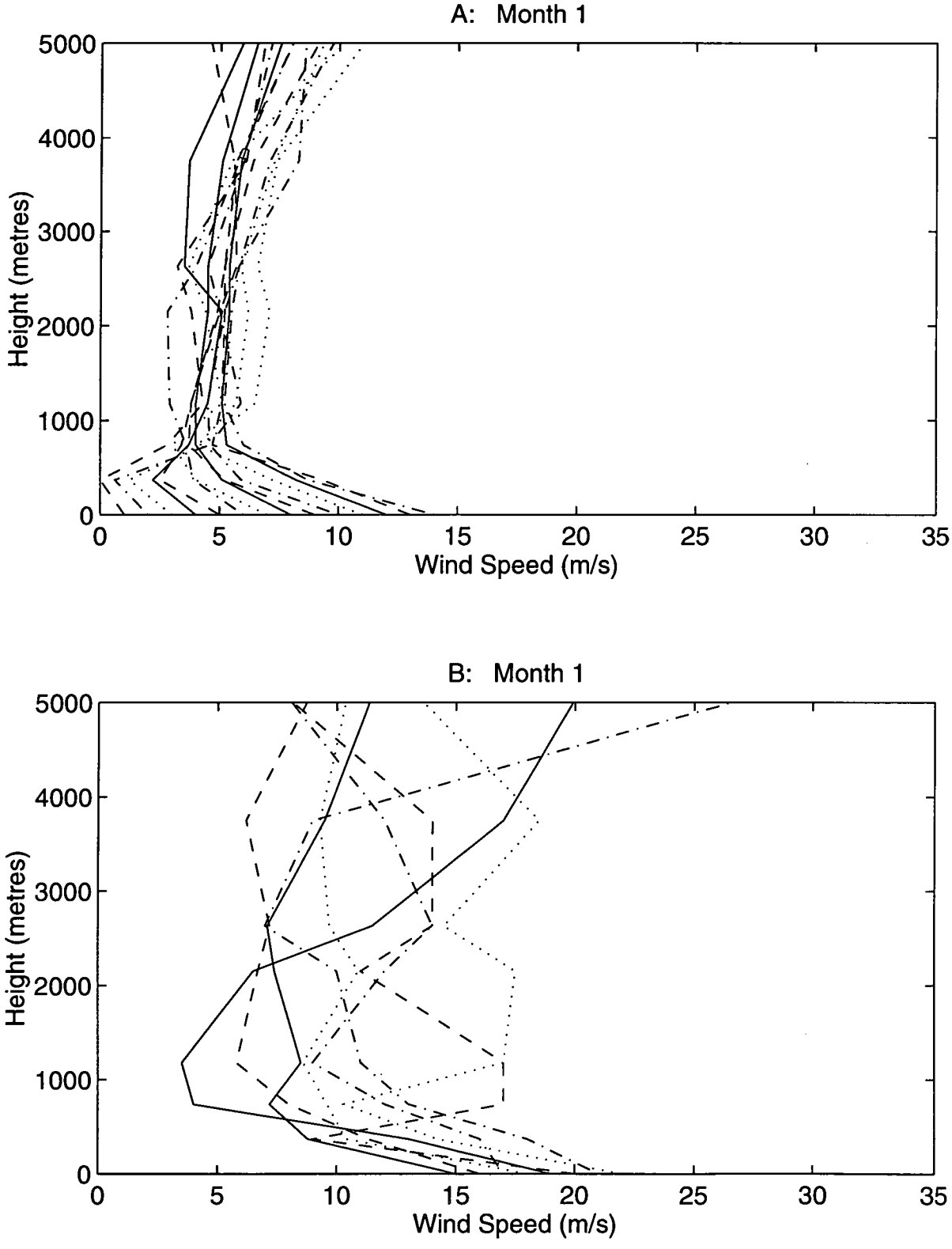

Figure 7.3: Katabatic January monthly mean wind speed profiles for surface wind speeds: A: 1-14 m/s, B: 15-24 m/s.

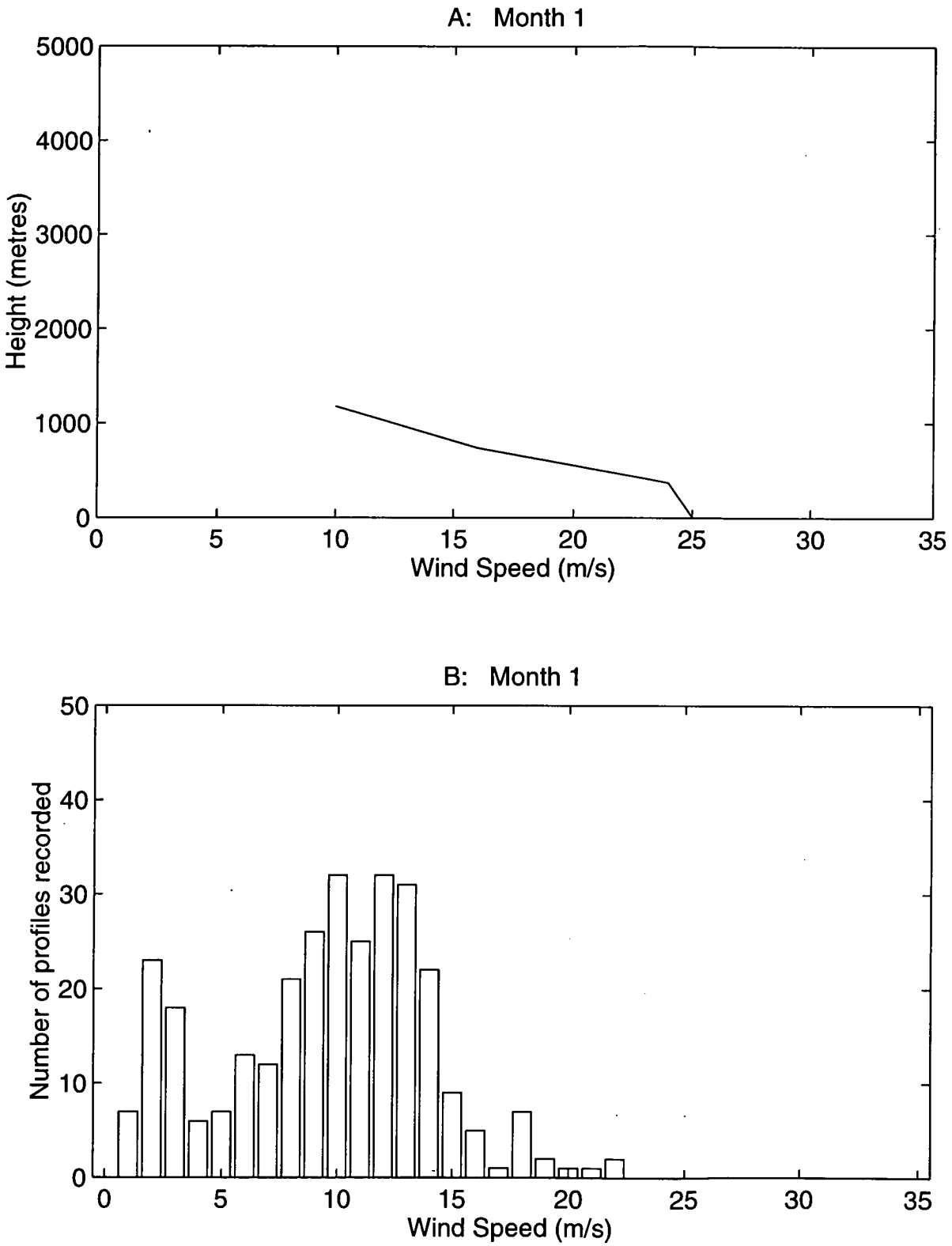

Figure 7.4: Katabatic January monthly mean wind speed profiles for surface wind speeds: A: 25+ m/s. Sub-figure B shows the number of profiles corresponding to each surface wind speed used in this analysis of January AUW data.

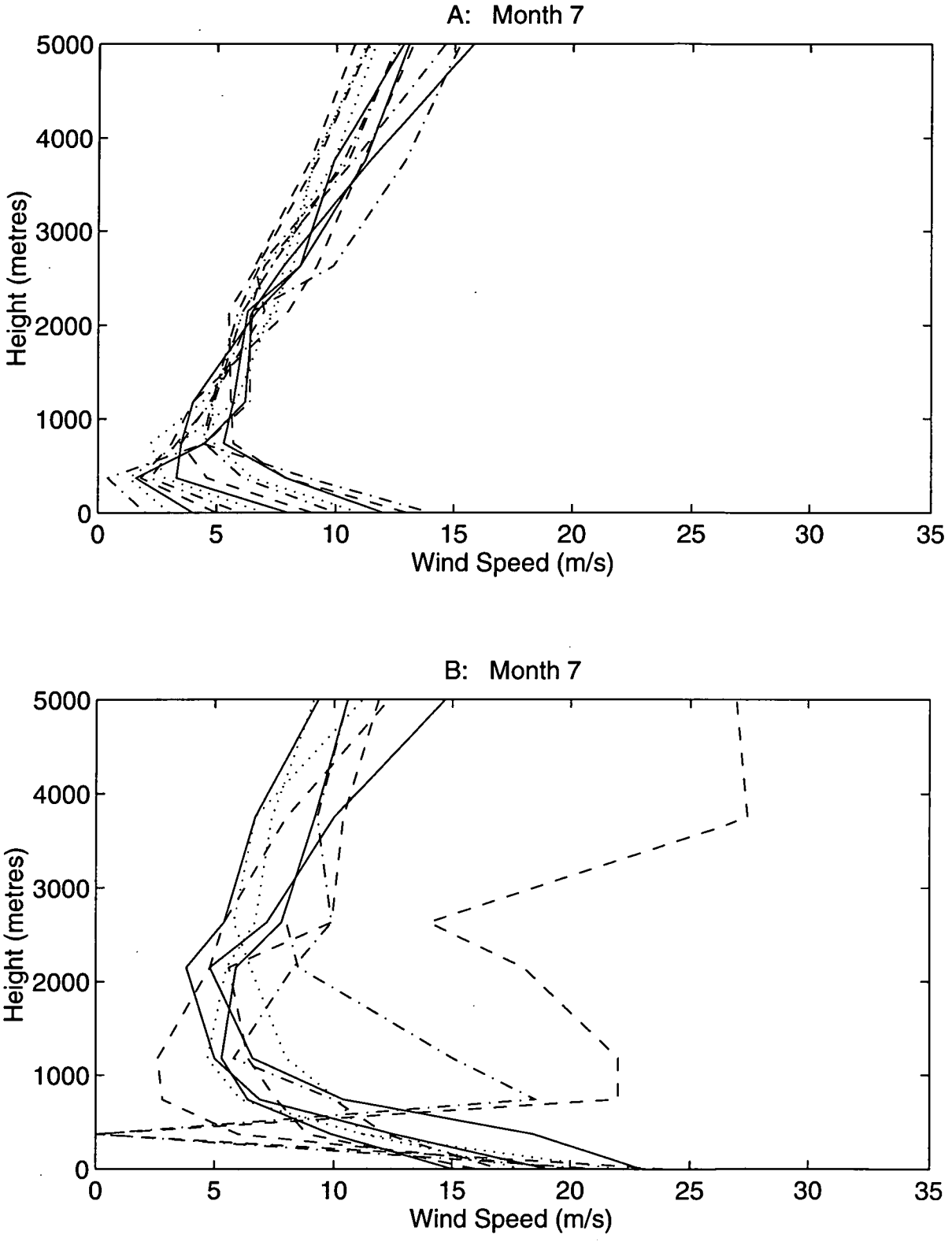

Figure 7.5: Katabatic July monthly mean wind speed profiles for surface wind speeds: A: 1-14 m/s, B: 15-24 m/s.

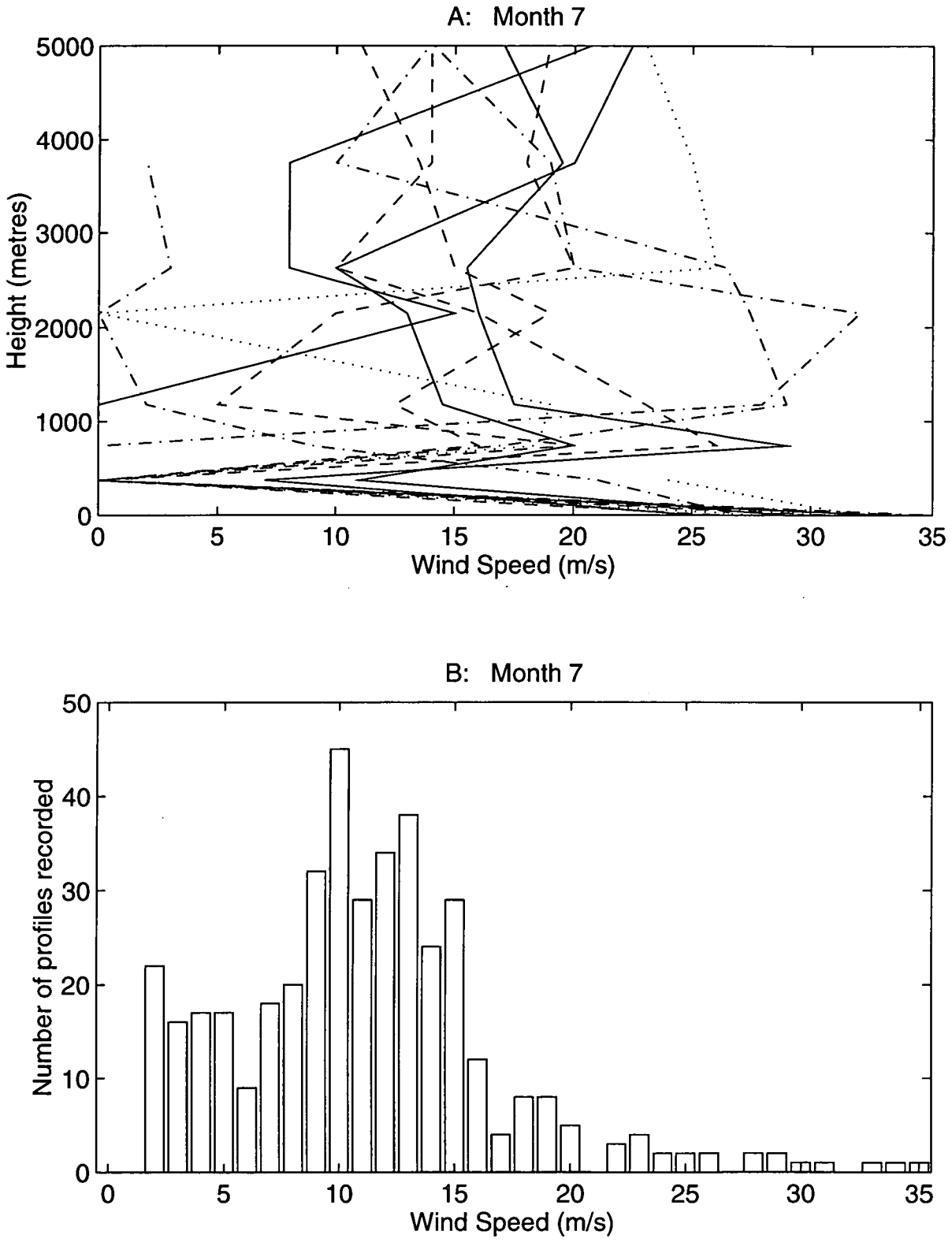

Figure 7.6: Katabatic July monthly mean wind speed profiles for surface wind speeds: A: 25+ m/s. Sub-figure B shows the number of profiles corresponding to each surface wind speed used in this analysis of July AUW data.

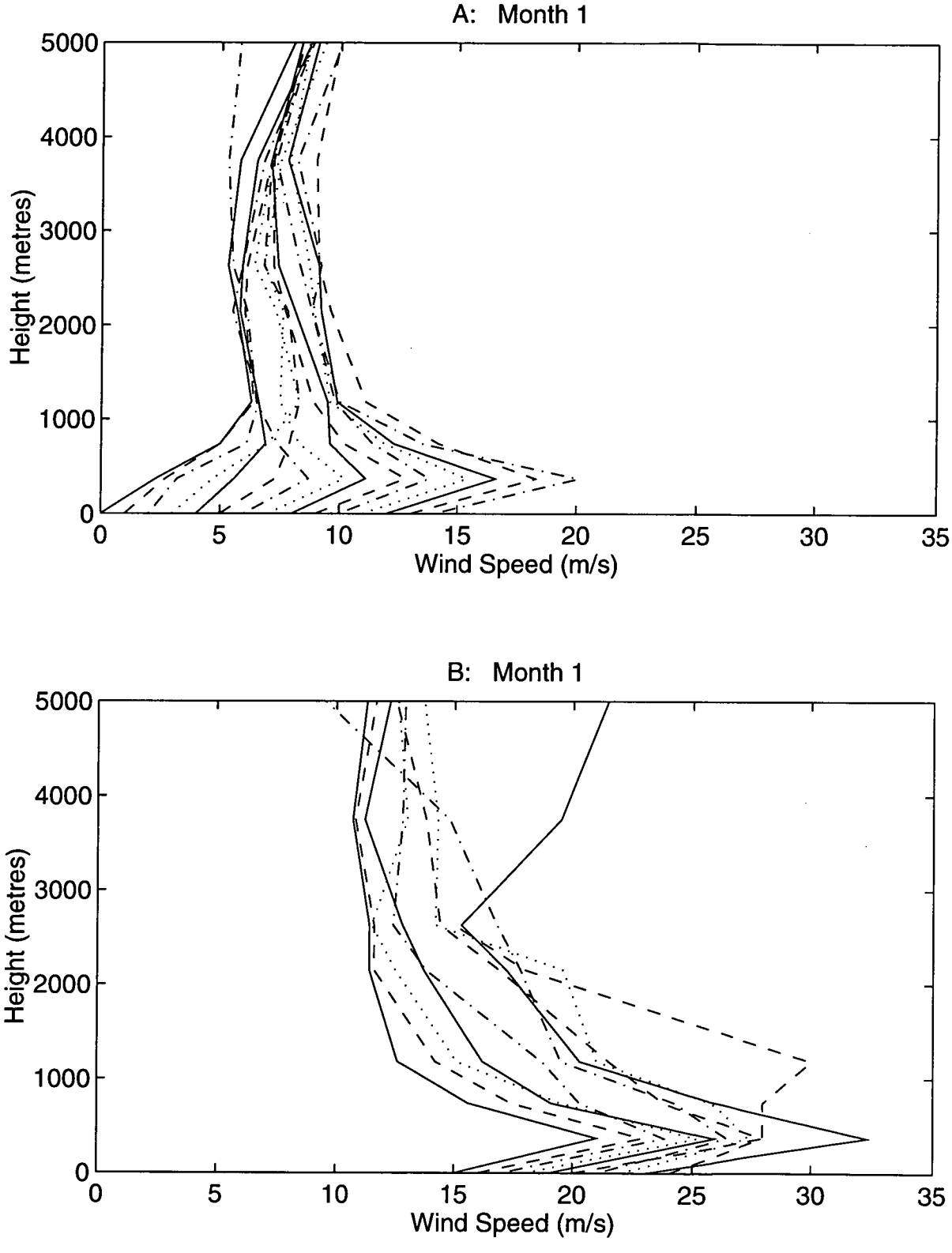

Figure 7.7: Non-katabatic January monthly mean wind speed profiles for surface wind speeds: A: 1-14 m/s, B: 15-24 m/s.

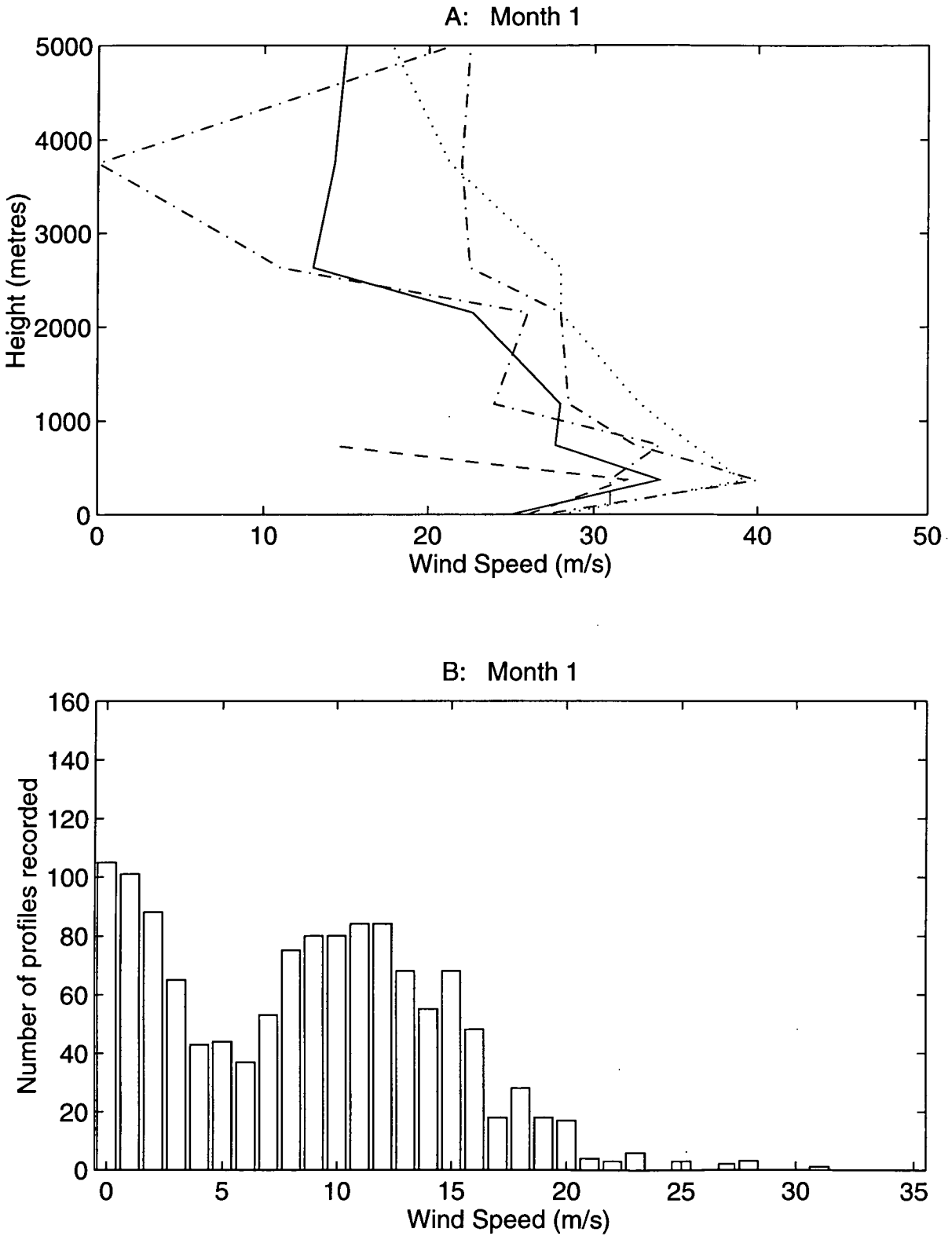

Figure 7.8: Non-katabatic January monthly mean wind speed profiles for surface wind speeds: A: 25+ m/s. Sub-figure B shows the number of profiles corresponding to each surface wind speed used in this analysis of January AUW data.

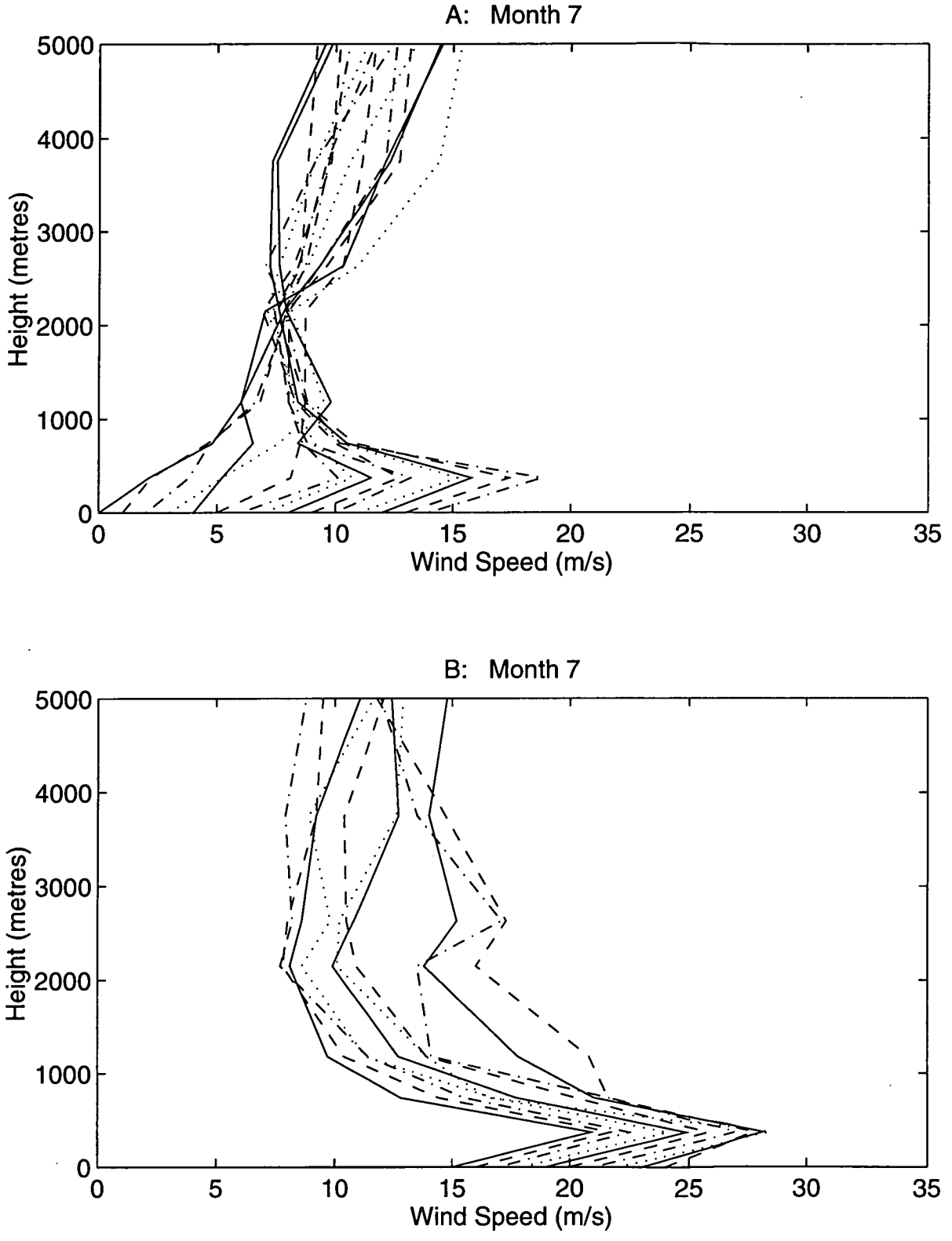

Figure 7.9: Non-katabatic July monthly mean wind speed profiles for surface wind speeds: A: 1-14 m/s, B: 15-24 m/s.

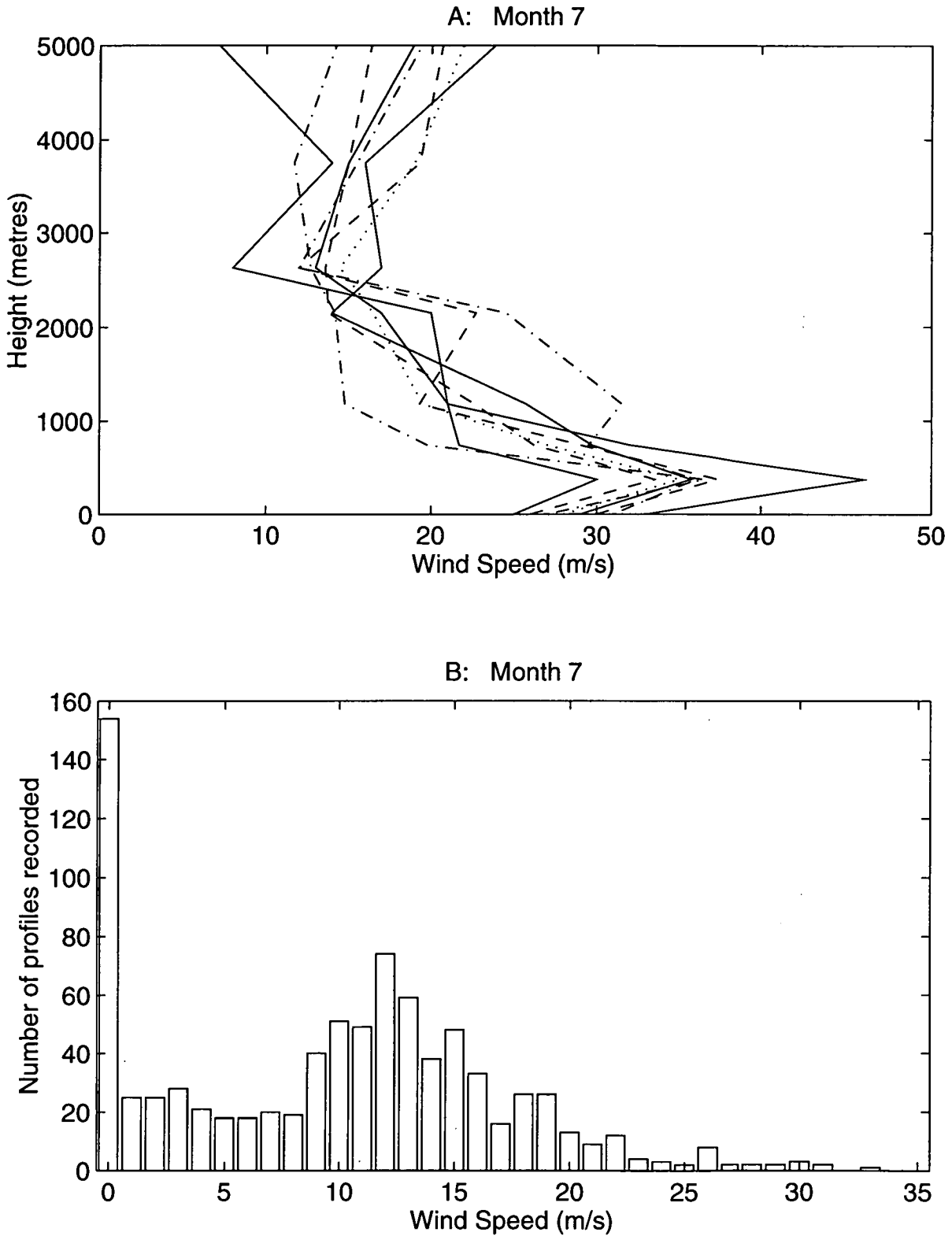

Figure 7.10: Non-katabatic July monthly mean wind speed profiles for surface wind speeds: A: 25+ m/s. Sub-figure B shows the number of profiles corresponding to each surface wind speed used in this analysis of July AUW data.

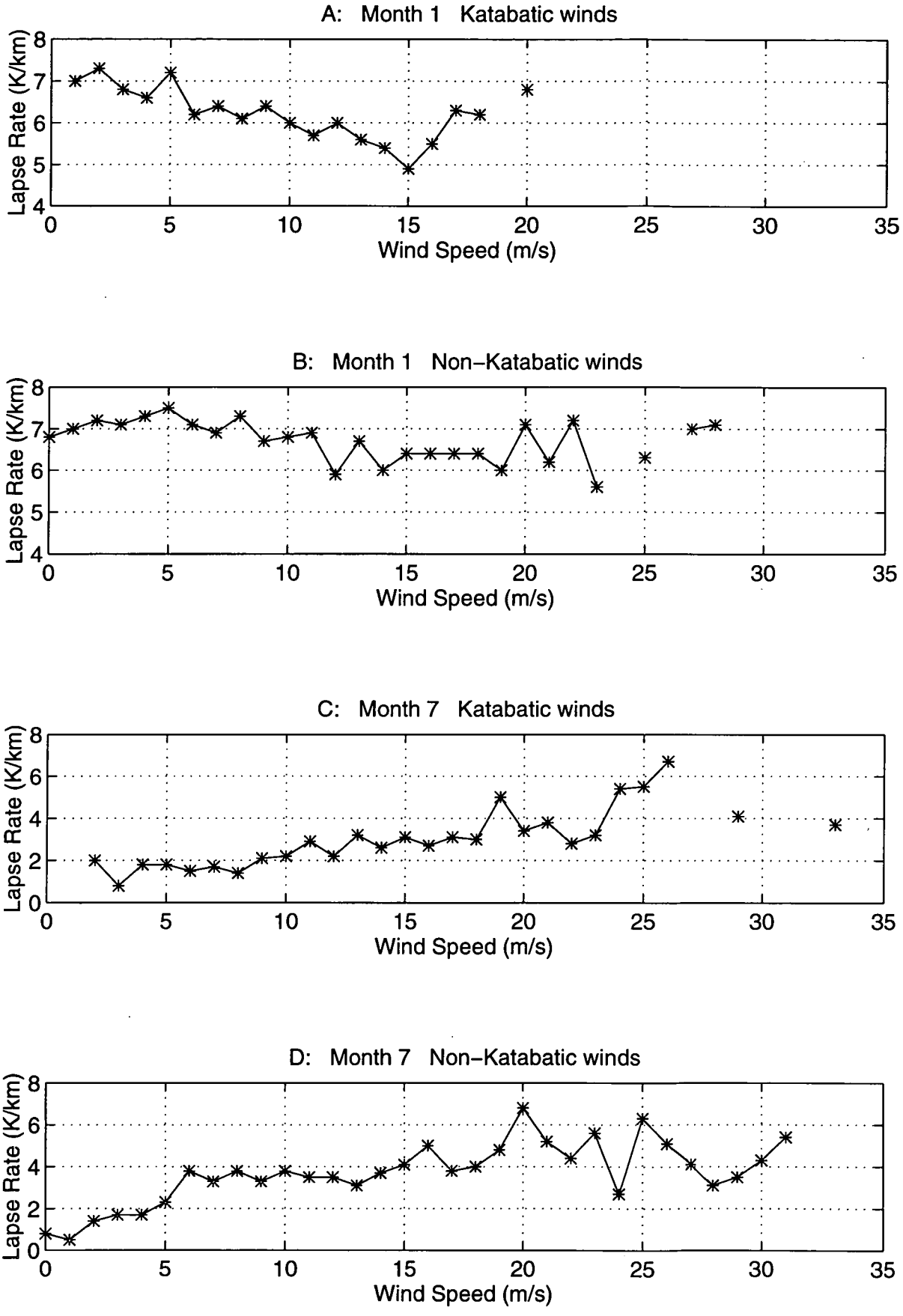

Figure 7.11: Mean monthly lapse rates corresponding to different wind speeds for katabatic and non-katabatic type winds, for January and July at Mawson. These lapse rates are calculated between the surface and 700hPa, a height of about 2600 metres.

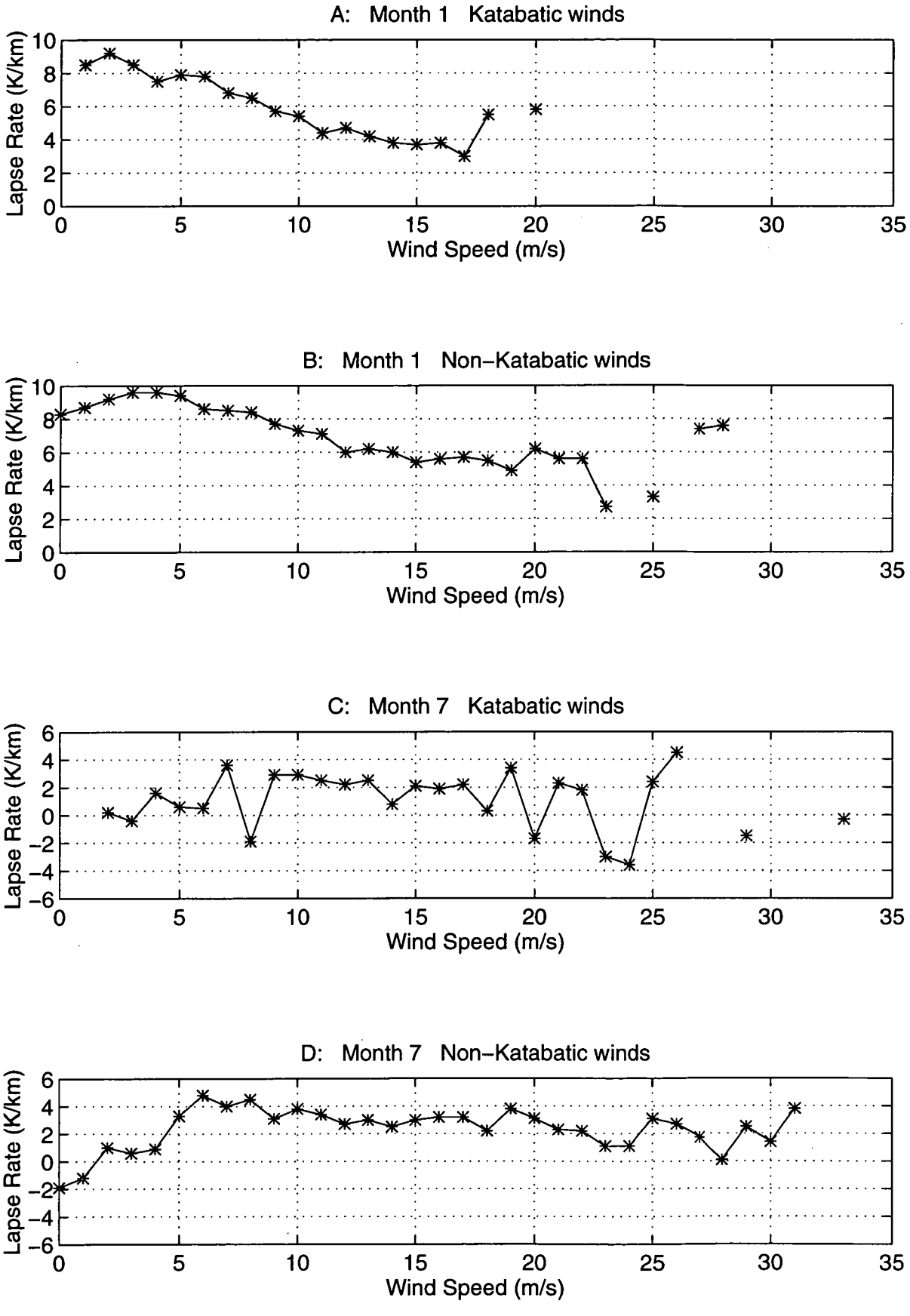

Figure 7.12: Mean monthly near-surface lapse rates corresponding to different wind speeds for katabatic and non-katabatic type winds, for January and July at Mawson. These near-surface lapse rates are calculated between the surface and a height of about 740 metres.

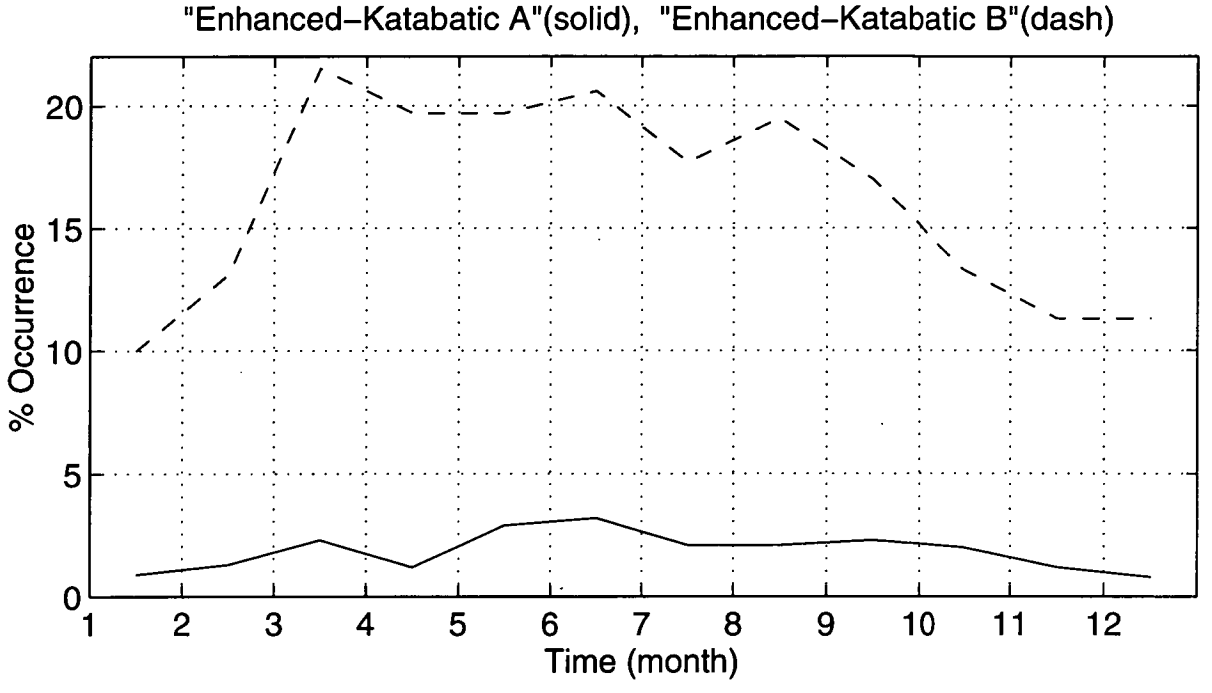

Figure 7.13: Monthly mean percentage occurrences of Enhanced-katabatic A and Enhanced-katabatic B winds at Mawson.

7.3 ANALYSES OF SURFACE AND 700hPa WINDS AT MAWSON

7.3.1 INTRODUCTION

The upper wind (AUW) data set provides a good representation of winds over Mawson station, but a larger scale wind pattern can only be inferred by examining other parameters, such as changes in cloud amount, relative humidity and pressure. Such changes may be used as indicators of the synoptic pattern, as was done in Chapter 3.

The Southern Hemisphere Analyses (SHANAL) data set is used to provide a synoptic scale wind pattern over the area of interest. The dates of occurrences of different wind types at Mawson were extracted from the upper wind data set. These dates were then used to select the SHANAL 700 hPa height and wind fields, corresponding to different wind types, that were then totalled and averaged. This resulted in mean synoptic situations corresponding to the various wind types defined in Section 3.4 of Chapter 3; katabatic, blizzard, calm, katabatic-blizzard, katabatic-non-blizzard and blizzard-non-katabatic.

The validity of these mean SHANAL fields was examined by comparing them with the Mawson upper wind analyses. It was found that although not all of the mean SHANAL fields corresponded with the results from the Mawson upper wind analyses, the comparison yielded useful information, discussed further in Section 7.3.3.

7.3.2 UPPER WIND (AUW) DATA: RELATIONSHIP BETWEEN SURFACE AND 700 hPa WINDS

The general relationships between wind directions at the surface and 700 hPa for the months of January and July, as shown by Figures 7.14 to 7.20 are discussed.

The January and July monthly mean structures of the atmosphere over Mawson from the surface to 500 hPa, in terms of wind directions is shown in Figure 3.20, Chapter 3.

The relationships between surface and 700 hPa level wind directions differ depending on the wind type. The discussion in Section 3.5.1 is relevant and is expanded upon here.

January average, blizzard and blizzard-non-katabatic type winds are consistent with the January inter-level forcings, with wind directions of neighbouring levels not differing by very large angles, and the relationship between levels fairly clear. Analyses in Chapter 3 revealed that blizzard winds were associated with cyclonic depressions. These systems are consistent with lack of inversion, and lack of near surface jets, two features that can complicate the relationship between wind directions at different levels.

The January katabatic-blizzard wind direction analysis, Figure 7.18 shows a similar relationship but the forcing at the 700 hPa level has greater scatter, probably because the near-surface jet was included in this wind type, and caused the relationship between wind directions at different levels to be less clear than for the January average wind case, or other blizzard winds types.

The wind directions at 700 hPa that accompany katabatic winds at the surface show no definite direction; katabatic winds typically form under anticyclonic synoptic patterns, and are primarily influenced by the cooling of the surface and air near the surface, that then drains downslope. Actual forcing, as in transfer of momentum from higher levels by synoptic winds is not required, and katabatic winds have been noted as being independent of the synoptic pattern, Chapter 2. Katabatic-non-blizzard winds show similar results, with no apparent corresponding upper wind direction frequency during summer.

The winter situation is different however. Katabatic and katabatic-non-blizzard winds have corresponding maxima in 700 hPa wind direction frequency occurrences from west to southwest. Rusin (1961) noted a similar upper air forcing for katabatic winds at Mirny station. However, this result must be viewed with some caution for several reasons.

If such a relationship exists it must be significantly influenced by an inversion,

or at least a more stable atmosphere during winter, because the relationship is not apparent during summer. As mentioned above, and also in Chapter 2, katabatic flow is likely to form in the presence of anticyclonic conditions, without forcing by synoptic scale winds and independent of the synoptic situation; therefore it may be concluded that the relationship between specific wind directions at the 700 hPa level and katabatic winds during July is coincidental and not an actual relationship.

Anticyclonic patterns do not encourage cloud formation but rather allow significant radiational cooling at the surface and formation of inversions and near-surface jets, and katabatic type flow.

Although not very apparent from the July 700 hPa level wind direction frequencies of Figure 7.14, the most commonly occurring winds are from the west to southwest, showing that the general circulation is such. Wilson (1968) also shows that the upper air general circulation pattern over the Mawson area is easterly during summer but westerly during winter. This suggests that the 700 hPa wind direction maxima corresponding to katabatic flow may be coincidental.

The numerical modelling presented in Chapter 8 resolves the question of the synoptic wind direction forcing katabatic flow at Mawson.

The relationship between blizzard and blizzard-non-katabatic surface wind directions and 700 hPa level wind directions is similar in July to that found for January; Figures 7.16 and 7.20. This is probably so because these are controlled by off-shore depressions, systems that do not significantly vary their characteristics from season to season, unlike the occurrence and strength of inversions over the continent. However, the July 700 hPa level forcings of these systems is less pronounced than in January.

The July occurrence of upper wind directions corresponding to katabatic-blizzard surface winds displays no definite influence, Figure 7.18. Compared with the January data, that suggests some degree of cyclonic influence, it is concluded that katabatic-blizzard winds present during July can occur without significant

enhancement due to an off-shore depression. This is explained as follows.

Greater cooling of air near the surface during winter than summer means that air is more dense, and the resultant force due to gravitational acceleration is larger. Stronger inversions, that develop during winter, allow relatively strong winds near the surface, as surface frictional effects are somewhat damped by the intense stable stratification of the air overlying the surface. Katabatic near-surface jets that form during winter are therefore likely to be stronger than those during summer.

In Figure 7.18, the lack of a specific wind direction at 700 hPa, that may force katabatic-blizzard winds, is attributed to low-level flow and its formation; as noted previously, katabatic jets have been observed to occur independently of synoptic flow. Therefore, the corresponding 700 hPa wind directions may only have a minor influence. This means that katabatic winds of blizzard strength are difficult to predict using synoptic analysis.

Analyses of mesoscale and sub-mesoscale air masses, upstream of Mawson, may be useful for investigating the supply and demand of air draining towards this station. However, there are not adequate numbers of observations available in this region for a comprehensive study, but use can be made of numerical modelling to help explain some patterns of air flow. This technique is used in Chapter 8.

There are various mechanisms by which calm conditions can form at Mawson station. That related to the supply and demand of air is discussed here because it appears to be the most important. Other mechanisms shall be discussed in a later section.

The 700 hPa level wind direction occurrence analyses, Figure 7.17, for the month of July show a similar response as to that found for katabatic flow. Although such upper wind directions may not actually force the katabatic winds, the similarity between the katabatic and the calm suggest that the occurrence of these two wind types is related. Figure 3.10B of Chapter 3, shows that the maximum occurrences of the calm conditions are during the coldest winter months,

WIND TYPE	JANUARY		
	SURFACE (°)	AUW 700 hPa (°)	SHANAL 700 hPa (°)
AVERAGE	130	110	101
KATABATIC	130	110	94
BLIZZARD	130	100	100
CALM	—	110	91
KAT-BLZ	130	90	100
KAT-NON-BLZ	130	110	93
BLZ-NON-KAT	120/130	100	100

Table 7.1: Most frequent upper wind direction forcings for seven wind types for January at Mawson, taken from Figures 7.14 to 7.20. For cases without a single most frequent upper wind direction, multiple values are shown. The SHANAL values were interpolated to the Mawson location from a 5° x 5° (latitude x longitude) data set.

when drainage of air via katabatic flow is very efficient. Calms are less likely to occur in the presence of strong winds associated with off-shore depressions because such systems do not depend on a supply of air upwind in the same manner that katabatic winds do. The more efficient the drainage, the more likely it is for calm conditions to occur. There are also similarities between the upper wind direction analyses of katabatic and calm winds during summer, but to a lesser extent.

In the following section, composites of synoptic patterns are produced that correspond to the seven wind types, and these are compared with the analyses produced in this section.

Apart from showing most frequent synoptic wind direction forcings for each wind type, for January and July respectively, Tables 7.1 and 7.2 show that there is a more "direct" relationship between surface and 700 hPa level wind directions during January than during July. During January there is a similarity between surface and 700 hPa wind directions, with values differing between these levels by about 20 to 30°, generally, but during July the differences are greater and more

WIND TYPE	JULY		
	SURFACE (°)	AUW 700 hPa (°)	SHANAL 700 hPa (°)
AVERAGE	130	130/240	142
KATABATIC	130	250	208
BLIZZARD	130	90	111
CALM	—	260	235
KAT-BLZ	130	90/150/260	196
KAT-NON-BLZ	130	250	250
BLZ-NON-KAT	130	90	100

Table 7.2: Most frequent upper wind direction forcings for seven wind types for July at Mawson, taken from Figures 7.14 to 7.20. For cases without a single most frequent upper wind direction, multiple values are shown. The SHANAL values were interpolated to the Mawson location from a 5° x 5° (latitude x longitude) data set.

varied for different types of winds.

The data in these tables can also be used to compare AUW and SHANAL data. The AUW values have been computed from data spanning a greater period than the SHANAL values, and are therefore expected to be more valuable, at least for the column of air over Mawson.

For numerical modelling, it is desirable to use an accurate spatially-varying synoptic wind field to provide forcing. If SHANAL fields are found to be accurate, these should be used in preference to the AUW value (that provides just one value for the synoptic wind field, not spatially-varying). The quality of the SHANAL fields can be estimated by comparison with AUW values above Mawson. This is done by calculating the root mean square (RMS) differences in wind direction. For cases of multiple values (see Table 7.2), the smallest difference is used.

For January: RMS = 12.46°.

For July: RMS = 27.23°.

These values indicate that for the examination of the relationship between synoptic and surface winds at Mawson, the January SHANAL fields are considerably

more reliable than the July SHANAL fields. This is probably not a reflection of the methods of compilation of the SHANAL data set, but rather it suggests that the inversion and its effect on the wind regime are not well considered. It may therefore seem best to dismiss the SHANAL field and use the AUW value, for the month of July, but this would mean that the single value at the 700 hPa level above Mawson is to be imposed over the entire 80x74 grid, that is probably also not highly accurate.

It is decided that the SHANAL fields shall be used as synoptic forcings in numerical modelling of January and July wind types: calm, katabatic-blizzard, katabatic-non-blizzard and blizzard-non-katabatic. In addition, modelling is carried out with upper wind directions incremented by 45° between runs, to investigate the basic relationships between synoptic and surface wind directions at Mawson station. These modelling results are presented in Chapter 8.

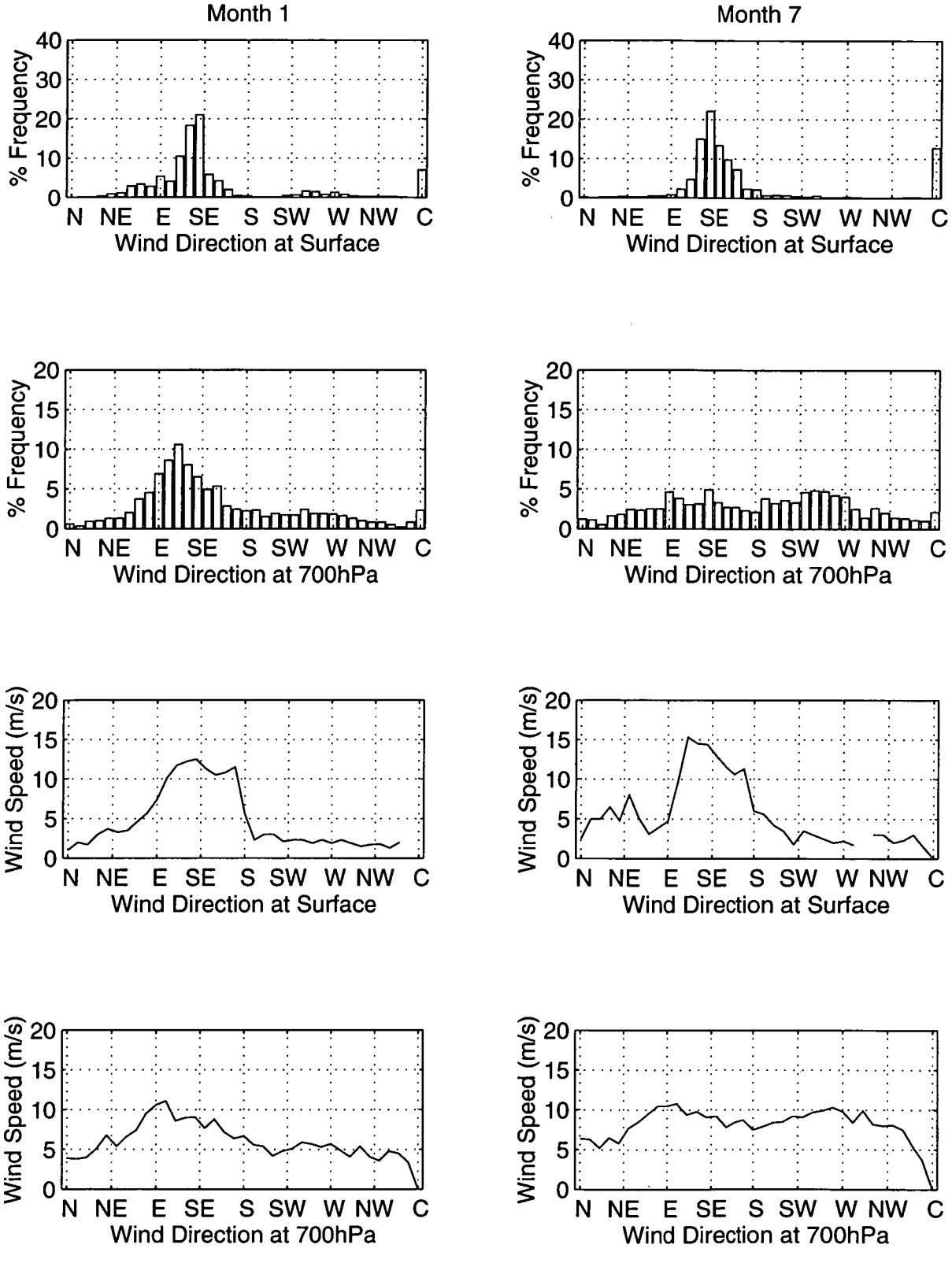

Figure 7.14: Percentage frequency occurrence of wind directions at the surface at Mawson and the corresponding percentage frequencies of winds directions at the 700 hPa level. Monthly mean wind speeds calculated for each wind direction are also shown for the surface and 700 hPa level. The left hand column represents January; the right hand column represents July.

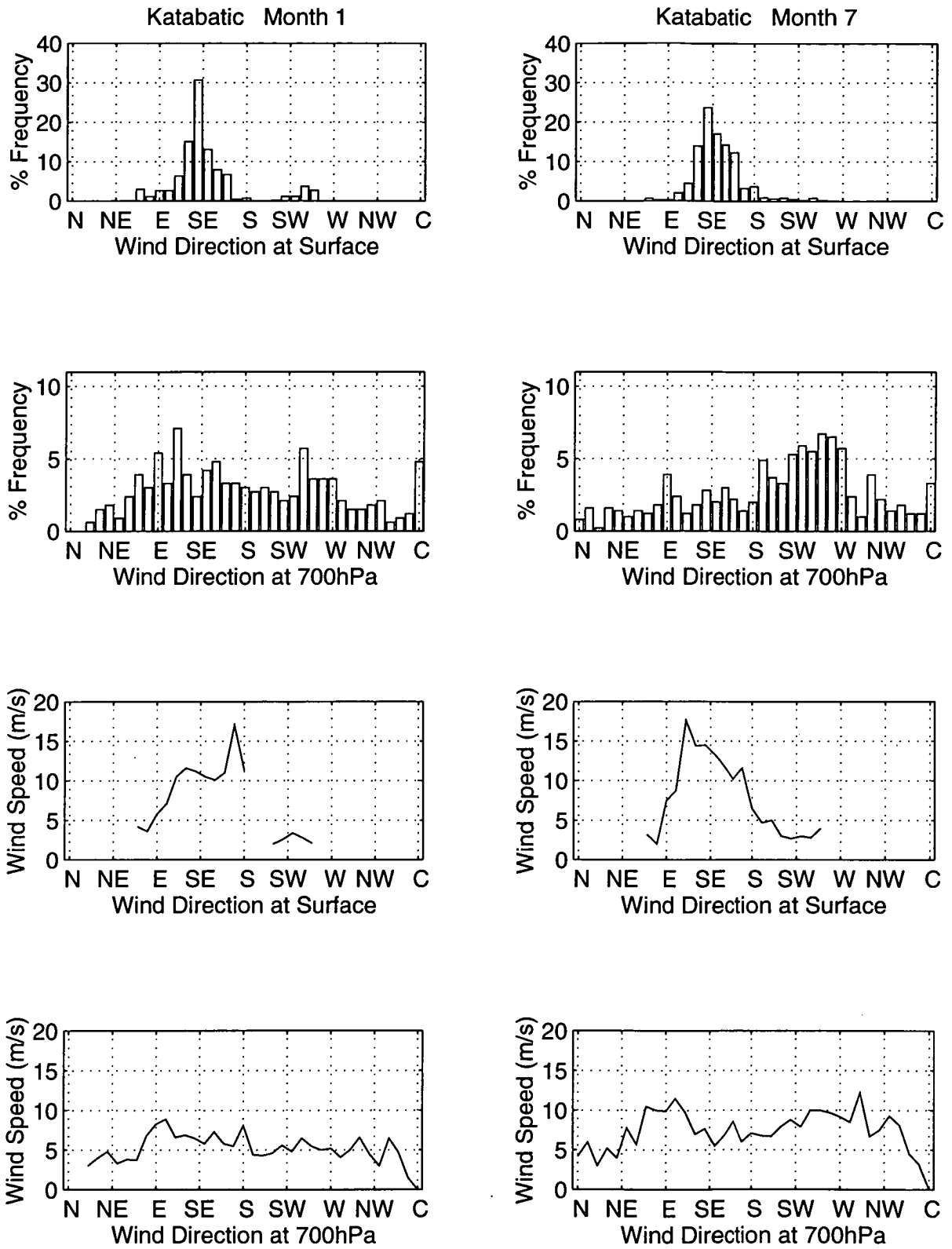

Figure 7.15: Katabatic winds: Percentage frequency occurrence of wind directions at the surface at Mawson and the corresponding percentage frequencies of winds directions at the 700 hPa level. Monthly mean wind speeds calculated for each wind direction are also shown for the surface and 700 hPa level. The left hand column represents January; the right hand column represents July.

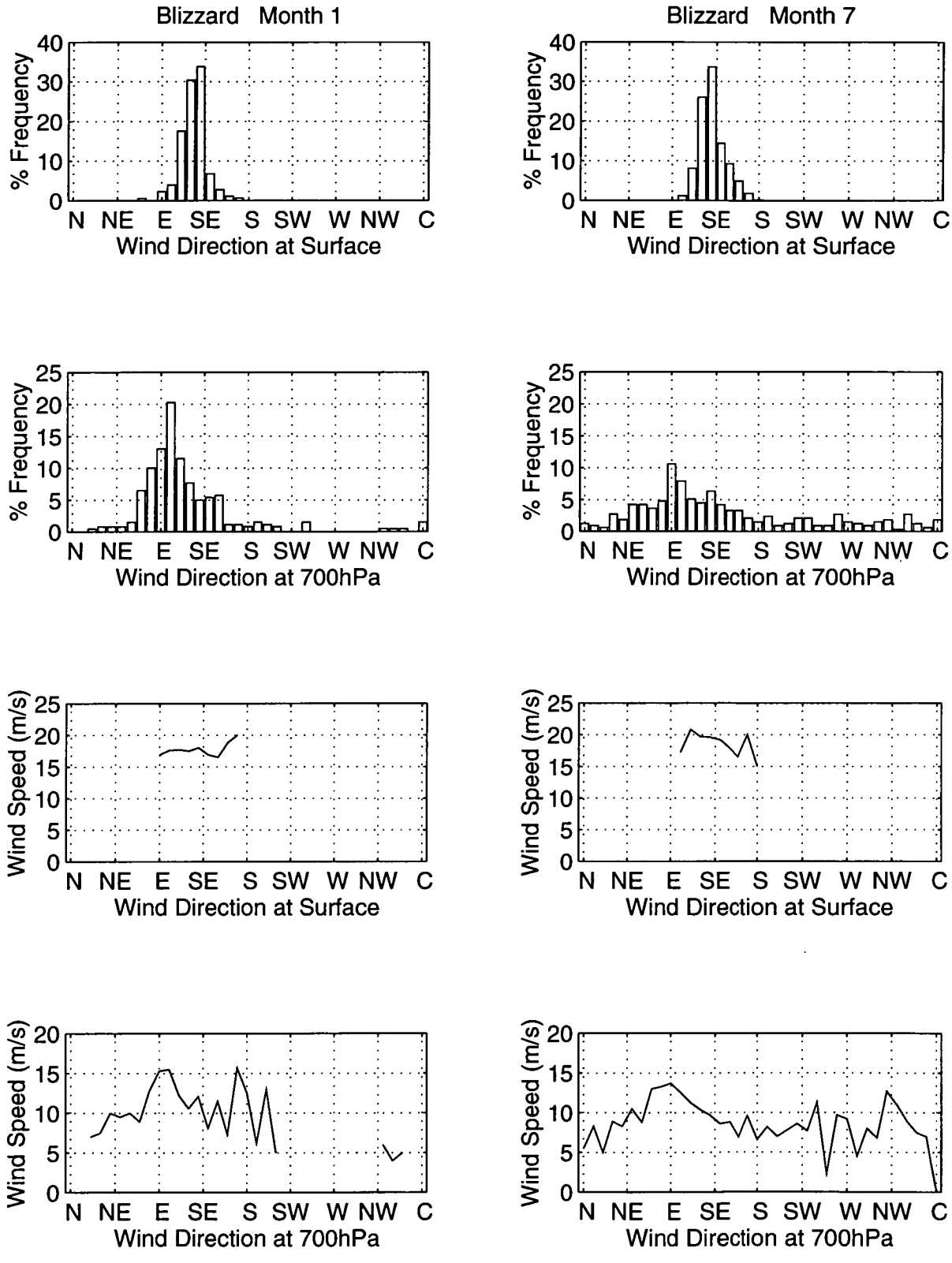

Figure 7.16: Blizzard winds: Percentage frequency occurrence of wind directions at the surface at Mawson and the corresponding percentage frequencies of winds directions at the 700 hPa level. Monthly mean wind speeds calculated for each wind direction are also shown for the surface and 700 hPa level. The left hand column represents January; the right hand column represents July.

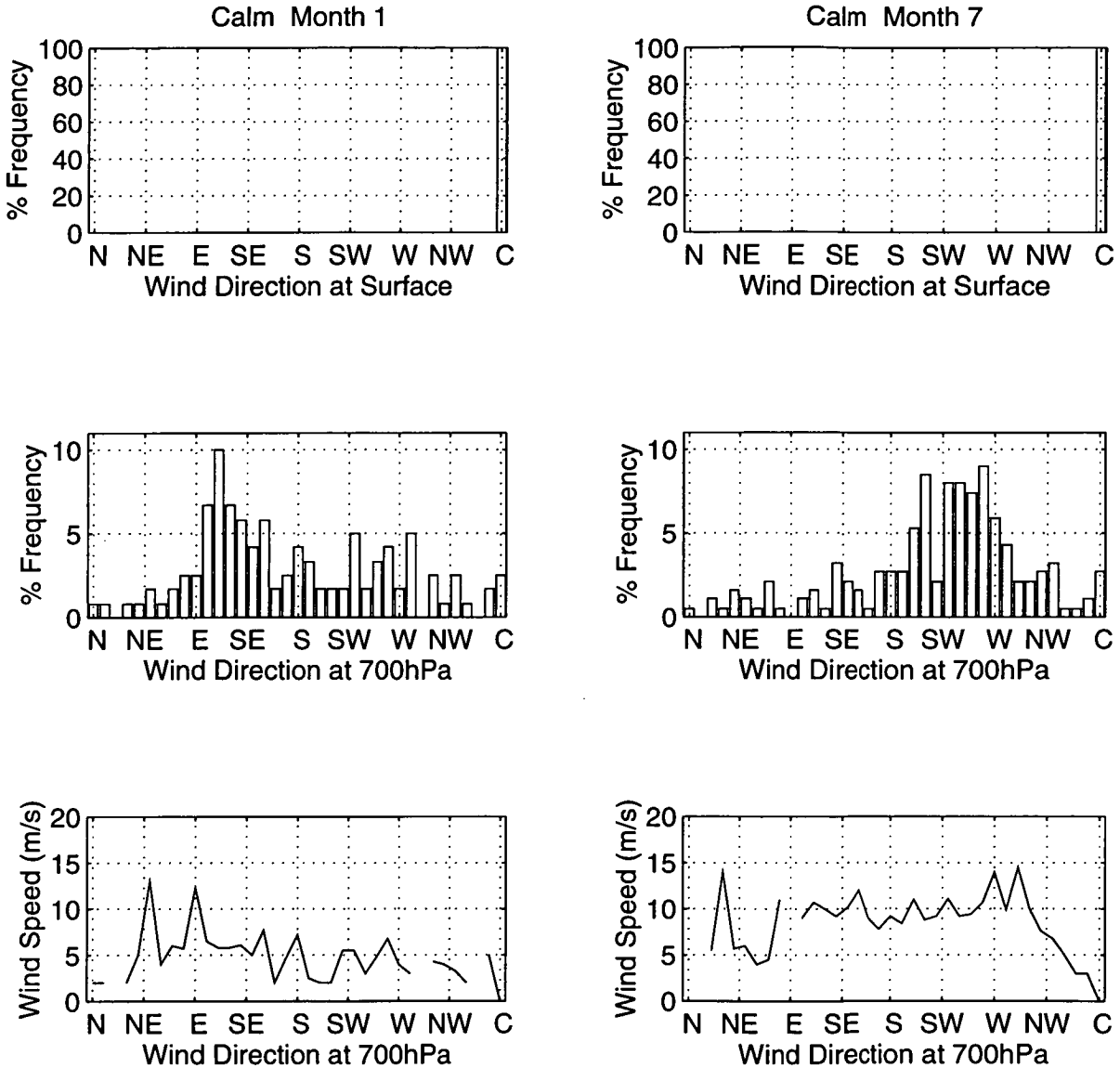

Figure 7.17: Calm: Percentage frequency occurrence of wind directions at the surface at Mawson and the corresponding percentage frequencies of winds directions at the 700 hPa level. Monthly mean wind speeds calculated for each wind direction are also shown for the surface and 700 hPa level. The left hand column represents January; the right hand column represents July.

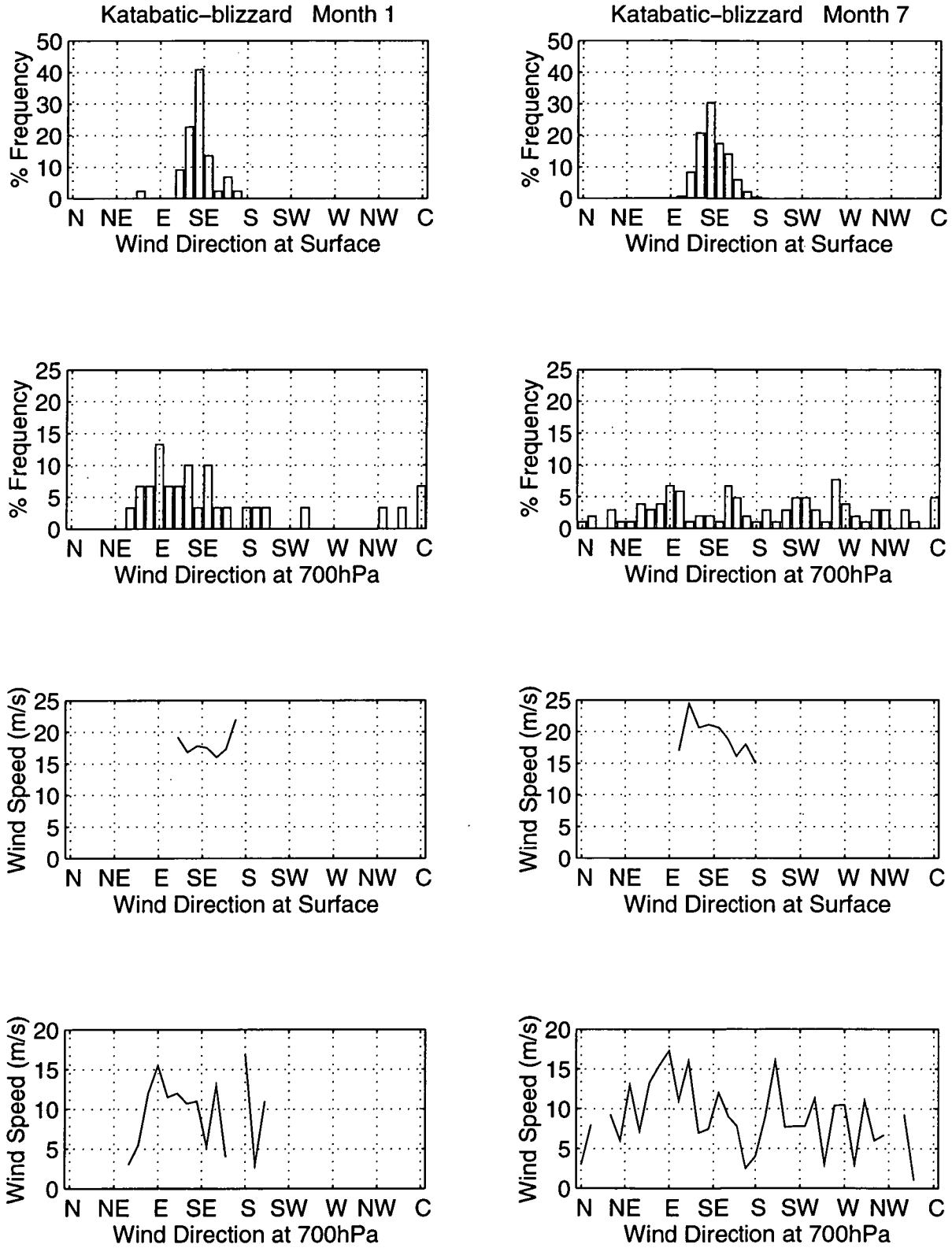

Figure 7.18: Katabatic-blizzard: Percentage frequency occurrence of wind directions at the surface at Mawson and the corresponding percentage frequencies of winds directions at the 700 hPa level. Monthly mean wind speeds calculated for each wind direction are also shown for the surface and 700 hPa level. The left hand column represents January; the right hand column represents July.

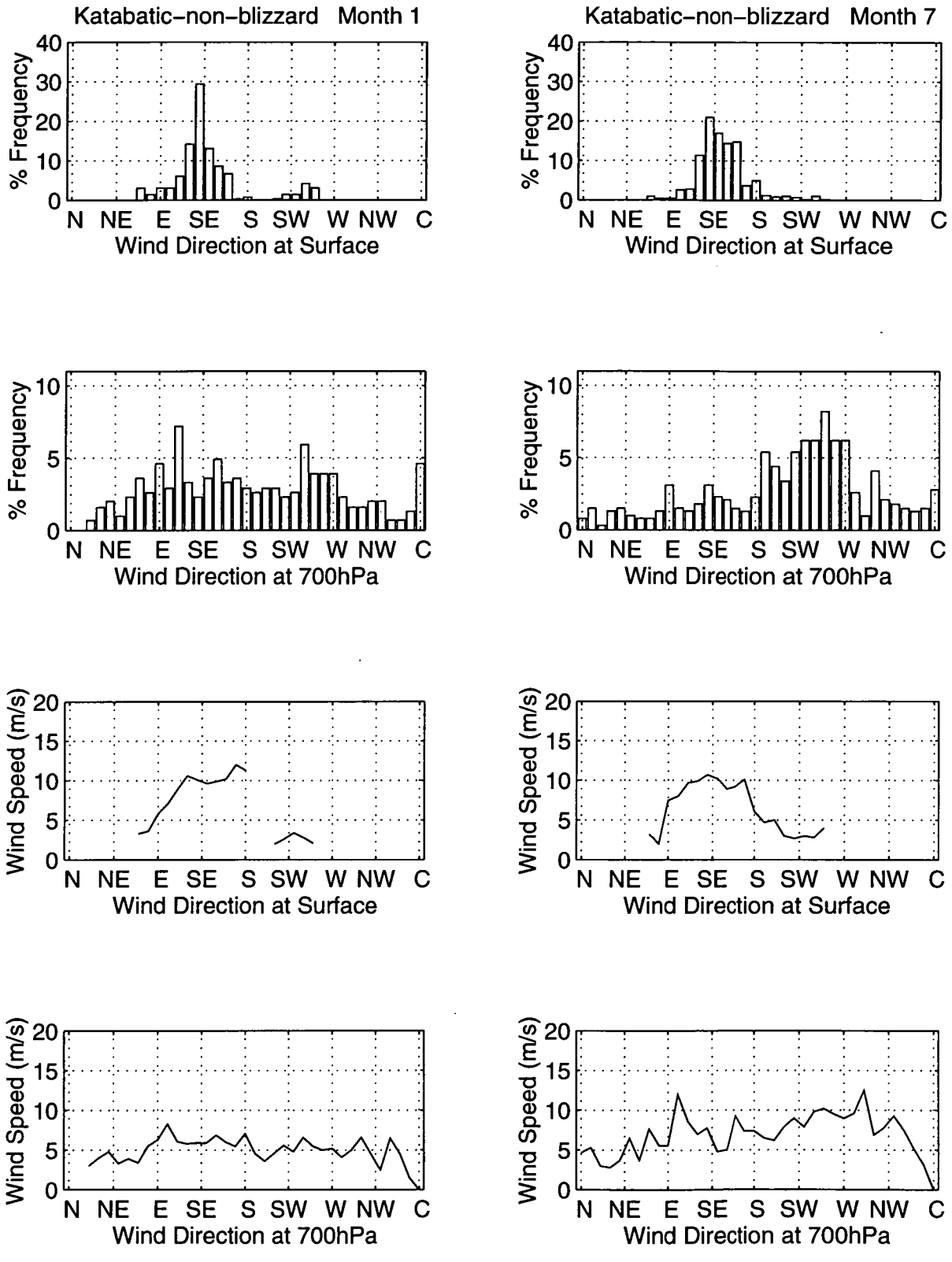

Figure 7.19: Katabatic-non-blizzard: Percentage frequency occurrence of wind directions at the surface at Mawson and the corresponding percentage frequencies of winds directions at the 700 hPa level. Monthly mean wind speeds calculated for each wind direction are also shown for the surface and 700 hPa level. The left hand column represents January; the right hand column represents July.

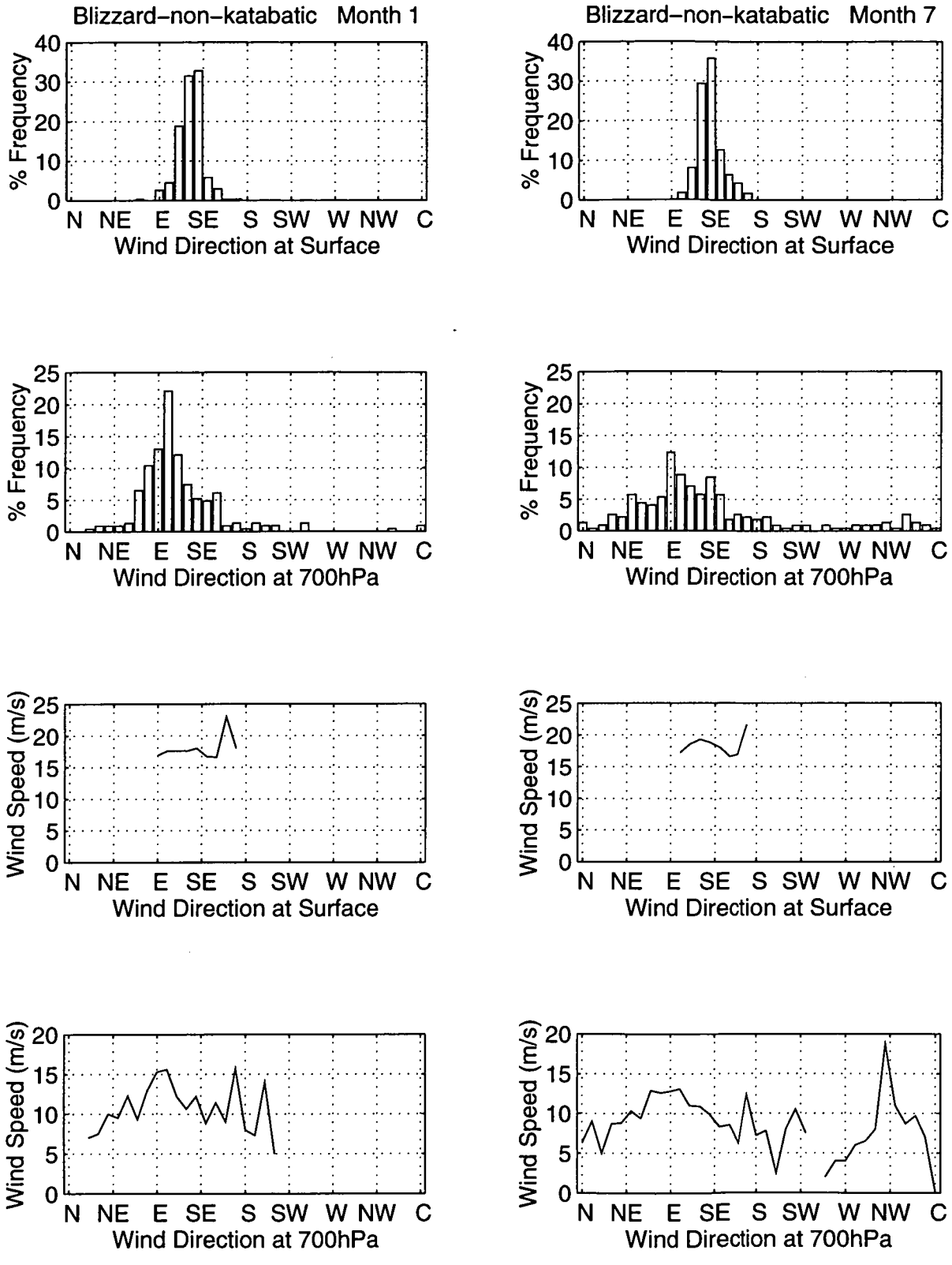

Figure 7.20: Blizzard-non-katabatic: Percentage frequency occurrence of wind directions at the surface at Mawson and the corresponding percentage frequencies of winds directions at the 700 hPa level. Monthly mean wind speeds calculated for each wind direction are also shown for the surface and 700 hPa level. The left hand column represents January; the right hand column represents July.

7.3.3 SOUTHERN HEMISPHERE ANALYSES DATA: RELATIONSHIP BETWEEN SURFACE AND 700hPa WINDS

Mean 700 hPa height and vector fields are computed from the Southern Hemisphere Analyses (SHANAL) data set corresponding to each of the seven wind types analysed in the previous section. These fields are compared with those analyses of the previous section and conclusions about the relationships between winds at 700 hPa and those at the surface are examined.

The advantage of the SHANAL data is that they can be used to examine the synoptic patterns, not just a single column of the atmosphere, as was done in the previous section above Mawson station. It was found that the synoptic situations suggested by the AUW analyses are confirmed by the SHANAL synoptic pattern composites for most wind types during January.

The mean January 700 hPa synoptic situation shown in Figures 7.21 and the corresponding wind field shown in Figure 7.22 have been used as the upper wind forcing for the mean January model run and the tuning of the model's energy balance, as discussed in Chapter 6. For the modelling of the July mean, the synoptic situation shown in Figure 7.35 was used, and the corresponding wind field, Figure 7.36.

The synoptic fields over the Lambert Glacier region are considered. The synoptic patterns corresponding to the different wind types are compared with the monthly mean patterns; the various wind types can be considered as perturbations from the mean, and conclusions about synoptic influence on near surface winds can be made.

The synoptic pattern corresponding to katabatic flow during January is given by Figure 7.23. The contours are less closely spaced (compared with the mean) over the Lambert Glacier region, that again shows that the presence of the weak anticyclonic flow contributes to the formation of katabatic flow. This is in good agreement with the analysis of synoptic influence on katabatic flow in the previous section. Also, Streten (1963) noted that katabatic winds have weak synoptic

influence and that there appears to be no relationship between the strength of upper and surface winds at Mawson. The explanation given in the previous section with regard to the formation of katabatic flow is consistent with Streten's remarks.

Downslope and katabatic are the dominant winds at Mawson, (Streten (1962) and Figure 3.10, Chapter 3), and this can be explained by the presence of the anticyclonic system over the continent, (allowing cooling by loss of long-wave radiation, and development of surface inversions over sloped terrain), that is necessary as a component of the general circulation and large scale atmospheric continuity. Formation of katabatic flow is favoured by the surface cooling that accompanies anticyclonic conditions and therefore these winds must be present quite often because the mean January pattern shows the presence of such a synoptic pattern. The comparison between the mean and katabatic mean synoptic patterns shows that there is weaker upper air flow associated with the katabatic, that probably allows greater cooling to occur at the surface because there is less air motion to cause turbulent mixing, and therefore the formation of katabatic flow is enhanced.

Figure 7.25 shows that the synotic forcing associated with blizzard winds at Mawson involves the presence of a cyclone to the north to northeast. This agrees with analyses in the previous section, conclusions made in Chapter 3, work by Ball (1960) and various papers by Streten, discussed in Section 2.4, Chapter 2. The "tightening" of the contours over the coastal region of Mawson shows that there is a significant synoptic influence associated with the presence of blizzard winds.

The synoptic pattern associated with January calm conditions, Figure 7.27, indicates weak upper air flow, and therefore weak or non-existant air flow at the surface. This could also mean that under such synoptic conditions katabatic flow can exist and calms may then occur due to the supply of air upwind of Mawson becoming exhausted. It may be expected that during summer the drainage is

less efficient and therefore this mechanism of formation of a period of calm is less likely than it is in winter. However, Streten (1963) notes that between October and January (1960 - 1961), a period that is not considered to represent "typical winter" conditions, but probably closer to "summer" conditions, 83 percent of katabatic onsets did occur from previously calm conditions.

During summer it has been observed that weak anabatic winds can form during the afternoons when air temperatures are highest and the air is relatively less dense, meaning that katabatic flow is somewhat discouraged. Periods of calm may occur in transition from katabatic to anabatic, and also with anabatic flow being strong enough to oppose and equal katabatic flow.

Calms may also occur with a depression situated to the northwest of Mawson, with the northerly wind component of the eastern side of the system opposing katabatic drainage outflow. This was noted by Streten (1963) for a case of a low pressure system that directed north to northwest upper winds over Mawson during May 1960, but it was also noted that on another occasion a similar synoptic pattern did not retard katabatic flow, again showing that Antarctic weather cannot be predicted using synoptic analysis alone.

Calms may also be present at the surface with the occurrence of hydraulic jumps, discussed in Chapter 2.

Wave formations in the lower atmosphere over the areas immediately surrounding Mawson may also account for relatively short periods of calm. These were documented by Streten (1963), noting that wave periods may range from several minutes to several hours. Such motions may originate from disturbances in the air flow caused as it encounters the various peaks of the Framnes Mountains, south of Mawson. Streten notes that Mt. Henderson may play a part.

The synoptic patterns corresponding to January mean blizzard and blizzard-non-katabatic winds, Figures 7.25 and 7.33, are quite similar. There is an offshore depression, the continental anticyclone and a "tightening" of the upper air gradient between the two systems over the coastal area, that causes winds of blizzard

strength at Mawson. This "tightening" of the pressure gradient was noted by Streten (1968b) and Streten (1968a) in regard to persistently strong winds.

The other blizzard type to be analysed, katabatic-blizzards, resulted in a different January mean 700 hPa synoptic pattern, Figure 7.29. There is a depression present off the coast but it seems to dominate a large part of the East Antarctic coast, as well as hundreds of kilometres inland. Also, the inland anticyclone is not nearly as well defined as for the blizzard and blizzard-non-katabatic winds. As shown in Chapter 3, Figure 3.14, katabatic-blizzard monthly mean wind speeds were actually greater than those for blizzard or blizzard-non-katabatic winds for all months. Primary examination of the corresponding synoptic pattern may suggest that katabatic-blizzard winds should be weaker than the other two blizzard types during summer because the contours are not so "tight".

Under the influence of an intense offshore depression, the winds can reach blizzard strength at Mawson, but the katabatic drainage may be quite insignificant during some of these events, with wind speeds largely determined by the cyclone, (blizzard and blizzard-non-katabatic wind types). In the presence of less intense depressions, the katabatic wind has a greater effect on the resultant wind at Mawson because the winds associated with the depression do not dominate. The mean wind speeds are greater under the influence of less intense depressions because both the katabatic and cyclonic winds contribute, instead of just one or the other dominating, (katabatic-blizzard winds). This shall be further investigated using the numerical model.

The relationship between coastal lows and air flow at places where there is great katabatic activity, and the resultant intensification of blizzards, was noted to be a "peculiar effect" by Streten (1962). This may be better understood by applying different synoptic wind patterns over the Lambert Glacier region and comparing the resultant near-surface winds produced by the numerical model for each of these patterns. However, as previously noted, the synoptic wind field alone does not control the evolution of surface wind fields. Other parameters

that have significant influence are cloud amount and the vertical temperature profile, but only changes in synoptic forcing are considered for the investigation discussed in Chapter 8.

The relationship between synoptic and surface winds during July is less clear than it is during January. This contrast between summer and winter wind direction profiles was previously noted in Chapter 3.

The synoptic patterns corresponding to the July mean blizzard wind types, Figures 7.39, 7.43 and 7.47 do not show the characteristic "tightening" of the contours as was found for the January cases (Figures 7.25, 7.29 and 7.33).

Following on from the above discussions, it may be concluded that strong winds at Mawson during July occur due to drainage of air that has cooled over the regions to the south, not directly forced by the synoptic scale winds. The synoptic wind direction may have a comparitively greater influence than the synoptic wind speed, particularly during winter.

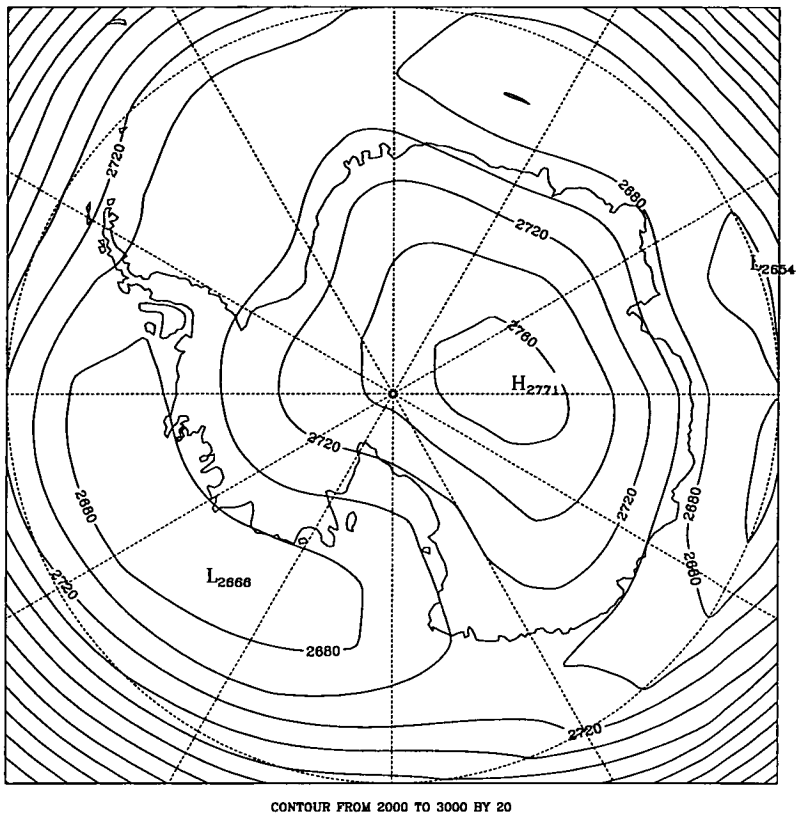

Figure 7.21: Mean monthly height of SHANAL January 700 hPa pressure level.

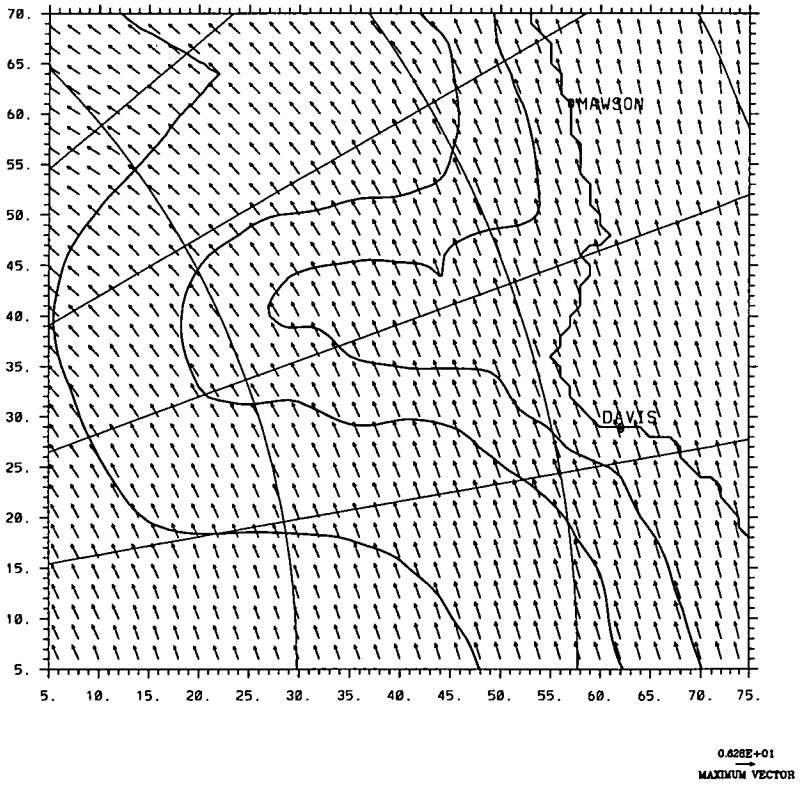

Figure 7.22: Mean monthly SHANAL January 700 hPa level wind field interpolated to the 80x74 mesoscale model grid, over the Lambert Glacier Basin region. For clarity, only vectors located at even-numbered grid points are plotted. This field was used to force the January model runs in Chapter 6, listed in Table 6.1.

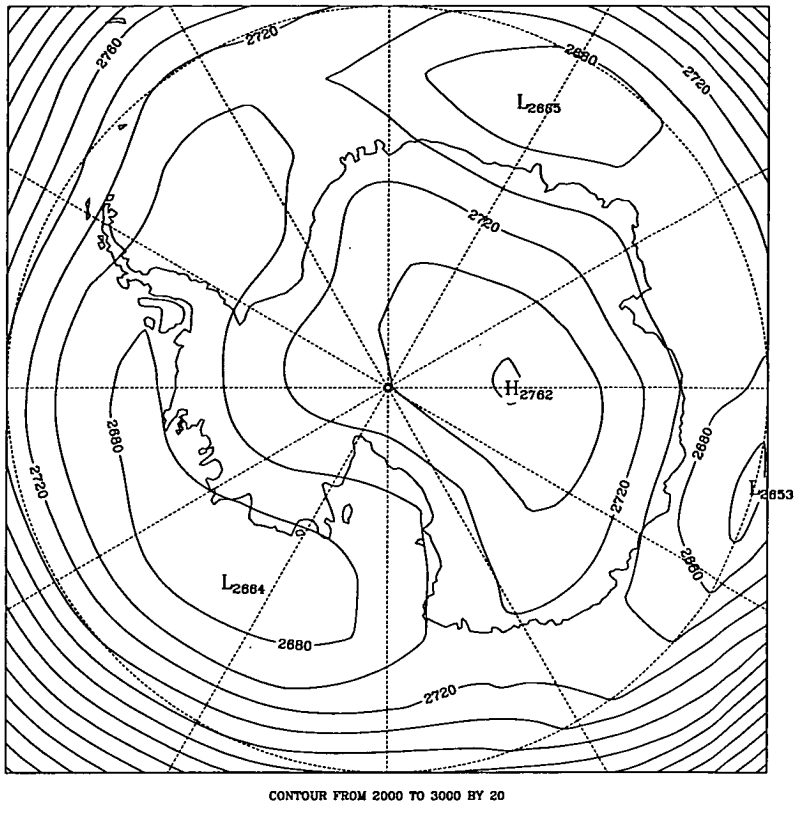

Figure 7.23: Mean monthly height of SHANAL January 700 hPa pressure level corresponding to katabatic winds at Mawson.

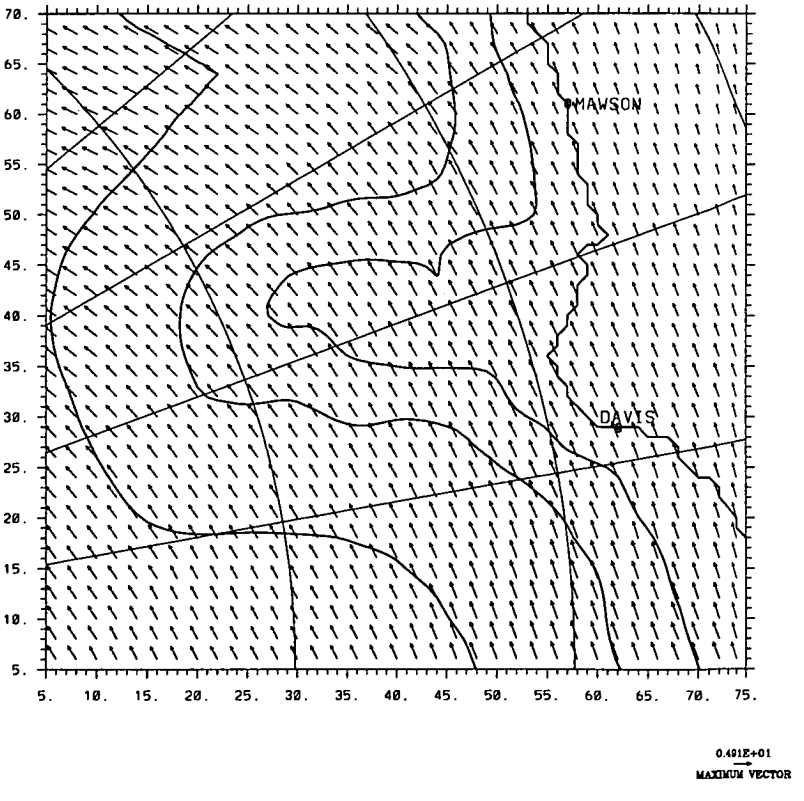

Figure 7.24: Mean monthly SHANAL January 700 hPa level wind field corresponding to katabatic winds at Mawson, interpolated to the 80x74 mesoscale model grid, over the Lambert Glacier Basin region. For clarity, only vectors located at even-numbered grid points are plotted.

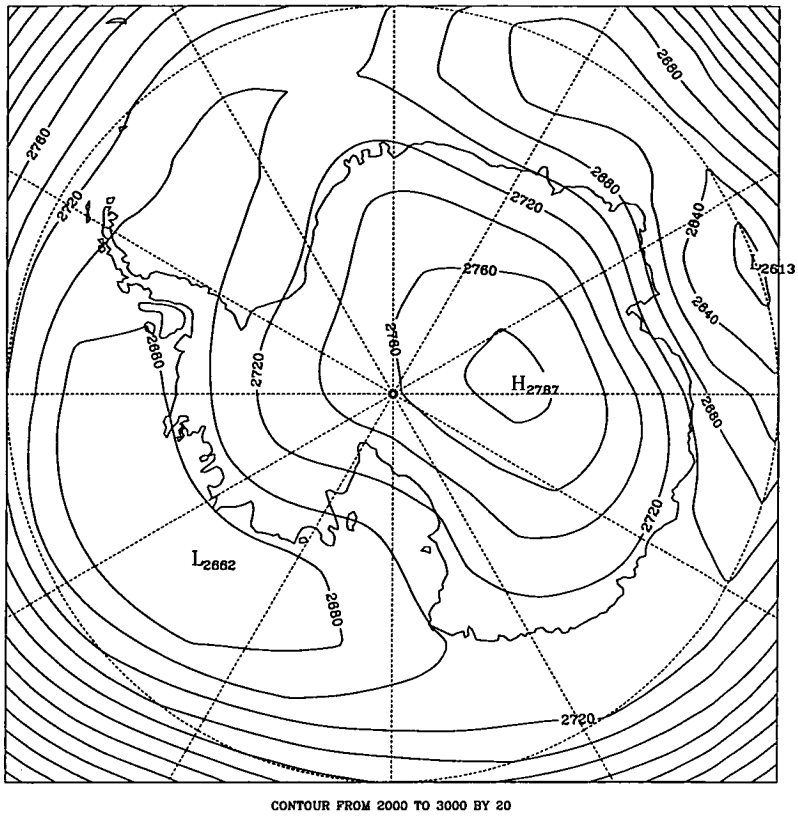

Figure 7.25: Mean monthly height of SHANAL January 700 hPa pressure level corresponding to blizzard winds at Mawson.

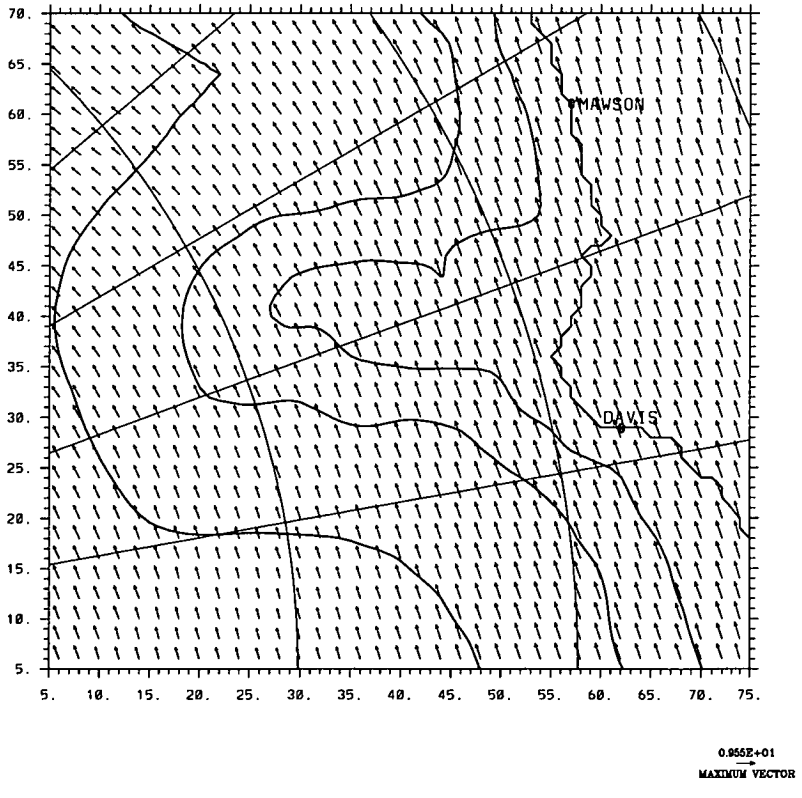

Figure 7.26: Mean monthly SHANAL January 700 hPa level wind field corresponding to blizzard winds at Mawson, interpolated to the 80x74 mesoscale model grid, over the Lambert Glacier Basin region. For clarity, only vectors located at even-numbered grid points are plotted.

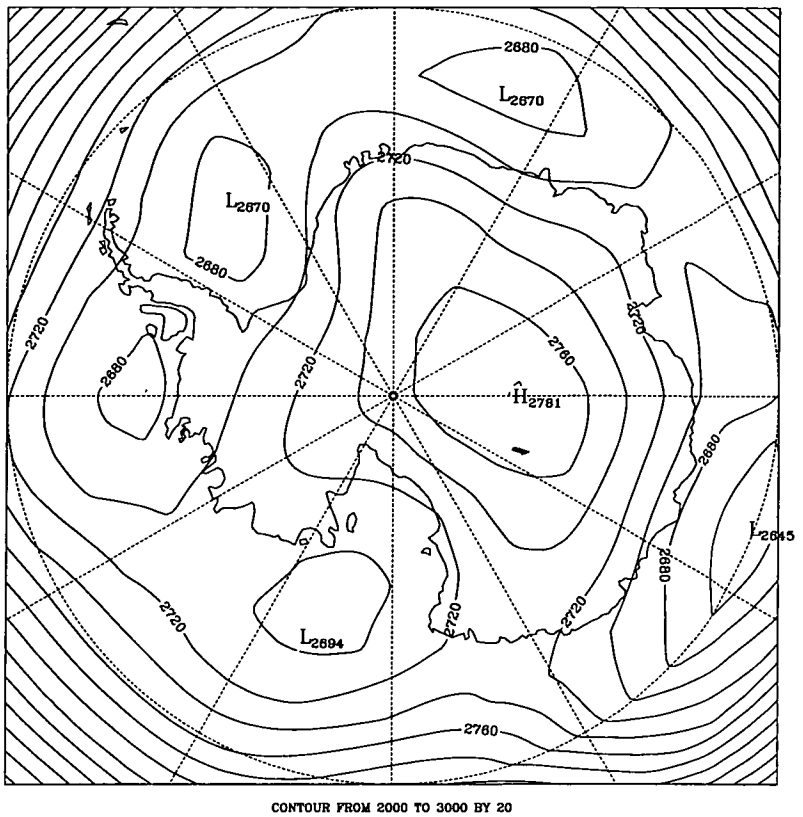

Figure 7.27: Mean monthly height of SHANAL January 700 hPa pressure level corresponding to calm conditions at Mawson.

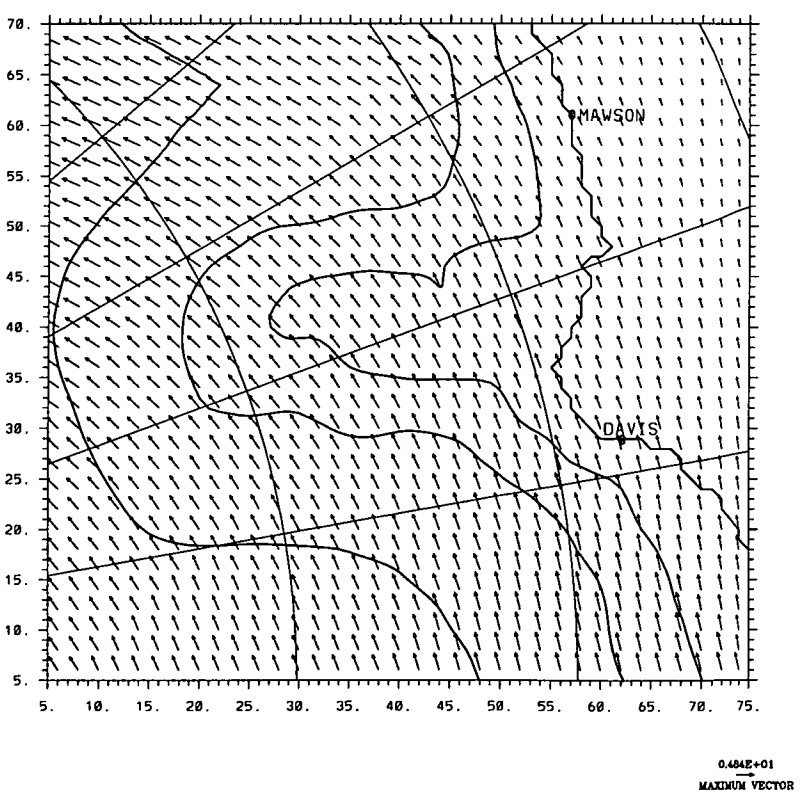

Figure 7.28: Mean monthly SHANAL January 700 hPa level wind field corresponding to calm conditions at Mawson, interpolated to the 80x74 mesoscale model grid, over the Lambert Glacier Basin region. For clarity, only vectors located at even-numbered grid points are plotted. This field is used to force model run R41, Chapter 8.

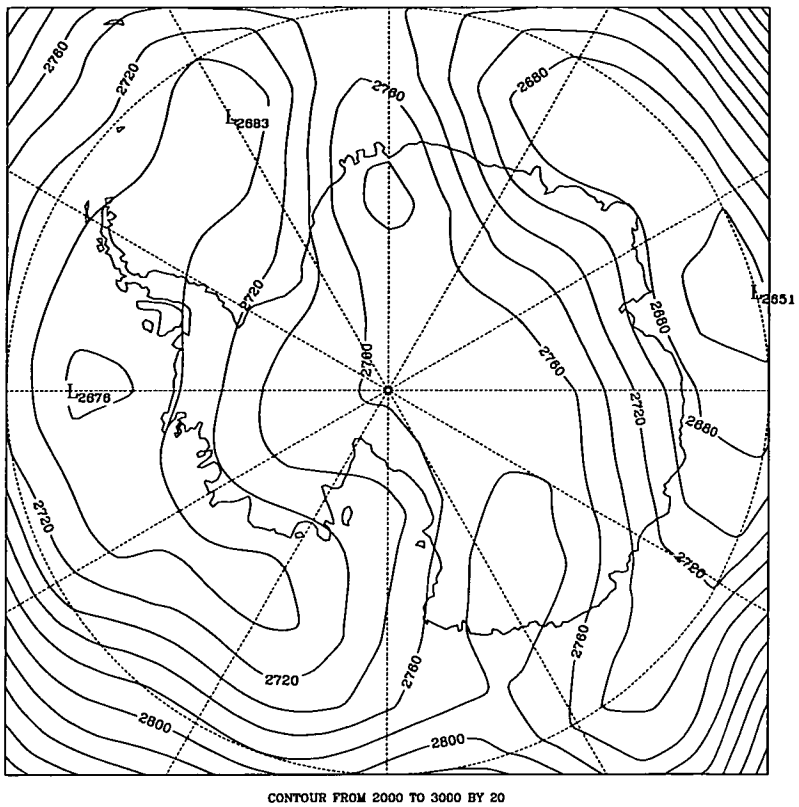

Figure 7.29: Mean monthly height of SHANAL January 700 hPa pressure level corresponding to katabatic-blizzard winds at Mawson.

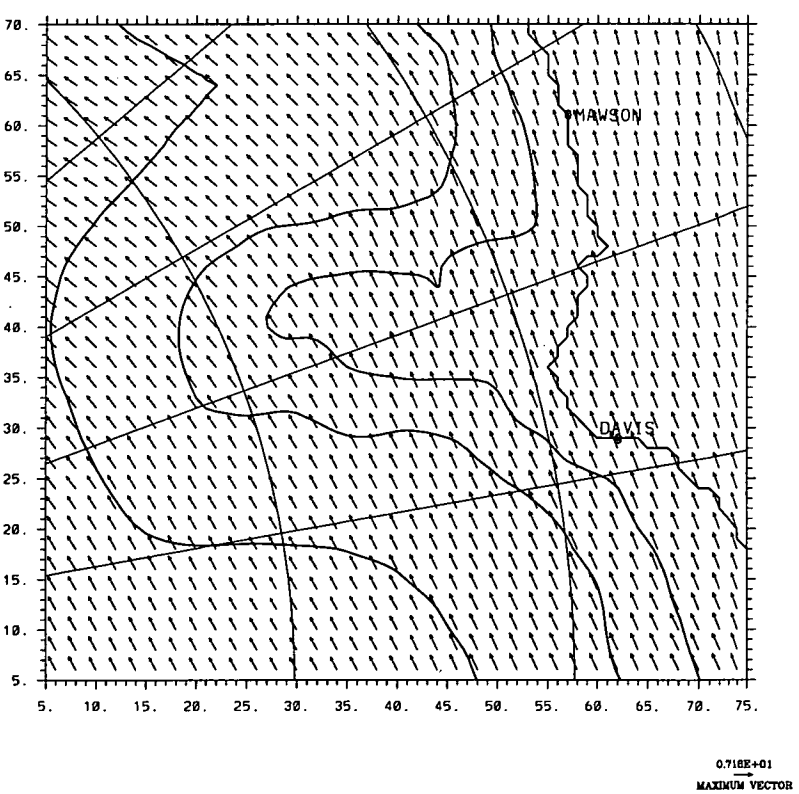

Figure 7.30: Mean monthly SHANAL January 700 hPa level wind field corresponding to katabatic-blizzard winds at Mawson, interpolated to the 80x74 mesoscale model grid, over the Lambert Glacier Basin region. For clarity, only vectors located at even-numbered grid points are plotted. This field is used to force model run R42, Chapter 8.

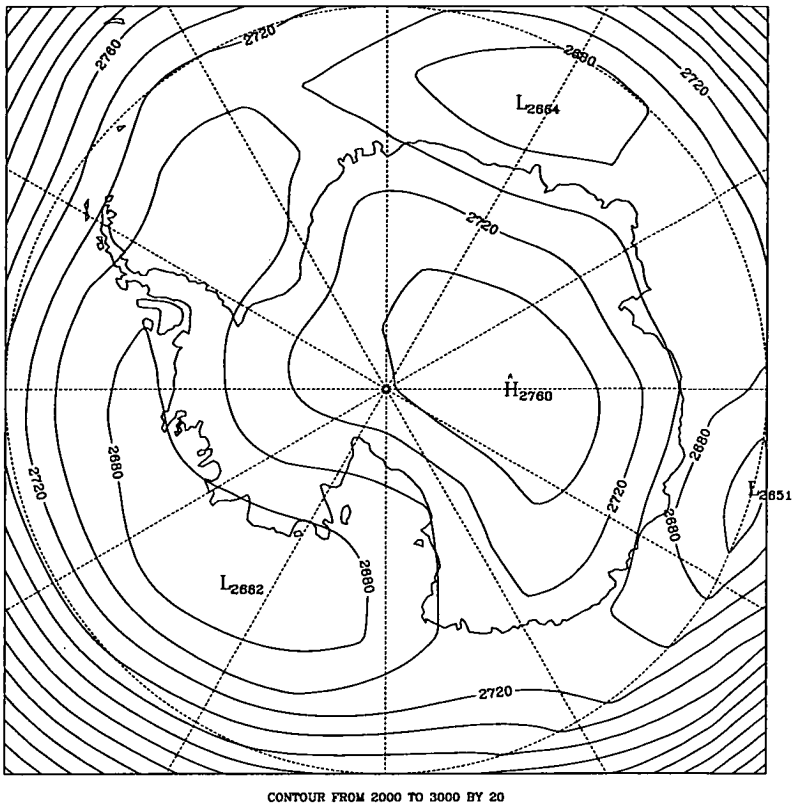

Figure 7.31: Mean monthly height of SHANAL January 700 hPa pressure level corresponding to katabatic-non-blizzard winds at Mawson.

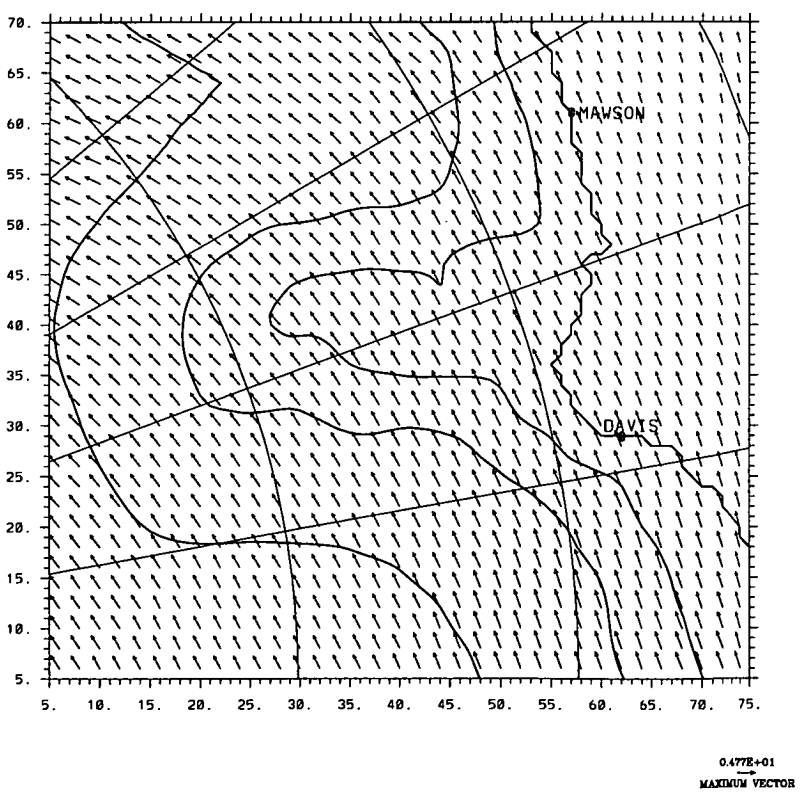

Figure 7.32: Mean monthly SHANAL January 700 hPa level wind field corresponding to katabatic-non-blizzard winds at Mawson, interpolated to the 80x74 mesoscale model grid, over the Lambert Glacier Basin region. For clarity, only vectors located at even-numbered grid points are plotted. This field is used to force model run R43, Chapter 8.

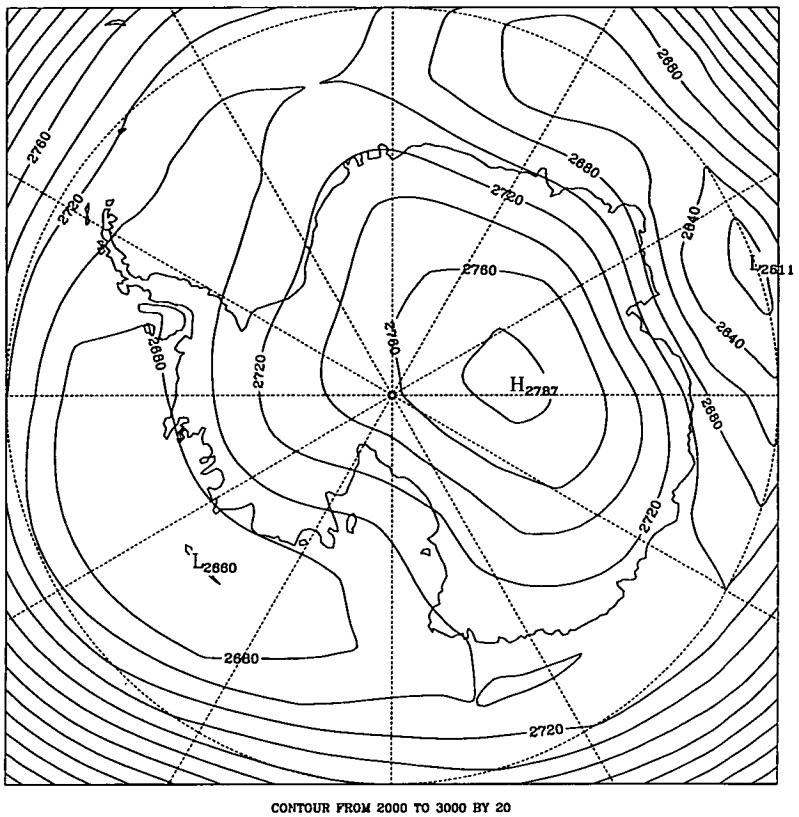

Figure 7.33: Mean monthly height of SHANAL January 700 hPa pressure level corresponding to blizzard-non-katabatic winds at Mawson.

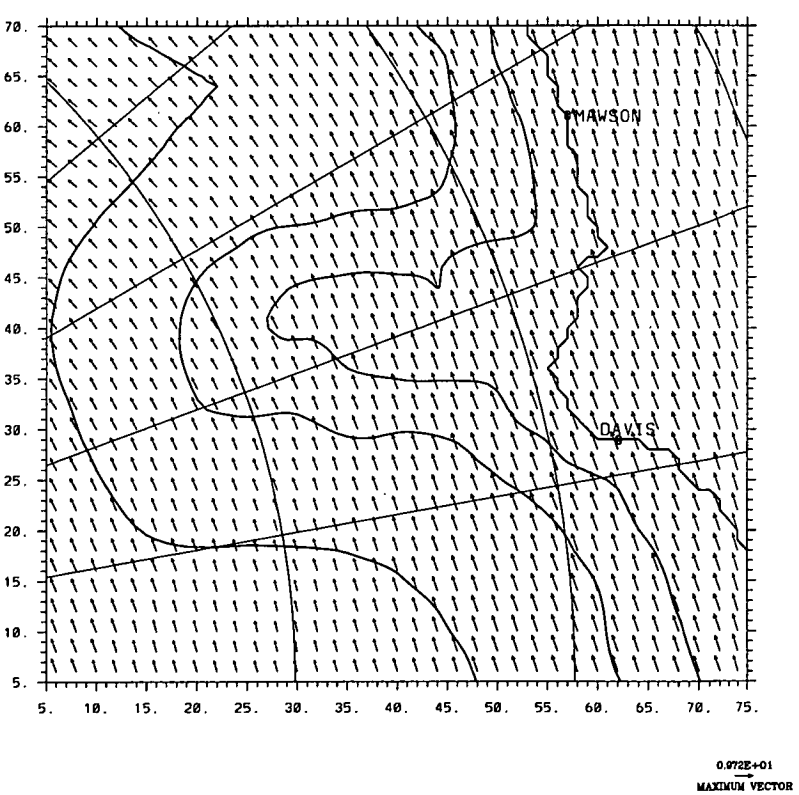

Figure 7.34: Mean monthly SHANAL January 700 hPa level wind field corresponding to blizzard-non-katabatic winds at Mawson, interpolated to the 80x74 mesoscale model grid, over the Lambert Glacier Basin region. For clarity, only vectors located at even-numbered grid points are plotted. This field is used to force model run R44, Chapter 8.

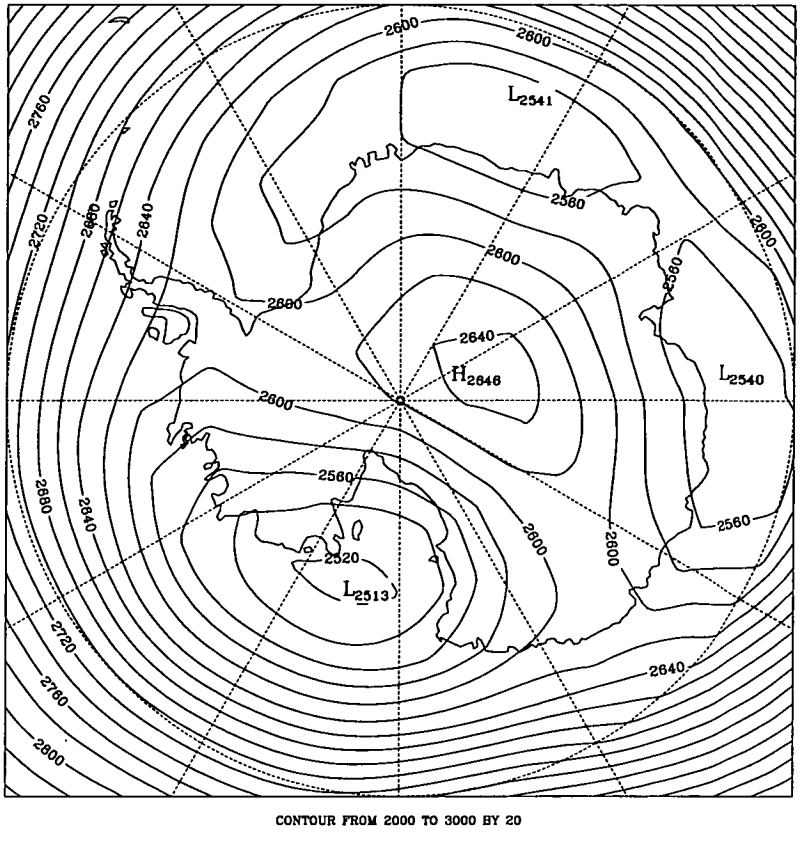

Figure 7.35: Mean monthly height of SHANAL July 700 hPa pressure level.

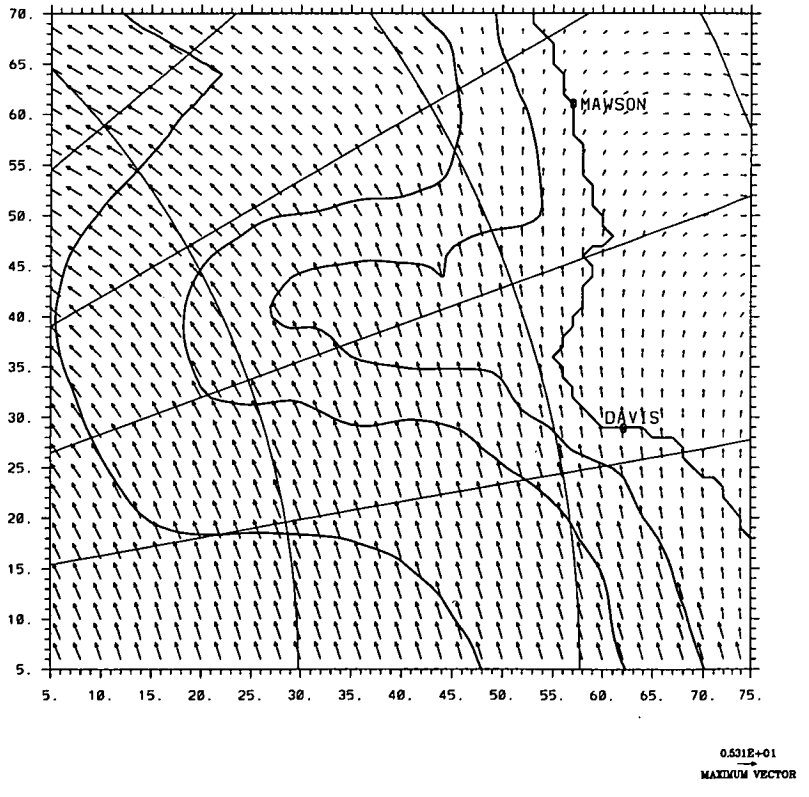

Figure 7.36: Mean monthly SHANAL July 700 hPa level wind field interpolated to the 80x74 mesoscale model grid, over the Lambert Glacier Basin region. For clarity, only vectors located at even-numbered grid points are plotted. This field was used to force the July model runs in Chapter 6, listed in Table 6.1.

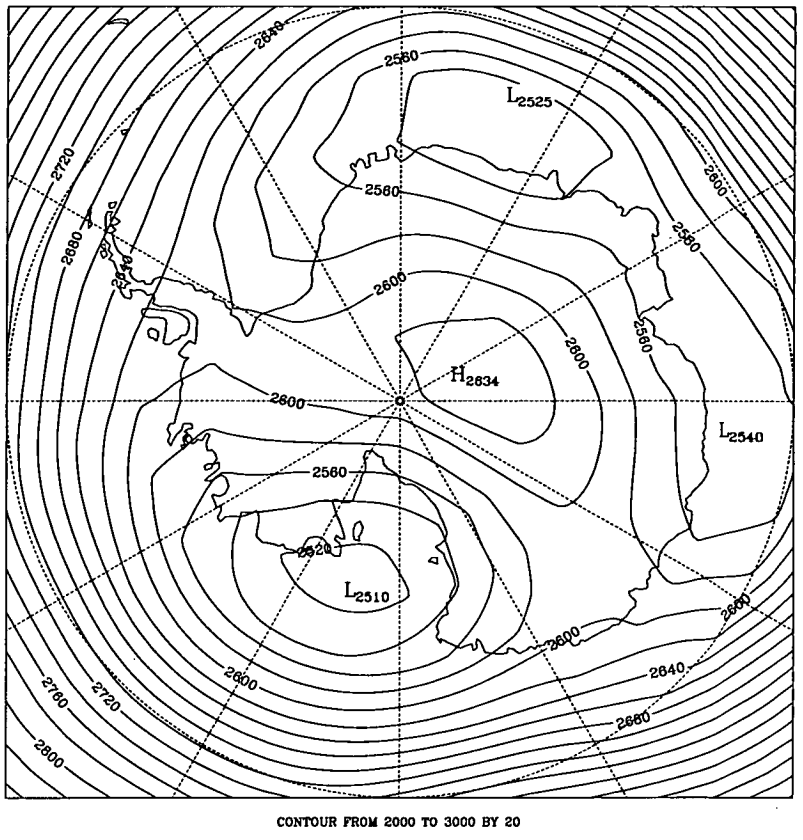

Figure 7.37: Mean monthly height of SHANAL July 700 hPa pressure level corresponding to katabatic winds at Mawson.

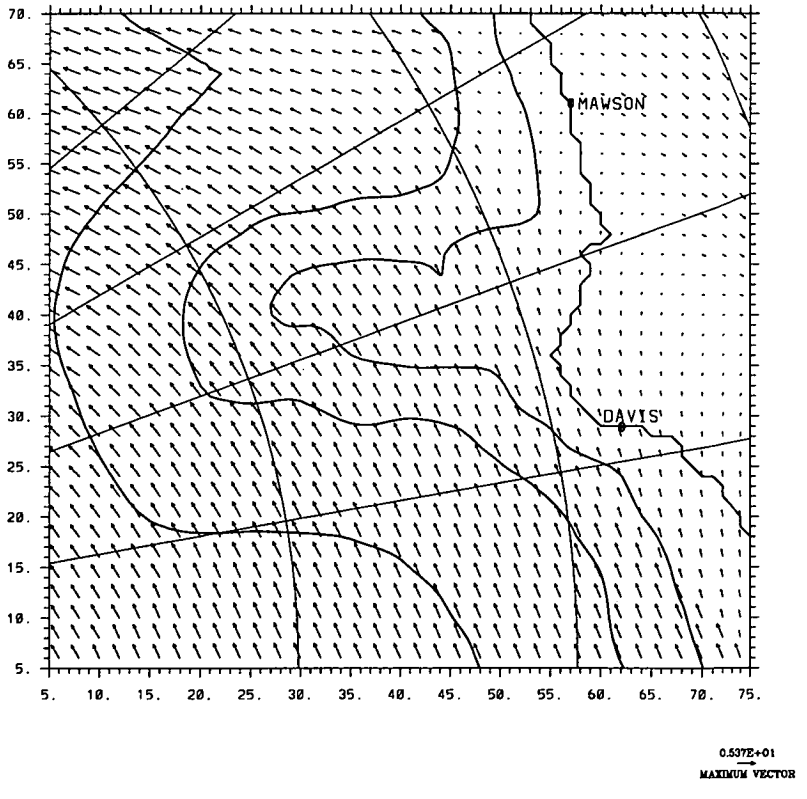

Figure 7.38: Mean monthly SHANAL July 700 hPa level wind field corresponding to katabatic winds at Mawson, interpolated to the 80x74 mesoscale model grid, over the Lambert Glacier Basin region. For clarity, only vectors located at even-numbered grid points are plotted.

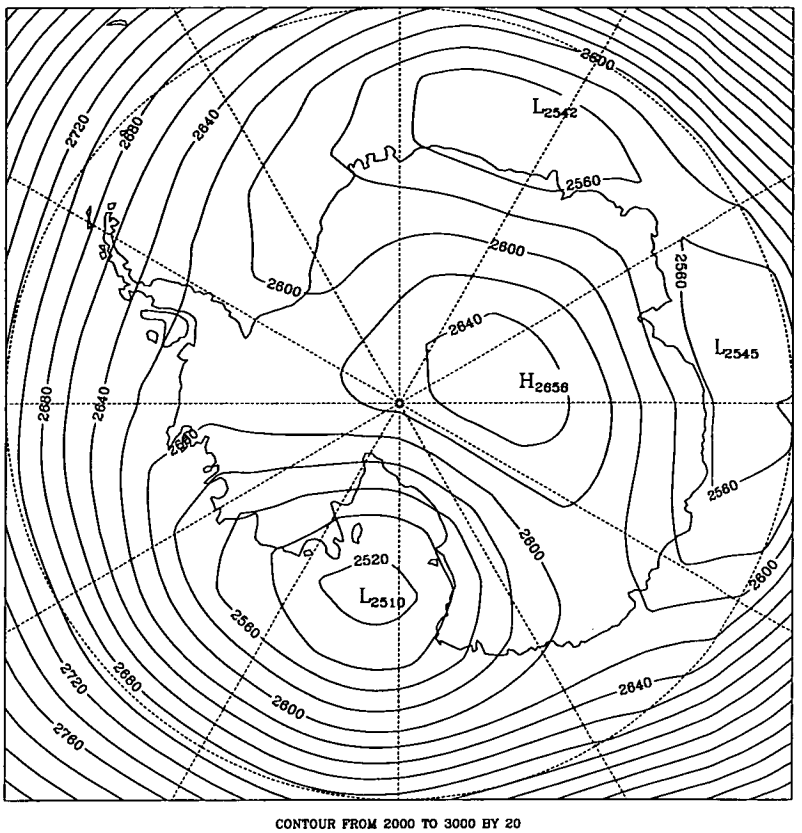

Figure 7.39: Mean monthly height of SHANAL July 700 hPa pressure level corresponding to blizzard winds at Mawson.

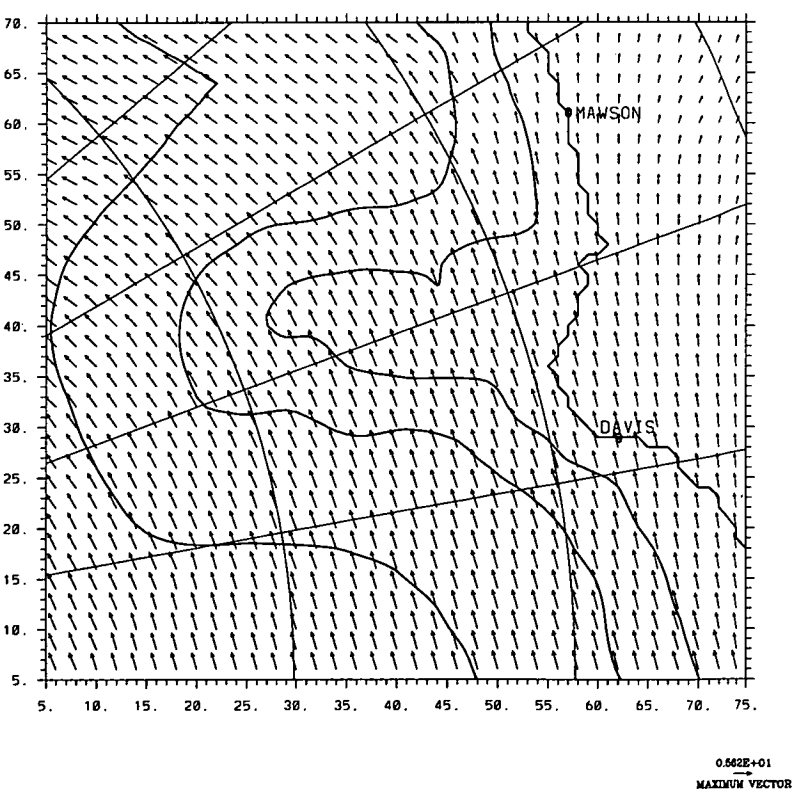

Figure 7.40: Mean monthly SHANAL July 700 hPa level wind field corresponding to blizzard winds at Mawson, interpolated to the 80x74 mesoscale model grid, over the Lambert Glacier Basin region. For clarity, only vectors located at even-numbered grid points are plotted.

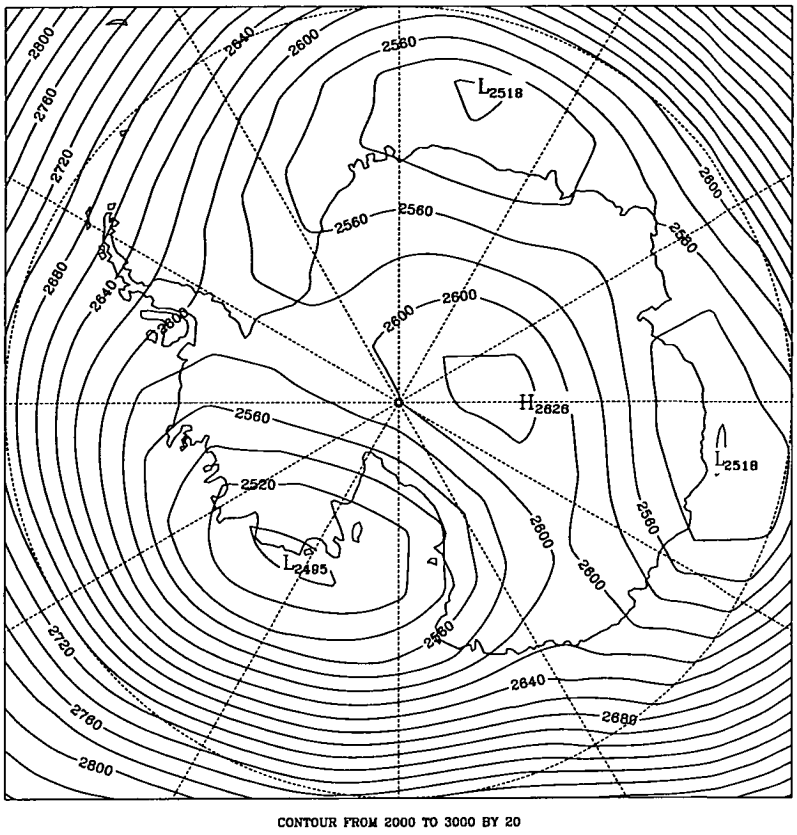

Figure 7.41: Mean monthly height of SHANAL July 700 hPa pressure level corresponding to calm conditions at Mawson.

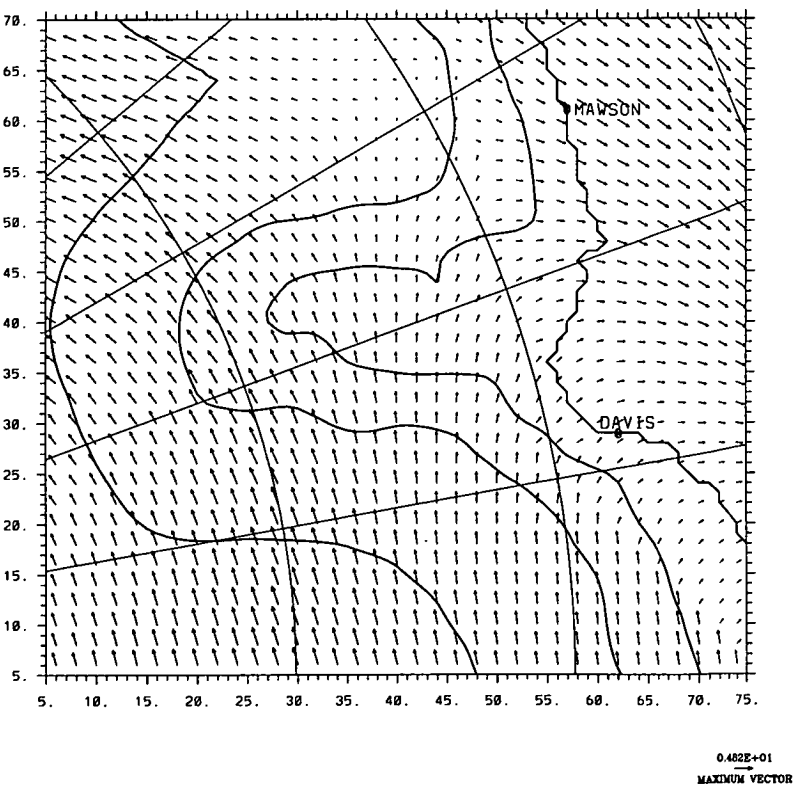

Figure 7.42: Mean monthly SHANAL July 700 hPa level wind field corresponding to calm conditions at Mawson, interpolated to the 80x74 mesoscale model grid, over the Lambert Glacier Basin region. For clarity, only vectors located at even-numbered grid points are plotted. This field is used to force model run R45, Chapter 8.

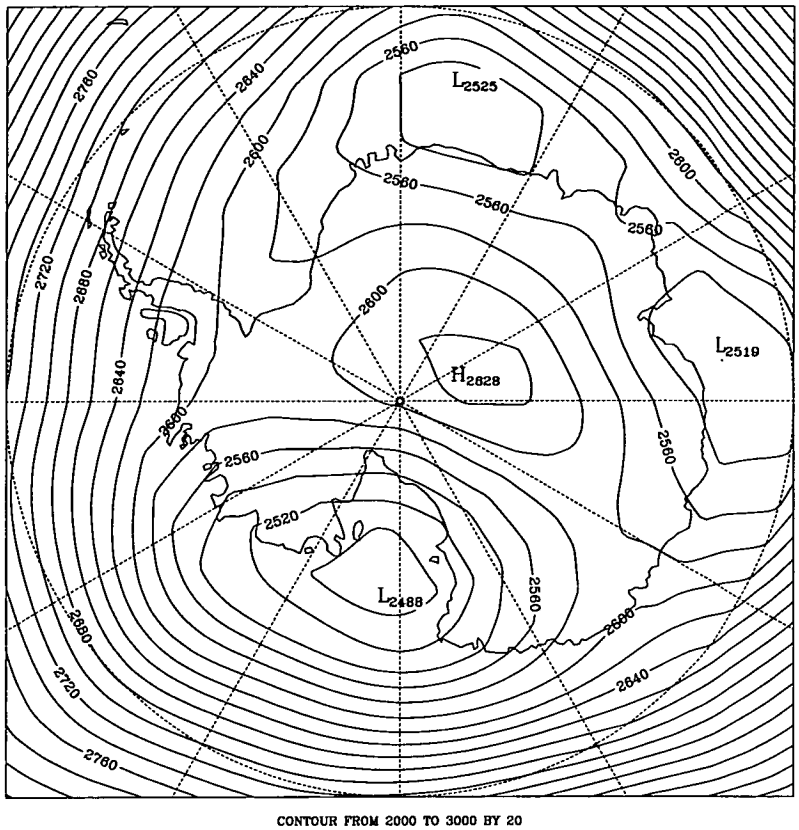

Figure 7.43: Mean monthly height of SHANAL July 700 hPa pressure level corresponding to katabatic-blizzard winds at Mawson.

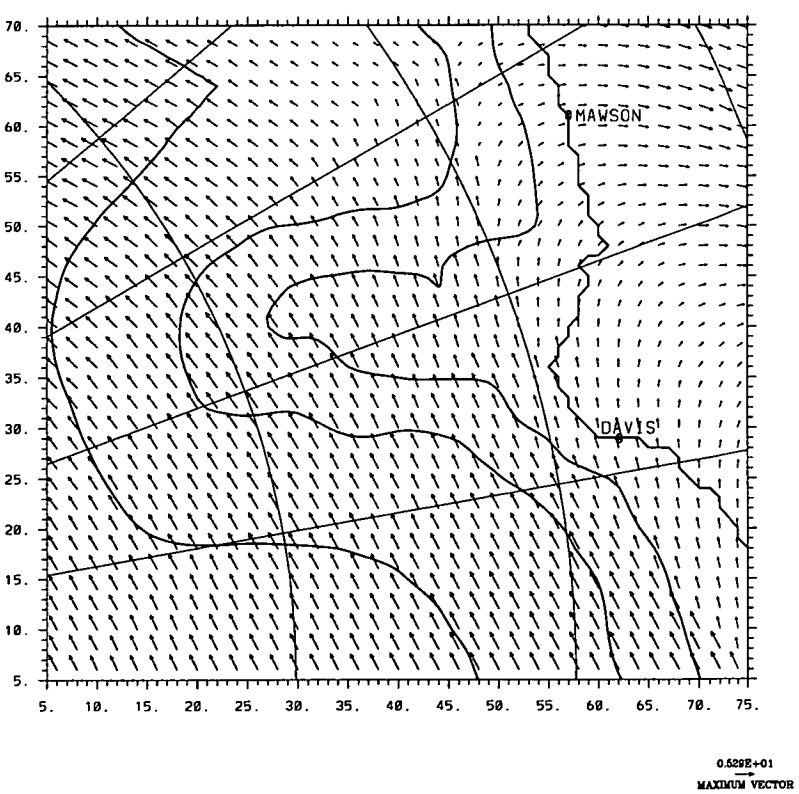

Figure 7.44: Mean monthly SHANAL July 700 hPa level wind field corresponding to katabatic-blizzard winds at Mawson, interpolated to the 80x74 mesoscale model grid, over the Lambert Glacier Basin region. For clarity, only vectors located at even-numbered grid points are plotted. This field is used to force model run R46, Chapter 8.

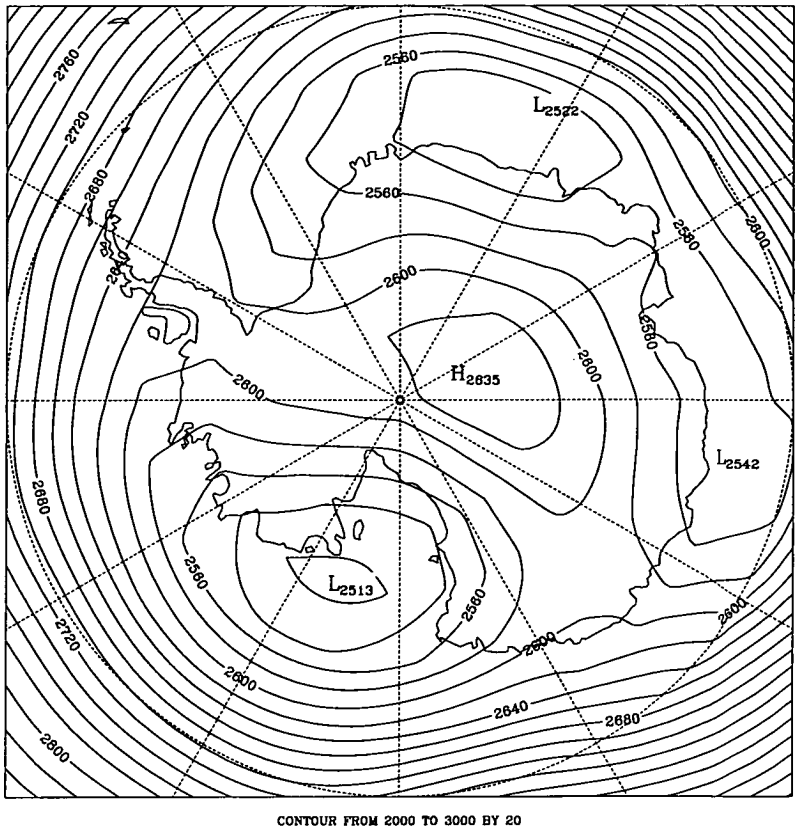

Figure 7.45: Mean monthly height of SHANAL July 700 hPa pressure level corresponding to katabatic-non-blizzard winds at Mawson.

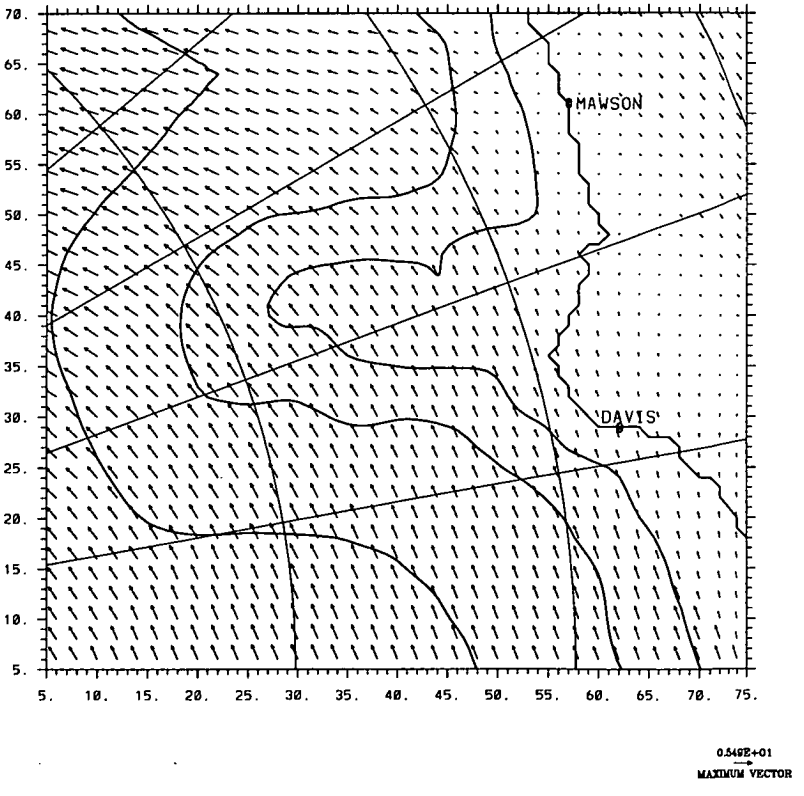

Figure 7.46: Mean monthly SHANAL July 700 hPa level wind field corresponding to katabatic-non-blizzard winds at Mawson, interpolated to the 80x74 mesoscale model grid, over the Lambert Glacier Basin region. For clarity, only vectors located at even-numbered grid points are plotted. This field is used to force model run R47, Chapter 8.

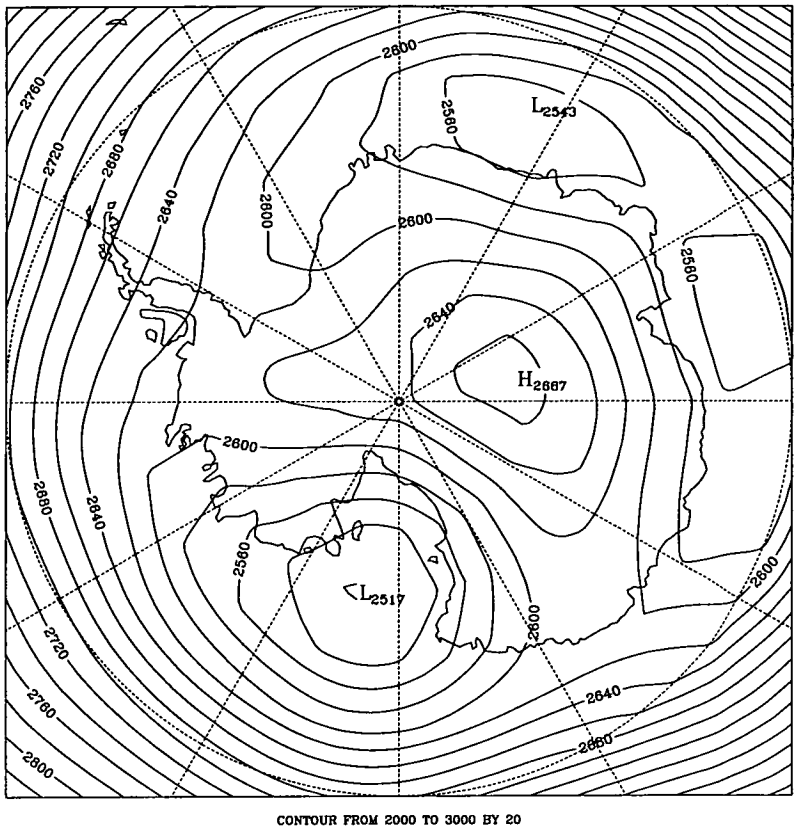

Figure 7.47: Mean monthly height of SHANAL July 700 hPa pressure level corresponding to blizzard-non-katabatic winds at Mawson.

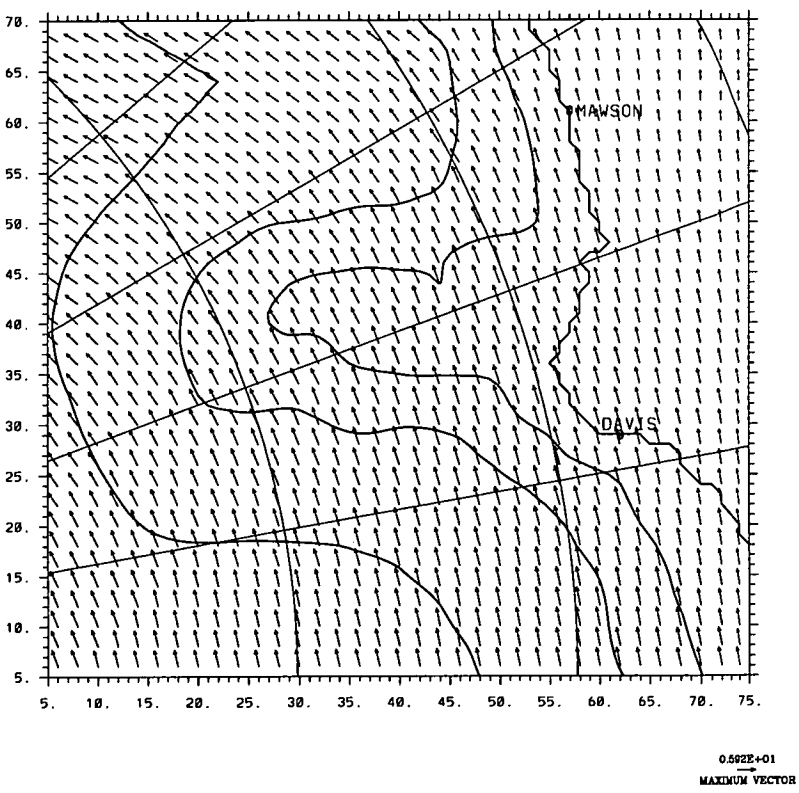

Figure 7.48: Mean monthly SHANAL July 700 hPa level wind field corresponding to blizzard-non-katabatic winds at Mawson, interpolated to the 80x74 mesoscale model grid, over the Lambert Glacier Basin region. For clarity, only vectors located at even-numbered grid points are plotted. This field is used to force model run R48, Chapter 8.

7.4 CONCLUSION

The analyses discussed throughout this chapter establish probable synoptic conditions for various surface winds observed at Mawson. The relationships are considerably clearer during summer than winter.

In the case of the near-surface katabatic jet, the lack of synoptic influence appears evident from vertical wind speed profiles. Figures 7.5 and 7.6A suggest that the katabatic jet is isolated from the atmosphere above, in terms of momentum transfer from higher levels, and that such winds are independent of significant synoptic control, existing as relatively dense parcels of air draining downslope from the plateau. However, not all katabatic wind profiles show such characteristics, and they are less pronounced during January.

Forcings of katabatic-blizzard upper winds are not clear, unlike blizzard-non-katabatics, that have corresponding E-SE upper wind, related to a cyclonic system to the north-east of Mawson, for both summer and winter.

At lower wind speeds, katabatic winds have E-SE upper winds during January, but W-SW during July. At these low wind speeds, non-katabatic winds have E-SE upper winds during January and the July upper wind forcing is highly variable, except for the surface wind speeds within the interval 0-5 m/s, for which there is a corresponding W-SW upper wind.

During January, upper wind forcings are in about the same direction as the surface winds, and the strength of the upper winds probably affect surface wind strength; direct transfer of momentum in the vertical. The case is more complicated during July.

Figure 7.15 demonstrates that katabatic winds are likely to be influenced by SW - W wind directions at the 700 hPa level during July. Rusin (1961) found a similar relationship at Mirny station.

The numerical model, that has been shown previously to be well tuned and perform realistically in modelling boundary layer winds over the Lambert Glacier

Basin region, is used to clarify the relationship between synoptic forcing and surface winds. Results of the numerical modelling are presented in Chapter 8.

Chapter 8

NUMERICAL MODELLING OF SYNOPTIC INFLUENCE ON SURFACE WINDS AT MAWSON

8.1 INTRODUCTION

The aim of this chapter is to use results from numerical modelling of the atmosphere to assist in clarifying the relationships between synoptic and surface winds at Mawson station.

January and July mean conditions are modelled for synoptic wind directions over Mawson station that differ by margins of 45°, from one run to the next. Explanations as to why these runs are conducted and results from the numerical modelling are discussed in Section 8.2.

The relatively poor representation of the terrain slope at the model grid point corresponding to Mawson station was noted in Chapter 6 as one cause of the low modelled wind speeds. Throughout this chapter, the modelled surface wind speeds at Mawson were closer to those observed because the synoptic forcing was stronger. The major aim of Section 8.2 is to compare surface meteorological conditions generated by different synoptic wind forcings; although the winds produced by the model may not exactly match observed values, the interest lies in the comparison of results between runs.

Numerical modelling that expands on the discussions in Chapter 7 is car-

ried out for the synoptic wind fields compiled from SHANAL data for different wind types: calm, katabatic-blizzard, katabatic-non-blizzard and blizzard-non-katabatic.

These upper wind fields are shown by Figures 7.28, 7.30, 7.32 and 7.34 for January and by Figures 7.42, 7.44, 7.46 and 7.48 for July. Results from numerical modelling carried out using these wind fields as synoptic forcings are discussed in Section 8.3.

As noted in the previous chapter, the SHANAL data are somewhat suspect in comparison with AUW data at Mawson. Therefore, the results of the modelling that use these as input data, (for synoptic forcing), must be examined carefully.

Findings are summarised in Section 8.4.

8.2 MODELLING OF SYNOPTIC WIND DIRECTION INFLUENCES

8.2.1 INTRODUCTION

Numerical modelling is a powerful technique for studying the atmosphere because a chosen parameter can be varied while all others are kept constant. The resultant changes to the system must be due to the one parameter varied, assuming that the model is functioning correctly and realistically. This is a safe assumption for the experiments conducted in this chapter because the model was tuned and results verified, as shown in Chapter 6.

A total of eighteen numerical model runs were carried out in this section; nine January and nine July runs. Respective monthly mean conditions were used. Runs for a particular month differ only by the synoptic forcing used.

As shown in Table 8.1, the synoptic (upper) wind direction forcings used differ from one run to the next by 45°. The specific wind directions are valid for the longitude of Mawson station, 62°52′48″E. This series of model runs produced data that can be used to further the understanding of interactions between terrain, boundary layer winds and inversion strengths at Mawson, under the influence of

Synoptic wind		Run name	
Direction (°)	Speed (m/s)	January	July
0	10	R23	R32
45	10	R24	R33
90	10	R25	R34
135	5	R26	R35
135	10	R27	R36
180	10	R28	R37
225	10	R29	R38
270	10	R30	R39
315	10	R31	R40

Table 8.1: January and July mean monthly conditions are used (as in runs R22 and R20 respectively, Chapter 6.). The runs listed in this table differ from these mean monthly runs only by the synoptic wind direction forcings used. Wind directions and speeds are spatially-constant, with wind directions valid for the longitude of Mawson station.

various synoptic wind directions. The results are discussed in Section 8.2.2.

The synoptic wind fields used are spatially-constant, with wind directions over Mawson station duplicated to every other grid point. This method is used for simplicity, so that a plane of constant wind direction, instead of an actual spatially-varying synoptic pattern, can be applied as forcing to the top of the boundary layer. Wind speeds of 10 m/s are used, except for two runs as shown in Table 8.1. This wind speed value was selected because it is a "round" figure close to both January and July 700 hPa level mean wind speeds.

The orientation of the fall line of the terrain at Mawson is approximately 135°. Mean resultant wind directions have been found to be quite closely aligned with the fall line. Apart from altering the synoptic wind direction from run to run while keeping the wind speed constant, additional experiments are conducted in which the synoptic wind speed is halved (from 10 m/s to 5 m/s) for the upper wind direction of 135°. Results are discussed in Section 8.2.3.

8.2.2 SYNOPTIC WIND DIRECTION FORCING OF THE BOUNDARY LAYER

Figure 8.1 displays resultant modelled January and July surface wind directions at Mawson corresponding to applied synoptic wind directions.

Generally, the resultant January surface wind directions are about 45° "greater" (that is, 45° further clockwise) than the synoptic wind directions. These changes in wind direction with height are accounted for by surface friction; surface winds turning to the right (in the Southern Hemisphere) of the geostrophic winds, as described by the Ekman spiral.

During January, exceptions to this pattern are for surface wind directions corresponding to the applied synoptic wind directions from the east and from the southeast. This probably occurs because the fall line of the terrain is most closely aligned with these wind directions and this results in channelling of the winds at the surface; winds from other directions tend to flow "across" the fall line.

In reality the terrain is steeper at this location and surface winds are influenced to a greater degree, resulting in surface wind directions closer to the orientation of the fall line.

During July, the relationships between surface and synoptic wind directions are less clear, but Figure 8.1B shows that the synoptic wind direction has significant influence on the direction of the surface wind. The presence of an inversion somewhat inhibits the influence of the synoptic wind on surface winds. This is investigated further in Section 8.2.3.

The two columns corresponding to applied synoptic winds from the southeast with speeds of 5 and 10 m/s respectively, are very similar for the summer runs, but the winter results show a difference of about 20°. This occurs because during summer the main influences on the surface wind direction are the synoptic wind direction and the topography, but during winter, the inversion partly isolates the boundary layer flow from the synoptic forcing, as well as modifying the vertical hodograph of the wind. This means that lower synoptic wind speeds during winter

allow the local wind regime to have a relatively greater effect on the surface wind. During summer, lower synoptic wind speeds result in lower surface wind speeds but similar wind directions.

Figure 8.2 shows modelled January and July surface wind speeds at Mawson corresponding to applied synoptic wind directions.

Comparing the January and the July wind speeds for the applied synoptic wind directions, ranging from northerly (clockwise) to sou-easterly, less momentum is transferred from the synoptic level to the surface during July. For synoptic winds ranging from southerly (clockwise) to nor-westerly, the July surface wind speeds are greater than the corresponding January wind speeds.

The strongest January surface wind speed was produced when the applied synoptic wind direction ranged from easterly to sou-easterly. This explains why strong surface winds are observed during January at Mawson station; the vertical hodograph of winds and the easterly to sou-easterly synoptic wind directions result in surface wind directions closely aligned with the fall line of the terrain, resulting in enhancement of downslope flow.

Mean January synoptic (700 hPa) forcings observed over Mawson reveal maximum frequencies of easterly to sou-easterly wind directions. This means that the mean January synoptic forcings encourage formation of strong downslope surface winds. Therefore, strong winds frequently occur at Mawson, apart from blizzards directly related to cyclonic vortices to the north or northeast.

An analogous case is found for July, but the synoptic wind directions are sou-westerly to westerly. Numerical modelling showed that these synoptic winds produced the highest surface wind speeds and these synoptic wind directions were the most frequently observed over Mawson during July.

Mawson station is a site of strong and frequent winds because the structure of the boundary layer is such that it varies between summer and winter, and allows production of strong surface flow by the synoptic wind directions that happen to correspond to mean seasonal synoptic forcings.

Figure 8.2, that displays data produced by numerical modelling, and the above discussion clarify a question discussed in Chapter 7; downslope winds are enhanced by sou-westerly synoptic winds during July. "Katabatic" wind forcing mechanisms are more difficult to decipher because they are more related to sub-mesoscale air masses inland of Mawson and less related to synoptic forcings than are "downslope" winds.

Figure 8.3 shows lapse rates at Mawson, as produced by the numerical model for January and July conditions, corresponding to applied synoptic wind directions. The lapse rates were calculated as the negative of the changes in temperature over the changes in height; a stable atmosphere has a negative lapse rate.

The most stable conditions result from synoptic wind directions of southerly (clockwise) to nor-westerly during summer and northerly (clockwise) to southerly during winter.

Although the magnitudes differ substantially, the patterns of lapse rate for applied upper wind directions southerly (clockwise) to nor-westerly are the same for January and July. The major differences between the lapse rates for these two months were found for upper winds northerly (clockwise) to sou-easterly. For this range of wind direction, thermally unstable conditions were generated from January model runs, but stable conditions from the July model runs.

Model runs for both summer and winter showed that the column of air over Mawson was more stable when the larger (10 m/s) synoptic wind speed from the southeast was applied.

Despite the substantial scatter, Figure 8.4 shows that there is a loss of stability for modelled surface winds of greater strength, for both January and July. This is the generally accepted relationship between wind speed and thermal stability, but as shown by analyses of observed data in Chapter 7, this relationship varies between summer and winter, and with the type of wind in the real atmosphere.

A conclusion of Chapter 6 was that surface wind speeds at Mawson were too

low due to the poor representation of the terrain using 20 km horizontal grid spacings within the numerical model. The results from these runs have shown that with more realistic synoptic wind speeds than those present in SHANAL data, the surface wind speeds at Mawson have been closer to observed values.

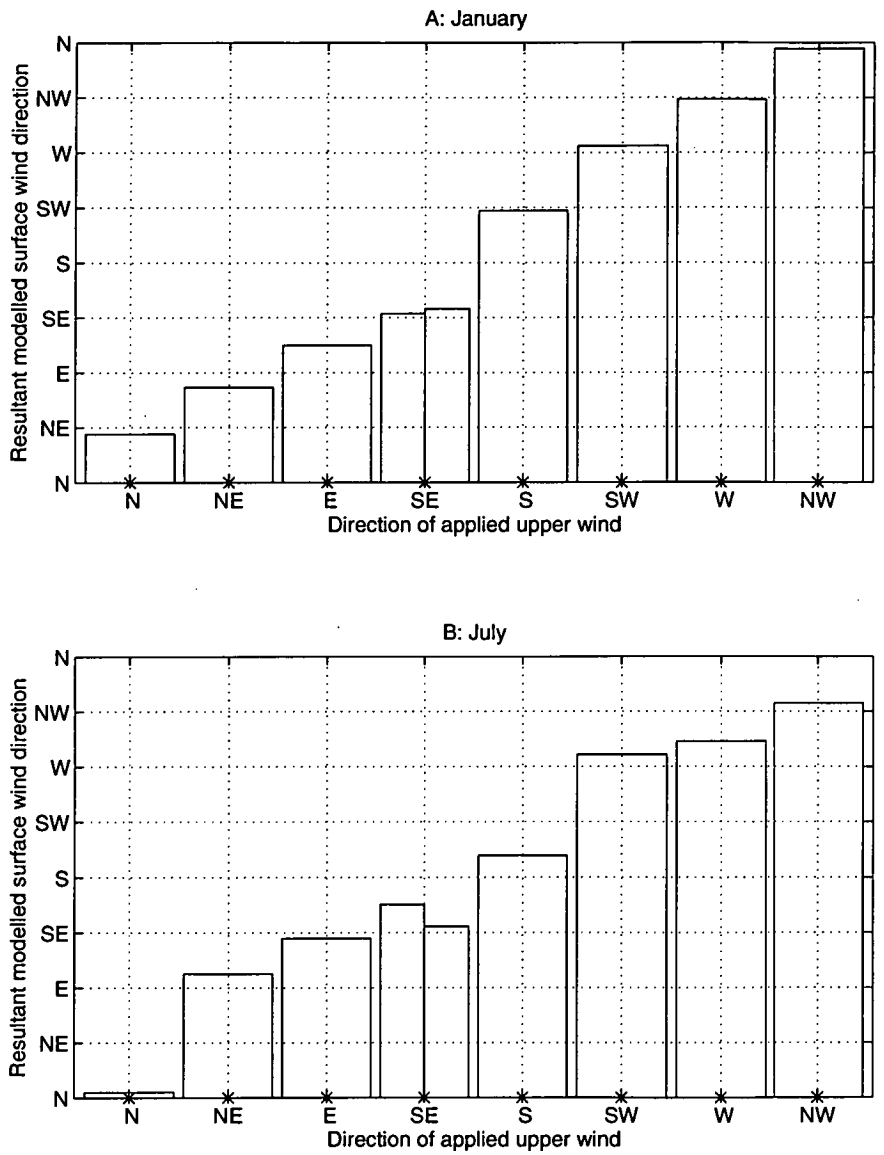

Figure 8.1: Resultant modelled surface wind direction at the 8 metre level at Mawson versus various applied upper wind directions for A: January and B: July. Each model run used an applied synoptic wind direction (N, clockwise to NW, differing from one run to the next) over the entire 80x74 grid, and a spatially-constant wind speed of 10 m/s. There are two values plotted corresponding to the applied SE wind direction; the value on the left of the SE corresponds to an applied synoptic wind speed of 5 m/s and the value on the right to a wind speed of 10 m/s.

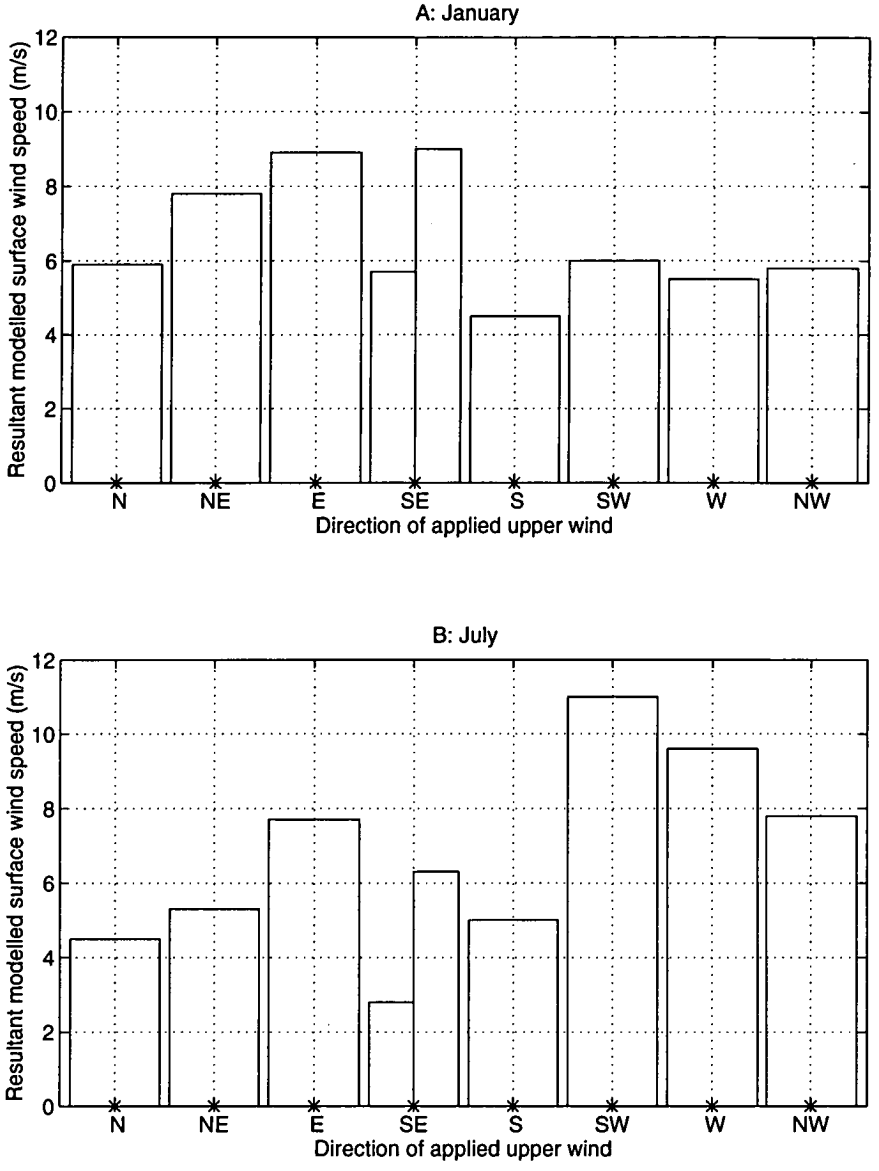

Figure 8.2: Resultant modelled surface wind speed at the 8 metre level at Mawson versus various applied upper wind directions for A: January and B: July. Each model run used an applied synoptic wind direction (N, clockwise to NW, differing from one run to the next) over the entire 80x74 grid, and a spatially-constant wind speed of 10 m/s. There are two values plotted corresponding to the applied SE wind direction; the value on the left of the SE corresponds to an applied synoptic wind speed of 5 m/s and the value on the right to a wind speed of 10 m/s.

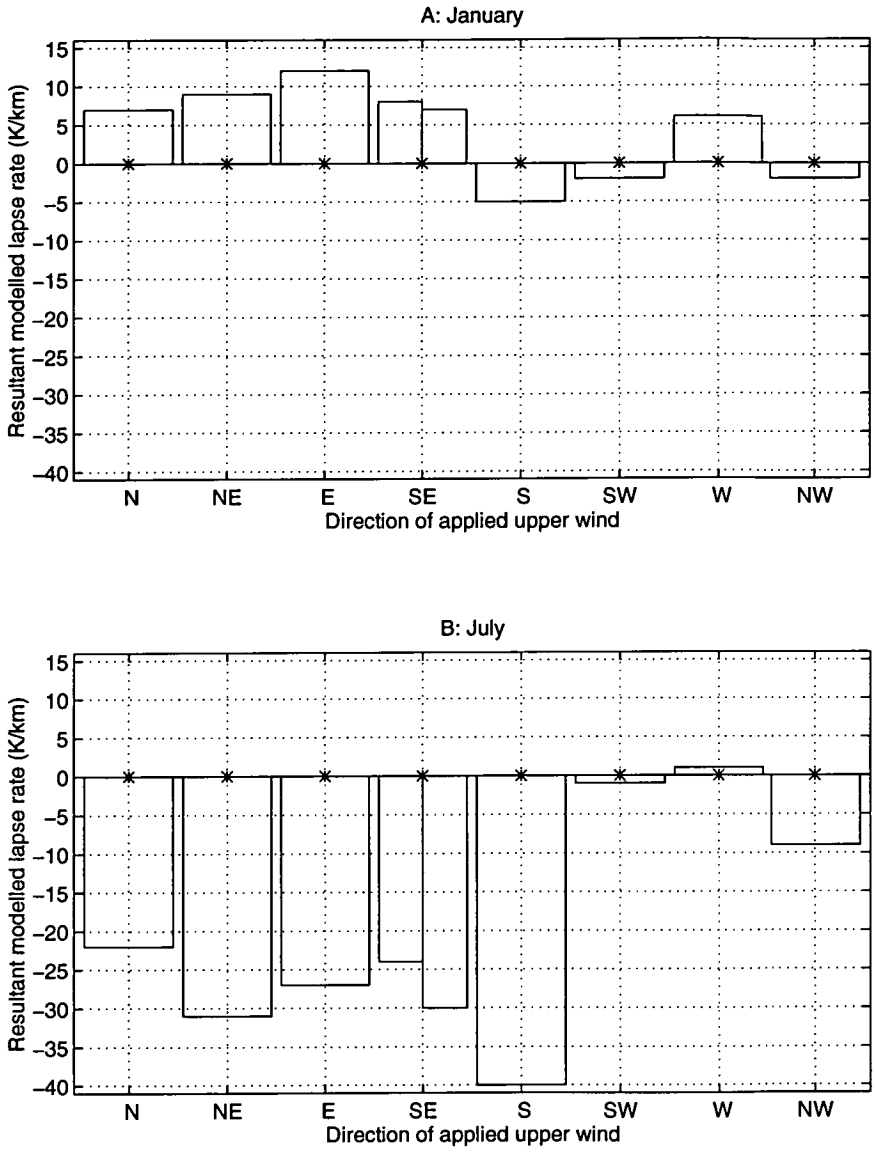

Figure 8.3: Resultant modelled lapse rate at Mawson versus various applied upper wind directions for A: January and B: July. The lapse rate was calculated as the negative of the change in temperature over the change in height; a stable atmosphere has a negative lapse rate. Each model run used an applied synoptic wind direction (N, clockwise to NW, differing from one run to the next) over the entire 80x74 grid, and a spatially-constant wind speed of 10 m/s. There are two values plotted corresponding to the applied SE wind direction; the value on the left of the SE corresponds to an applied synoptic wind speed of 5 m/s and the value on the right to a wind speed of 10 m/s.

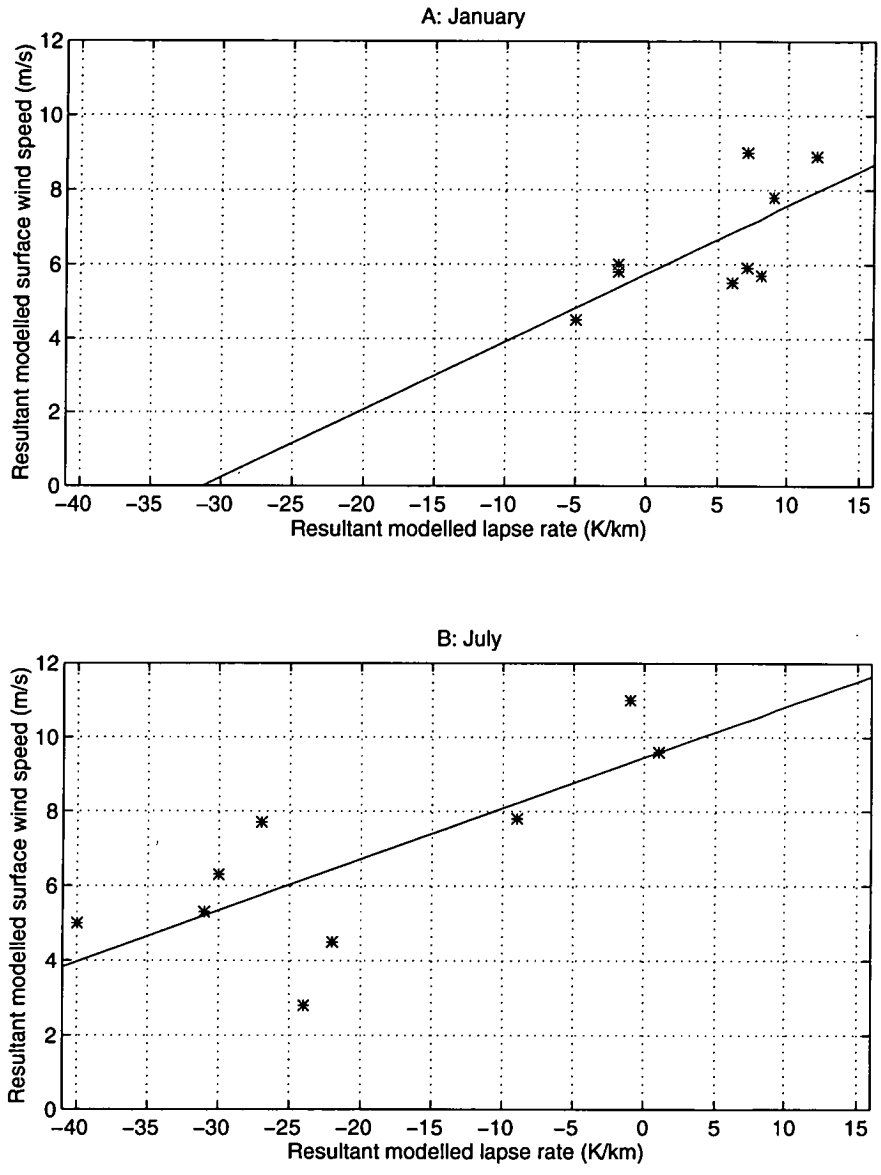

Figure 8.4: Resultant modelled surface wind speed at Mawson versus resultant modelled surface lapse rate for A: January and B: July.

8.2.3 BOUNDARY LAYER STRUCTURE: JANUARY vs JULY

Figures 8.5 and 8.6 are hodographs at Mawson (model grid point (57,61)) from model runs R26 and R27; January, synoptic wind 135°, 5 m/s and 10 m/s respectively. The u- and v-components of the wind are relative to the real world, derived from those relative to the model grid.

Comparing the two hodographs, the results from run R27 show stronger wind speeds than for run R26, but the amounts of turning of wind directions with height are similar. These hodographs indicate that the height of the wind speed maximum increases with greater synoptic wind speeds.

Hodographs from July model runs R35 and R36, (July, 135°, 5 m/s and 10 m/s respectively), (Figures 8.7 and 8.8 respectively) show that there were significant changes in wind veering with height when synoptic wind speeds were varied.

Comparing the two July hodographs, the results from run R36 show that more momentum is transferred to the lower levels because the upper wind speed is stronger. Also, this run has a deeper Ekman layer (about 150 metres; vectors A to H) than does run R35 (about 75 metres; vectors A to F), that has weaker synoptic forcing.

The wind speeds to the right of each hodograph show that for a synoptic wind speed of 10 m/s, the wind maxima in the column of air over Mawson is located at heights of 50 to 100 metres above the surface, as noted in Chapter 2. However, for run R35 (5 m/s synoptic wind speed), the wind maxima are at lower levels (15 metres), indicating the presence of a steady near-surface katabatic jet; the relatively low synoptic wind speed has not contributed adequate amounts of momentum to cause significant vertical mixing in the lower atmosphere.

Figures 8.9 and 8.10 are vertical profiles of wind speed and sensible temperature at Mawson station (model grid point (57,61)) produced by model runs R27 (January) and R36 (July) respectively. Both runs were forced with 10 m/s synoptic winds from the southeast.

An inversion is not generated by the summer run and the wind speed profile is not katabatic. There is low-level air flow but the layer is relatively deep and well mixed. The wind speed profile from winter run R36 has a near-surface jet (about 100 metres above the surface). This corresponds to a shallow temperature inversion extending from the surface to a height of about 200 metres. As shown by analyses of observed data in Chapter 7, there is a characteristic minimum in wind speed within about 500 metres above a near-surface katabatic jet; this feature is simulated by the numerical model.

There is transfer of momentum from the synoptic to surface level during both January and July. This is clearly shown for January by the hodographs and vertical profile of wind speed. For July, the near-surface winds are stronger when synoptic forcing is stronger, but above this surface flow is a region of low wind speeds. The temperature profile shows that an inversion is not present through this region and the July hodographs show that the wind directions in the boundary layer are approximately perpendicular to the synoptic wind directions. It is concluded that mixing occurs in this region above the near-surface jet.

This well mixed region above the July katabatic jet may form by the following process. An inversion forms extending from the surface to a height of about 1000 metres. Properties of this inversion are laminar flow and significant turning of wind direction with height. The strong synoptic forcing causes mixing in the upper region of the inversion, resulting in weakening of the inversion and reductions in wind speeds. The near-surface inversion remains, as does the near-surface jet, effectively isolated from the synoptic flow by the turbulent layer above. Surface wind gusts may be caused by transfer of parcels of air with higher momentum from the turbulent to the near-surface layer. Synoptic wind speeds greater than 10 m/s would probably be required to cause the breakdown of the near-surface inversion.

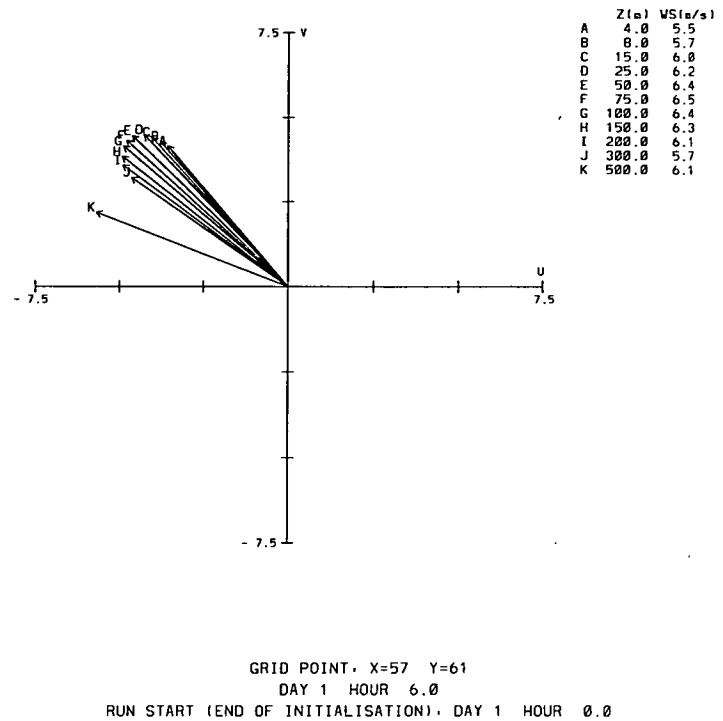

Figure 8.5: Hodograph at Mawson (model grid point (57,61)) from run R26; January, synoptic wind 135°, 5 m/s. The u- and v-components of the wind are relative to the real world, computed from those relative to the model grid.

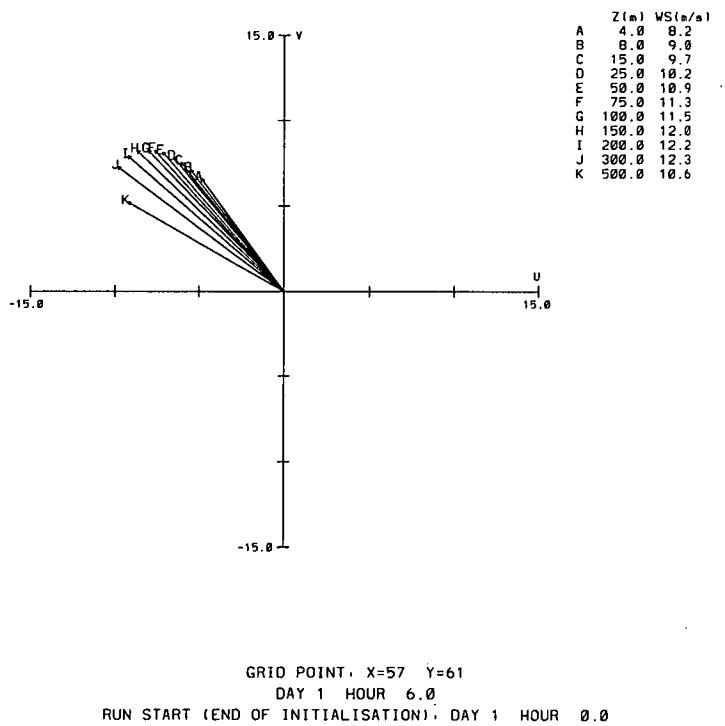

Figure 8.6: Hodograph at Mawson (model grid point (57,61)) from run R27; January, synoptic wind 135°, 10 m/s. The u- and v-components of the wind are relative to the real world, computed from those relative to the model grid.

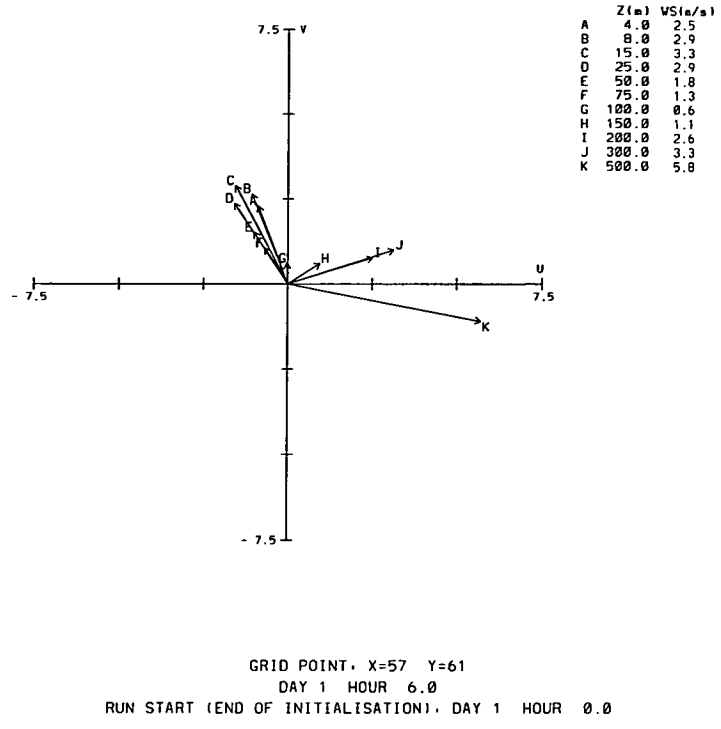

Figure 8.7: Hodograph at Mawson (model grid point (57,61)) from run R35; July, synoptic wind 135°, 5 m/s. The u- and v-components of the wind are relative to the real world, computed from those relative to the model grid.

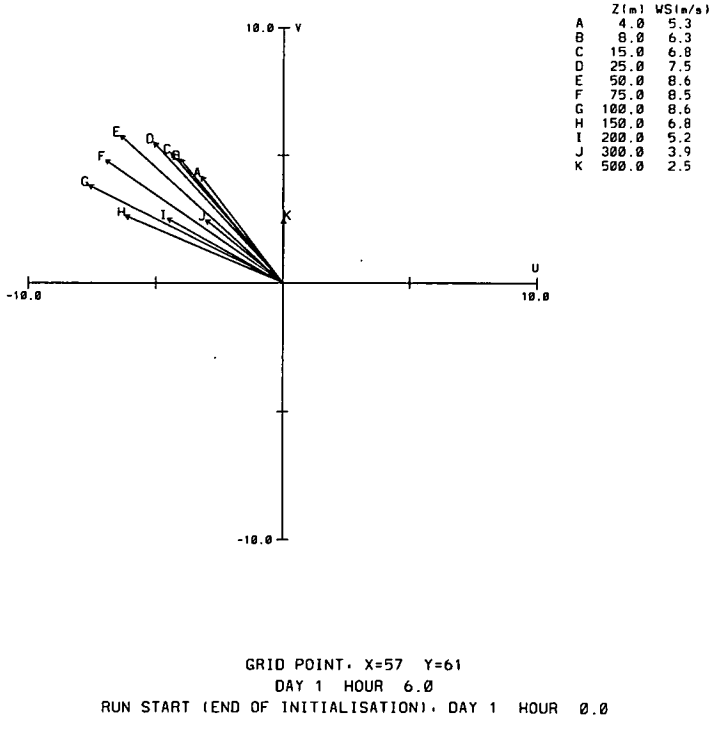

Figure 8.8: Hodograph at Mawson (model grid point (57,61)) from run R36; July, synoptic wind 135°, 10 m/s. The u- and v-components of the wind are relative to the real world, computed from those relative to the model grid.

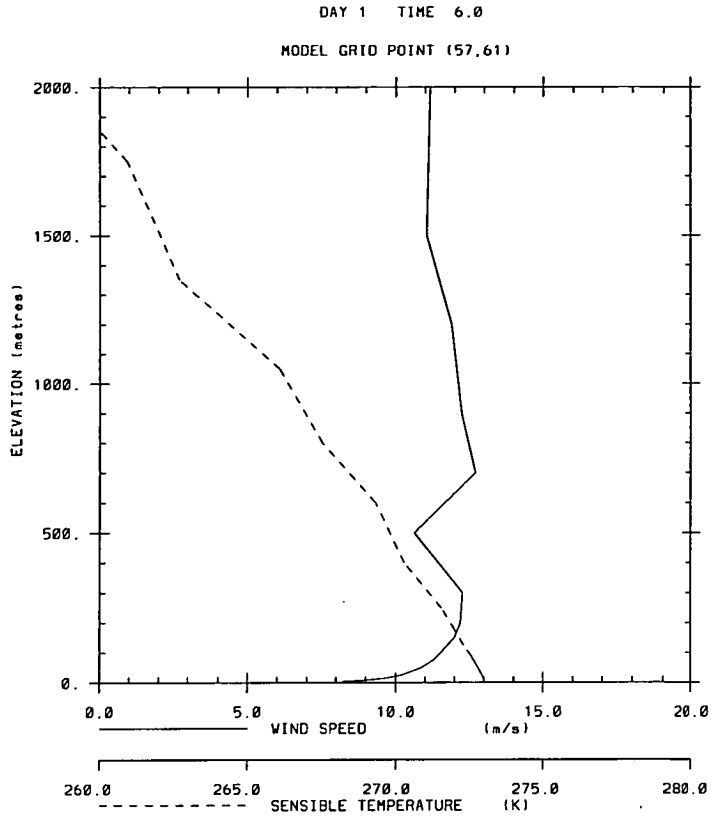

Figure 8.9: Vertical wind speed and sensible temperature profiles at Mawson (model grid point (57,61)) from run R27; January, synoptic wind 135°, 10 m/s.

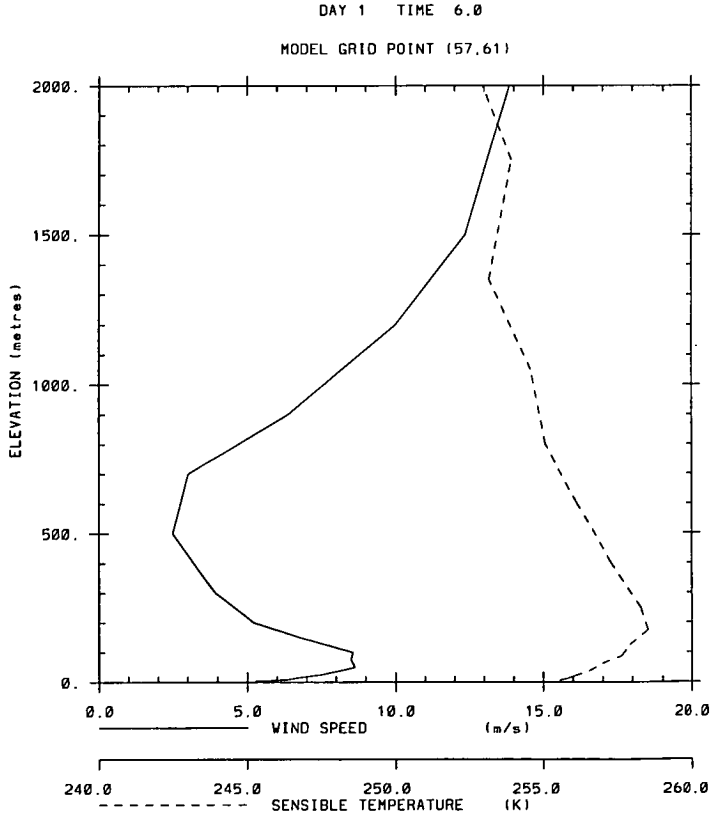

Figure 8.10: Vertical wind speed and sensible temperature profiles at Mawson (model grid point (57,61)) from run R36; July, synoptic wind 135°, 10 m/s.

8.3 SYNOPTIC FORCING OF SURFACE WINDS AT MAWSON

8.3.1 INTRODUCTION

Numerical modelling was carried out for summer and winter conditions, forced with synoptic wind fields compiled in Chapter 7 for calm, katabatic-blizzard, katabatic-non-blizzard and blizzard-non-katabatic winds at Mawson station. These runs were conducted to find the likely surface wind fields accompanying these four types of wind. The runs are listed in Table 8.2.

8.3.2 VERIFICATION OF MODELLED SURFACE WINDS AT MAWSON

It was found in Chapter 7 that SHANAL data are less accurate during July than January. This means that results from July model runs R45 to R48 may not be as accurate as results from January runs R41 to R44.

Verifications of monthly mean conditions produced by the numerical model were made in Chapter 6. Model runs R41 to R48 used different (not monthly means that were used in runs R20 and R22) synoptic forcings, and cannot be verified using monthly mean data. However, comparison between modelled and observed wind directions, at Mawson station for the four different wind types, can be used to indicate the accuracy of the model-generated wind fields. If accurate, it is assumed that the wind field inland of Mawson is also reasonably accurate.

Table 8.3 shows that surface winds generated by the January model runs are reasonably accurate, differing from observed values by about 15°. Comparisons for the calm wind type are not taken into account.

Table 8.3 shows that for July, the only wind type that has a corresponding modelled wind direction that matches the observed value well is blizzard-non-katabatic. The July katabatic-blizzard modelled surface wind direction at Mawson station does not agree with observations, differing by 83.5°.

The model runs conducted in Section 8.2 formed a database of summer and

Surface wind condition	Run name	
	January	July
Calm	R41	R45
Katabatic-blizzard	R42	R46
Katabatic-non-blizzard	R43	R47
Blizzard-non-katabatic	R44	R48

Table 8.2: January and July mean monthly conditions are used (as in runs R22 and R20 respectively). The runs listed in this table differ from these mean monthly runs only by the synoptic wind forcings used. Synoptic patterns were compiled from SHANAL data for each of the four surface wind conditions in the left hand column, for both January and July. Synoptic wind directions and speeds are spatially-varying. Problems with accuracy of these fields were discussed in Chapter 7.

winter surface winds corresponding to synoptic wind direction forcings, ranging from northerly (clockwise) to nor-westerly. These results may be used to substitute for the surface wind field generated by July model run R46 (katabatic-blizzard), that was found to be inaccurate.

The probable synoptic (AUW 700 hPa) wind directions over Mawson that were found to correspond to July katabatic-blizzard surface winds were at angles 90°, 150° and 260°, as shown in Table 7.2, Chapter 7. Numerical model runs in Section 8.2 that were forced with similar synoptic wind directions were runs R34 (90°), R36 (135°) and R39 (270°). The surface wind directions at Mawson station generated by these three model runs were compared with observed surface wind directions of katabatic-blizzard winds, Table 8.4. It was found that the result from run R34 had the best match with observations. It can therefore be assumed that the modelled surface wind field is realistic, in the vicinity of Mawson station. Over the remainder of the region, the surface wind fields produced are probably less reliable because run R34 used synoptic wind fields that were spatially-constant.

The surface wind field generated by July run R34, shown by Figure 8.16, is a probable representation of surface air flow associated with katabatic-blizzard winds at Mawson station.

Surface wind condition	Surface Wind Direction at Mawson					
	January			July		
	Observed	Modelled	Run	Observed	Modelled	Run
Calm	—	114.4	R41	—	250.2	R45
Katabatic-blizzard	130	114.0	R42	130	213.5	R46
Katabatic-non-blizzard	130	113.5	R43	130	175.3	R47
Blizzard-non-katabatic	120/130	115.0	R44	130	130.5	R48

Table 8.3: Comparison between observed and modelled surface wind directions at Mawson for the four types of wind: calm, katabatic-blizzard, katabatic-non-blizzard, blizzard-non-katabatic, for January and July. In reality, calm wind conditions do not have accompanying wind directions, but wind directions are defined by the numerical model for winds of all speeds, no matter how small.

Observed		Model		
Wind Direction			Wind Direction	
Surface	700 hPa	Run	Synoptic Forcing	Surface
130	90	R34	90	130.3
130	150	R36	135	140.0
130	260	R39	270	290.6

Table 8.4: Comparison between observed (left hand column) and modelled (right hand column) surface wind directions corresponding to katabatic-blizzard winds at Mawson station during July.

The July katabatic-non-blizzard modelled surface wind direction at Mawson station differed from the mean observed value by 45.3°. Using the method described above did not improve the match between modelled and observed wind directions at Mawson. It is concluded that katabatic winds below blizzard strength (< 15 m/s) are virtually independent of synoptic forcing. This result was also suggested from the analyses of data in Chapter 7.

Although katabatic-non-blizzard winds at Mawson do not seem to be forced by synoptic winds, it has been shown previously that katabatic-blizzard winds and also downslope winds are influenced by synoptic winds.

8.3.3 SURFACE WIND FIELDS

Figures 8.11 to 8.14 show surface streamlines produced by January model runs R41 to R44. These represent calm, katabatic-blizzard, katabatic-non-blizzard and blizzard-non-katabatic winds at Mawson station.

Although the synoptic forcing patterns differ, these four January model runs show the characteristic cross-slope flow that was produced by January mean run R22 in comparison with mean July run R20. This demonstrates the significant influence that terrain has on surface winds, despite changes in synoptic forcings. Compared with the results from July runs (Figures 8.15 to 8.17), similarities between surface wind fields over the continent, generated by the January runs, show that seasonal influences are more significant than differences in synoptic patterns.

January runs show generally easterly surface air flow over the sea. The calm wind case (Figure 8.11) shows that there is divergence of flow north of Mawson station. The synoptic forcing corresponding to calm wind conditions at Mawson station causes this divergence of flow, but the convergence over the central Lambert Glacier region is mainly due to the influence of the underlying terrain. The divergence over the sea may partly explain the calm conditions at Mawson station; this possibility was not found by analyses of real data in Chapter 7, and

it demonstrates another powerful aspect of numerical modelling. The pattern of divergence over the sea was not apparent in the other January model runs, Figures 8.12 to 8.14.

Figure 8.15 shows surface streamlines expected over the Lambert Glacier Basin region when forced with the mean synoptic pattern corresponding to calm wind conditions at Mawson during July. Despite the convergence of air over the central region of the grid, the streamlines show that south of Mawson station there is divergence. As discussed in Chapter 2, winds can persist in coastal regions of Antarctic with the presence of a zone of convergence upstream. The modelled divergence suggests that calm wind conditions occur at Mawson because there is not an adequate supply of air.

Figure 8.16 was generated by run R34, as a substitute for run R46, the case of the July katabatic-blizzard wind at Mawson station. This figure displays the surface air flow only in the vicinity of Mawson because run R34 was forced by spatially-constant synoptic winds, and therefore not strictly valid for large areas.

In comparison with mean July surface winds, the air flow over the sea/seaice area differs from the mean westerly flow. This figure suggests that the surface outflow from over the Lambert Glacier - Amery Ice Shelf is partially directed towards Mawson station in the easterly flow, thereby providing a good supply of air and possibly continuous and strong winds, because this outflow results from the region of significant convergence over the Lambert Glacier to the south. In addition, there is the mean surface wind that approaches Mawson from the south/southeast.

For the case of July blizzard-non-katabatic winds at Mawson station (run R48), Figure 8.17 shows that a surface jet of easterly flow was formed from convergence of drainage of continental air and northerlies (north of Mawson). The northerly winds were forced by the synoptic pattern that was present over the sea/seaice; Figure 7.48.

There is westerly flow north of Davis. Between this flow and the easterly jet

north of Mawson, a region of positive vorticity (anticyclonic rotation) developed. This suggests that the interaction between the terrain-induced continental surface air flow and the air flow over the sea/seaice region forced by the synoptic pattern (for blizzard-non-katabatic July winds at Mawson), causes formation of this mesoscale antocyclonic rotation.

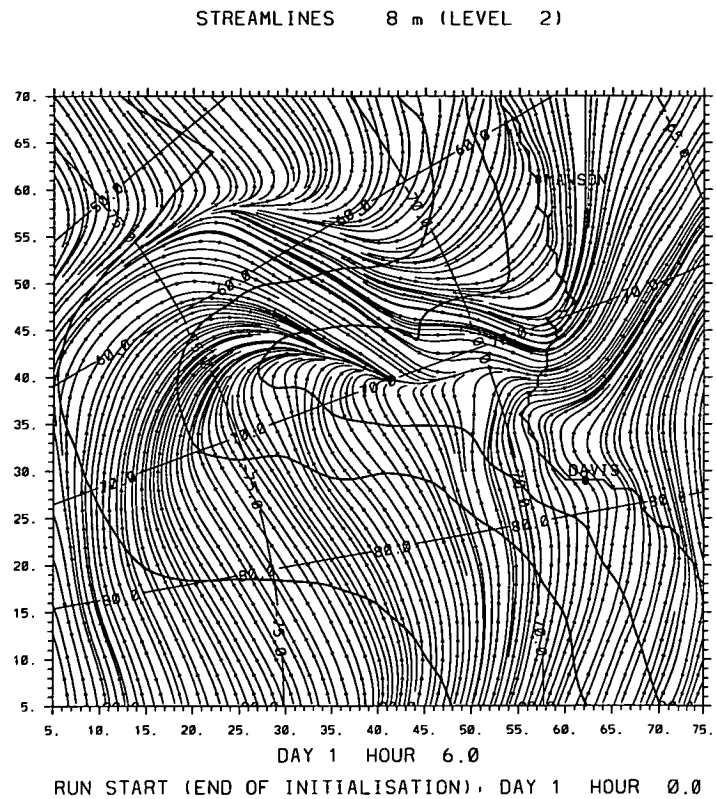

Figure 8.11: Surface (8 metres height) streamlines as produced by January "calm" run R41. These lines do not represent trajectories but rather the air flow over the region at one time.

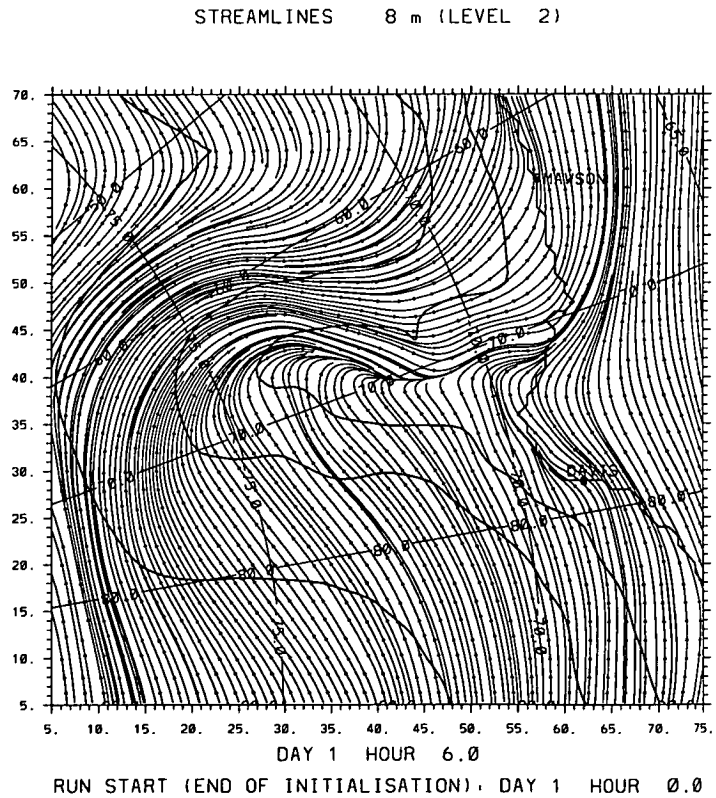

Figure 8.12: Surface (8 metres height) streamlines as produced by January "katabatic-blizzard" run R42. These lines do not represent trajectories but rather the air flow over the region at one time.

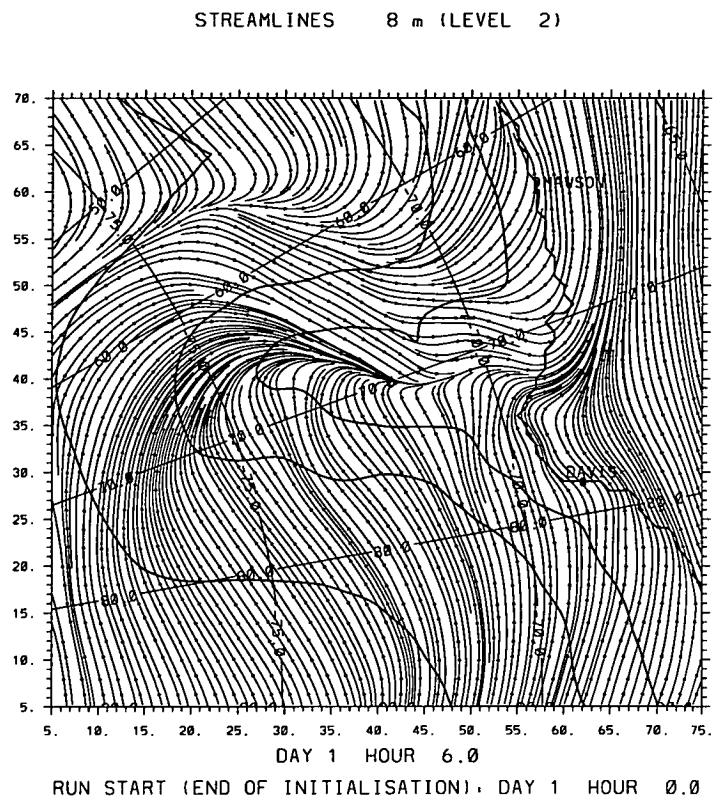

Figure 8.13: Surface (8 metres height) streamlines as produced by January "katabatic-non-blizzard" run R43. These lines do not represent trajectories but rather the air flow over the region at one time.

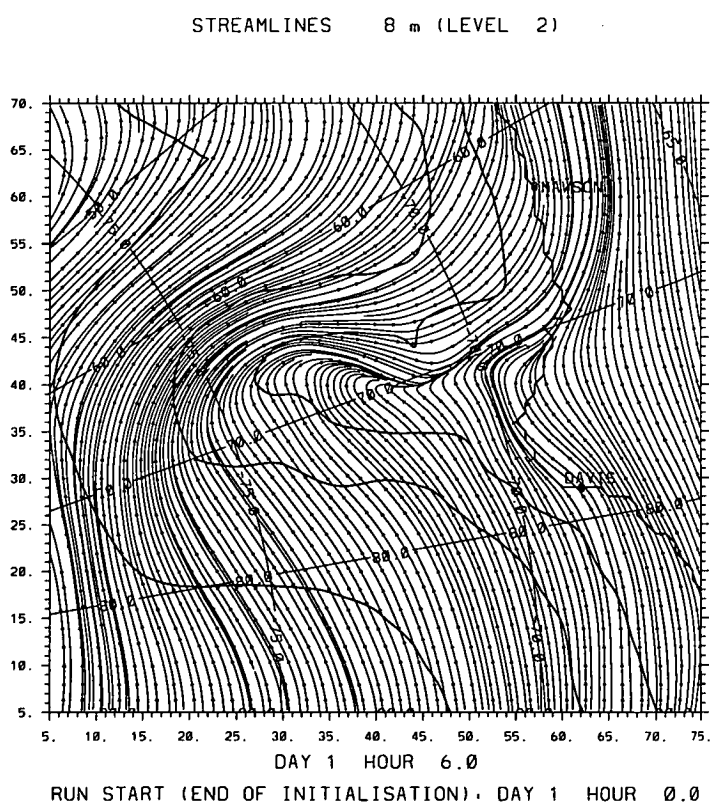

Figure 8.14: Surface (8 metres height) streamlines as produced by January "blizzard-non-katabatic" run R44. These lines do not represent trajectories but rather the air flow over the region at one time.

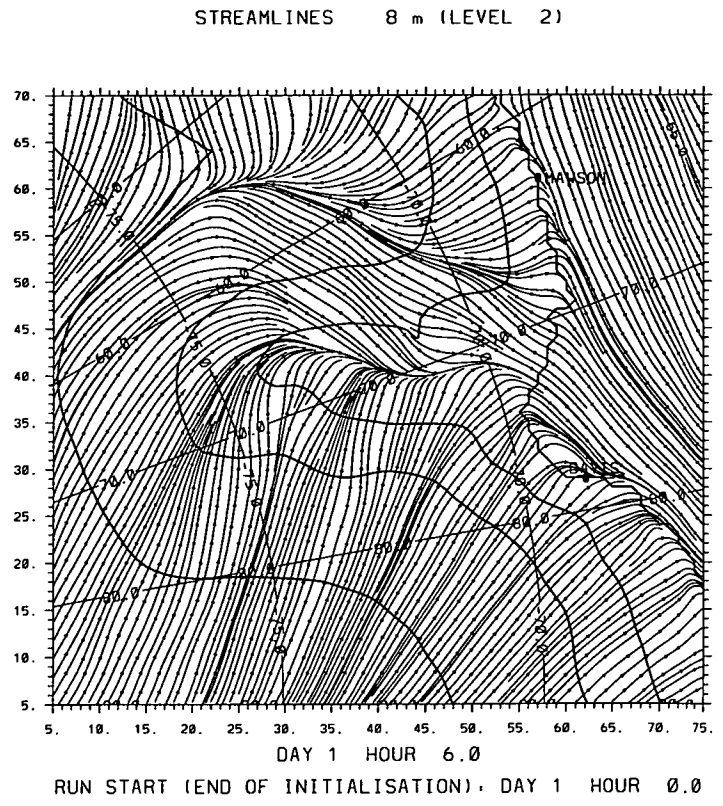

Figure 8.15: Surface (8 metres height) streamlines as produced by July "calm" run R45. These lines do not represent trajectories but rather the air flow over the region at one time.

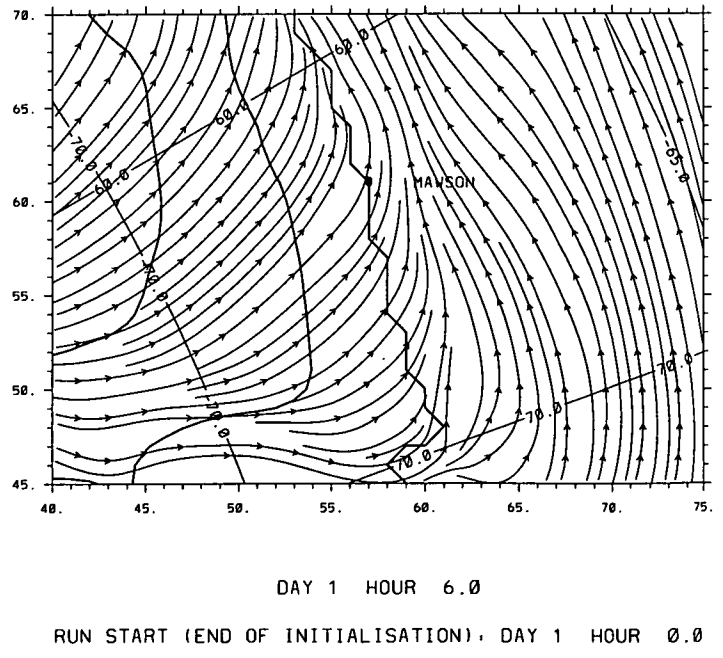

Figure 8.16: Surface (8 metres height) streamlines as produced by July run R34; synoptic forcing 10 m/s from 90°, substituted for July "katabatic-blizzard" run R46 that was found to be inaccurate; refer to text. These lines do not represent trajectories but rather the air flow over the region at one time. Only streamlines in the vicinity of Mawson are shown because the model was forced with a spatially-constant wind that was valid at Mawson.

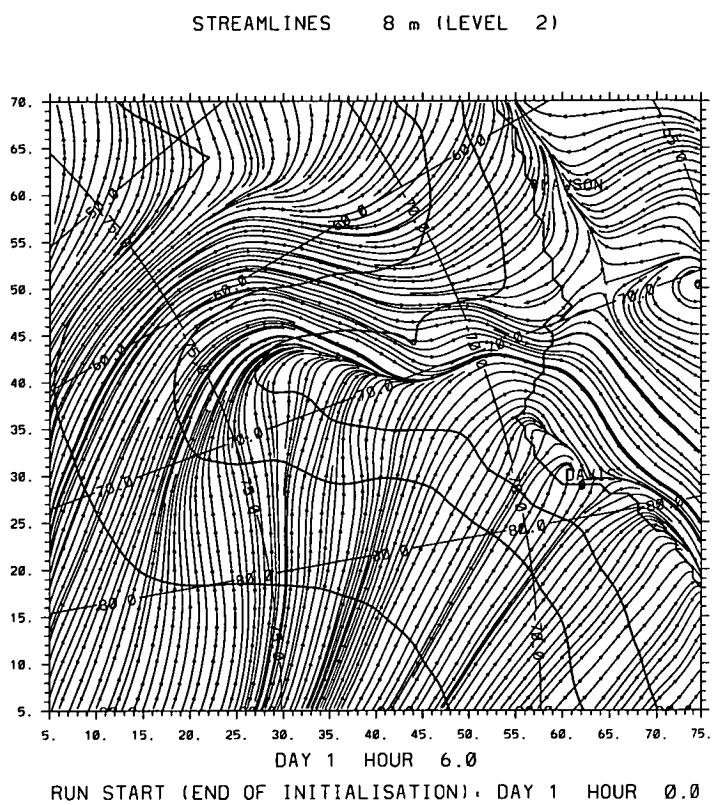

Figure 8.17: Surface (8 metres height) streamlines as produced by July "blizzard-non-katabatic" run R48. These lines do not represent trajectories but rather the air flow over the region at one time.

8.4 CONCLUSION

Numerical modelling of boundary layer meteorological conditions, forced by various synoptic winds, has been used to clarify relationships between synoptic and surface winds during summer and winter.

As found from analyses of observations in Chapter 7, there are relatively "direct" relationships between synoptic and surface winds during summer at Mawson station. This was confirmed by numerical modelling.

Following Chapter 7, synoptic-surface wind relationships were not as clear for winter as they were for summer. Numerical modelling conducted in this chapter has shown that sou-westerly synoptic winds is the likely forcing of winter downslope flow.

The mean winter surface air flow over the sea/seaice region is westerly, but blizzard winds at Mawson have corresponding easterly flow.

Katabatic-non-blizzard winds were found to be virtually independent of synoptic forcing.

The differences in boundary layer structure between summer and winter, and the corresponding seasonal differences in synoptic flow (general circulation) explained why Mawson station is a site of strong and persistent winds.

Chapter 9

CONCLUSION

The aims of this project were to establish mean seasonal (particularly summer and winter) atmospheric boundary layer meteorological conditions over the Lambert Glacier Basin Region of East Antarctica and to clarify the relationship between synoptic weather conditions and surface winds at Mawson station.

Previous studies of the Antarctic atmospheric planetary boundary layer were reviewed in Chapter 2. Meteorological conditions, and their variations over different regions, and basic principles which were found to apply in other regimes where observations were available, were examined for application to the Lambert Basin, where little observational information was available, were discussed.

In Chapter 3, measurements from over the Lambert Glacier Basin of East Antarctica were examined to establish the validity of compiling a climatology of this region. It was concluded that presently, due to the sparseness of the data coverage, a reliable climatology over the whole region could not be compiled. However, there were adequate data to be used in verification of results of numerical modelling, which could cover the area.

At Mawson and Davis stations, however, there were many data available. Several different types of winds were defined and analysed from observations at these stations. Meteorological conditions accompanying katabatic and blizzard winds were found. Mawson is a "katabatic wind site". The climatology of winds at Davis station, which is located some 20 km beyond the edge of the steep ice slope, demonstrated that not all coastal regions of Antarctica are subject to

katabatic flow.

To summarise, at Mawson, blizzard winds were warm, moist and related to cyclonic forcing, but winds categorised as katabatic were from cold, dry air originating further south and flowing as a shallow surface density current to the coast, from strong surface inversions. Katabatic-blizzard winds were the strongest mean winds found; characteristics of these winds showed they were forced by a combination of cyclonic flow and drainage flow from the interior of the continent. At Davis station, mean wind speeds were about 5 m/s less than those at Mawson station, and strong winds were largely related to offshore depressions. Winds at Mawson station were investigated in more detail in Chapters 7 and 8.

Features of the CSU-Pielke numerical mesoscale model and data used to initialise the model were discussed in Chapter 4. The aim of using the model was to establish summer and winter climatologies over the Lambert Glacier Basin region, using the data that are available to verify the results.

The model was tested for its suitability in modelling Antarctic meteorological conditions in Chapter 5. The first problem involved the surface energy balance iteration scheme that functioned correctly in terms of mathematics, but converged to unrealistic surface temperatures. It was found that the scheme was over-sensitive to initial conditions, and adjustments were made to overcome this problem.

Comparisons between observed and modelled surface temperature fields showed that modelled values were unrealistically low over the sea ice region of the model domain. The flat terrain of this region, and the weak winds, prevented mixing of air, and the result was significant cooling of the surface due to loss of long-wave radiation. In reality, surface temperatures of sea ice are relatively warm compared with those over the Antarctic plateau due to heat conduction through the ice from the water below. After several test runs, the monthly mean sea ice surface temperatures were prescribed. The surface temperatures of the firn (snow and ice) over the continent were calculated at every timestep of a model run.

The strong temperature inversions, (typically 20 - 25 K), that occur over the plateau of Antarctica during winter, caused the PBL height, predicted using the Deardorff (1974) scheme, to fall to very low values (about 6 metres). Such values were unrealistic and also disrupted the numerical computations within the PBL layer. The problem was overcome by introducing the Arya (1981) PBL height parameterisation, for "extremely stable" atmospheres. Tests showed that the combination of these two schemes produced the best results, with PBL heights comparable to those observed in the Antarctic by Bromwich (1976). This modification and model test runs were discussed in Chapter 5.

The sensitivities of the numerical model's thermal fields to surface parameters, such as albedo, diffusivity and inclusion of blue ice, were discussed in Chapter 6. This chapter also discussed the tuning of the model's radiation with respect to cloud influences. Cloud amount was an unknown parameter over the region of interest, but estimations were made using the limited observations and knowledge of cloud occurrence over Antarctica.

Cloud had not previously been included in the model, apart from emissivities at different levels due to water vapour. This process had not taken into account cloud albedo, absorption of long-wave radiation or variations in these factors due to cloud amount. These were represented in the model by making adjustments to the long-wave output and short-wave input terms in the surface energy balance equation.

Following the adjustments to parameterisation schemes in Chapter 5, and tuning of the numerical model's energy balance in Chapter 6, monthly mean January and July results were verified using observed data. The data generated for these two months were then used to represent mean summer and winter boundary layer climatologies of surface winds and thermal patterns over the Lambert Glacier Basin region. These were presented in Chapter 6, and were shown to provide close agreement with the results from the oversnow traverses and new Automatic Weather Stations.

Analyses of observations, in Chapter 7, were used to further investigate winds at Mawson station, and relationships between synoptic conditions and surface winds. Near-surface jets, particularly during winter, complicate these relationships because they are fairly independent of synoptic control, existing as relatively dense parcels of air draining downslope from the plateau.

Upper wind forcings of katabatic-blizzards were not as clear, as for blizzard-non-katabatics, that have corresponding E-SE upper winds, related to a cyclonic system to the north-east of Mawson, for both summer and winter.

Figure 7.15 demonstrates that katabatic winds are likely to be influenced by SW - W wind directions at the 700 hPa level during July. Rusin (1961) found a similar relationship at Mirny station.

Investigations of relationships between wind speeds and lapse rates, at Mawson, showed that during summer, wind speed increases were accompanied by increases in thermal stability, but during winter, wind speed increases corresponded to reductions in stability.

During January, upper wind forcings are in about the same direction as the surface winds, and the strength of the upper winds probably affect surface wind strength, through direct transfer of momentum in the vertical. The case is more complicated during July, with vectorial components contributing to the surface flow forcing.

The numerical model was previously shown to realistically model boundary layer winds over the Lambert Glacier Basin region. It was again used to clarify relationships between synoptic and surface winds, at Mawson, during summer and winter. Results of the numerical modelling were presented in Chapter 8.

As found from analyses of observations in Chapter 7, there are relatively "direct" relationships between synoptic and surface winds during summer at Mawson station. This was confirmed by the numerical modelling. It was also shown that winter downslope flow is forced by sou-westerly synoptic winds.

The mean winter surface air flow over the sea/ice region is westerly, but bliz-

zard winds at Mawson have corresponding easterly flow. Katabatic-non-blizzard winds were found to be virtually independent of synoptic forcing.

The differences in boundary layer structure between summer and winter, and the corresponding seasonal differences in synoptic flow (general circulation) explained why Mawson station is a site of strong and persistent winds.

Once appropriately adapted for Antarctic use, the numerical model was found to produce reasonable thermal fields with corresponding wind regimes. It then served as a powerful tool for improving the general understanding of air flow over Antarctica, on the regional scale, and also for explaining relationships between surface and synoptic winds over Mawson station.

REFERENCES

Abbs, D. ,(1986). Sea-breeze interactions along a concave coastline in southern Australia: observations and numerical modeling study. *Mon. Wea. Rev.* **114**, 831–848.

Adachi, T. (1984). Analytical Solutions of Katabatic Winds at Mizuho and Syowa Stations, Antarctica. Proceedings of the Sixth Symposium on Polar Meteorology and Glaciology. Tokyo: Memoirs of National Institute of Polar Research Special Issue No. 34.

Allison, I., Wendler, G. and Radok, U. ,(1993). Climatology of the East Antarctic Ice Sheet (100°E to 140°E) Derived From Automatic Weather Stations. *Journal of Geophysical Research* **98, No.D5 May 20**, 8815–8823.

Alt, J., Astapenko, P. and (Jr)., N. J. R. ,(1959). Some aspects of the Antarctic atmospheric circulation in 1958. *IGY General Report* **Series no. 4.**

Ambach, W. ,(1974). The Influence of Cloudiness on the Net Radiation Balance of a Snow Surface with High Albedo. *J. Glaciology* **13**, 73–84.

Arking, A. and Childs, J. D. ,(1985). Retrieval of Cloud Cover Parameters from Multispectral Satellite Images. *Journal of Climate and Applied Meteorology* **Vol. 24, April**, 322–333.

Arya, S. P. S. ,(1981). Parameterizing the Height of the Stable Atmospheric Boundary Layer. *Journal of Applied Meterology* **20**, 1192–1202.

Arya, S. P. ,(1988). Introduction to Micrometeorology . *International Geophysics Series* **Vol. 42.**

Ball, F. K. ,(1956). The Theory of Strong Katabatic Winds. *Australian Journal of Physics* **9, No. 3**, 373–386.

Ball, F. K. ,(1957). The Katabatic Winds of Adelie Land and King George V Land. *Tellus IX* **2**, 201–208.

Ball, F. K. (1960). Winds on the Ice Slopes of Antarctica. Proceedings of the Symposium on Antarctic Meteorology, Melbourne 1959. London: Pergamon Press.

Blumen, W. , (1984). An observational study of instability and turbulence in nighttime drainage winds. *Boundary Layer Meteorology* **28**, 245–269.

Bromwich, D. (1976). Boundary Layer Characteristics Of The Wilkes Ice Cap. M.Sc. Thesis, Meteorology Department, University Of Melbourne.

Bromwich, D. H. , (1991). Mesoscale Cyclogenesis over the Southwestern Ross Sea Linked to Strong Katabatic Winds. *Mon. Wea. Rev.* **119**, 1736–1752.

Bromwich, D. H. and Kurtz, D. D. , (1984). Katabatic Wind Forcing of the Terre Nova Bay polynya, Antarctica. *Journal of Geophysical Research* **89, No.C3**, 3561–3572.

Bromwich, D. H., Parish, T. R. and Zorman, C. A. , (1990). The Confluence Zone of the Intense Katabatic Winds at Terra Nova Bay, Antarctica, as Derived From Airborne Sastrugi Surveys and Mesoscale Numerical Modeling. *Journal of Geophysical Research* **Vol. 95 No. D5**, 5495–5509.

Budd, W. F. , (1966). Glaciological Studies In The Region Of Wilkes, Eastern Antarctica, 1961. *ANARE Scientific Reports. Series A (IV) Glaciology* **Publication No. 88.**

Budd, W. F. , (1969). The Dynamics of Ice Masses. *ANARE Scientific Reports. Series A (IV) Glaciology* **Publication No. 108.**

Budd, W. F., Dingle, R. and Radok, U. , (1966). Byrd snow drift report. *Studies in Antarctic Meteorology, Antarctic Research Series* **9.**

Budd, W. F., Jenssen, D. and Radok, U. (February 1971). Derived Physical Characteristics Of The Antarctic Ice Sheet. Mark 1. Publication No. 18, Meteorology Department, University Of Melbourne.

Businger, J. A. (1973). *Workshop on Micrometeorology*. Amer. Meteor. Soc..

Clark, T. L. and Farley, R. D. , (1984). Severe Downslope Windstorm Calculations in Two and Three Spatial Dimensions Using Anelastic Interactive Grid Nesting: A Possible Mechanism for Gustiness. *Journal of the Atmospheric Sciences* **41, No. 3**, 329–350.

Clarke, R. H. , (1970). Recommended methods for the treatment of the boundary layer in numerical models. *Aust. Met. Mag.* **18**, 51–73.

Coulter, R. L., Martin, T. J. and Porch, W. M. , (1991). A Comparison of Nocturnal Drainage Flow in Three Tributaries. *Journal of Applied Meteorology* **30**, 157–169.

Dalrymple, P. C. , (1966). A Physical Climatology of the Antarctic Plateau. *Studies in Antarctic Meteorology, Antarctic Research Series* **9**, 195–231.

Dalrymple, P. C., Lettau, H. H. and Wollaston, S. H. , (1966). South Pole micrometeorology program: Data analysis. *Studies in Antarctic Meteorology, Antarctic Research Series* **9**.

Dare, R. A. (1995). Characteristics of Surface and Upper Winds at Mawson and Davis. Antarctic CRC Report, To be published.

Deardorff, J. W. , (1972). Parameterisation of the planetary boundary layer for use in general circulation models. *Mon. Wea. Rev.* **100**, 93–106.

Deardorff, J. W. , (1974). Three-Dimensional Numerical Study of the Height and Mean Structure of a Heated Planetary Boundary Layer. *Boundary Layer Meteorology* **7**, 81–106.

Deaven, D. G. (1974). A solution for boundary problems in isentropic co-ordinate models. Ph.D. dissertation, Florida State University.

Defant, A. (1951). Local Winds. Compendium of Meteorology. Boston, Mass.: American Meteorological Society.

Drewry, D. J. (1983). *Antarctica, glaciological and geophysical folio.* Cambridge: Scott Polar Research Institute.

Dzerdzeevskii, B. L. (1960). Certain features of weather in the coastal area of Eastern Antarctica. Proceedings of the Symposium on Antarctic Meteorology, Melbourne 1959. London: Pergamon Press.

Gallée, H. and Schayes, G. , (1992). Dynamical Aspects Of Katabatic Wind Evolution In The Antarctic Coastal Zone. *Boundary Layer Meteorology* **59, April**, 141.

Goodwin, I. D. , (1988). Firn Core Data From shallow Drilling Investigations In Eastern Wilkes Land, East Antarctica. *ANARE Research Notes, Antarctic Division, Australia* **65**.

Hootman, B. W. and Blumen, W. , (1983). Analysis of Nighttime Drainage Winds in Boulder, Colorado, During 1980. *Mon. Wea. Rev.* **111**, 1052–1061.

Kitabayashi, (1977). Wind tunnel and field studies of stagnant flow upstream of a ridge. *J. Meteor. Soc. Japan* **55**, 193–203.

Lee, R. (1978). *Forest Microclimatology*. New York: Columbia University Press.

Lettau, H. H. , (1966). A Case Study of Katabatic Flow on the South Pole Plateau. *Studies in Antarctic Meteorology, Antarctic Research Series* **9**.

Lettau, H. H. and Schwerdtfeger, W. , (1967). Dynamics of the Surface-Wind Regime Over the Interior of Antarctica. *Antarctic Journal of U.S.* **II, No.5**, 155–158.

Lied, N. T. , (1964). Stationary Hydraulic Jumps in a Katabatic Flow Near Davis, Antarctica, 1961. *Aus. Met. Mag.* **47**, 40–51.

Liljequist, G. H. , (1958). Long-wave radiation and turbulent heat transfer in the Antarctic winter and the development of surface inversions. *Polar Atmosphere Symposium* **part I**, 167–181.

Linacre, E. and Hobbs, J. (1977). *The Australian Climatic Environment*. John Wiley & Sons.

Loewe, F. ,(1974). Die tagliche Windschwankung uber dem Innern von Inlandeisen in Sommer. *Archiv fur Meteorologie, Geophysik und Bioklimatologie B* **22**, 219–232.

Madigan, C. T. (1929). Sci. Rep. Aust. Antarctic Expedition 1911-14 B.

Mahrer, Y., Segal, M. and Pielke, R. , (1985). Mesoscale modelling of wind energy over non-homogeneous terrain. *Bound. Layer Meteorol.* **31**, 13–23.

Mahrer, Y. and Pielke, R. A. ,(1977). A Numerical Study of the Airflow over Irregular Terrain. *Beitrage zur Physik der Atmosphare* **50**, 98–113.

Mahrer, Y. and Pielke, R. A. , (1978). A Test of an Upstream Spline Interpolation Technique for the Advective Terms in a Numerical Mesoscale Model. *Mon. Wea. Rev.* **106**, 818–830.

Mahrt, L. and Larsen, (1982). Small Scale Drainage Front. *Tellus* **34**, 579–587.

Manins, P. C. and Sawford, B. L. , (1979a). A model of katabatic winds. *Journal of the Atmospheric Sciences* **36**.

Manins, P. C. and Sawford, B. L. , (1979b). Katabatic winds: A field case study. *Quart. J. R. Met. Soc.* **105**, 1011–1025.

Mather, K. B. (1960). Katabatic Winds South of Mawson. Antarctic Meteorology, Proceedings of the Symposium, Melbourne, 1959. London: Pergamon Press.

Mather, K. B. , (1962). Further observations on sastrugi, snow dunes and the pattern of surface winds in Antarctica. *Polar Record* **11**, 158–171.

Mather, K. B. , (1969). The Pattern of Surface Wind Flow in Antarctica. *Pure Appl. Geophys.* **75**, 332–354.

Mawson, D. (1915). *Home of the Blizzard.* Vol. **Vol. 1**. London: Heinemann.

Mellor, M. , (1960). Sea Ice Measurements At Mawson and Davis, 1954-58. *ANARE Interim Reports 19* **November 1960**.

vanMeurs, B. and Allison, I. (1986). An application of automatic weather station data to the study of katabatic flow in East Antarctica. Proceedings of second International Conference on Southern Hemisphere Meteorology. Boston, Mass.: American Meteorological Society.

vanMeurs, B. and Allison, I. (1988). Numerical Simulation of Katabatic Flow and its Interaction with Synoptic Pressure Fields in East Antarctica. Unpublished report.

vanMeurs, B. and Allison, I. (1989). The Structure of Katabatic Flow Along 112°E as Inferred from Model and Automatic Weather Station Results. Paper delivered at Conference and Workshop on Antarctic Weather and Climate.

Miller, S. A. (1974). An Analysis of Heat and Moisture Budgets of the Inversion-Layer over the Antarctic Plateau, for Steady State Conditions. Ph.D. Thesis (shortened version).

O'Brien, J. , (1970). A note on the vertical structure of the eddy exchange coefficient in the planetary boundary layer. *J. Atmos. Sci.* **27**, 1213–1215.

Oke, (1973). City Size and the Urban Heat Island. *Atmos. Environ.* **7**, 769–779.

Parish, T. R. , (1982). Surface Airflow Over East Antarctica. *Mon. Wea. Rev.* **110**, 84–90.

Parish, T. R. , (1984). A Numerical Study of Strong Katabatic Winds over Antarctica. *Mon. Wea. Rev.* **112**, 545–554.

Parish, T. R. , (1992). On the role of Antarctic Katabatic Winds in Forcing Large-Scale Tropospheric Motions. *Journal of the Atmospheric Sciences* **49, No.15**, 1374–1385.

Parish, T. R. , (1988). Surface Winds over the Antarctic Continent: A Review. *Review of Geophysics* **26 No.1 Feb.**, 169–180.

Parish, T. R. and Bromwich, D. H. , (1987). The surface windfield over the Antarctic ice sheets. *Nature* **328**, 51–54.

Pettré, P. and André, J. C. ,(1991). Surface-Pressure Change through Loewe's Phenomena and Katabatic Flow Jumps: Study of Two Cases in Adelie Land, Antarctica. *Journal of the Atmospheric Sciences* **48**, 557–571.

Phillpot, H. R. (1989). On Surface Weather Behaviour On The Australian Antarctic Territory Coastline, I: An Observational Overview, II: Near-Surface Pressure Systems and Associated Coastal Weather. Conference and Workshop on Antarctic Weather and Climate.

Phillpot, H. R. and Zillman, J. W. ,(1970). The Surface Temperature Inversion over the Antarctic Continent. *Journal of Geophysical Research* **75, No.21.**

Pielke, R., McNider, R. T., Segal, M. and Mahrer, Y. ,(1983). The use of a mesoscale numerical model for evaluations of pollutant transport and diffusion in coastal regions and over irregular terrain. *Bull. Amer. Met. Soc.* **64**, 243–249.

Pielke, R. A. ,(1974). A Three-Dimensional Numerical Model of the Sea Breezes Over South Florida. *Mon. Wea. Rev.* **102**, 115–139.

Pielke, R. A. and Mahrer, Y. ,(1975). Representation of the Heated Planetary Boundary Layer in Mesoscale Models with Coarse Vertical Resolution. *Journal of the Atmospheric Sciences* **32**, 2288–2308.

Pielke, R. A. (1984). *Mesoscale Meteorological Modelling.* Academic Press.

Pielke, R. A. and Martin, C. L. ,(1981). The Derivation of a Terrain-Following Coordinate System for use in a Hydrostatic Model. *Journal of the Atmospheric Sciences* **38**, 1707–1713.

Porch, W. M., Clements, W. E. and Coulter, R. L. ,(1991). Nighttime Valley Waves. *Journal of Applied Meteorology* **30**, 145–156.

Prandtl, L. (1942). *Fuehrer durch die Stroemungslehre.* Braunschweig: Vieweg & Sohn.

Purnell, D. K. ,(1976). Solution of the advective equation by upstream interpolation with a cubic spline. *Mon. Wea. Rev.* **104**, 42–48.

Radok, U., Brown, T. J., Jenssen, D., Smith, I. N. and Budd, W. F. ,(1986). Antarctic ice accumulation basins and their main discharge regions. *On The Surging Potential Of Polar Ice Streams* **IV**.

Ramanathan, V. E., Pitcher, E. J., Malone, R. and Blackmon, M. L. ,(1983). The response of a spectral general circulation model to refinements in radiative processes. *Journal of the Atmospheric Sciences* **Vol. 40, March**, 605–630.

Rubin, M. J. and Giovinetto, M. B. ,(1962). Snow Accumulation in Central West Antarctica as Related to Atmospheric and Topographic Factors. *Journal of Geophysical Research* **67**, 5163–5170.

Rusin, N. P. (1961). *Meteorological and Radiational Regime of Antarctica.* Leningrad, (Translated Jerusalem 1964): Gidrometeorizdat.

Schwerdtfeger, P. (1963). Theoretical derivation of the thermal conductivity and diffusivity of snow.. International Union of Geodsey and Geophysics, International Association of Scientific Hydrology, Symposium of Berkeley.

Schwerdtfeger, W. ,(1970). The climate of the Antarctic. *World Survey of Climatology* **Vol. 14**, 253–355.

Schwerdtfeger, W. (1974). Mountain barrier effect on the flow of stable air north of the Brooks Range. Climate of the Arctic, Proceedings of the 24th Alaskan Science Conference, Fairbanks, August 1975, G. Weller and S.A. Bowling, Eds.. University of Alaska Press.

Schwerdtfeger, W. (1984). *Weather and Climate of the Antarctic.* Amsterdam: Elsevier.

Schwerdtfeger, W. and Mahrt, L. J. (1968). The relation between the Antarctic temperature inversion in the surface layer and its wind regime. Paper delivered at ISAGE Conference, Glacial Meteorology.

Segal, M., Avissar, R., McCumber, M. and Pielke, R. ,(1988). Evaluation of vegetation effects on the generation and modification of mesoscale circulations. *J. Atmos. Sci.* **45**, 2268–2292.

Shaw, P. J. R. ,(1957). Climate of Mawson in 1955. *Australian Meteorological Magazine* **18**, 1–20.

Shaw, P. J. R. (1960). Local winds in the Mawson area. Antarctic Meteorology, Proceedings of the Symposium, Melbourne, 1959. London: Pergamon Press.

Simmonds, I. and Budd, W. F. ,(1991). Sensitivity of the southern hemisphere circulation to leads in the Antarctic pack ice. *Quart. J. R. Met. Soc.* **117**, 1003–1024.

Steyn, D. and McKendry, I. ,(1988). Quantitative and qualitative evaluation of a three-dimensional mesoscale numerical model simulation of a sea-breeze in complex terrain. *Mon. Wea. Rev.* **116**, 1914–1926.

Stone, R. S., Dutton, E. G. and DeLuisi, J. J. ,(1989). *Antarctic Journal* **1989 Review**, 230–232.

Streten, N. A. ,(1961). A note on observations at Mawson and field stations in Mac.Robertson Land in 1960. *Aus. Met. Mag.* **34**, 45–62.

Streten, N. A. ,(1962). Notes on Weather Conditions in Antarctica. *Aus. Met. Mag.* **No. 37, June**, 1–30.

Streten, N. A. ,(1963). Some observations of Antarctic katabatic winds. *Aus. Met. Mag.* **42**, 1–23.

Streten, N. A. ,(1968a). A note on two prolonged Antarctic gales. *Weather* **23**, 162–167.

Streten, N. A. ,(1968b). Characteristics of strong wind periods in coastal East Antarctica. *Journal of Applied Meteorology* **7**, 46–52.

Streten, N. A. ,(1990). A review of the climate of Mawson - a representative strong wind site in East Antarctica. *Antarctic Science* **2(1)**, 79–89.

Tauber, G. M. (1960). Characteristics of Antarctic Katabatic Winds. Antarctic Meteorology, Proceedings of the Symposium, Melbourne, 1959. London: Pergamon Press.

Turner (1973). *Buoyancy Effects in Fluids.* Cambridge University Press.

Vowinckel, E. (1957). Climate of the Antarctic Coast.. Meteorology of the Antarctic. Weather Bureau of South Africa, Government Printer, Pretoria.

Weller, G. , (1969). A Meridional Surface Wind Speed Profile in MacRobertson Land, Antarctica. *Pure Appl. Geophys.* **77**, 193–200.

Weller, G. , (1980). Spatial and Temporal Variations in the South Polar Surface Energy Balance. *Mon. Wea. Rev.* **108**, 2006–2014.

Weller, G. and Schwerdtfeger, P. , (1977). *Antarctic Research Series* **25.**

Weller, G. E. , (1967). Radiation Fluxes over an Antarctic Ice Surface, Mawson 1961-62. *ANARE Scientific Reports. Series A (IV) Glaciology* **Publication No. 96.**

Weller, G. E. , (1968). The Heat Budget And Heat Transfer Processes In Antarctic Plateau Ice And Sea Ice. *ANARE Scientific Reports. Series A (IV) Glaciology* **Publication No. 102.**

Wendler, G., André, J., Pettré, P., Gosink, J. and Parish, T. , (1993). Katabatic winds in Adelie Coast. *Antarctic Research Series (Antarctic Meteorology and Climatology: Studies based on Automatic Weather Stations)* **61**, 23–46.

Wendler, G. , (1986). The "Radiation Paradox" on the Slopes of the Antarctic Continent. *Polarforschung* **56 (1/2)**, 33–41.

Wendler, G. and Kodama, Y. , (1993). The Kernlose Winter in Adelie Coast. *Antarctic Research Series (Antarctic Meteorology and Climatology: Studies bas ed on Automatic Weather Stations)* **61**, 139–147.

Wilson, C. , (May 1968). Climatology of the Cold Regions, Southern Hemisphere. *Cold Regions Science and Engineering* **Monograph I-A3c** .

Wilson, J. (1992). Wind Flow Around Law Dome, East Antarctica. M.Sc. Thesis, Department of Mathematics, Monash University.

Zeman, O. , (1979). Parameterisation of the Dynamics of Stable Boundary Layers and Nocturnal Jets. *Journal of the Atmospheric Sciences* **36**, 792–804.

Zilitinkevich, S. S. (1970). Dynamics of the Atmospheric Boundary Layer. Paper delivered at Leningrad Gidrometeor.